Targeting NAD^+ for retinal ganglion cell protection in experimental glaucoma

Gloria Cimaglia

2023

School of Optometry and Vision Sciences

Cardiff University

Thesis submitted for the degree of

Doctor of Philosophy

To Red,

Mo chuisle.

Acknowledgements

"It was a dark and stormy night" as my beloved Snoopy would have said but, even with a pandemic in the middle, we made it!

Firstly, I wish to thank Professor James E. Morgan, Professor Marcela Votruba, and Associate Professor Pete A. Williams for giving me the opportunity to undertake this project and to become part of their research groups at Cardiff University and Karolinska Institutet. I am very grateful for the scientific and personal influence you had on me. Your enthusiasm, guidance, and support transformed this project into one of the most satisfying scientific experience I ever had. I hope that our collaboration can continue for many years to come.

A huge thank goes to Fight for Sight without whom this project would have not been possible, and to the Swedish Metabolomics Centre for processing the optic nerve samples.

I am grateful to Dr. Veronica Walker, Nicky for us, who taught me how to approach a rat for the first time, and now is calling me the "rat whisperer". Without her knowledge and competence I would have never been able to take such a good care of my animals. Her advices have been precious.

I want also to extend my gratitude to all the people I have been lucky to meet over the past years. Thanks to James Tribble for his endless patience and kindness in answering all my science related questions. Thanks to Erini Kokkali and Ryan Bevan for teaching me how to perform the essential techniques from day one, and for sharing with me part of this journey. Thank to my amazing friend and colleague Andrew Want. You taught me "how to be Brit", that the weather is never just weather and that a good cup of tea can solve everything. After three years together I must say that your Mediterranean temper might be a little bit more than "just one drop of milk in a espresso". I hope that in London you will find everything you have whished for. Thank to Cristina Llinares Benadero and Sara Jörgensen for the chats, coffees and the international dinners.

I huge thank goes to my best friend Minna Christiansen Lund, now Dr. in Neuroscience. We have started this journey together many years ago, when we could only dream about this amazing profession. Even if we could not continue in the same place together, we have always been there for each other with silent video calls, sudden laughs while we were both writing and reading

ours “scientific masterpieces”. It was a shared journey anyway. I promise you that, if I will be able to have my own group at some point, we will collaborate together again!

Last but not least I want to thank my parents. Thank you for your endless love and support throughout all this journey. Although it has been a huge sacrifice to have me away from home, you have always given me the confidence to pursue what I really loved. And a special thank goes to you dad. You have been my example and if I never give up and I am able to walk arduous paths is because you taught me how to do it.

Gloria

“Nothing in life is to be feared, it is only to be understood”

Marie Sklodowska-Curie

Summary

Glaucoma is the leading cause of irreversible blindness worldwide. It is characterised by progressive degeneration and loss of retinal ganglion cells (RGCs) and their axons. Despite ocular hypertension (OHT) being the major and only treatable risk factor, increasing evidences suggest that nicotinamide adenine dinucleotide (NAD^+) age related decline may exacerbate neuronal vulnerability to glaucomatous damage.

NAD^+ is an important metabolite, central to neuronal health and energy metabolism. RGCs due to their compartmentalised structure and function are among the most energy consuming neurons of the central nervous system (CNS), and rely on mitochondria to fulfil their energy requirements. Reduced NAD^+ bioavailability has an impact on mitochondrial functions, affecting mitochondrial ability to produce ATP, increasing at the same time oxidative stress and inflammatory reactions. This leads to an altered cellular homeostasis which influences RGCs degeneration.

Here we show that nicotinamide adenine mononucleotide (NAM) supplementation, a precursor of NAD^+, can mitigate RGC dendritic atrophy in *ex vivo* retinal explants and *in vivo* following induction of unilateral OHT. NAM enrichment maintained RGCs cellular homeostasis, restoring energy metabolism and cellular antioxidant capacity, which were lost in untreated OHT models. Proof of concept experiments explored whether overexpression of NMNAT2, the rate limiting enzyme of the salvage pathway, could enhance RGCs survival.

These findings suggest that supporting energy metabolism can reduce RGCs vulnerability to glaucomatous damage. Preserving RGC integrity is pivotal to visual functions, and considering the ongoing nicotinamide trials, these data further confirm the significant neuroprotection that can be achieved with NAD^+-related therapies.

Contributions

All the work presented in this thesis is my own except for the following contributions.

In all the experimental chapters Dr. Veronica Walker and JBIOS (animal facility at Cardiff University) assisted with housing and transferring of the animals.

Chapter 3:

Assistant Prof. James Tribble and Dr. Eirini Kokkali introduced me to the microbead model.

Chapter 5:

Dr. Eirini Kokkali assisted during retinal explant procedures and image acquisition.

Chapter 7:

Andrew Want assisted with optic nerves collection and the Metabolomic Swedish Centre analysed optic nerves samples. Assistant Prof. James Tribble and Associate Prof. Pete Williams supported during metabolomics raw data analysis.

Chapter 8:

Associate Prof. Pete Williams provided the AAV-NMNAT2 construct.

Publications

Papers

Tribble J.R., Otmani A., Sun S., Ellis S.A., **Cimaglia G.**, Vohra R., Jöe M., Lardner E., Venkataraman A.P., Domínguez-Vicent A., Kokkali E., Rho S., Jóhannesson G., Burgess R.W., Fuerst P.G., Brautaset R., Kolko M., Morgan J.E., Crowston J.G., Votruba M. and Williams P.A. (2021) Nicotinamide provides neuroprotection in glaucoma by protecting against mitochondrial and metabolic dysfunction. *Redox Biology* **43**

Cimaglia G., Votruba M., Morgan J.E., Helder A. and Williams P.A. (2020) Potential therapeutic benefit of NAD^+ supplementation for glaucoma and age-related macular degeneration. *Nutrients* **12**: 9

Book chapters

Cimaglia G., Bevan R.J., Want A. and Morgan J.E. (2023) Gene gun DiOlistic labelling of retinal ganglion cells. Submitted to *Methods in Molecular Biology*

Table of Contents

Table of Figures

List of Tables

Abbreviations

%	Percentage
°C	Degree Celsius
µg	Microgram
µm	Micrometre
3-MH	3-Methyhistidine
5-ALA	5-aminolevulinic acid
AA	Arachidonic acid
AAV	Adeno-associated virus
ACG	Angle closure glaucoma
AD	Alzheimer's disease
ADMA	N-N Dimethylarginine (asymmetric dimethylarginine)
ALS	Amyotrophic lateral sclerosis
ANOVA	Analysis of variance
ARM	Armadillo/HEAT motif
ATP	Adenosine triphosphate
AUC	Area under the curve
BBB	Blood brain barrier
BDNF	Brain derived neurotrophic factor
BN	Brown Norway
C.HNAM	Control high NAM
C.LNAM	Control low NAM
C.sham	Control normotensive no treatment (naïve)
CDNF	Ciliary derived neurotrophic factor
cm	Centimetre
CNS	Central nervous system
DEV	Days ex vivo
DHAP	Dihydroxyacetone phosphate
DiD	1,1'-dioctadecyl-3,3,3',3'-tetramethylindodicarbocyanine, 4-chlorobenzenesulfonate
DiI	1,1'-dioctadecyl-3,3,3',3'-tetramethylindocarbocyanine perchlorate
DiO	3,3'-Dioctadecyloxacarbocyanine perchlorate
DNA	Deoxyribonucleic acid
DRP1	Dynamin related protein 1
em	Emission
ETC	Electron transport chain
ex	Excitation
F6P	Fructose-6-phosphate
G	Gauge
G.HNAMint	Glaucoma high NAM intervention

G.HNAMproph	Glaucoma high NAM prophylactic
G.LNAMint	Glaucoma low NAM intervention
G.LNAMproph	Glaucoma low NAM prophylactic
G.sham	Glaucoma not treated
G3P	Glyceraldehyde 3 phosphate
G6P	Glucose-6-phosphate
gc	Genome copies
GCL	Ganglion cell layer
GDNF	Glia derived neurotrophic factor
GFP	Green fluorescent protein
GPC	Glycerophosphocholine
GPx	Glutathione peroxidase
GR	Glutathione reductase
GSH	Glutathione
GSSG	Glutathione disulfide
h	Hour(s)
H_2O	Water
H_2O_2	Hydrogen peroxide
HBSS	Hank's balanced salt solution
HNAM	High dose NAM treatment
HT	Hypertensive
IL	Interleukin
INL	Inner nuclear layer
Int	Intervention
IOP	Intraocular pressure
IPL	Inner plexiform layer
IVI	Intravitreal injection
KEGG	Kyoto Encyclopaedia of Genes and Genomes (database)
LGN	Lateral geniculate nucleus
LNAM	Low dose NAM treatment
max	Maximum
MBI	Microbead
Met	Methionine
mg	Milligram
min	Minimum
min	Minute(s)
ml	Millilitre
mM	Millimolar
mm	Millimetre
mm^2	Milli square metre
mmHg	Millimetre of mercury
mtDNA	Mitochondrial DNA
n	Cellular sample size (RGC)
N	Cohort sample size (rat)
NA	Nicotinic acid

NAD	Nicotinamide adenine dinucleotide
NAD^+	Oxidised form of nicotinamide adenine dinucleotide
NADH	Reduced form of nicotinamide adenine dinucleotide
NAG	N-acetylglutamate (N-acetylglatamic acid)
NAM	Nicotinamide adenine mononucleotide
NAMPT	Nicotinamide phosphoribosyl transferase
ND	Neurodegenerative disease
nDNA	Nuclear DNA
NFL	Nerve fibre layer
NFL	Nerve fibre layer
NGF	Nerve growth factor
nm	Nanometre
NMN	Nicotinamide mononucleotide
NMNAT2	Nicotinamide nucleotide adenylyl transferase 2
NR	Nicotinamide riboside
NRK	Nicotinamide riboside kinase
NT	Normotensive
NTG	Normal tension glaucoma
NTG	Normal tension glaucoma
OAG	Open angle glaucoma
OHT	Ocular hypertension
ON	Optic nerve
ONH	Optic nerve head
ONL	Outer nuclear layer
OPA1	Optic atrophy type 1
O-PE	O-phosphoethanolamine
OPL	Outer plexiform layer
OXPHOS	Oxidative phosphorylation
p	Probability value
PARPs	Poly ADP-ribose polymerases
PBS	Phosphate Buffer Saline
PCA	Principal component analysis
PD	Parkinson’s disease
PEP	Phosphoenolpyruvate (Phosphoenolpyruvic acid)
PFA	Paraformaldehyde
Proph	Prophylactic
psi	Pound per square inch
RBPMS	RNA-binding protein with multiple splicing
RBPMS	Ribonucleic acid-binding protein with multiple splicing
RGC	Retinal ganglion cell
RNA	Ribonucleic acid
ROCK	Rho-associated kinase
ROS	Reactive oxygen species
RPE	Retinal pigmented epithelium
RPE	Retinal pigmented epithelium
RPM	Revolution per minute
SARM1	Sterile alpha and Toll/interleukin-1 receptor motif-containing 1

SC	Superior colliculus
SD	Standard deviation
SEM	Standard error of the mean
SIRTs	Sirtuins
T.G.AAVNMNAT2	Transgenic hypertensive AAV-NMNAT2 injected group
T.NT.AAVNMNAT2	Transgenic normotensive AVV-NMNAT2 injected group
TCA	Tricarboxylic acid cycle
TCA	Tricarboxylic acid
TIR	Toll/interleukin-1 receptor
TLR	Toll like receptor
TNF	Tumour necrosis factor
UPR^{mt}	Mitochondrial unfolded protein response
W	Tungsten
w	Week(s)
Σ	Sum

1 Introduction

1.1 The retina

Despite its external location, due to its embryological origin, the retina is part of the central nervous system (CNS). Consistent with its neural identity, the retina comprises complex neural networks that convert electrical activity and action potentials into visual information that travel through the optic nerve to the designated brain areas (lateral geniculate nucleus (LGN), superior colliculus (SC) and visual cortex) (Armstrong and Cubbidge, 2019, Gregg et al., 2013).

Five distinct classes of neurons populate the retina: photoreceptors, horizontal cells, bipolar cells, amacrine cells and retinal ganglion cells (RGCs). Somas and processes of these neurons are structurally organised in five layers. The cell bodies are located in the outer nuclear layer (ONL), inner nuclear layer (INL) and ganglion cell layer (GCL), while the processes and synapses sit in the outer plexiform layer (OPL) and inner plexiform layer (IPL) (Dowling, 1987). Along with the neuronal population, glial cells – Müller cells, astrocytes and microglia – provide metabolic, structural and functional support to the neuronal retina (Fig. 1.1) (Karlstetter et al., 2015, Pfeiffer et al., 2016).

Each retinal cell has a specific function, which contributes to the transfer of visual information from the eye to the brain.

The retinal pigment epithelium (RPE) is formed by a single layer of retinal pigment epithelial cells which absorb the light and participate in photoreceptor outer segment homeostasis (Boulton and Dayhaw-Barker, 2001). The photoreceptors, rods and cones, modulate the first step in the conversion of light stimuli into electrical signals, which are then further processed by horizontal cells. Horizontal cells modulate and integrate the output photoreceptors signal. Bipolar cells, the main retina interneurons, form the main pathway from photoreceptors to retinal ganglion cells (Grünert, 2009). Bipolar cells synapse with amacrine cells within and below the ganglion cell layer to create a signalling loop between bipolar cells and retinal ganglion cells and bipolar cells and photoreceptors (Dowling, 2015).

Finally retinal ganglion cells summate information from the outer retina within the inner plexiform layer. If the change in membrane potential is sufficient, they will generate an action potential for transmission to visual centres within the CNS.

RGC degeneration and loss underpin vision loss in glaucoma, one of the commonest causes globally of vision loss. Their protection and repair is the subject of this thesis.

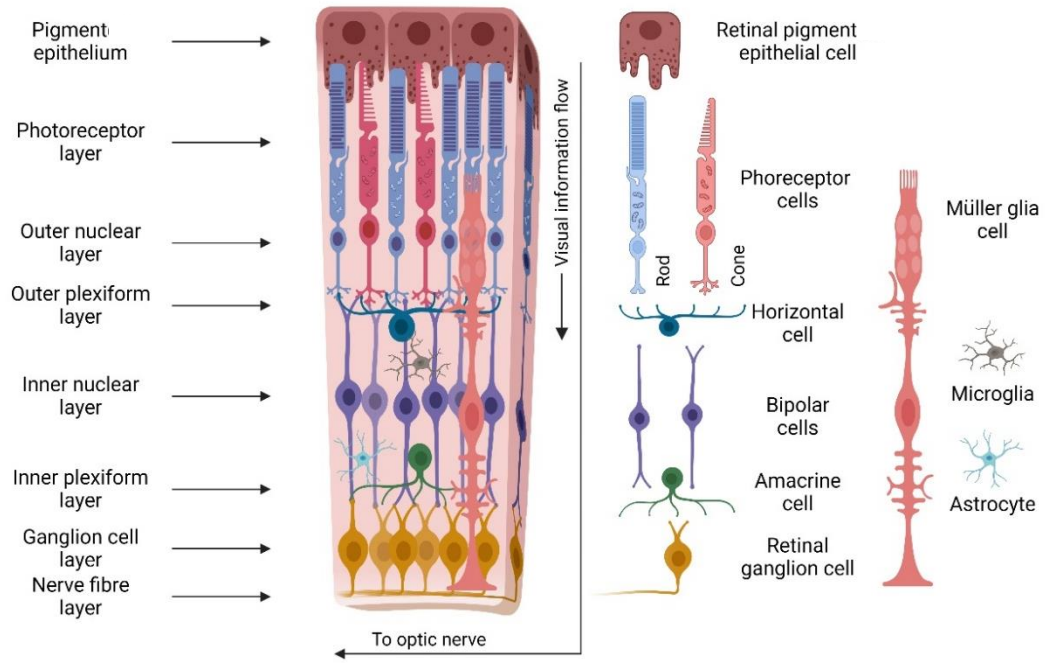

Figure 1. 1. Schematic retinal structure.

1.2 Retinal ganglion cells

1.2.1 Structure and function

RGCs are the output neurons of the retina and their main function is to process and convey visual information to the visual centres of the brain. There are approximately 1.2 millions RGCs in the human retina (Kim et al., 2021), and around 82,800 to 89,200 in the rat depending on strain and pigment (Salinas-Navarro et al., 2009), with both human and rodent RGCs distributed within the retina following a central-peripheral gradient (Sernagor et al., 2001). In the human retina, the RGC layer is more than one RGC thick, forming the macula, an area of high RGC density to manage the outputs from the centrally located fovea.

RGC cell bodies lie in the GCL, while their broad and intricate dendritic trees extend their branches in the IPL where they form synapses. RGCs excitation is glutaminergic while the lateral inhibitory pathway depends on GABA and the release of glycine from amacrine cells (Kolb H., 1995). Unlike any other CNS neuron, RGCs receive synaptic inputs on the actual dendrite shaft,

with a Gaussian distribution of synaptic connections which determines the RGC receptive field (Marshak, 2009).

RGCs axons form the retinal nerve fibre layer lying on the inner retina; they exit the retina at the optic disc. Then these axons, when they travel trough the lamina cribrosa, bundle together to form the optic nerve and become myelinated (Boiko et al., 2003).

1.2.1.1 Subtypes

RGCs are classified according to morphology, gene expression, spacing and physiological properties. Following these parameters at least 30 different subtypes have been classified based on their morphology (Sanes and Masland, 2015) and many more based on their transcriptomic profile (Huang et al., 2022).

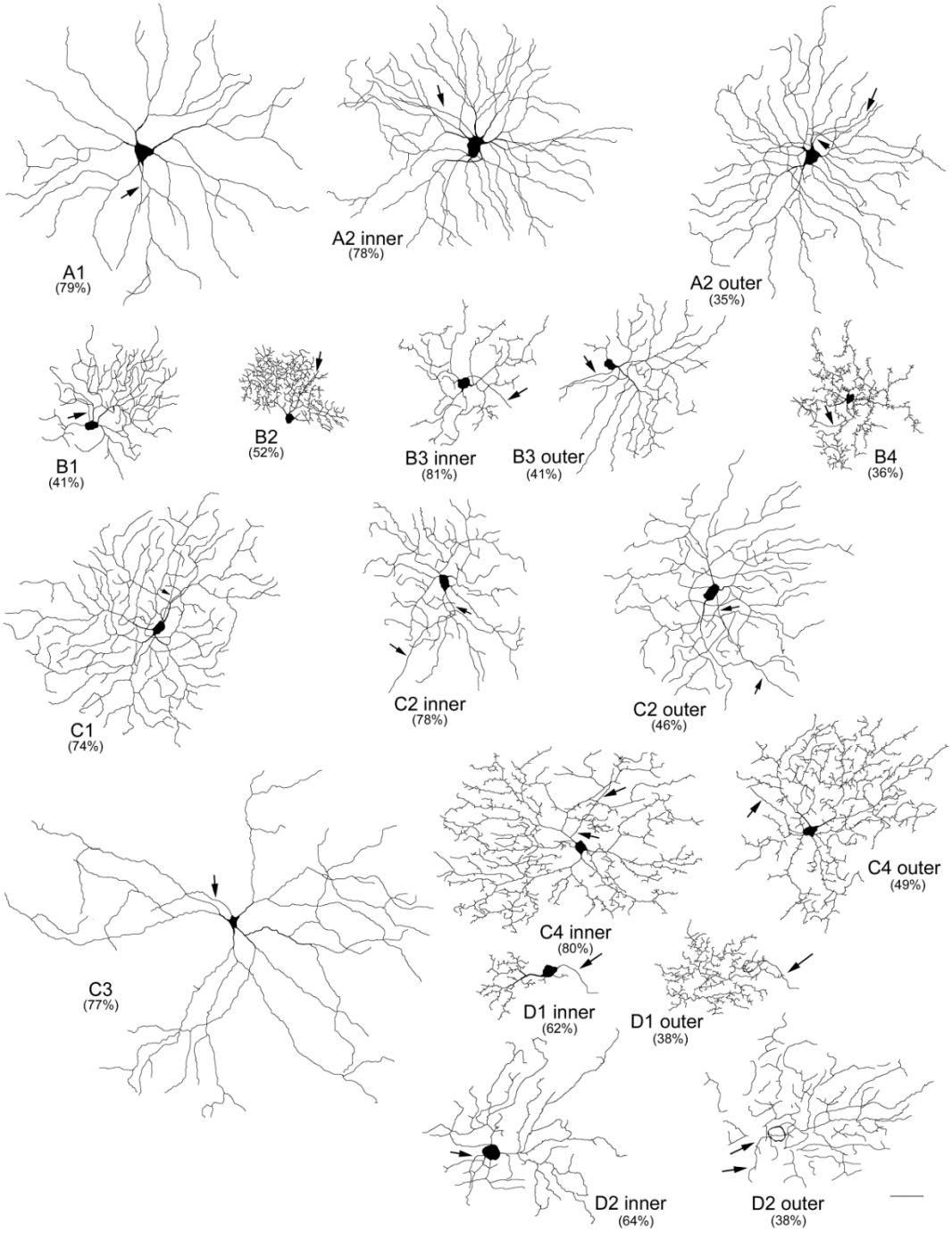

Figure 1. 2. Rat RGCs classification based on dendritic morphology. *From (Sun et al., 2002a)*

One of the most basic RGCs classification is as ON, OFF or ON/OFF. ON and OFF characterization is not only functional, based on the synaptic connection with ON and OFF bipolar cells respectively, but it also based on the morphology of the dendritic arbour. ON RGCs spread their dendrites in the sublamina b of the IPL, while OFF in the deeper sublamina a. ON/OFF RGCs are bistratified, with one layer of dendrites branching in each lamina (Fig. 1.3). Some authors suggest

that due to their high energy demand ON RGCs are more susceptible to damage (Sanes and Masland, 2015), but this is controversial and is still debated (VanderWall et al., 2020).

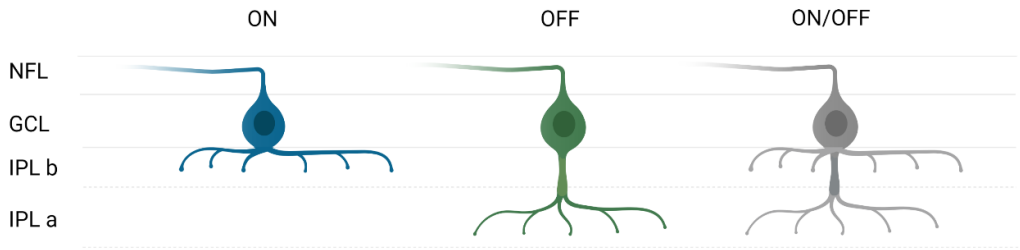

Figure 1. 3. RGC classification based on dendritic arborization depth in the IPL.

Although the variation in RGC dendritic configuration would suggest a random distribution of cell types (Fig. 1.2), RGCs dendritic trees are organised so that each type tiles with cells of the same class to cover the retina. This process is part of RGCs development and their spatial distribution become stable once they mature (Parrish et al., 2007, Koleske, 2013, Jan and Jan, 2010, Lin et al., 2020). The way in which RGCs spread their dendrites is defined by the relation with their neighbouring cell (Wässle et al., 1981). The tiling can be space filling and slightly overlapping or space filling and self avoiding, all as a function of the distance with the adjacent cells in order to ensure the best coverage (Fig. 1.4 a-d) (Reese and Keeley, 2015).

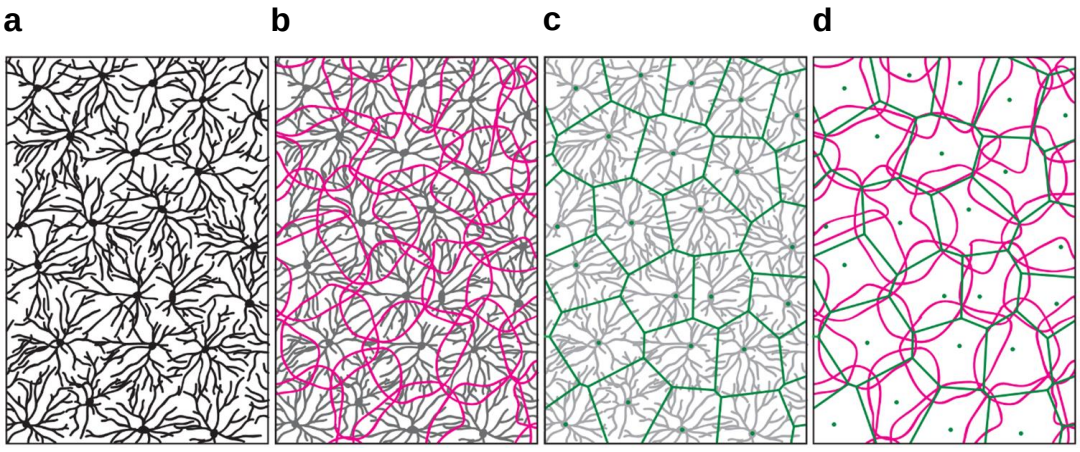

Figure 1. 4. Principle of retinal mosaic. a) Example of dendritic tiling; b) space filling and overlapping tiling; c) space filling and self avoiding tiling; d) graphical representation of dendritic field coverage modulated by a combination of b) and c). From (Reese and Keeley, 2015)

1.2.2 Energy metabolism

RGCs possess an active metabolism which renders them vulnerable to energy insufficiency. In addition to that, their compartmentalised structure into dendrites, soma and axon, with different functions and locations along the retinal layers, makes these neurons energetically more complex. The variation in energy requirements within a cell is reflected by the uneven mitochondrial distribution which reflects the energy demand of each component (Liu and Prokosch, 2021).

1.2.2.1 Dendrites

RGC dendrites, located in the IPL, are the site where input signals are collected and integrated before an action potential can be initiated at the axon hillock (Yu et al., 2013). This process imposes a high energy demand on the RGC and makes them as major consumers of ATP (Casson et al., 2021). Although the IPL has a low oxygen tension, the oxygen consumption rate is very high because RGCs dendrites rely almost exclusively on oxidative phosphorylation (OXPHOS) for the generation of ATP (Chidlow et al., 2019). However, when oxygen supply is very limited ATP can be also generated via anaerobic glycolysis (Viegas and Neuhauss, 2021).

1.2.2.2 Soma

RGC somas sit in the GCL and are the place where all RGC organelles, including mitochondria, are synthesised (Yu et al., 2013). In contrast to dendrites, RGC somas have a relative low oxygen consumption (Yu and Cringle, 2001), but this low oxidative profile may sound contradicting considering the large amount of mitochondrial proteins and histochemical evidence of cytochrome c oxidase activity (Yu et al., 2013, Casson et al., 2021). RGCs can use more than one substrate to fulfil their energy requirements. Although glucose is the preferred fuel source, pyruvate and lactate can be used as well. That strategic flexibility is what guarantees RGCs to remain viable under different condition, and preserves intact functions even in adverse circumstances. If that adaptability would not be possible that would have devastating effects on the entire cell (Munemasa and Kitaoka, 2012, Casson et al., 2021, Country, 2017).

1.2.2.3 Axons

RGCs axons connect the eye to the brain and comprise 80% of an RGC by volume (Curcio and Allen, 1990). RGCs axons have a location-based myelin distribution which defines their energy requirements, with unmyelinated intraocular portion and myelinated fibres when they exit the

lamina cribrosa. The absence of myelin, and the consequent lack of saltatory conduction, places the axon confined in the intraocular portion (NFL and ONH) in high energetic need (Ito and Di Polo, 2017). Indeed, mitochondria density is higher in that portion in order to maintain a stable membrane potential (Neishabouri and Faisal, 2011). In contrast, when the axons exit the lamina cribrosa they become myelinated and competent of saltatory conduction, whose speed is a direct function of fibre diameter, myelin thickness, and internode distance (Cragg and Thomas, 1957, Brill et al., 1977, Waxman, 1980). This acquired "electrical efficiency" drastically reduces the energy demand, as the decreased cytochrome c oxidase levels have confirmed (Kageyama and Wong-Riley, 1984).

1.2.3 Vulnerability

RGCs as a result of their high energy requirements, lives on a metabolic knife edge. This metabolic challenge is aggravated by RGCs compartmentalised energy needs. In a physiological state, mitochondria can keep up with RGCs ATP requirements but, with aging and increased production of reactive oxidative species (ROS), RGCs become more vulnerable and prone to damage (Baltan et al., 2010). For this reason, moderate alterations to the cellular environment can degrade RGC viability. For example, the elevation of eye pressure (ocular hypertension, OHT) can compromise RGC health, even at low levels of elevation. OHT is one of the major risk factor for developing glaucoma (Smith, 1879, Coleman and Miglior, 2008), and the inducible glaucoma related factor in this project, therefore it will be extensively discussed throughout this dissertation.

1.3 Glaucoma

1.3.1 Aetiology

Glaucoma defines a group of optic neuropathies characterised by the progressive and selective loss of RGCs and their axons which ultimately leads to vision loss (Weinreb et al., 2014). Glaucoma remains the leading cause of irreversible blindness worldwide, estimated to affect around 80 million people, which is expected to increase to 111.8 million by 2040 (Tham et al., 2014). Glaucomatous optic neuropathies are generally associated with increased intraocular pressure (IOP), referred as OHT, where the IOP raises above the normal range 11 – 21 mmHg (Hollows and Graham, 1966). Glaucomatous damage can also progress in the absence of OHT, with IOP in the normal range, which in that case is referred as normal tension glaucoma (NTG) (Jonas et al., 2017). Besides NTG, glaucomas can be divided into two main categories which

modify the aqueous humor outflow pathway depending on the morphology of the anterior chamber angle, open angle glaucoma (OAG) and angle closure glaucoma (ACG). In OAG aqueous outflow is reduced due to and increase in resistance at the level of the trabecular meshwork. In contrast, in ACG the drainage pathway at the iridocorneal angle is blocked by the peripheral iris preventing aqueous outflow (Weinreb et al., 2014). Glaucomas are also classified as primary, secondary or congenital depending on the triggering cause.

1.3.2 Mechanisms of RGCs degeneration

RGC degeneration is central to all forms of glaucoma. Detrimental changes to these cells lead to visual field loss, NFL thinning (axon loss), usually expressed as an increased disc:cup ratio, which are the characteristic clinical features to define the pathology (Quigley, 2011). It has been well established that prior apoptosis RGCs undergo through a period of intense remodelling which tremendously affects RGC dendrites, soma volume and axon diameter (Morgan, 2012, Weber et al., 1998, Morgan et al., 2006, Morgan, 2002). However, the underlying causes that contribute to progressive RGCs degeneration and ultimately lead to cell death have not been completely clarified yet. Mitochondrial dysfunctions, oxidative stress, inflammation, neurotrophic factors deprivation along with bioenergetic insufficiency have been proposed as contributing factors, showing similarities with other age related neurodegenerative diseases (Chan et al., 2021). In line with this assumption, multiple studies have been carried out to understand these processes (discussed in the upcoming sections), which aim to improve our understanding of the pathology that will hopefully define new therapeutic strategies.

1.3.2.1 Mitochondrial dysfunctions and oxidative stress

Mitochondria are central to RGC function and survival. These organelles are the principal source of cellular ATP through oxidative phosphorylation (OXPHOS) and key players in the apoptosis pathway (Kroemer et al., 1998, Green and Reed, 1998, Kong et al., 2009), two main biological events that influence RGCs fate. With aging mitochondria ATP production rate decreases, and considering the late age onset of glaucoma and RGCs energy requirement this “energy crisis” has been shown to negatively impact RGCs functions (Tribble et al., 2021c, Almasieh et al., 2012). However, functional perturbation of mitochondria homeostasis is also highly dependent on mitochondrial dynamics – fusion/fission, mitophagy and biogenesis (Ju et al., 2022). Optic Atrophy Type 1 (OPA1) and dynamin-related protein 1 (DRP1) – both members of the dynamin-related GTPases family – respectively regulate mitochondria fusion and fission. Indeed, mutations of those genes have been associated with optic neuropathies which both lead to RGCs

death (Liao et al., 2017, Williams et al., 2010, Kim et al., 2015). Mitophagy and mitochondrial biogenesis, which complete the dynamic life cycle of mitochondria, together define what is commonly called mitochondrial turnover, ensuring that damaged mitochondria are degraded and replaced to maintain mitochondrial homeostasis. However, the molecular machinery that controls these processes is extremely complex, and with the detrimental effect of age the chances to accumulate mutations in the genes that control these mechanisms increase (*e.g.* PINK1, Parkin – mitophagy; PGC-1α, AMPK – mitochondrial biogenesis) (Muench et al., 2021, Ma et al., 2020, Jornayvaz and Shulman, 2010).

While mitochondria are regarded as the "powerhouse", the downside of their support is the generation of reactive oxygen species (ROS). ROS production in excess of a cell's antioxidant capacity generates oxidative stress. Surprisingly, mitochondrial DNA (mtDNA) it is very vulnerable to ROS damage. The effect of this damage is significant since mtDNA codes for the 13 proteins which comprise the enzymatic complexes of the ETC (Anderson et al., 1981)(with the exception of complex II which is encoded by nuclear DNA (nDNA)). Both mitochondrial respiration and mtDNA are located in the mitochondrial matrix and collocate with the site of ROS generation (Nissanka and Moraes, 2018). mtDNA, by contrast with nuclear DNA, is not protected by chromatin packing; it exists as circular genome which is vulnerable to oxidative damage (Nass and Nass, 1963). In non-pathological conditions, this cycle of damage is moderated by mitochondrial quality control mechanisms, which are Parkin-independent (*e.g.* BNIP3, NIX), and promote the autophagic clearance of damaged mitochondria, especially when the damage is due to ROS accumulation (Ni et al., 2015, Pickles et al., 2018). In both OHT and NT glaucoma, cellular senescence and mechanical stress at the level of the ONH contribute to oxidative stress and perturbation of mitochondrial dynamics (Lee et al., 2011). As a consequence, damaged mitochondrial are not cleared, ROS production – mainly due to complex I and III deficits – increases, and ATP production drops, which all contribute to the opening of the mitochondrial transition pore with cytoplasmic cytochrome c release and the initiation of the intrinsic apoptotic pathway (Redza-Dutordoir and Averill-Bates, 2016, Elmore, 2007, Qu et al., 2010).

1.3.2.2 Inflammation

Whether or not RGCs degeneration is a direct or indirect consequence of age-related inflammation (Fulop et al., 2021, Franceschi et al., 2018, Fulop et al., 2017), acute or chronic neuroinflammatory processes are starting to be seen as key players in the glaucomatous

degenerative mechanisms (Mac Nair and Nickells, 2015). Functional and structural changes in retinal glial cells (astrocytes, Müller cells and microglia) have been identified in a range of glaucoma models and in human tissue samples (Melik Parsadaniantz et al., 2020). For instance, in the DBA/2J mouse model, a widely used model of congenital glaucoma of pigment dispersion age-related OHT, Müller glia activation was detected before clear signs of OHT and RGCs changes (Inman and Horner, 2007). Likewise could be said for astrocyte reactivity (Soto and Howell, 2014). However, the issue is not glial activation but the level of this activation and the interaction with the surrounding cells. Moderate activation plays a substantial role in maintaining RGCs and retina homeostasis, achieved by nerve growth factor and antioxidant release, and scavenging functions (Bringmann et al., 2009). By contrast, overactivation brings with it the release of several detrimental effectors as tumour necrosis factor alpha (TNFα), interleukin-1 (IL-1) and RGCs activation of cell death receptors (Melik Parsadaniantz et al., 2020). As well as Müller glia, microglia has been found activated in both human and animal model of glaucoma, but if this activation is protective or detrimental is still unclear (Williams et al., 2017d, Vecino et al., 2016).

Microglia, in both the developing and mature CNS and retina, maintains normal cellular homeostasis by clearing cellular debris from the GCL and INL (Bodeutsch and Thanos, 2000). In normal conditions, quiescent microglia releases several anti-inflammatory and neurotrophic factors as tumour necrosis factor beta (TNFβ), brain derived neurotrophic factor (BDNF), glial cell-line derived neurotrophic factor (GDNF), and ciliary neurotrophic factor (CNTF) which promote and regulate RGC survival (Langmann, 2007, Tezel, 2021). Resident microglia senses changes that can potentially damage RGCs, like oxidative stress, and as a consequence, proliferates and moves to the potential site of injury. Although this “inflammatory” response can be beneficial, if the toxic cellular environment is not normalised, persistent microglia activation can exacerbate RGCs neurodegenerative process (Rashid et al., 2019). The analysis of microglia from patients with glaucoma have shown the expression of several toll like receptors (TLRs; TLR2, TLR4 and TLR7) which activate innate immunity, along with TNFα and IL-6 which promote inflammation and lead to RGCs apoptosis (Ramirez et al., 2017).

1.3.2.3 Neurotrophic support deprivation

The contextualisation of the factors that damage RGC structure rests on the appreciation that the axon comprises 80% of an RGC by volume. Axonal transport deficits, especially retrograde transport, are one of the characteristics of glaucomatous pathology, which purportedly lead to neurotrophic factors deprivation (Claes et al., 2019). Whether or not this is one of the triggering

mechanisms, the purpose of neurotrophic factors is to sustain and promote neuronal survival in stressful circumstances (*e.g*. aging, disease, OHT insults).

It is important to understand that neurotrophic support plays different roles depending on the stage of neuronal development. In development, the withdrawal of neurotrophic support will results in the rapid onset of apoptosis; surgical removal of SC and dLGN in newly born rodents, the recipient brain areas for RGC afferents, results in a severe loss of RGCs (Harvey and Robertson, 1992). By contrast, when the same ablation is performed during adulthood, the loss of RGCs it is delayed, appearing months after the initial lesion, consistent with the prolonged time-frame of RGCs degeneration in glaucoma (Pearson and Thompson, 1993). One factor which may account for this delayed degeneration is that the release of neurotrophic factors, such as BDNF from RGCs, increases immediately after damage and could temporarily compensate for the lack of retrograde support (Almasieh et al., 2012).

RGCs possess receptors for nerve growth factor (NGF), BDNF, neurotrophin-3 (NT-3) and neurotrophin-4/5 (NT-4/5) as for CNTF and GDNF (Almasieh et al., 2012, Claes et al., 2019), and interestingly treatment with NGF and BDNF have shown to increase RGCs survival rate (Weber et al., 2010, Binley et al., 2016, Lambiase et al., 2009). The role of these factors in the protection of retinal ganglion cells is complex. For example, the experimental overexpression of CNTF, normally secreted by Müller glia, has been shown to be more effective on axonal injury repair rather than RGC distal projections in the inner retina (Leaver et al., 2006). Although retinal cells can provide a certain amount of neurotrophins, these compartmentalised effects may suggest that retinal secreted neurotrophic molecules can only provide a temporary neuroprotection which with protracted degenerative insults fail due to death of the secreting cells. However, with axonal transport deficits, “neurotrophic fuel” from the brain stem cannot reach the insulted area, thus RGCs progress to cell death.

1.3.3 Current therapeutic strategies and possible therapeutic approaches

Although advances in understanding the pathophysiology of glaucoma have clearly defined that it is a multifactorial condition, to date available treatments only target IOP. Clinical therapies for glaucoma management include topical medications and surgical procedures. Non invasive strategies as IOP lowering eye drops (*i.e.* prostaglandin analogues, β-blockers, carbonic anhydrase inhibitors, adrenergic agonists, cholinergic agonists), act by either reducing the outflow resistance or decreasing the aqueous formation, and even among normotensive patients seem to delay the disease progression (Cvenkel and Kolko, 2020, Hoyng and Kitazawa,

2002). When these first line of treatments fail, more invasive procedures such as laser trabeculoplasty, trabeculectomy, and drainage implants are required to limit the progression to complete visual loss (Conlon et al., 2017, Marquis and Whitson, 2005). However, when the disease diagnosis is confirmed around 30% to 50% of RGCs have already been lost. Therefore even if the available treatment can slow down the disease progression, none can neither halt, reverse or prevent the underlying disease mechanisms (Weinreb et al., 2014).

The lack of comprehensive treatments with the burden of an aging population has supported the search for treatments that act independently of treatments to reduce IOP. The new translational approaches aim to tackle the disease from a neuroprotective perspective in which they reduce RGCs death by interfering with the triggering mechanisms at the level of dendrite, soma and axon (Naik et al., 2020). In this context, a number of recent studies have identified nicotinamide adenine dinucleotide (NAD) as a very promising molecule for the protection of RGCs integrity and viability. NAD based treatments target the preservation of mitochondrial function and axonal transport (Williams et al., 2017b). Due to these characteristics, ongoing clinical trials are already testing NAD precursors, alone or in combination with IOP lowering drugs, to verify the feasibility as neuroprotective agent of this molecule (Hui et al., 2020, De Moraes et al., 2022, NCT05275738, 2022, NCT05405868, 2022). Although nicotinamide has already reached the human experimental phase, a deeper insight into this molecule's function and effect is required to understand the wide spectrum of action against RGC degeneration.

1.4 Nicotinamide adenine dinucleotide

Nicotinamide (NAD^+) was first described in 1906 as product of yeast fermentation (Harden et al., 1906a, Harden et al., 1906b). Then, in 1937 when Joseph Goldberg identified deficiency in vitamin B, the common name of nicotinic acid and a precursor of NAD^+, as the cause of pellagra the importance of NAD^+ metabolism in health and disease emerged (Morabia, 2008). Besides a severe epidermic photosensitivity, pellagra is also characterised by extended CNS deficits (Brown, 2010, Hegyi et al., 2004), which have risen a growing interest around the link between NAD^+ and CNS functions and aging.

To understand this link and the potential relationship between NAD^+ and RGCs neuroprotection, in the next paragraphs we will address in details NAD^+ metabolism and its biological functions.

1.4.1 NAD^+ metabolism

NAD^+ is an important cofactor in vital reactions which regulate the mammalian physiology, and being a major component in both bioenergetic and signalling pathways its homeostatic levels are kept under control with a highly regulated balance between biosynthesis and consumption.

1.4.1.1 NAD^+ biosynthesis

NAD^+ biosynthesis has three major routes (Fig 1.5 a): the *de novo* or kynurenine biosynthetic pathway (from tryptophan (trp)), the Preiss-Handler pathway (from nicotinic acid (NA)), and the salvage pathway (from nicotinamide adenine mononucleotide (NAM) or nicotinamide riboside (NR) outside the CNS (Fletcher et al., 2017))(Yang and Sauve, 2016). The *de novo* NAD^+ biosynthesis begins with the essential amino acid trp which is enzymatically degraded into kynurenine, after with eight further enzymatic reactions result in NAD^+ (Castro-Portuguez and Sutphin, 2020). The Preiss-Handler is a three step NAD^+ biosynthesis pathway which starts with the phosphoribosylation of NA and culminates with the amidation of nicotinic acid adenine dinucleotide into NAD^+ (Preiss and Handler, 1958a, Preiss and Handler, 1958b). Although those two pathways may seem sufficient to guarantee enough NAD^+ bioavailability, 80% of cellular NAD^+ comes from the salvage pathway. This pathway maintains NAD^+ homeostasis through the action of nicotinamide phosphoribosyl transferase (NAMPT), which converts NAM into nicotinamide mononucleotide (NMN), and nicotinamide mononucleotide adenylyl transferase (NMNATs) which aminates NMN into NAD^+. When the NAD^+ precursor is NR, the latter is firstly converted to NMN by nicotinamide riboside kinase 1 and 2 (NRK 1, NRK2) and then by NMNATs in NAD^+ (Cimaglia et al., 2020, Canto et al., 2015). The rate limiting step in NAD^+ biosynthesis is the one catalysed by NMNAT isoforms (NMNAT1, NMNAT2 and NMNAT3). These have different cellular localisations, which have differential effects on the cellular bioenergetic depending on the paralogue involved in NAD^+ biosynthesis (Felicitas Berger, 2005). NMNAT1 and NMNAT3 are ubiquitously expressed, but in the mammalian system NMNAT1 is predominantly nuclear while NMNAT3 is mitochondrial. NMNAT2 is confined to the neurons, where localises to the Golgi and the cytosolic compartments (Covarrubias et al., 2020). Moreover, NMNAT2 plays a fundamental role in axon development and survival (Gilley and Coleman, 2010, Gilley et al., 2018) and its depletion has been associated with Wallerian degeneration (Funakoshi and Araki, 2021, Loreto et al., 2019).

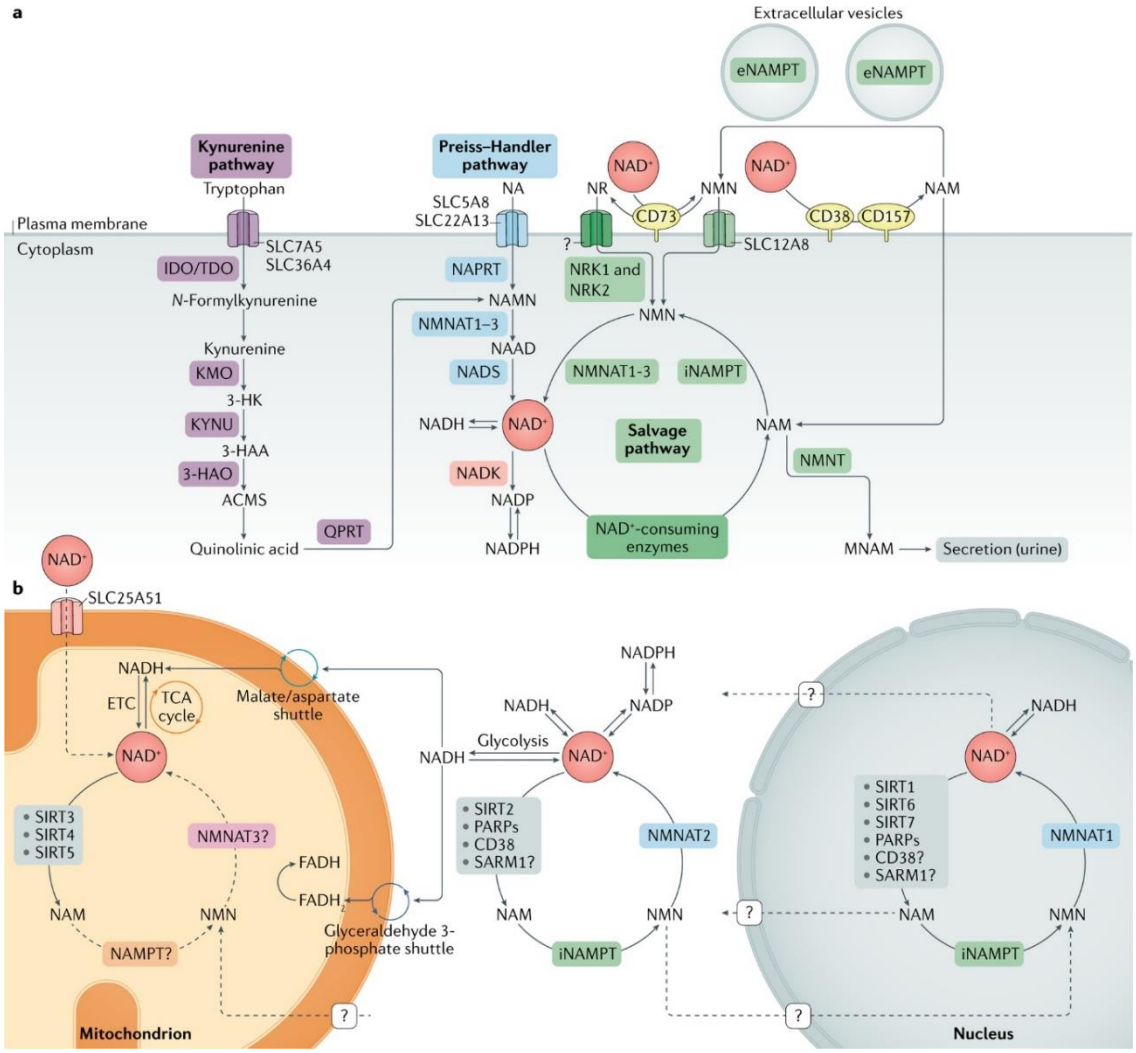

Figure 1. 5. NAD⁺ biosynthesis and metabolism. a) NAD⁺ biosynthetic pathways. NAD⁺ is biosynthesised by three main routes: the kynurenine or *de novo* pathway from tryptophan, the Preiss-Handler pathway from nicotinic acid, and the salvage pathway. b) NAD ⁺metabolism in different subcellular compartments. Mitochondrial, cytoplasmic and nuclear NAD⁺ metabolism is regulated by subcellular NAD⁺ consuming enzymes and redox reactions. From (Covarrubias et al., 2020)

1.4.1.2 NAD⁺ consumption

The impact of NAD⁺ to mammalian physiology is given by the end-use of this molecule through different pathways. This can either be to generate energy or as "signalling executive" that defines cell fate.

1.4.1.2.1 NAD⁺ in energy metabolism

Cytosolic and mitochondrial NAD⁺ pools contribute to the maintenance of normal energy levels *via* glycolytic and tricarboxylic acid (TCA) metabolic pathways (Fig. 1.5 b). In the cytoplasm, two

molecules of NAD^+ are required to convert glucose into pyruvate, which provide a net of two NADH molecules (reduced form of NAD^+) that are then transported into the mitochondria either with the malate-aspartate shuttle or the glyceraldehyde-3-phosphate shuttle. In the mitochondria, NADH from the glycolysis and the TCA cycle is passed to the ETC and oxidised by complex I. The two electrons (e^-) gained by this transformation conveys to complex II, complex III, cytochrome c and complex IV. This flux of electrons along the complexes, generated from NADH, creates a proton gradient which then enables the F_0F_1-ATP synthase (complex V), generating ATP while pumping the protons back into the mitochondrial matrix (Xie et al., 2020, Canto et al., 2015).

It is important to note that the use of NAD^+ to maintain cellular energy homeostasis results in a net expenditure of NAD^+ for the production of ATP.

1.4.1.2.2 NAD^+-dependent signalling pathways

NAD^+ is the substrate of key signalling pathways that modulate neuronal development, neuroprotection, cell senescence, mitochondrial homeostasis, inflammation and even DNA repair (Katsyuba and Auwerx, 2018, Katsyuba et al., 2020). The molecules that are capable to execute all these functions are: sirtuins (SIRTs), poly ADP-ribose polymerases (PARPs), cluster of differentiation 38 (CD38), also known as cyclic ADP ribose hydrolase, and sterile alpha and toll/interleukin-1 receptor [TIR] motif containing 1 (SARM1). These four classes of enzymes are important in maintaining NAD^+ since NAM which is generated as a by-product of their reactions is then reconverted in NAD^+ through the salvage pathway.

Situins

Sirtuins are a family of seven (SIRT1-SIRT7) NAD^+ consuming enzymes with different subcellular localisation (SIRT1 nucleus and cytosol, SIRT2 only cytosol, SIRT3 and SIRT4 mitochondrial specific, SIRT5 mitochondria and cytosol, SIRT6 nucleus and SIRT7 nucleolus). Nuclear SIRT1 and SIRT6 seem to regulate genome stability and life span (interacting with p53 apoptotic pathway), while mitochondrial SIRT3 and SIRT4 can prevent cell death maintaining NAD^+ mitochondria pools following stress responses (Finkel et al., 2009). Another key role of sirtuins activity has been discovered following experimental caloric restriction, where SIRT1 and SIRT3 promoted mitochondrial turnover and mitophagy (Lombard et al., 2011). In the CNS, SIRT1 is involved in neurite and axon development, and modulates dendritic arborisation (Gao et al., 2010).

PARPs

The PARPs family comprises seventeen proteins, 3 of which (PARP1, PARP2 and PARP3), have been characterised with respect to the NAD^+-dependent role (Lautrup et al., 2019, Covarrubias et al., 2020). PARPs consume NAD^+ to initiate the signalling cascade that culminates in DNA repair (Javle and Curtin, 2011). NAD^+-PARPs mediated DNA repair is one of the main NAD^+-consuming mechanism in aging, and it has been shown to really compromise NAD^+ homeostasis. As a consequence, PARPs overactivation during aging has been shown to promote NAD^+-dependent neuronal loss and to be the root of several neurodegenerative diseases (Fang et al., 2016).

CD38

CD38 is a transmembrane glycoprotein which has both receptor and enzyme mediated functions (Malavasi et al., 2008). Its enzyme functions are all NAD^+ mediated and are particularly relevant to the brain physiology, since CD38 is predominantly expressed in neurons, astrocytes and microglia (Yamada et al., 1997). The importance of CD38 as one of the NAD^+ consuming enzymes came from aging and inflammation studies where CD38 knockout mice demonstrated less age-related brain ischemic damage and mitochondrial dysfunction (Camacho-Pereira et al., 2016, Guerreiro et al., 2020). It has been hypothesised that NAD^+-age dependent decline, especially in pathological conditions may be due to CD38 overactivation (Li and Wu, 2021). However, further studies are needed to completely clarify the NAD^+-dependent activity of this enzyme.

SARM1

The link between SARM1 activity and NAD^+ levels was revealed in studies of Wallerian axonal degeneration (Waller, 1850). SARM1 is a multidomain protein with a N-terminal autoinhibitory Armadillo/HEAT motif (ARM) domain followed by a C-terminal catalytic TIR domain (Chuang and Bargmann, 2005). SARM1 has a NAD^+ hydrolase function (Osterloh et al., 2012), which is confined to the TIR domain which determines the active state of the protein. SARM1 activity is regulated downstream by NMNAT2, which catalyses the conversion of NMN into NAD^+ (Bratkowski et al., 2020). Since SARM1 is active in pathological settings, especially in the absence of axonal NMNAT2, it has been suggested that low rates of NAD^+ synthesis rather than the absolute NAD^+ level *per se* trigger SARM1 activation (Figley and DiAntonio, 2020, Figley et al., 2021). Indeed, the by-products of SARM1 NAD^+-hydrolase activity are NAM and ADP-ribose (ADPR) and cyclic ADPR (cADPR), with the latter found only in degenerating axons (Sasaki et al.,

2020). It has therefore been suggested that SARM1 can be regarded as a NAD^+ sensor, activated by low NMN:NAD ratios (Jiang et al., 2020).

1.4.2 NAD^+ in brain aging and neurodegenerative diseases

There is a substantial evidence that NAD^+ declines with age in vertebrates and invertebrates (Fang et al., 2014, Mills et al., 2016, Stein and Imai, 2014). Whether this reflects decreased biosynthesis or increased consumption is still unclear (McReynolds et al., 2020, McReynolds et al., 2021). However, all experimental conditions that have attempted to increase life or health span of an organism (*e.g*. by calorie restriction, exercise, glucose deprivation) have reported conditional increases in NAD^+, while the opposite was found in aging and senescence studies (Verdin, 2015). This physiological link has been further clarified by evidence that decline in NAD^+ is highly involved in governing the ten hallmarks of brain aging (*i.e.* mitochondrial dysfunction, oxidative damage, impaired waste disposal, compromised stress response, inflammation, impaired neurogenesis, telomerase activity, disrupted DNA repair, dysfunctional neuronal network and calcium dysregulation) (Fang et al., 2017, Lautrup et al., 2019). NAD^+ bioavailability is significantly reduced by NAD^+ catabolic pathways increased activity during aging. That pathological vicious cycle leads an aberrant disease state where NAD^+ insufficiency severely compromise cellular health and homeostasis.

Age related neurodegenerative diseases (NDs) such as Alzheimer's disease (AD), Parkinson's disease (PD), amyotrophic lateral sclerosis (ALS) and glaucoma are accompanied by decreased NAD^+ levels (Hikosaka et al., 2021, Cunnane et al., 2020, Blaszczyk, 2020). Experimental evidences have shown that NAD^+ metabolic manipulation, either by silencing NAD^+-dependent enzymes expression or by dietary enrichment with NAD^+ precursors, can improve neuronal functions by restoring mitochondrial functions, inflammatory responses and ROS defensive strategies (Strømland et al., 2021, Campbell, 2022).

The cross cutting role of NAD+ in a range of pathways, especially in regards of mitochondrial functions, has come from the Deletor mouse which carries a mtDNA replicative helicase mutation (Khan et al., 2014), and has been studied as a model of mitochondrial myopathy. Daily oral administration of NR to these mice was sufficient to restore mitochondrial turnover, and to prevent mtDNA deletion. In addition to that, Khan *et al.* reported that mitochondrial integrity was maintained by an enhanced mitochondrial unfolded protein response (UPR^{mt}), which promotes cell survival, mitochondrial recovery and biogenesis (Shpilka and Haynes, 2018, van de Ven et al., 2017). NAD^+ can also act as a very powerful anti-inflammatory molecule. This effect

appears to be achieved through PARP1 and SIRT1 mutual conditioning (Chung and Joe, 2014). PARP-1 promotes inflammatory responses by positively regulating the pro-inflammatory NF-kB transcription factors, that on the contrary can be suppressed by SIRT1 activation (Kauppinen et al., 2013, Pazzaglia and Pioli, 2019). Thus, impaired NAD^+ homeostasis induces a cascade of detrimental effects which can compromise cellular viability.

1.4.3 NAD^+ and retinal diseases

The retina is one of the most energy consuming tissues. NAD^+-related impairments have been described in many retinal pathologies (Jadeja et al., 2020). Leber congenital amaurosis 9 (LCA9) was one of the first to link pathology with impaired energy maintenance. LCA9 is caused by a mutations in *NMNAT1* which results in complete vision loss (Sasaki et al., 2015, Falk et al., 2012). Impaired NAD^+ metabolism has been also associated with accelerated loss of rods and cones (Lin et al., 2016). RPE cells are also critically dependent on NAD^+ for their metabolic support. The restoration of NAD^+ homeostasis in mouse models of AMD reduced light induced RPE damage arising from ROS and inflammation (Bai and Sheline, 2013, Sheline et al., 2010, Fisher and Ferrington, 2018, Zhu et al., 2016, Bergen, 2017).

1.4.3.1 NAD^+ and glaucoma

The view that NAD^+-related optic nerve damage may be an important component in glaucoma arose from Williams *et al.*'s report that retinal NAD^+ declined with age in the DBA/2J mouse model of glaucoma (Williams et al., 2017b). RNA sequencing of RGCs at different time points (pre OHT, 4months old; early glaucoma (OHT without neuronal damage), 9 months old) indicated abnormalities in mitochondrial functions that increased with age. These observations emphasised the importance of mitochondrial degeneration in RGC loss in glaucoma. A metabolic analysis of DBA/2J/control matched for age up to 12 months indicated a progressive decline of NAD^+ / NAD^+-related metabolites, and scavenger species such as oxidised and reduced glutathione (Williams et al., 2017b). Although RGCs can meet their energy requirements by switching to β-fatty acid oxidation this only aggravated the oxidative state of the cell and increased the risk of DNA damage. Collectively these changes caused NAD^+ depletion which impaired RGCs homeostasis, increasing the risk of apoptosis cell death. Critically, NAM administration in DBA/2J significantly reduced ON degeneration (further confirmed in (Williams et al., 2018)), prevented RGCs loss and NFL thinning, and preserved visual functions as assessed by pattern electroretinogram – PERG), all hallmarks features of glaucomatous damage. NAM treatment normalised also PARP1 activity, indication that the restoration of NAD^+ metabolism

could effectively protect against DBA/2J optic nerve degeneration. Williams *et al.* also demonstrated that *Nmnat1* gene therapy either alone or in combination with NAM conferred significant RGC protection (and the preservation of RGC axons) in the DBA2J model. *Nmnat1* is of interest because of its role in slow Wallerian degeneration mutation (*Wld*^{s}), an in-frame fusion of the N-terminal E4 ubiquitin ligase Ube4b that incorporates full length *Nmnt1* and delays axon degeneration (Conforti et al., 2007).

Further support for the importance of NAD in RGC metabolism has come from human studies. Reynier *et al.* analysed plasma from POAG patients to determine the relationship between systemic NAD^+ levels and glaucomatous damage. Although the study is small (54 patients) they demonstrated a negative correlation between systemic NAD+ levels and glaucoma damage, consistent with observations in the mouse (Kouassi Nzoughet et al., 2019). Clinical studies of NAD^+ supplementation in glaucoma patients suggests a role for the remediation of NAD deficits as a treatment for glaucoma. Hui *et al.* demonstrated that NAM supplementation (1.5g day for 6 weeks plus 3g day for other 6 weeks) improved visual function in 23% of the patients (Hui et al., 2020). A number of studies have since been registered to evaluate the effect of NAM treatments in larger patients cohorts (NCT05275738, SW – NAM; NCT05405868, UK – NAM; NCT05695027, US – NAM + pyruvate; NCT03797469, US – Vit B3). While the proliferation of clinical studies is encouraging it is unclear if the appropriate therapeutic levels of NAM are being targeted or indeed will be achieved. To date the functional benefits are marginal and have only been reported in small studies. Further work is needed to determine the appropriate dose of NAM to achieve the greatest preservation of RGC structure and function. Without definitive data on the best dose levels, clinical studies that report marginal benefits risk the termination of work on NAM therapies that might, at the correct dose be very effective.

1.4.4 NAD^+ precursor and safety

While NAD^+-mediated neuroprotection can only be achieved through NAD^+-precursor supplementation, selection of the best precursor of choice can be challenging. NA, NR or NAM will each increase NAD^+ levels (Martens et al., 2018, Khan et al., 2014, Mehmel et al., 2020, Bogan and Brenner, 2008, Braidy et al., 2019), but their effects on NAD^+ levels need to be considered with respect to the desired treatment target since the distribution of NAD^+ synthesising enzymes varies considerably between tissues. For the conversion to NAD^+, NA must first be converted by nicotinic acid phosphoribosyl transferase (NAPRT) into nicotinic acid mononucleotide (NaMN), and then by NMNATs (that can recognise both NMN and NaMN as

substrates (Rongvaux et al., 2003)) into NAD^+. Since NAPRT is predominantly expressed in the liver, kidney and intestine but in the brain (Bogan and Brenner, 2008, Mori et al., 2014), NA is a poor candidate for the treatment of neurodegeneration. Indeed, the very high doses needed to reach therapeutically useful levels of NAD^+ for CNS treatment incurred side effects that adversely affected drug compliance (Knip et al., 2000).

The use of NR is also influenced by the target organ of interest (Fletcher et al., 2017, Ratajczak et al., 2016). NR is one of the precursors in the NAD^+ salvage pathway that do not necessarily need to be converted to NAM to form NMN, since this can occur in a NRK- dependent pathway in which is converted to NAM by purine nucleoside phosphorylase. NRK has two isoforms, NRK 1 and NRK2. NRK1 is ubiquitously expressed while NRK2 is mainly expressed in the liver, skeletal muscle and heart (Katsyuba and Auwerx, 2018). The utility of NR for the treatment of neurodegeneration has been questioned following experimental studies using this precursor which failed to demonstrated any meaningful benefits (Brakedal et al., 2022, Mehmel et al., 2020). Even so, *in vitro* and invertebrate studies have reported some benefits with NR (Schondorf et al., 2018, Veenhuis et al., 2021), suggesting that CNS effects might be species or phenotype-specific (*e.g.* NRK1 or NRK2 are only minimally expressed in RGCs (Williams et al., 2017c)).

By contrast, NAMPT, the first enzyme of the NAM salvage pathway, is neuron specific (Zhang et al., 2010, Lundt and Ding, 2021), and can provide a sustained increase in neuronal NAD^+ levels. NAM is also the major *in vivo* NAD^+ precursor in mammals and a physiological inhibitor of NAD^+ catabolic enzymes (Magni et al., 2008, Magni et al., 2009).

While these considerations suggest that NAM would be the most appropriate choice for the protection of CNS neurons such as RGCs, they do not address the safety of long term NAM consumption. A large body of toxicology and therapeutic studies suggest that NAM consumption is clinically safe. The UK expert group on vitamins and minerals (EVM) and the European commission scientific committee on food (EU SCF) have set guidance values for vitamin B_3 supplementation from 500mg to 900mg a day for a healthy adult population (Poljsak and Milisav, 2018). However, there has been some confusions over the terminology used to describe vitamin B_3 supplementation. Both niacin, the common name for nicotinic acid, and NAM are considered under the umbrella of vitamin B_3. However, when vitamin B_3 has been introduced to the market as healthy supplement the molecule branded as B_3 was nicotinic acid, therefore the

guidance values were based upon NA and not on NAM, which is the active form of NA and chemically different from the latter (Fig. 1.6).

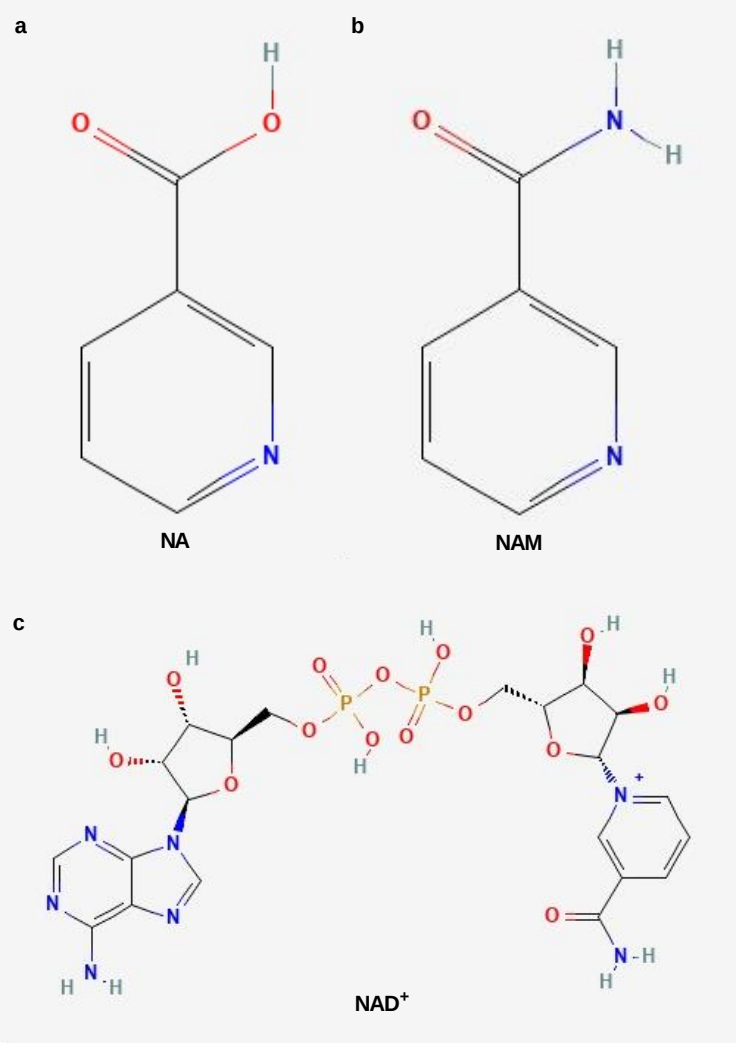

Figure 1. 6. Chemical structure of NA, NAM and NAD$^+$. Modified from PubChem.

Toxicology studies have determined NAM LD_{50} (lethal dose in 50% of the test animal) at 2.5 g/kg (oral administration) and 2.05 g/kg (intraperitoneal injections), that would equate in humans at a daily dose 150g and 120g respectively (Hwang and Song, 2020). Clinical studies have reported minimal adverse effects (*e.g.* headache and dizziness) at doses over 18 g a day; these doses are considerably higher than the 3 g/day suggested for CNS treatment (Hwang and Song, 2020). Therefore, it can be concluded that NAM administration is safe and can be used in long term therapies. The only adjustment that can be conceived to improved patients compliance in case of high doses is to design a sustained release NAM supplement, since the available formulation

contain max 500 mg/tablet, and a hypothetical dose of 9 g/day would require 18 tablets which would not be taken regularly by any patient.

1.5 Experimental models of glaucoma

Animal models, even if they cannot replicate each pathological aspect, offer a valid method to mirror some of the damage seen in humans and potentially uncover the underlying molecular mechanism. A single animal model will never be able to reproduce all the aspect of this multifactorial neurodegenerative disease, but with knowledge of each model strength and limitation, they can help to gain new insight into the condition and support the development of new therapeutic strategies.

Many species have been used for the development of experimental models of glaucoma, such as primates, cats, dogs, pig, rabbits and rodents. Of these, rodents have retained their popularity as experimental animal due to the relatively similar human physiological aspects, eye structure, and the multiple techniques available for genetic manipulation (Johnson and Tomarev, 2010). Broadly, the available experimental models can be grouped in two categories: non-hypertensive and hypertensive models.

1.5.1 Non-hypertensive models

1.5.1.1 Genetic models

Some genetic normotensive models have been proposed to recapitulate RGCs loss independent of the increase in IOP. The optineurin E50K overexpressing mice ($E50K^{tg}$) were developed based on the identifications of mutations in optineurin in a family with NT glaucoma (OPTN E50K). By the age of 16 months these mice have already lost 25% of RGCs. A major drawback of this model was the conspicuous loss of other retinal neurons along with ONL and INL thinning, which is not observed in glaucoma patients (Fernandes et al., 2015). However, when this mutation was inserted in a BAC transgenic mouse expressing human OPTN E50K (BAC-$hOPTN^{E50K}$), RGCs loss was similar to human NT glaucoma, with preservation of other retinal neurons (Fernandes et al., 2015).

Other models that recapitulate NT glaucoma RGCs loss have deficits in glutamate transporters GLAST or EAAC1 function. Although there are no hereditary studies that suggest any implication of genetic disfunction of glutamate regulation in human NT glaucoma, GLAST and EAAC1 deficient mice show different levels of RGCs degeneration (GLAST 50% RGCs loss by 8 months;

EAAC1 RGCs degeneration already at 8 weeks old), as well as ON cupping and axonal degeneration (Harada et al., 2007).

1.5.1.2 Optic nerve crush

Murine models of optic nerve crush (ONC) are a valuable tool to study RGCs progressive loss following traumatic injury to the ON. This is experimentally achieved with a surgical controlled, spatially discrete, compression (just for few seconds) of the optic nerve, that damages the axons without severing them and leads to axon-driven RGCs death (Tang et al., 2011). According to the mechanisms of compartmentalised RGCs degeneration, this method offers the opportunity to study the details of axonal transport failure and degeneration in a predictable way, even though does not reflect the clinical pathogenesis of glaucoma.

1.5.1.3 Retinal explants

Axotomised retinal explants, for the same principle of ONC without the need of sophisticated surgical skills, enable the study of progressive RGCs degeneration in a predictable way (Murali et al., 2019). Following ON transection, retinas can be removed immediately after death and cultured in a controlled environment for several days. While this model only shares the selective degeneration of RGCs with glaucoma, it is straightforward and allows preliminary therapeutic screening of neuroprotective agents (Pattamatta et al., 2016, Bull et al., 2011).

1.5.2 Hypertensive models

Since elevated IOP remains the principal clinical determinant of glaucoma, animal model of ocular hypertension have been used to provide an approximation of retinal and optic nerve changes in clinical glaucoma. Genetic and inducible OHT murine models are the most used in glaucoma research and by far are the one that have given the most useful insights to understand this pathology.

1.5.2.1 Genetic models

The DBA/2J mouse model is the most widely used genetic animal model of congenital ocular hypertension. These mice develop OHT by the age of 8 months, at 10 months significant optic nerve damage, and by 12 months severe glaucomatous damage, and most importantly their RGC loss is IOP dependent (Libby et al., 2005). Their IOP elevation is subsequent to a congenital iris disease (recessive mutation in glycosylated nonmetastatic melanoma protein b, *Gpnmb*, and

tyrosinase related protein 1, *Tyrp 1* (Anderson et al., 2002)) with pigment dispersion which deposits in the ocular drainage structures obstructing the outflow pathway. It is important to note that not all DBA/2J mice developed elevated IOP and glaucoma-like damage and that studies require large animal numbers to provide meaningful data. As a result the model is expensive since animals need to be maintained for 12 months for the generation of typical optic nerve damage.

The CYP1B1 deficient mice are modelled over a gene responsible for congenital glaucoma which encodes for cytochrome P450, family 1 , subfamily b, polypeptide 1. These mice develop abnormalities in their aqueous outflow pathway similar to the one observed in ACG (Ishikawa et al., 2015).

Then, there are two models available which tend to mimic OAG. One with a mutation on the alpha-1 subunit of collagen type 1, which leads to progressive RGCs loss induced by OHT without sever structural changes in the drainage pathway. And, the myocilin Tyr423His mutated mice that show severe glaucoma with RGCs and axon loss (Ishikawa et al., 2015).

1.5.2.2 Inducible models

Inducible models of OHT try to reproduce ACG with either acute or chronic and progressive IOP increase depending on the procedure.

1.5.2.2.1 Laser photocoagulation

Laser photocoagulation of the trabecular meshwork obstructs the outflow of the aqueous humor leading to IOP increase. When properly executed, this method can produce IOPs above 30 mmHg, but it requires fine equipment and high standard surgical skills which make it difficult to be perform in all research settings (Biswas and Wan, 2019).

1.5.2.2.2 Episcleral vein cauterisation

Episcleral vein cauterisation was reported in 1995 as a less invasive method to induce OHT compared to photocoagulation (Shareef et al., 1995). Episcleral veins are cauterised using handheld devices until is observed a large venous swelling, which creates a marked IOP increase due to increased outflow resistance. Although effective, this method produced a rapid elevation IOP that decreased a week after the procedure, therefore it is more appropriate for

experimental designs which focus on early mechanism of RGC degeneration (Biswas and Wan, 2019).

1.5.2.2.3 Hypertonic saline injection

Sclerosis of the episcleral veins by hypertonic saline injections it is probably one of the most accurate and precise model to induce chronic IOP elevation, and it is generally referred as the Morrison model (Morrison et al., 2008). Although extremely effective this procedure is technically challenging. The proper execution demands a delicate cannulation of the episcleral veins, that in mice and rats are almost invisibles. Unless this technique is performed by a very experienced surgeon it is not the most accessible option, despite having the highest OHT-induction rate among all the other animal models of glaucoma (Morgan and Tribble, 2015).

1.5.2.2.4 Microbead models

Another alternative method to reliably increase IOP is through the injection of microparticles, which accumulate in the trabecular meshwork and obstruct the outflow pathway. Microbead models of glaucoma have a long history of experimental application and through all these years many refinements have been made to the beads materials and injection technique in order to be tailored to the specific animal model and study (Claes et al., 2021, Ito et al., 2016, Morgan and Tribble, 2015, Sappington et al., 2010, Samsel et al., 2011). Several materials have been used to produce injectable microbeads, such as polyurethane, latex, polymethylmethacrylate as polystyrene, which are characterised by different specific material properties that suit the different study designs (Rho et al., 2014, Morgan and Tribble, 2015).

If the animal strain is appropriately chosen (Cone et al., 2012, Claes and Moons, 2022, Eastlake et al., 2021) and the injections correctly executed, this model can mimic a chronic model of glaucoma with moderate IOP elevation and give reliable readouts.

1.6 Hypothesis and Aim

Progressive RGCs dysfunction and atrophy is now accepted as a critical prelude to cell loss in glaucoma, and a phase that may present a therapeutic window for the prevention of RGC loss and their potential recovery (Morgan, 2012). The majority of studies to date have focussed on RGC loss rather than structural changes that can provide a very sensitive marker of pathological progression (Tribble et al., 2019).

Mitochondria have been shown to have a clear role in the mediation of the damaging effect of glaucoma (Tribble et al., 2021c), and it has been shown that increasing levels of NAM and genetic overexpression of *Nmnat1* can profoundly mitigate RGC degeneration (Williams et al., 2018, Williams et al., 2017b).

Considering the ongoing clinical trials, a comprehensive understanding of NAM efficacy is paramount. This study will focus on sensitive and early metabolic and structural RGC changes following the induction of unilateral ocular hypertension in rats (Tribble et al., 2021b), alone and in combination with NAM dietary enrichment, but also using gene therapy to overexpress *NMNAT2* (the human gene of the neuronal specific NAD^+ salvage pathway rate limiting enzyme).

In order to investigate the feasibility of NAM-mediated neuroprotective strategies in glaucoma the following issues will be addressed:

a) Safety and tolerance of NAM administration in wild type Brown Norway rats established in relation to Brown Norway baseline parameters (chapter 4).
b) Proof of concept of NAM-mediated RGCs neuroprotection in axotomised mice retinal explants (chapter 5).
c) NAM-mediated RGCs neuroprotection in unilateral hypertensive model of glaucoma following two therapeutic regimes: prophylactic and intervention (chapter 6).
d) Metabolic changes following NAM treatments (chapter 7).
e) Effect of *hNMNAT2* overexpression on RGCs neuroprotection (chapter 8).

2 Materials and methods

2.1 Animals

The use of animals in this study was approved by the Cardiff University Ethical Review Board, and all the experiments performed in accordance with the Home Office Animals Act 1986 (Scientific Procedures) under licences PLL PB89BF24D and PIL I73025511. All animals were housed at Cardiff University licensed facility on a 12-hour light/dark cycle (6 am – 6 pm), at a room temperature of 20-24° C, and humidity of 55%. All animals had access to food and water *ad libitum*.

2.1.1 Animal strains and husbandry

2.1.1.1 C57BL/6J mice

12 weeks old male C57BL/6J mice were purchased from Charles River Laboratories, housed 2-5 mice per cage, and habituated for one week before being used for experiments. All mice were used for retinal explants and were not exposed to any treatment of procedure prior their experimental use. All the animals were culled by cervical dislocation (schedule 1) and tissue sample (eyes) were collected upon death.

2.1.1.2 Brown Norway rats (BN/RijHsd)

Male Brown Norway rats were purchased in a UK licensed establishment (ENVIGO) at different ages in order to be ready for experimental purposes at 16 weeks old. They were pair housed in environmentally enriched cages, and habituated and handled for at least 2 weeks prior any procedure. All the rats were trained for unrestrained intraocular pressure measurements and had regular check-ups (*e.g.* weight, responsiveness to stimuli). To maintain the rats' wellbeing they were handled without any training or experimental purpose and had plenty of play time (*e.g.* rat friendly hard plastic balls). At the end of the experimental period the rats were culled by increasing CO_2 concentrations confirmed by cervical dislocation (schedule 1). Samples were collected upon death and either processed immediately afterwards (retinas) or stored at -80° C (optic nerves) until analysis.

According to the project design the rats were divided into different experimental groups (Table 2.1), each group had a specific diet to meet the experimental requirements (NAM enriched diet). To avoid any dietary confounder among the groups, the control groups during the experimental

period were switched to sugary water (H_2O plus commercial caster sugar) which was used to mask NAM bitterness in the treated groups.

Due to the precise timing of the experimental setting, and the age of the animals when they were purchased, the experimenter was not blind to any of the parameters for the grouping for the entire project.

Strain	Group	Procedure	Treatment	Treatment delivery	Treatment duration	End point	Diet[1]
BN	C.sham (NT control)	/	/	/	/		RM3 (P); SDS diet
BN	G.sham (unilateral glaucoma control)	Induction of OHT	/	/	/	4 w after OHT	RM3 (P); SDS diet
BN	C.LNAM (NT)	/	NAM low dose, 200 mg/day/kg	Normal drinking water	4 weeks	4 w after NAM	RM3 (P); SDS diet
BN	C.HNAM (NT)	/	NAM high dose, 600 mg/day/kg	Normal drinking water + food	4 weeks	4 w after NAM	RM3 (P) + 9380 ppm NAM (P) 25kGy; SDS diet
BN	G.LNAMproph (unilateral glaucoma)	Induction of OHT	NAM low dose prophylactic treatment, 200 mg/day/kg	Normal drinking water	6 weeks	4 w after OHT	RM3 (P); SDS diet
BN	G.HNAMproph (unilateral glaucoma)	Induction of OHT	NAM high dose prophylactic treatment, 600 mg/day/kg	Normal drinking water + food	6 weeks	4 w after OHT	RM3 (P) + 9380 ppm NAM (P) 25kGy

[1] Diet was customised by SDS for this project specific experimental purposes. NAM (Apollo Scientific ltd) was shipped to the manufacturer and irradiated in their RM3 (P) diet.

							; SDS diet
BN	G.LNAMint (unilateral glaucoma)	Induction of OHT	NAM low dose intervention treatment, 200 mg/day/kg	Normal drinking water	25 days	4 w after OHT	RM3 (P); SDS diet
BN	G.HNAMint (unilateral glaucoma)	Induction of OHT	NAM high dose intervention treatment, 600 mg/day/kg	Normal drinking water + food	25 days	4 w after OHT	RM3 (P) + 9380 ppm NAM (P) 25kGy ; SDS diet
BN	T.NT.AAVNMNAT2 (unilateral overexpression of *hNMNAT2*)	Intravitreal injection of AAV-*hNMNAT2*	Gene therapy with AAV-*hNMNAT2*	Intravitreal injection	3 weeks	3 w after IVI	RM3 (P); SDS diet
BN	T.G.AAVNMNAT2 (unilateral overexpression of hNMNAT2 followed by unilateral glaucoma)	Intravitreal injection of AAV-*hNMNAT2*; induction of OHT	Gene therapy with AAV-*hNMNAT2*	Intravitreal injection	3 weeks prior OHT	4 w after OHT	RM3 (P); SDS diet

Table 2. 1. Experimental groups with corresponding experimental procedures and treatments. Male Brown Norway were divided into ten experimental group. C.sham and G.sham were used as positive and negative controls. Each NAM group had a specific diet according to the experimental purpose. Overexpression of *hNMNAT2* was used to promote the production on NAD^+.

2.2 Induction and monitoring of ocular hypertension

Ocular hypertension was induced with intracameral magnetic microbead injection in the left eye with the contralateral eye used as internal control. Intracameral magnetic microbead injections were adapted from Tribble et al. protocol (Tribble et al., 2021b), with the adjustments described in detail in chapter 3. Induction and maintenance of OHT was checked every other day after the injection until the animal was culled. Baseline IOP measurements were taken prior the injection and/or treatment on all the animals.

2.2.1 Intraocular pressure measurement

IOP measurements for experimental purposes were taken on awake not anesthetised rats trained with positive reinforcement for unrestrained IOP recordings. IOP was measured with a rebound tonometer calibrated for rat eye (Morrison et al., 2009) (Tonolab, Icare). Five complete IOP recordings were taken for each eye. Each complete recording consisted of six single measurements automatically averaged by the Tonolab to a final reading. The Tonoprobe was positioned 1 to 2 mm from the eye with a 90° angle between the cornea apex and the tonometer handle. IOP checks were performed every other day always between 7 and 9 am to avoid any effects of the circadian rhythm.

2.2.2 Induction of ocular hypertension

Unilateral ocular hypertension was inducted using a paramagnetic bead model. Rats were anaesthetised with 5% isoflurane (Piramal Healthcare UK Ltd)/ 2L O_2/min and kept at 2.5% throughout the procedure. The contralateral eye (NT) was protected from dryness by Viscotears gel (Bausch & Lomb) while the ipsilateral eye (HT) furtherly numbed with 0.4% Oxyburprocaine eye drops (Bausch & Lomb). Magnetic microbeads injectable solution (Dynabeads™ M-450 Epoxy; Thermo Fisher Scientific) was prepared was 1x Hank's Balanced solution (HBSS -$CaCl_2$, -$MgCl_2$, -phenol red; Gibco) to reach a final concentration of ≈2.7 x 10^6 beads/µl (240 mg/ml). 8-10 µl of bead solution was slowly injected (100 µl NanoFil Hamilton syringe, World Precision Instruments; 33G tribevelled needle, World Precision Instruments) into the anterior chamber. During the injection beads were directed to the iridocorneal angle with a hand held magnet to block the aqueous humor outflow. Once the needle was removed 0.5% Chloramphenicol eye drops (Bausch & Lomb) were applied to minimise the risk of infection.

2.3 Induction of *hNMNAT2* overexpression

Over expression of *human nicotinamide nucleotide adenylyltransferase 2* (*hNMNAT2*) was induced by intravitreal injections of 3 µl of 2.2x10^{11} gc/ml AAV2 CMV-eGFP-T2A-CMV-NMNAT2 (AVV-216829, Vector Biolabs). Rats were anaesthetised as described above. The contralateral eye (NT.AAVnull) was protected from dryness by viscotears gel (Bausch & Lomb) while the ipsilateral eye (HT) furtherly numbed with 0.4% Oxyburprocaine eye drops (Bausch & Lomb). To have a clear view of the optic nerve head few drops of 1% Tropicamide (Bausch & Lomb) were applied to the eye to dilate the pupil. Once the pupil was dilated Viscotears and a cover slip were applied to the cornea to allow a direct visualisation of the optic nerve head and vasculature. The

viral vector was intravitreally injected pointing the needle toward the ONH (10 µl NanoFil Hamilton syringe, World Precision Instruments; 35G tribevelled needle, World Precision Instruments). The needle was kept in place for at least 10-30 seconds and then slowly withdrawn. Once the needle was removed 0.5% Chloramphenicol eye drops (Bausch & Lomb) were applied to minimise the risk of infection.

2.4 Tissue harvest and dissection

2.4.1 Retinas

Mice (for retina axotomy explant models) and rats were euthanised as described in section 2.1.1.1 and 2.1.1.2. Once death was confirmed eyes were immediately enucleated and the cornea marked with a hand-held cauteriser to maintain orientation during dissection. The eyes were immediately transferred into Hank's Balanced Salt Solution (Gibco™, Fisher Scientific). Under a dissecting microscope, each eye was dissected with Pierce Notched Forceps (Duckworth & Kent ltd) and straight Vannas Scissors (Duckworth & Kent ltd). A 26G needle was used to puncture the globe at limbus and afterwards cut along the ora serrata, allowing the removal of the cornea, lens and vitreous. The retina was then detached from the sclera and choroid, cutting the optic nerve at the optic nerve head to separate it entirely. If some vitreous was still attached it was gently removed with the forceps. Thereafter, four cuts were made to the retina to allow the tissue to be flat mounted with the GCL upward and used for experiments.

2.4.2 Optic nerves

Rat optic nerves for metabolomics analysis were collected immediately after culling. Brains were removed and optic nerves dissected and separated at the chiasm in NT (right eye) and HT (left eye). The samples were weighted and snap froze with liquid nitrogen. The tissue was stored at -80° C and shipped in dry ice to the Swedish Metabolomics Centre for sample processing.

Group	Sample size	Treatment
G.sham	NT = 6; HT = 6	/
G.HNAMint	NT = 6; HT = 6	Intervention; NAM 600 mg/day/kg
G.HNAMproph	NT = 6; HT = 6	Prophylactic; NAM 600 mg/day/kg

Table 2. 2. Optic nerves sample groups. Optic nerves were collected from G.sham, G.HNAMint and G.HNAMproph as RGC enriched tissue for metabolomic analysis.

2.5 Retina axotomy explant model

The axotomy explant model was used to screen the effect of nicotinamide on RGC prior *in vivo* experiments. This model was performed with slight modifications from previously established protocols (Binley et al., 2016, Bull et al., 2011). The dissected retinas were flat mounted, with the GCL upward, on a cell culture insert (Millicell 0.4 µm pore; Merck). The retinas were kept in culture (37° C, 5% CO_2) for 72h in a six well plate and fed by culturing media (Neurobasal®-A, Gibco™), 1.5 ml/well, supplemented with 2mM L-glutamine (GlutaMAX™, Gibco™), 2% B27 (Gibco™), 1% N2 (Gibco™) and 1% penicillin/streptomycin (Gibco™). Half of the media volume was changed every other day. For the NAM groups (NAM, Apollo Scientific ltd; molecular weight: 122.12 g/mol) the culturing media was further supplemented with either 100 mM NAM (low NAM; LNAM) or 500 mM NAM (high NAM; HNAM). After 72h the retinas were removed from culture, transferred to a microscope slide and processed.

Strain	Group	Culturing period	Treatment
C57BL/6J	E.0DEV.sham	/	/
C57BL/6J	E.3DEV.sham	72h	Culturing media
C57BL/6J	E.3DEV.LNAM	72h	Culturing media supplemented with [100 mM] NAM
C57BL/6J	E.3DEV.HNAM	72h	Culturing media supplemented with [500 mM] NAM

Table 2. 3. Mouse retinal explant experimental groups. Retinas from C57BL/6J have been divided into four experimental groups. E.0DEV.sham and E.3DEV. sham have been used as positive and negative controls. NAM neurotrophic support has been tested with media supplemented with two different NAM concentrations, 100mM LNAM and 500mM HNAM. DEV = days ex vivo.

2.6 Analysis of RGC dendritic structure

Analysis of RGCs morphology was the core of this project. Neuronal labelling typically relies on the expression of fluorescent markers. However, not all markers are reliable when used to investigate degeneration, since they are dependent on cells' viability. In contrast, Diolistics is a very efficient method that does not depend on the status of the cell (Honig and Hume, 1986),

and consists of ballistic delivery of fluorescent dyes with random cell labelling where the dyes have diffused (Gan et al., 2000, Sherazee and Alvarez, 2013). Using multiple dyes has several advantages, *i.e.* higher cellular yield that can be achieved increasing the chance of hitting RGCs with different dyes. Labelled cells can be visualised separating the channels once the tissue sample are analysed at the confocal. That allows a clear visualisation of RGC morphology reducing the probability of two overlapping cells being labelled by the same dye. Labelled RGCs are then semi automatically reconstructed and Sholl analysis performed (Binley et al., 2014).

2.6.1 DiOlistics bullet preparation

80 mg of tungsten particles (Ø ≈ 1.7 µm M-25 Tungsten, Bio-rad; Ø ≤ 1µm Tungsten, Alfa Aesar – Thermo Fisher), 2 mg of 1,1'-Dioctadecyl-3,3,3'3'-Tetramethylindocarbocyanine Perchlorate (DiI; D282, Invitrogen™) and 4 mg of 3,3'- Dioctadecyloxacarbocyanine Perchlorate (DiO; D275, Invitrogen™) or 1 mg of 1,1'-Dioctadecyl-3,3,3',3'-Tetramethylindodicarbocyanine, 4-Chlorobenzenesulfonate Salt (DiD; D7757, Invitrogen™) were weighted into separate 1.5 ml Eppendorf tubes. Under a fume hood, 400µl of methylene chloride were added to each dye and the tungsten particles evenly divided in two equal parts onto two glass slides. The tungsten particles were then finely grinded with a razor blade. Afterward, few drops of the dissolved dyes were added to each pile (DiI to one and DiO or DiD to the other). After each addition, the particles with dyes were left to dry for 3-5 min and then grinded again to avoid any clumps. This process was repeated until all 400 µl were used. Once all the solution was incorporated, the two piles of tungsten coated were mixed together and funnelled into the interior surface of Tefzel tubing (≈ 30cm; Bio-rad). The coated tubing was stored protected from light until use. Prior DiOlistics Gene Gun (Helios® Gene Gun; 1652432, Bio-Rad) shooting the coated tubing was cut into ≈ 12 mm bullets (bullet dyes combination were DiI/DiO- or DiI/DiD).

2.6.2 DiOlistics labelling

Retinas, dissected as described in section 2.4.1, were transferred to a microscope slide with the GCL upward, flattened out, and HBSS completely removed. DiOlistics bullets were then fired (mouse retinas, 100-110 psi; rat retinas, 120-140 psi) with a Helios® Gene Gun 5 cm from the retina surface through a polyethylene terephthalate membrane (3 µm pore size; Falcon cell culture inserts, Falcon 353092 – Fisher Scientific; gun barrel, 3cm height; cell culture insert, 2cm height) to help disperse tungsten particle and prevent clamping (Fig. 2.1). Once shot, Neurobasal-A media was added to the slides and the retinas transferred to an incubator for 30 min (37° C) to let the dye diffuse. After the diffusion the retinas were checked under a

fluorescence microscope to verify the labelling. In case of a poor labelling the retinas were re-shot and re-incubated for other 30 min. After incubation, Neurobasal-A was removed and the retinas fixed in 4% paraformaldehyde (PFA, Sigma-Aldrich; 30 min, mouse retinas; 1h, rat retinas). After fixation, samples were washed with 1 M phosphate buffered saline (10% 10x PBS – Gibco™ – diluted in UltraPure water, 7.4 pH), nuclei labelled (Hoesch 33442, 1:1000 in PBS; 15 min) and washed again (3 times with PBS). Samples were then mounted with FluoroSave (Millipore) mounting media, coverslipped and dried at room temperature for 1h and stored at 4° C until they were taken for confocal imaging.

However, the stain produced by this DiOlistic method will leak significantly after 48h, making the samples unusable. Therefore, all confocal imaging must be taken around the clock within this time.

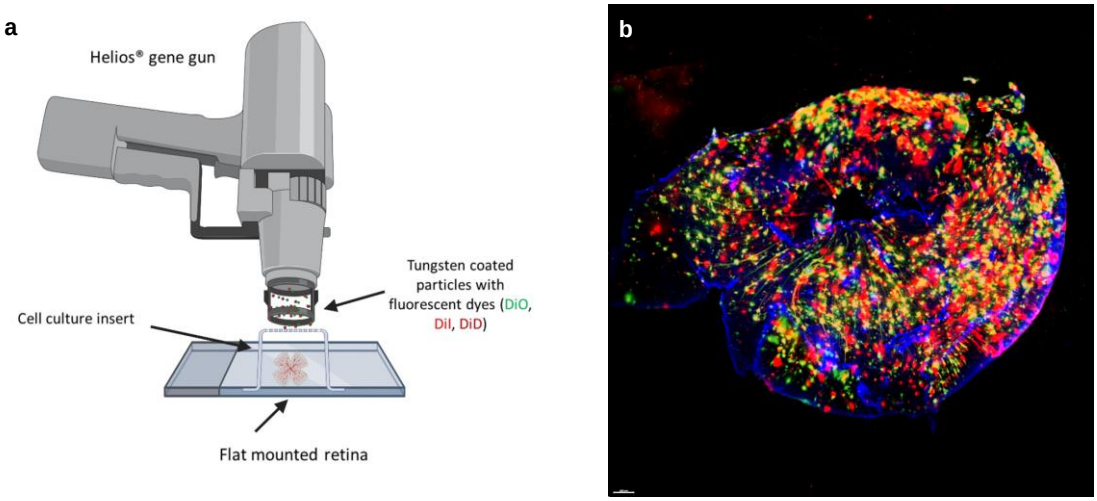

Figure 2. 1. Diolistics labelling. a) A bullet containing a mixture of tungsten coated particles (DiO/DiI or DiI/DiD) is shot with a Helios® gene gun. b) Shot particles hit the flat mounted retina and randomly label RGCs. Scale bar 600 µm.

2.6.3 Confocal microscopy

Images of individual RGC arbours were acquired with a Leica SP8 lightning confocal microscope (Leica; 20X magnification, 0.455 µm/pixel, 1 µm z-thickness) for mouse retinas, with a Zeiss LSM 780 confocal microscope (Carl Zeiss; 20X magnification, 0.345 µm/pixel, 1 µm z-thickness) for rat retinas. RGCs were identified by their location in the GCL, the presence of an axon projecting to the optic nerve, and a dendritic tree extending in the IPL. If these features were not present the cell was not included for analysis as there could be a high risk of including other retina cell

phenotypes. Bistratified RGCs were also excluded. The entire cell was imaged, including the axon and the full dendritic tree (tile size 1024 x 1024), using a separate channel for each dye (Fig. 2.2).

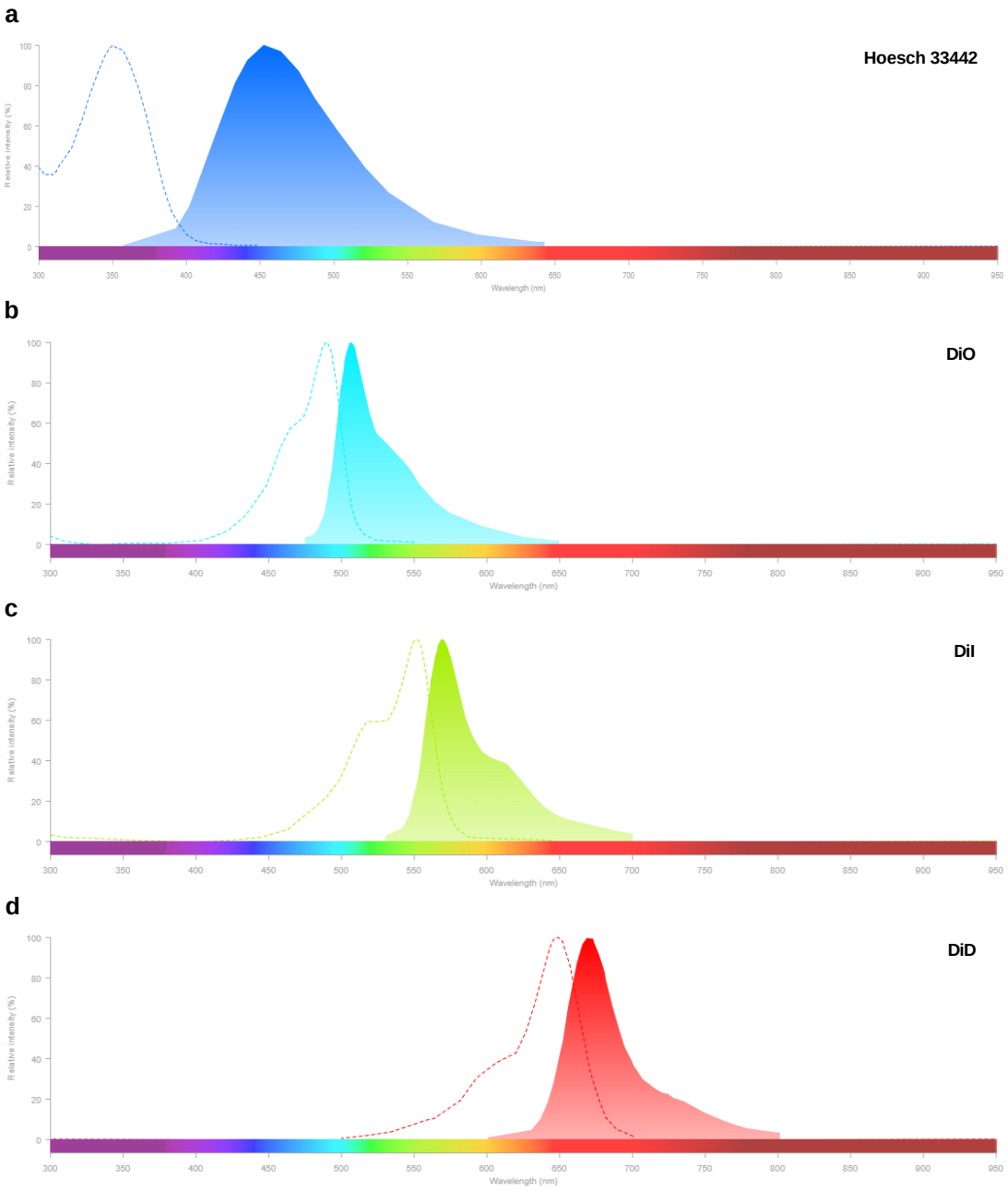

Figure 2. 2. Excitation and emission ranges for DiOlistics labelling. a) Hoechst 33442; ex. 352 nm, em. 445nm. b) DiO; ex. 487 nm, em 501 nm. c) DiI; ex. 551 nm, em. 565nm. d) DiD; ex. 648 nm, em. 670nm. Dashed line, excitation wavelength. Solid line, emission wavelength.

2.6.4 Retinal ganglion cell reconstruction

All imaged RGCs were reconstructed using the filament tracer module on Imaris software (Version 9.3.1, Bitplane). Once the image was selected the z-stack was reduced to include only the IPL (Fig. 2.3 a,b). A region of interest (ROI) was demarcated around the dendritic field and automatically traced to reconstruct the dendritic arbour (Fig. 2.3 c,d). The dendrites that were missed or erroneously included were either manually traced or erased. Once the arbour was accurately reconstructed the convex hull was calculated to determine the dendritic field area (Fig. 2.3 e,f). All parameters were then exported for data analysis with Sholl intervals set at 10 µm.

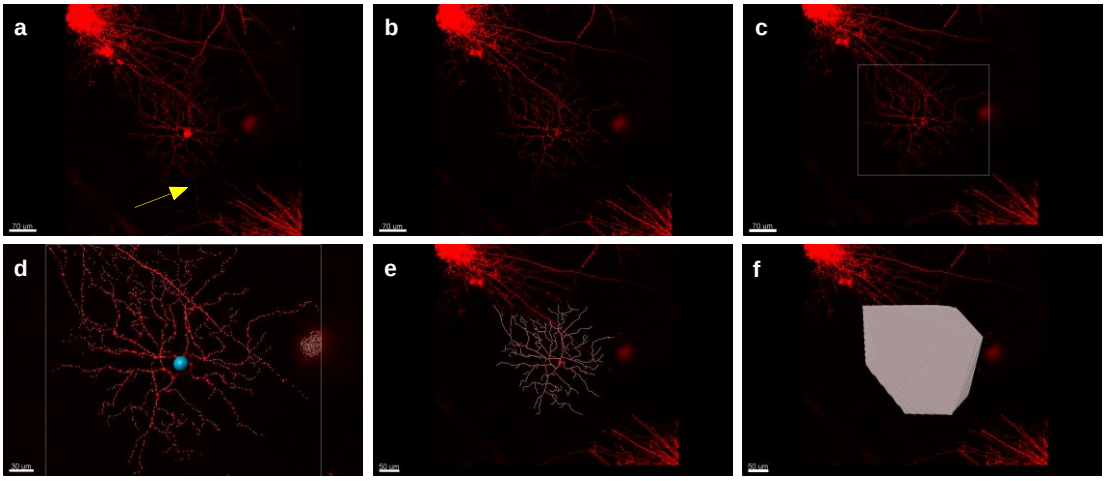

Figure 2. 3. Imaris reconstruction of labelled RGC. a) A RGC, identified by the presence of an axon (yellow arrow). b) Z-stacks at the IPL. c) Selection of a region of interest (ROI) which includes the entire dendritic tree. d) Automatic selection of the soma with reconstruction of the dendritic arbour. e) Reconstructed RGC dendritic tree with manual correction of missing/extra branches. f) Automatic computation of the dendritic field area.

2.6.5 Sholl analysis

Dendritic architecture is generally assessed by Sholl analysis (Sholl, 1953), which is a standard measure of dendritic complexity as function of the distance from the cell body, and quantifies dendrites intersecting at concentric rings at set intervals from the soma (10 µm). A shift in the Sholl curve typically determines a changes in the overall dendritic complexity (Fig. 2.4).

As a general rule for Diolistic labelling, RGCs from a given experimental groups are combined, and then mean number of dendritic intersections plotted at each interval. Due to the different

dendritic arbour morphology among RGC subtypes, Sholl profile of individual cells might be quite variable, but when averaged together a typical adult rat Sholl have a peak of ≈ 30 dendritic intersection at around 80 µm from the soma. After that point the curve generally declines with the final dendritic branches positioned around 350 µm from the soma. Given the variability in RGCs size and the associated standard deviation (SD) between cells, standard error of the mean (SEM) is used to simplify the visual understanding of the graphs.

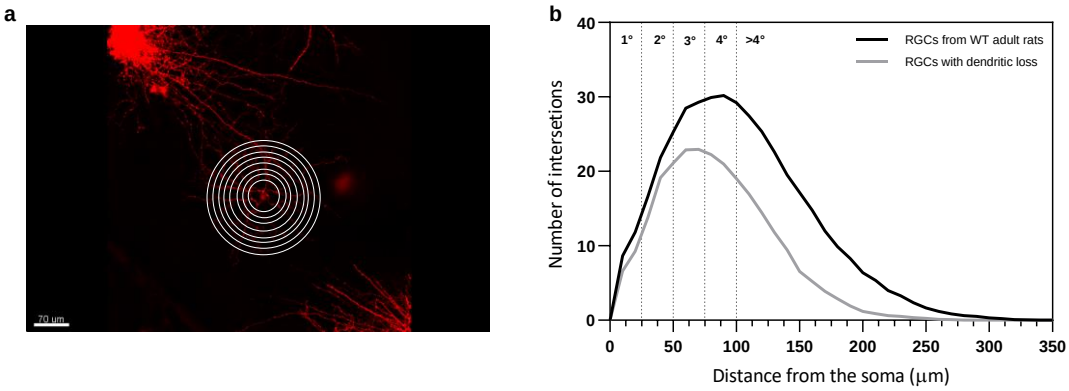

Figure 2. 4. Example of Sholl analysis. a) Quantification of dendrites intersecting concentric rings at 10 µm intervals from the cell body. b) Mean value of dendritic intersections at each intervals are plotted in function to the distance from the soma. A left shift in the curve describes loss of dendritic complexity. Dashed lines indicate the branching index.

Besides the Sholl profile other parameters can be assessed from the Imaris files, which will provide additional information on the RGCs morphology:

Area under the curve

This measure represents the area under the Sholl curve and gives an overall measure of dendritic complexity, allowing the comparison of different curves through a single numerical value.

Max Sholl or maximum number of intersections

This value represents the maximum number of dendritic intersection at any point of the Sholl curve, indicating the highest number of complexity, likely at the Sholl peak.

Total dendritic length

The sum of all branches within the dendritic tree measured in µm.

Branching level

This index represents a comparison of dendritic branches based on their branching level (*e.g.* primary, 1°; secondary, 2°; tertiary, 3°; quaternary, 4°).

RGCs field area

Area of the dendritic field measured in μm^2.

2.6.6 Nuclear count

A minimum of 24 random quadrants (1024 x 1024) from a tiled image of each retina were analysed on Imaris. GCL nuclei were identified automatically using the spot tool (5.5/6.5 µm diameter) and the density normalised to nuclei/mm^2. Average distance between neighbouring cell was automatically calculated by the software.

2.7 Metabolomics

Optic nerves for metabolomics analysis were collected as described in section 2.4.2 and the tissue shipped to the Swedish Metabolomics centre for sample processing. 200 µl of the 90:10 MeOH:H_2O was added to each frozen sample on dry ice, acid washed glass-beads (425-600 µm, Sigma Aldrich) were added to constitute 50% v/v of the MeOH:H_2O solution and samples were disrupted by shaking at 30 Hz for 2 minutes (Mixer Mill MM400, Retsch) using pre-chilled holding blocks (4°C). Following cell disruption samples were centrifuged at 4°C (14.000 RPM for 15 seconds). To obtain a 60:40 ratio of MeOH:H_2O, 100 µl of H_2O was added to the samples followed by shaking at 30 Hz for 15 seconds (Mixer Mill MM400, Retsch) using pre-chilled holding blocks. Samples were centrifuged at 4°C (14.000 RPM, 15 seconds) and the supernatant transferred into LC-MS vials (Thermo Fisher) and immediately analysed. 10 µl were injected into an Agilent 1290 UPLC-system connected to an Agilent 6546 Q-TOF mass spectrometer with an Agilent Jet Stream electrospray ionization (ESI) source. Data was collected in negative ionization mode with ESI settings: Gas temperature 150°C, drying gas flow 16 L/min, nebulizer pressure 35 psi, sheet gas temperature 350°C, sheet gas flow 11, Vcap 4000, nozzle voltage 300 V, Fragmentor 380, Skimmer1 45 V and OctapoleRFPeak 750 V. Metabolites were separated using HILIC HPLC column (iHILIC-Fusion(+), 100x2.1 mm, 3.5 µM, 100 Å, Hilicon AB). HILIC elution solvents were (A) H_2O, 50 mM ammonium formate and (B) 90:10 Acetonitrile:[50 mM ammonium formate in H_2O]. Chromatographic separation was achieved using the following linear gradient (flow rate

0.4 mL/min), min 0: 90% B; min 4: 85% B, min 5: 70% B, min 7: 55% B, min 10: 20% B, min 10.01: 90% B, min 15: 90%. Fifty-four low molecular weight metabolites verified with standards were detected. Metabolites were quantified as area under the curve of the mass spectrometry peak. Although internal standard data for AMP showed a fairly stable intensity, which suggested that data normalization was not required, all the data were normalized to tissue weight. Metabolic data were analysed using MetaboAnalyst (version 4.0(Chong et al., 2018, Chong et al., 2019, Xia and Wishart, 2011) and 5.0 (Pang et al., 2021, Pang et al., 2022)). Groups were compared by two-sample *t*-test with adjusted *p* value and cut-off of 0.05 considered significant. Principal component analysis was calculated using Pareto scaling to reduce the magnitude impact (van den Berg et al., 2006). Pathway analysis was performed in MetaboAnalyst using the *Rattus norvegicus* KEGG library.

2.8 Statistical analysis

Statistical analysis was performed on GraphPad Prism (version 9). Data from traced RGCs were used to plot the Sholl analysis showing number of dendritic intersections (y) against the distance from the soma at 10 µm intervals (x). Data are showed as mean value ± SEM. For all the other data, data are displayed as individual values with box and whiskers plots indicating 1st quartile, median and 3rd quartile (box), and minimum and maximum value (whiskers). For branching analysis, data are shown as individual value plus mean ± SD. Normality of data sets was tested using Shapiro-Wilk test. To compare two groups t-test or Mann-Whitney U test were used when appropriate. To compare three or more groups one-way ANOVA or Kruskal-Wallis, followed by Tukey *post-hoc*, Bonferroni or uncorrected Dunn's test were performed when appropriate. For the branching analysis, two-way ANOVA followed by uncorrected Fisher's LSD test. Results are denoted as follows: Ns = $p > 0.05$, * = $p < 0.05$, ** = $p < 0.01$, *** = $p < 0.001$, **** = $p < 0.0001$.

Statistical analysis was performed for the following groups with the following sample size (N, retinas; n, RGCs):

Group	N	n
E.0DEV.sham	10	75
E.3DEV.sham	12	47
E.3DEV.LNAM	12	53

E.3DEV.HNAM	12	62
C.sham	22	182
G.sham	NT = 12; HT = 12	NT = 66; HT = 83
C.LNAM	12	115
C.HNAM	12	113
G.LNAMproph	NT = 6; HT = 6	NT = 40; HT = 54
G.HNAMproph	NT = 12; HT = 12	NT = 102; HT = 136
G.LNAMint	NT = 6; HT = 6	NT = 62; HT = 79
G.HNAMint	NT = 12; HT = 12	NT = 107; HT = 104
T.AAVNMNAT2	NT.null = 6; NT.AAVNMNAT2 = 6	NT.null = 34; NT.NMNAT2 = 43
T.G.AAVNMNAT2	NT.null = 6; HT.AAVNMNAT2 = 6	NT.null = 42; HT.NMNAT2 = 41

Table 2. 4. Experimental groups sample size.

2.9 Normalisation parameters of the AUC of IOP profiles

To identify experimental IOP changes, post baseline IOP AUC was normalised to baseline IOP AUC using as normalising factor the number of IOP baseline recording, in order to have comparable AUCs between the different experimental stages.

2.10 Power analysis

Power calculations were performed on G*Power (version 3.1) (Faul et al., 2007). *A priori* power calculations were performed to decide the minimum sample size (Chow, 2007), estimating a 40 % AUC difference between the control and disease group (based on pilot data from the same model). Using G*Power the following sample sizes were calculated based on Wilcoxon-Mann-Whitney test of the means of two groups, with an α value of 0.05 and power value (1 – β) of 0.90. Mean AUC ± SD of control group and OHT glaucoma (based on preliminary trials) were estimated at 4151.86 ± 2120.55 for the control, and 2552.53 ± 1201.65 for OHT glaucoma (Table 2.5).

Effect size	Recommended RGC per group
0.9	29
0.8	36
0.7	46
0.6	63
0.5	90

Table 2. 5. Power calculations determining suggested RGC sample size based on estimated effect size.

Once all the experiments were concluded *post hoc* power calculation were performed to verify the goodness of the data. The actual effect size for each group was evaluated comparing the mean AUC ± SD and sample size of the positive and negative control group with the experimental group of interest (E.0DEV.sham and E.3DEV.sham for the explant experiments; C.sham and G.NT/HT.sham for the *in vivo* experiments; Table 2.6).

Group	Effect size (positive control)	Effect size (negative control)
E.3DEV.sham	1.28	/
E.3DEV.LNAM	0.17	1.12
E.3DEV.HNAM	0.19	1.07
G.NT.sham	0.90	/
G.HT.sham	1.21	/
C.LNAM	0.02	/
C.HNAM	0.34	/
G.NT.LNAMproph	0.01	0.73
G.HT.LNAMproph	0.47	1.17
G.NT.HNAMproph	0.41	0.94

G.HT.HNAMproph	0.39	1.26
G.NT.LNAMint	0.01	0.61
G.HT.LNAMint	0.34	0.50
G.NT.HNAMint	0.11	0.51
G.HT.HNAMint	0.16	1.05
T.NT.AAVnull	0.01	/
T.NT.AAVNMNAT2	0.13	/
T.G.NT.AAVnull	0.66	0.15
T.G.HT.AAVNMNAT2	0.25	1.19

Table 2. 6. Post hoc power calculation.

3 Brown Norway rats, characterization of baseline parameters and optimisation of inducible model of unilateral ocular hypertension

3.1 Overview

Our understanding of glaucomatous pathophysiology comes from the experimental models that have been developed over the years (chapter 1, insights on different glaucoma models)(Pang and Clark, 2020). Despite the different pathological features (e.g. ocular normotensive glaucoma, ocular hypertensive glaucoma) all lead to the progressive loss of retinal ganglion cells and the degeneration of the optic nerve. Since elevated intraocular pressure is highly associated with the disease and to date the only treatable factor, most of the *in vivo* models try to reproduce chronic IOP elevation (Biswas and Wan, 2019).

However, accurate assessment of glaucomatous-related changes, especially in inducible models of ocular hypertensions, depends on a robust experimental model and reliable and highly reproducible data. These factors are paramount for the choice of induction and assessment techniques, along with the intended species and strain. Hence, after a careful examination, it has been decided to perform experimental procedures on Brown Norway rats.

The Brown Norway (BN) rat (*Rattus Norvegicus*), even though it has Asiatic origins (Zeng et al., 2018), has become a popular species for modelling eye disease: principally by virtue of reasonably sized eye that responds well to manipulation. The utility of the model was further enhanced by the availability of a full genome sequence, raising the possibility of useful genetic models of eye disease (Gibbs et al., 2004).

In vision science most of the studies of inducible models of glaucoma are conducted on Brown Norway. There are several reasons why it is the strain of choice; one is certainly its visual acuity (Prusky et al., 2002) and above all because its physiological and structural parameters (*e.g.* intra ocular pressure (Morrison et al., 2009), retinal ganglion cells (Sun et al., 2002a, Sanes and Masland, 2015)) are well characterised. However, BN social behaviour (*e.g.* docile, easy to train) is also a determining factor since all inducible model of glaucoma require profuse handling and interaction (Schweinfurth, 2020).

Elevated intraocular pressure has been induced on BNs with the obstruction the aqueous outflow pathway. This can be experimentally obtained either with the sclerosis of episcleral vessel through hypertonic saline injections (Morrison et al., 2008) or through injection of

substances that mechanically block the outflow pathway (Johnson and Tomarev, 2010). Intracameral injections of microbeads are included in this last category, and can be made of latex microspheres (Urcola et al., 2006), polystyrene beads (Smedowski et al., 2014) and polystyrene ferromagnetic microbeads (Samsel et al., 2011, Tribble et al., 2021b). Although all microbead injections can induce ocular hypertension, each microbead has its own characteristics that need to be taken into account depending on the injection technique (Morgan and Tribble, 2015).

For the purpose of inducing moderate and controlled chronic IOP elevation Dynabeads® M-450 Epoxy microbeads (chapter 2 and appendix) were the best choice. Those are polystyrene epoxy coated microbeads with a diameter of 4.5 µm, that can be easily injected in the anterior chamber with a self healing tunnel injection which does not require a high degree of manual dexterity.

Although aqueous humor dynamics and response to IOP elevation have been well characterised in BNs (Ficarrotta et al., 2018, Eastlake et al., 2021), to perform the experiments with a high level of reproducibility all the experimental standard operating procedures have been optimised to increase the level of consistency and the reliability of the chosen model.

Characterization of baseline parameters, development and optimisation techniques for *in vivo* induction of ocular hypertension through intracameral injections of magnetic microbead particles will be discussed in the following sections.

3.2 Characterization of baseline parameters

3.2.1 Experimental setup

To obtain reproducible and reliable results, male Brown Norway rats – bought from a UK licensed establishment (Envigo UK) – have been extensively handled and trained only by one researcher. All the non surgical procedures have been refined in order to minimise animal discomfort and to avoid any restraining methods. Positive reinforcement and play time introduced to improve animal welfare and habituate the animal to regular IOP monitoring.

After culling, dissection techniques have been improved to reduce the dissection time to avoid retinal ganglion cells damage, and for DiOlistic delivery of tungsten coated fluorescent particles optimised for rat flat mounted retinas explants.

Since our work is mainly based on morphological analysis of retinal ganglion cells, Imaris parameters have been optimised to reliably reconstruct rat RGC dendritic arbours.

Readouts from these animals will constitute the normotensive control data (C.NT) throughout all the project and will be referred as control normotensive sham (C.NT.sham), sham due to the addition of caster sugar in the water during the experimental period, in this dissertation.

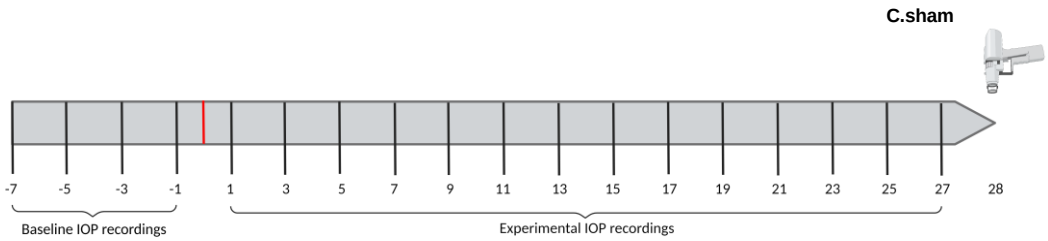

Figure 3. 1. Experimental workflow Brown Norway normotensive rats, C.sham.

3.2.2 Results

3.2.2.1 Animal welfare and training techniques

In order to provide the best living conditions, the laboratory rats once arrived from the licensed establishment were kept away from any training and experimental procedures for ten days. In these days of adaptation they were familiarised with the handler and the environment (*e.g.* procedure room, surgery room and recovery room). Exposing them to the different smells and noises, without experimental purpose, helped to reduce their vigilance and to improve the trust towards the handler. With constant supervision they were allowed to move freely outside the cage, alone or in pairs, and that developed a further bond with the researcher that was seen as a safe person to be around.

After this adaptation period, the rats entered their training period. Positive reinforcement (*e.g.* muesli, watermelon, nuts) was used to teach them to get accustomed to the situations they could have faced during the experiment (*e.g.* walk and sit on the handler's arm for IOP checks, held in certain ways for injections). They did not show any sign of distress during the training (*e.g.* apathy, weight loss, overgrooming, scruffy coat), but to confirm that their behaviour was reflecting their health their weight was constantly checked (Fig. 3.2). Indeed, it was not observed

anything different from a normal growing curve for rats of their age (10 - 12 week during training). Once all their training skills were impeccable (*e.g.* sitting on the handler arm, sit still without restraining methods in place), normal handling with few practice sessions were performed just prior the experiment.

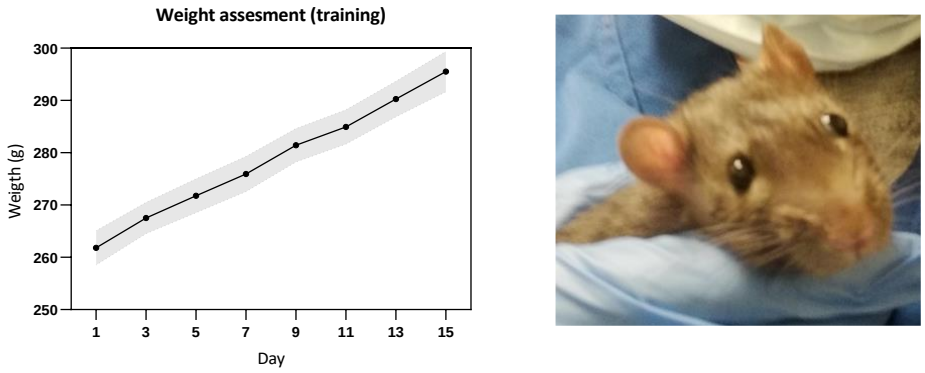

Figure 3. 2. Monitoring rat health through their weight gain during training. Intensive training did not affect Brown Norway wellbeing as shown by their growth curve (line mean value; shaded area ± SD) and a representative picture of one of the animal in training.

As part of the training, all rats received regular IOP checks. IOP recordings are a valuable way to detect retinal ganglion cells distress, and an important readout of this investigation. The common way to measure IOP in rodents in with a rebound tonometer; each single measurement is averaged on five single recordings that once are filed let the tonometer beep. That sound agitated the rats which tried to avoid what they perceived as danger. That initial reaction forced the introduction of a restraining method while measuring their pressure (Fig. 3.3 a). However, these animals were all normotensive and when their IOP recordings were tracked over time, their IOPs were too high to be their normal readout (Fig. 3.3 c). Some of their IOPs were above 25 mmHg, which is considered ocular hypertension and it was quite suspicious for wild type rats. Not convinced about these IOP readouts, they were taught to associate snack time with IOP readings. Even though it took some time to get them used to it, it was possible to train them to have their IOPs measured while they were freely nibbling on the handler arm (Fig. 3.3 b). That approach changed drastically the IOP redouts, which decreased by more than a half, with minimal standard deviation, compared to the restrained values (Fig. 3.3 d).

Considering the results obtained, this new technique was used throughout all the project for all the experimental groups.

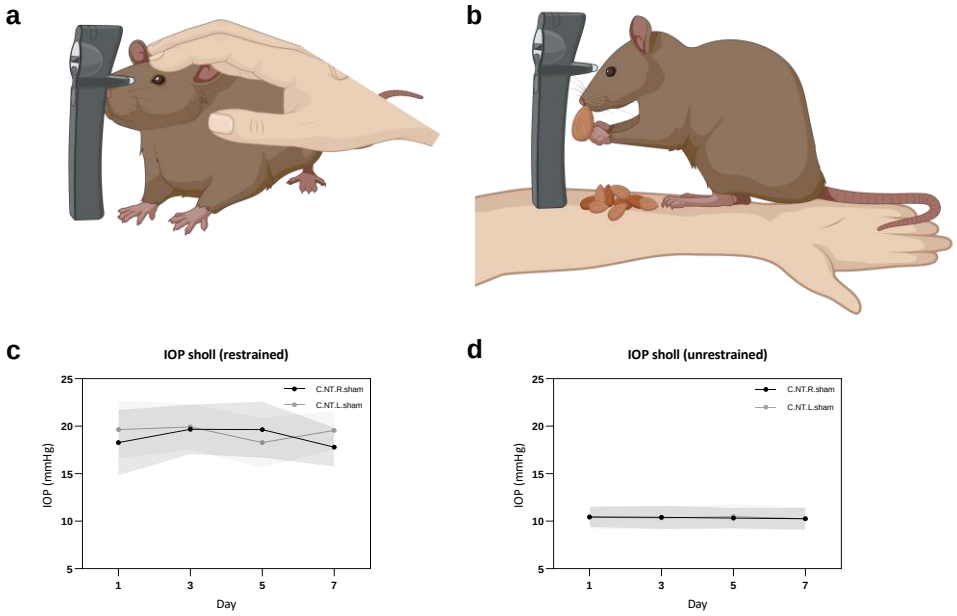

Figure 3. 3. Restraining method influences intra ocular pressure measurment. a) Gentle restrained IOP measurment. b) Unrestrained IOP measurment. c) Restrained IOP profile. d) Unrestrained IOP profile. Line mean value; shaded area ± SD. Cartoon created with Biorender.com.

3.2.2.2 Intraocular pressure and retinal ganglion cells dendritic baseline parameters

All the rats classified as C.NT.sham constituted the control group, whose parameters have been used to establish the positive or negative outcome of all the following experiments. Considering their touchstone role, all the baseline parameters were evaluated and the staining techniques optimised for the tissues sample and the material stock available (tungsten particles Ø ≈ 1.7 µm versus tungsten particles Ø ≤ 1µm).

3.2.2.2.1 IOP baseline parameters

Baseline IOPs were the first parameter that was observed as hallmark for normotension. The IOP recordings were prolonged to 5 weeks, with the purpose to have matching readouts for the upcoming experiments of 4 weeks induced ocular hypertension. However, that was the first time rats IOPs were monitored for a prolonged period of time and the effect on their health was unknown. Taking into account this unknown variable their weight was monitored at the same time they had their IOPs checked. As expected from their behavioural pattern, these frequent recordings did not negatively affect their growth curve (Fig. 3.4 a), and with this new measuring technique all the IOPs were at a normal normotensive level (Fig. 3.4 b-c; single rat IOPs are included in the appendix).

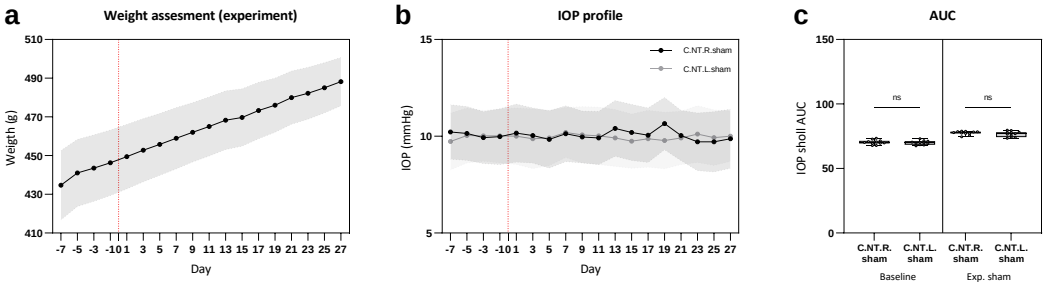

Figure 3. 4. Experimental assessment of unrestrained Brown Norway rats IOP profiles and the effect of repetitive recordings on their growth curve. a) Weight check-ups for the 5 weeks experimental period. Line mean value, shaded area ± SD (N = 11). b) Unrestrained IOP profiles measured with a hand held tonometer over a period of 5 weeks. Line mean value, shaded area ± SD (N = 11). c) Area under the Sholl IOP curve. Box and whisker plot with individual values; whiskers, min and max value; box plot, 1st quartile, median and 3rd quartile. Kruskal-Wallis test followed by uncorrected Dunn's test; ns = non significant. Exp. sham AUC IOP has been normalised to baseline following: $x(norm.factor) = \frac{\Sigma\, exp.sham\ recordings}{\Sigma\, baseline\ recordings}$.

3.2.2.2.2 RGC dendritic baseline parameters

Having established that all the animals were normotensive, to complete the evaluation of all the baseline parameters required for the project, RGCs structural parameters needed to be classified. RGCs dendritic arbours were Diolistically labelled with tungsten DiI -DiO coated fluorescent particles. That technique strongly relies on the lipophilic dye carrier, which can either be gold or tungsten. For our specific purpose tungsten is the most cost effective, but in the middle of the experiment the tungsten recommended by the Helios® gene gun manufacturer ran out of stock. Recommended tungsten particles had a diameter of ≈ 1.7 µm while the new stock comprised tungsten particles of less than Ø 1µm. To address whether this new tungsten could have changed the readouts of RGCs morphological analysis, data from two different C.NT.sham groups, one labelled with ≈ 1.7 µm tungsten particles and the other with ≤ 1µm (Fig.3.5 a-d), were compared. Although both Sholl and area under the Sholl curve (AUC) did not show any significant difference between the two groups, to obtain the same level of labelling with the smaller particles the shooting pressure was increased to 120/140 psi, while the 1.7 µm particles were shot at 110/120 psi. Having established that the change in particles diameter did not alter the outcome of the readouts, the data collected from both group were combined and processed to analyse baseline RGCs parameters.

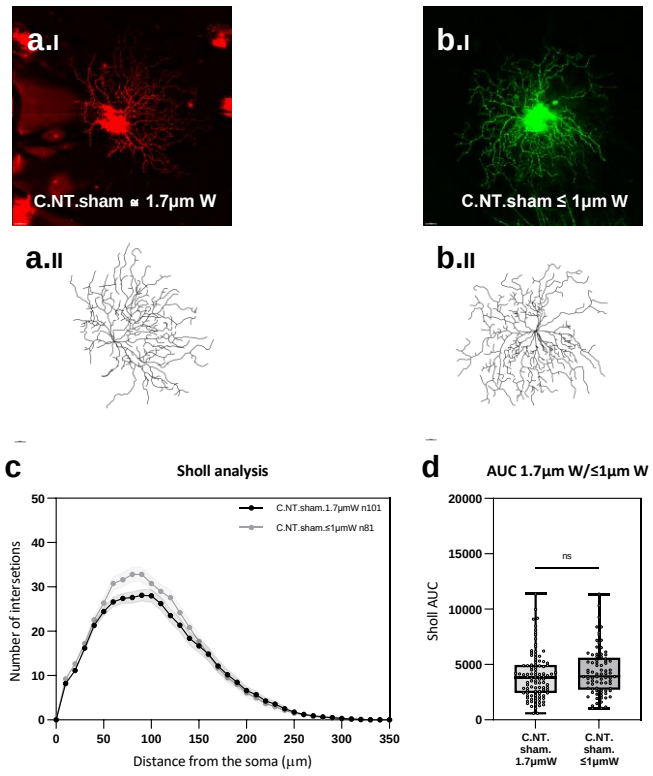

Figure 3. 5. Change in diameter of tungsten particles did not altered retinal ganglion cells morphological parameters. a, b) DiOlistically labelled RGC with corresponding Imaris reconstruction. C.NT.sham tungsten Ø ≈ 1.7 µm, . C.NT.sham tungsten Ø ≤ 1 µm. c) Sholl analysis of reconstructed RGCs. d) Area under the Sholl curve. Box and whisker plot with individual values; whiskers, min and max value; box plot, 1st quartile, median and 3rd quartile. Mann-Whitney test; ns = non significant. Scale bar 70µ

Analysis of dendritic parameters showed a normal Sholl curve, with a peak around 80 µm from the soma centre (Fig. 3.6 a). The area under the Sholl curve (AUC), with the individual values for each RGC traced, revealed the heterogeneity of the samples (mean ± SD, 4151.87 ± 2120.55; Fig. 3.6 b) , which confirmed the random DiOlistic labelling with no size-bias, further confirmed by the analysis of the field size (mean ± SD, 160982.05 ± 83949.21; Fig. 3.6 f). Both max Sholl (mean ± SD, 37.10 ± 14.56; Fig. 3.6 c) and dendritic length (mean ± SD, 6121.01 ± 3123.40; Fig. 3.6 d) reflected the different level of complexity and neurite extension, with a hierarchical gain of complexity (Fig. 3.6 e), which was expected from wild type RGCs. In addition, the average distance between cells and the GCL nuclei count provided an estimate measure of which kind of cellular disposition should be expected to be found in a rat retina in normal physiological condition (Fig. 3.6 g,h).

RGCs were classified also according to their dendritic extension in the IPL as ON-centre (dendrites terminating in the sublamina b) and Off-centre (dendrites terminating in the sublamina a). Based on this sub-classification no differences were observed between ON- and OFF-centre (Fig. 3.6 i-j).

Rat RGC DiOlistic labelling and classification are among the main expertise of the James Morgan group. Thus, it was possible to compare these parameters with previous classified RGC, and it was established that C.NT.sham morphologic patterns were equal to other wild type.

Based on the results obtained C.NT.sham was elected as positive control for the project.

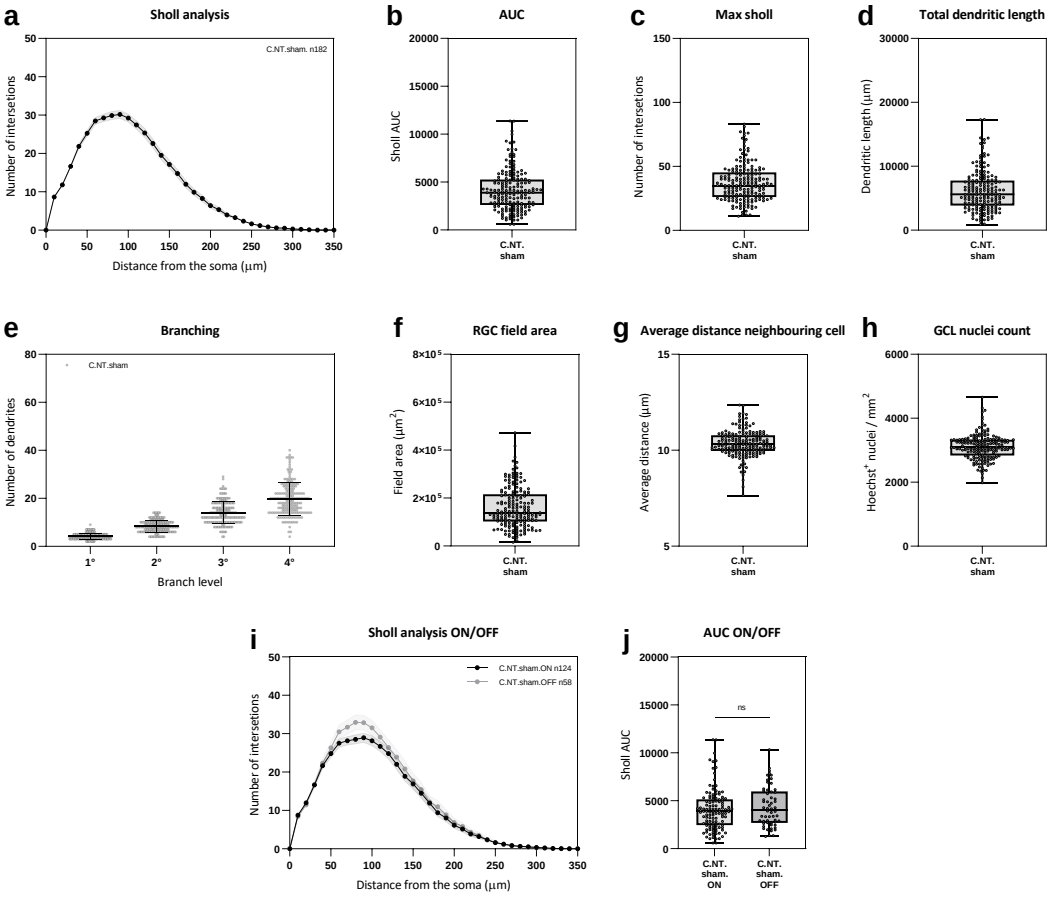

Figure 3. 6. Retinal ganglion cells morphological profile of normotensive Brown Norway rats. a) Sholl analysis of reconstructed RGCs. Line represents mean value at each interval, shaded area ± SEM. b) Area under the Sholl curve. c) Maximum number of dendrites intersections at the Sholl peak. d) Total length of all dendrites. e) Number of dendrites at each branching level proximal to the soma. Individual value ± SD. f) RGCs field size. g) Average distance between neighbouring cells. h) Ganglion cell layer nuclei count. i) Sholl analysis based on RGCs receptive field. j) Area under the Sholl curve of RGCs ON- and OFF-centre.

Box and whisker plot with individual values; whiskers, min and max value; box plot, 1st quartile, median and 3rd quartile. Mann-Whitney test; ns = non significant.

3.3 Development and optimisation of inducible unilateral model of ocular hypertension

3.3.1 Experimental setup

With all the baseline parameters available, and improved training techniques that guarantee the consistency of IOP recordings, three independent batches of Brown Norway were used to induce unilateral ocular hypertension and explore the effect of OHT on retinal ganglion cells (data from the first training batch are not included in the dissertation).

All animals were handled and trained as described in section 3.2 and their IOPs regularly checked with the same technique used for C.sham.

Self healing tunnel injections and microbead spreading technique were optimised in order to obtain a chronic moderate pressure increase for four weeks with just one injection.

Retina dissection techniques, labelling and morphological analysis performed as described in chapter 2 and in section 3.2.

Readouts from these animals will constitute the unilateral hypertensive glaucoma control data throughout all the project, and will be referred as glaucoma sham (G.sham) in this dissertation (sham due to the addition of caster sugar in the drinking water).

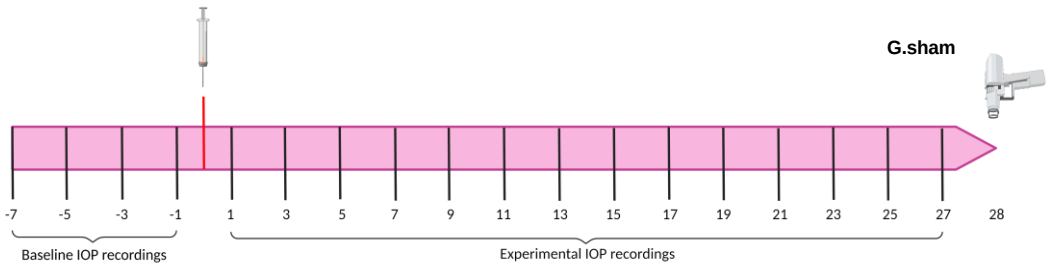

Figure 3. 7. Experimental workflow for in vivo model of induced unilateral ocular hypertension G.sham.

3.3.2 Results

3.3.2.1 Refinement of the injection technique

Microbead injections (MBI) when properly performed can induce chronic intraocular pressure increase. To properly occlude the trabecular meshwork also the concentration of the bead contained in the injectable solution has to be taken into account. Taking in consideration other successful studies performed by the Morgan and Williams groups where Dynabeads® M450 epoxy were used, for this model it was used a concentration of ≈ 2.7 x 10^6 beads/µl (injected volume 6-10 µl) to obtain a chronic moderate IOP increase.

The induction of ocular hypertension requires the complete coverage of the iridocorneal angle. However, when 6-7 µl of microbead solution was injected in a single shot with a 33G needle, with the beads spread along the iridocorneal angle, after needle was withdrawn (Fig. 3.8 a I-II) some of the beads moved towards the iris instead of remaining in the iridocorneal angle (Fig. 3.9 a). Although that injection technique raised the IOP, after two weeks the IOP was almost back to a normotensive state. Therefore, in order to maintain a sustained IOP increase for another two weeks a second injection was performed (Fig. 3.9 c).

To avoid the need of a second injection, the injection procedure was modified. The injection volume was increased from 6-7 to 8-10 µl keeping unmodified the Dynabeads® concentration. The self healing tunnel injection technique was kept the same, but the injection pace changed. The injection was slow and controlled, 2-2.5 µl/min/quadrant were displaced while injecting (Fig. 3.8 b). For the first and second quadrant the beads were displaced clockwise (9-12 o'clock first quadrant, 12-3 o'clock second quadrant), while the third and fourth quadrant anticlockwise (9-6 o'clock third quadrant, 6-3 o'clock fourth quadrant). Once all the beads were in place the 33G needle was withdrawn with no bead solution outflow (Fig. 3.9 b). This approach produced a sustained IOP elevation over a period of four weeks, with no need of further injections (Fig. 3.9 d). Procedure time, from the induction of anaesthesia to the needle removal, was typical 25-30 minutes which ensured a rapid recovery from the anaesthetic.

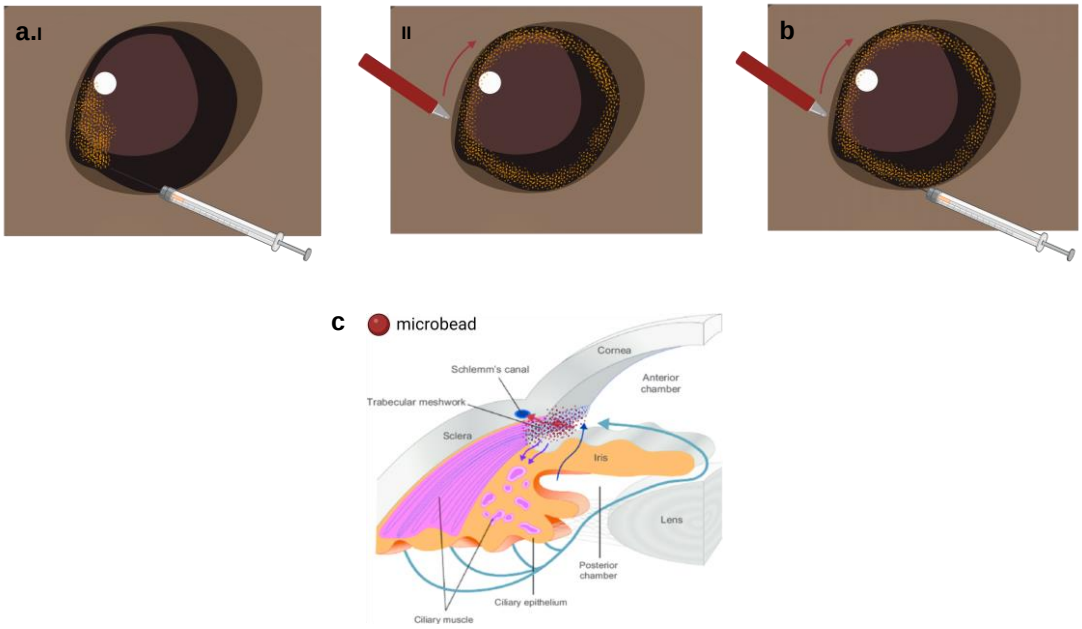

Figure 3. 8. Schematic representation of microbead injection techniques. a-I) Fast injection with microbead complete release, followed by -II) microbead displacing along the iridocorneal angle. b) Slow and controlled injection with simultaneous bead dispersion along the iridocorneal angle. c) Aqueous humor outflow pathway edited from (Crawley et al., 2012). Cartoon created with Biorender.com.

To understand whether or not the second microbead injection compromised the overall IOP profile, the area under the curve of the IOP profiles from both samples was analysed (Fig. 3.9 e). No significant difference was found between the two AUC IOPs (G.HT.sham 2MBI vs G.HT.sham 1MBI >0.9999), therefore the animals that received 2 MBIs were included in the G.sham group for RGCs morphological analysis.

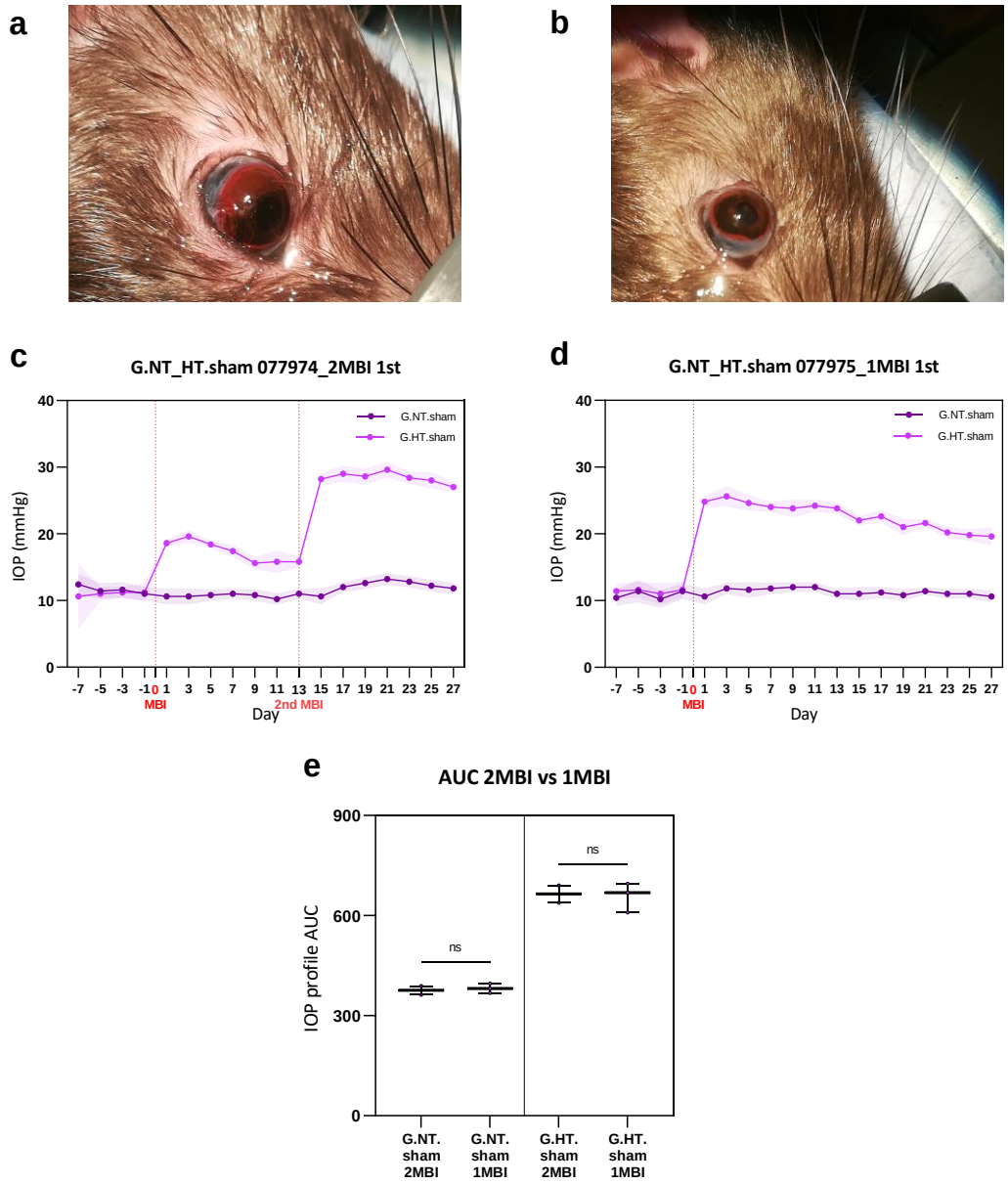

Figure 3. 9. Effect of different injection techniques on Brown Norway IOP profile. a) Representative picture of post fast intracameral microbeads injection. b) Representative picture of post slow and controlled intracameral microbeads injection. c) Injection technique illustrated in (a) required a second microbead injection to prolong a moderate IOP elevation for four weeks, as shown in the IOP profile. d) One microbead injection as illustrated in (b) was sufficient to produce a moderate IOP elevation for four week, as shown in the IOP profile. e) Area under the curve of IOP profile. Line mean value of complete set of IOP recording shaded area ± SD. Box and whisker plot; bottom whisker minimum value; box blot 1st quartile, median and 3rd quartile; upper whisker maximum value; dots single values. Mann-Whitney test; ns= non significant.

3.3.2.2 *Baseline glaucoma IOP profiles*

Ocular hypertension was induced unilaterally in 11 Brown Norway rats. The IOP was measured every other day, one week prior the induction and four weeks after (Fig. 3.10 a; Appendix A.2). All the rats had a sustained elevated IOP for all the experimental period, confirming the successful induction of chronic ocular hypertension. The peak IOP did not exceed 30 mmHg in any animals The post MBI AUC (Fig. 3.10 b) highlighted the significant difference between G.NT.sham and G.HT.sham (p = <0.0001), that proved the accurate induction of a chronic *in vivo* model of OHT glaucoma.

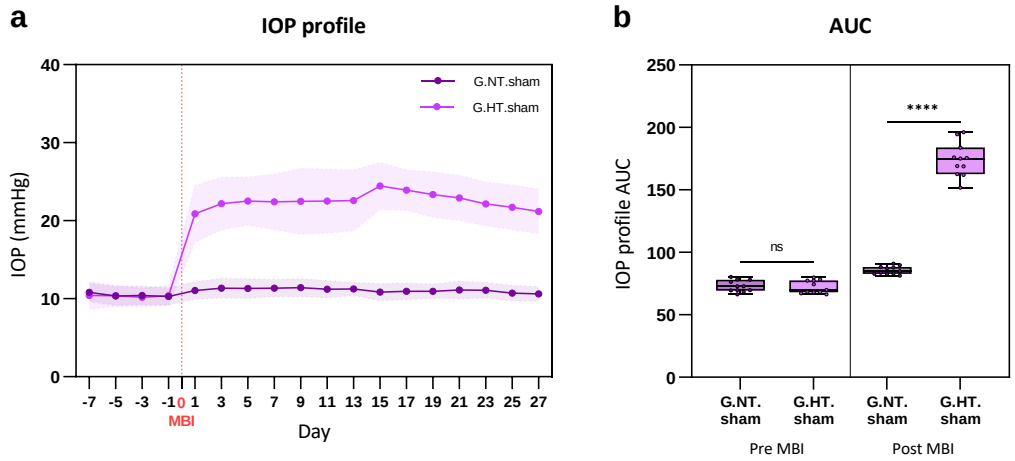

Figure 3. 10. Intraocular pressure profile unilateral model of OHT glaucoma. a) G.sham group IOP profile. Line mean value of complete IOP recordings ; shaded area ± SD. b) Area under the IOP curve. Box and whisker plot. Whiskers, minimum and maximum value; plot, 1st quartile, median and 3rd quartile. Dots, single rat value. Ordinary one-way ANOVA followed by Tukey's *post hoc* test; **** = p < 0.0001, ns = non significant, p = > 0.05. Post-MBI AUC IOP has been normalised to pre-MBI AUC IOP following: $x(norm.factor) = \frac{\Sigma\ post\ MBI\ recordings}{\Sigma\ pre\ MBI\ recordings}$.

3.3.2.3 *Ocular hypertension induces retinal ganglion cells dendritic atrophy*

A standard *in vivo* model of chronic hypertensive glaucoma, in order to mirror the pathophysiological features of the disease, should display retinal ganglion cell dendritic atrophy and at least 30% cell loss (McKinnon et al., 2009). To identify whether this model was accurately reproducing the disease parameters, the morphology of DiOlistically labelled RGCs was analysed and compared with the normotensive positive control C.NT.sham.

Analysing the Sholl profile of the group a profound left shift of the curve was observed, which represents the loss of dendritic arbours complexity (Fig. 3.11 c). A significant observation was that this trend was affecting both contralateral (G.NT.sham) and ipsilateral (G.HT.sham) eye, suggesting a contralateral effect of the pressure rise. In detail, based on the mean AUC of each group (C.NTsham 4151.87 ± 2120.55 SD; G.NT.sham 3140 ± 1048.18 SD; G.HT.sham 2552.53 ± 1201.66 SD) G.NT.sham displayed a 25% AUC decrease ($p = 0.0027$) and G.HT.sham 40% AUC reduction ($p = <0.0001$) compared to the control (Fig. 3.11 d). This extensive atrophy affected all the other parameters related to RGC dendritic architecture. The maximum number of intersection at the Sholl peak decreased 19% in the G.NT.sham group ($p = 0.0009$) and 23% in the G.HT.sham ($p = <0.0001$) compared to the C.sham, while there was just a 5% decrease in the G.HT.sham compared to the contralateral eye ($p = 0.3079$; Fig. 3.11 e). Similarly, the total length of the dendrites steadily decreased in each group compared to the control (26% G.NT.sham, $p = 0.0011$; 40% G.HT.sham, $p = <0.0001$; Fig. 3.11 f). Considering these parameters, the dendritic field area reduction (G.NT.sham 19%, $p = 0.0468$; G.HT.sham 40%, $p = <0.0001$; Fig. 3.11 h) and the dendrites distribution at each branching level (Fig. 3.11 g) goes beyond peripheral dendritic pruning, but reflects the dendritic reshaping that precedes RGCs cell loss.

At a cellular level, the average distance between cells in the G.sham decreased (Fig. 3.11 i), as well as the cellular density at the GCL (G.NT.sham, $p = 0.0039$; G.HT.sham $p = 0.0054$; Fig. 3.11 j), indicating OHT-induced RGC loss.

As expected, RGCs ON-centre were less affected than the OFF-centre. Although the level of damage was less prominent among the ON-centre, G.HT.sham.ON still lost 37% in overall complexity compared to the matched G.sham control. The effect on the OFF-centre was greater, with 36% reduction in the G.NT.sham.OFF and 43% in the G.HT.sham.OFF (Fig. 3.11 k-m).

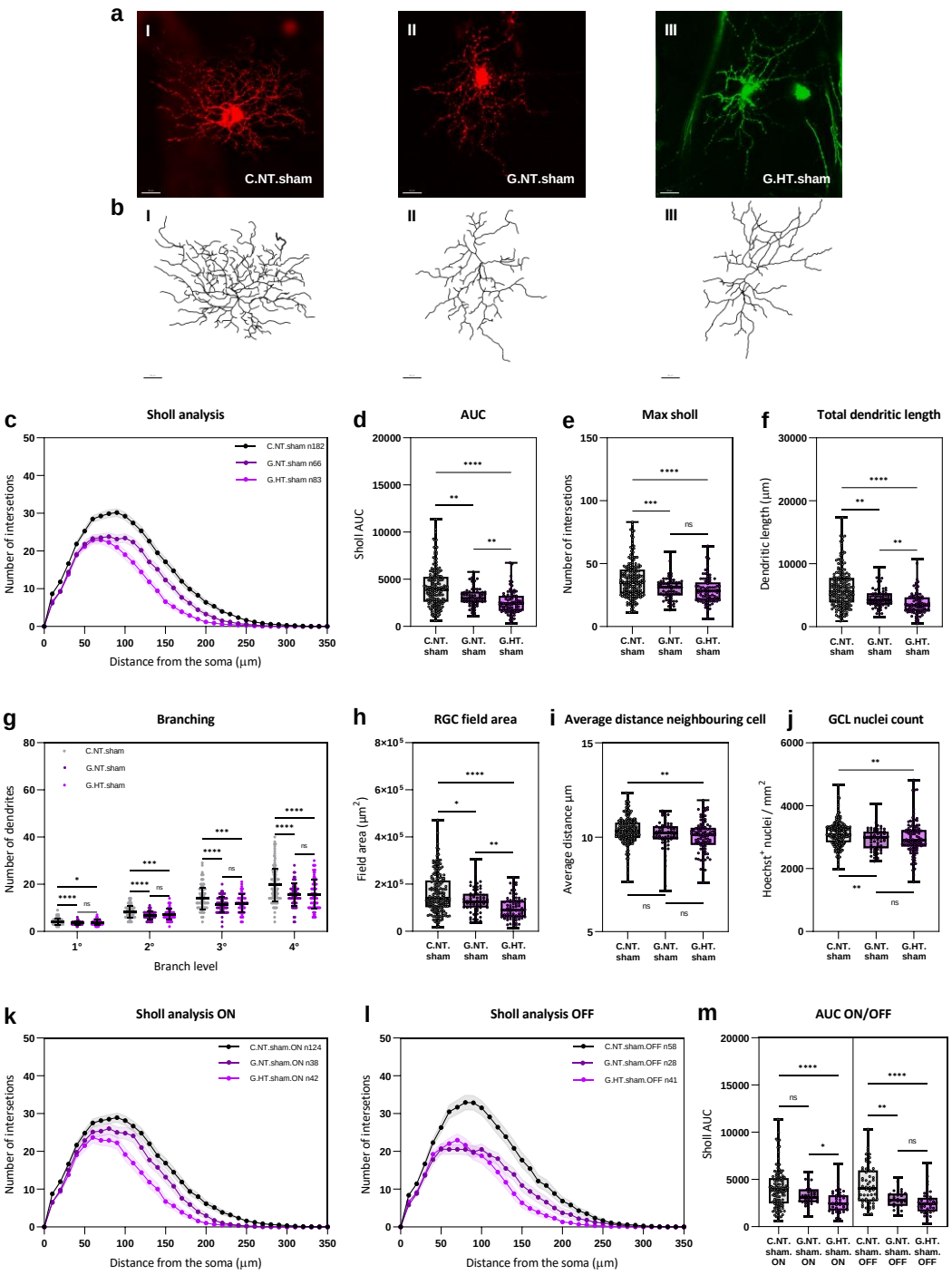

Figure 3. 11. Retinal ganglion cells morphological profile following induction of unilateral ocular hypertension. a, b) DiOlistically labelled RGCs with corresponding Imaris reconstruction. Scale bar 70 µm, image pixel size 2048 x 2048. c) Sholl analysis of all reconstructed RGCs. Line mean value at each interval; shaded area ± SEM. d) area under the Sholl curve (AUC). e) Maximum number of total dendritic intersections at the Sholl peak. f) Total dendrites length. g) Number of the dendrites at proximal soma branches. Individual values ± SD. h) Dendritic field area. i) Average distance between neighbouring cells at the GCL. j) Nuclei count at the GCL. k, l) Sholl Analysis of reconstructed RGCs according to their receptive

field. m) Area under the Sholl curve of RGCs divided according to their receptive field. Box and whiskers plot with individual values. Whiskers, minimum and maximum value; box plot, 1st quartile, median and 3rd quartile; dots, individual value. Kruskal-Wallis test followed by uncorrected Dunn's test. Ns = non significant. Ns = $p > 0.05$; * = $p < 0.05$; ** = $p < 0.01$; *** = $p < 0.001$; **** = $p < 0.0001$.

3.4 Discussion

Most of the scientific literature reports pressure around 20 mmHg as normotensive rat IOP parameter, but all the experimental recording were taken either on restrained or anaesthetised animals (Urcola et al., 2006, Eastlake et al., 2021, Jia et al., 2000, Tribble et al., 2021b, Tribble et al., 2021a). Although restraining methods and anaesthesia might be time-convenient, those technique introduce a pressure bias which affects both normotensive and hypertensive parameters. The introduction of training and positive reinforcement to acquaint the animals to unrestrained IOP measurements decreased by half the IOP and minimised the SD, in contrast to what has been commonly reported for Brown Norway rats (Morrison et al., 2009). This refinement strategy was humane-oriented, focusing on the animal wellbeing, which reduced the stress at the minimum. It has to be said that this method is time consuming and, if it not carefully planned in advance, can interfere with the tight deadlines each research has to respect (Smith and Lilley, 2019). To dedicate enough time to train each animal without interfering with the research plan, a maximum of six animals was in experiment simultaneously, while the others were in training (von Kortzfleisch et al., 2020). Splitting the experimental group in "mini-population" guaranteed the reproducibility of the data, which could also be tested with independent experiments.

These robust baseline parameters, and established training techniques, laid strong foundation for a reliable investigation of RGC OHT-related changes. With average C.sham IOPs of 10.05 mmHg ± 1.44 SD, and G.NT.sham of 11.08 mmHg ± 1.10 SD and G.HT.sham of 22.52 mmHg ± 3.41 SD, it was established that the pressure rise obtained with the refined injection technique, that ensured the complete and stable coverage of the iridocorneal angle, was moderate and sufficient to mimic chronic hypertensive glaucomatous damage. Although experimental pressure above 30 mmHg produce RGCs damage, this magnitude of pressure increase can also induce uveitic RGC damage (Baneke et al., 2016, Cunningham and Zierhut, 2017), which is different and more severe that normal glaucomatous OHT and introduces a confounder in the analysis (Lewkowicz et al., 2015, Din et al., 2014, Baneke et al., 2016).

Without any apparent inflammatory confounder, this model of moderate chronic OHT produced a dendritic remodelling that was not affecting only the terminal branches but also the proximal dendrites, which is a hallmark of extensive degeneration (Tribble et al., 2014). When these characteristics are combined with cell loss they meet the clinical criteria of end point glaucomatous pathology.

The choice of having a naïve control instead of using the contralateral not injected eye as normotensive control might be in conflict with a "reduction principle". However, that choice unveiled a conspicuous contralateral effect that would not have been detected otherwise. Published works suggest that ipsilateral OHT may activate microglia responses in the contralateral eye (Ramírez et al., 2015, Ramírez et al., 2010, Tribble et al., 2021a), which supports the contralateral damage detected in G.NT.sham. In light of that, if the contralateral eye would have been used as control, the degree of dendritic atrophy in the ipsilateral eye would have been underestimated. In addition, this observation is highly relevant in the clinical practice because supports topical IOP management on both eyes, even in the absence of clinically established OHT.

To have a wider overview, an electroretinogram for each rat should have been included to determine the degree of visual loss (Wilsey and Fortune, 2016). Although it could have been informative, it was outside the scope of the project, and already well documented in the same Brown Norway microbead model of glaucoma, showing a major impairment of retinal ganglion cell functions (Eastlake et al., 2021).

In summary, it can be said that the refinements on both C.sham and G.sham helped to produce a reliable model that can be reproduced over time, redefining the classical murine IOP parameters without stress and restraining confounders. The new injection technique guaranteed a sustained moderate OHT over a period of 4 weeks, reproducing the typical feature of ocular hypertensive-induced degeneration, including different degree of RGC atrophy among ON- and OFF-centre RGCs (Della Santina and Ou, 2017). Which might be the causes of this neurodegeneration and whether can be either prevented or reversed will be subject of discussion in the next chapters.

4 Effect of long term nicotinamide adenine mononucleotide administration on normotensive Brown Norway rats

4.1 Overview

The success and feasibility for any NAD^+-related treatment for retinal ganglion cells neuroprotection depends on the baseline effect that every NAD^+ precursor has on wild type animals at doses that exceed those advised for nicotinamide-based dietary supplements (Hwang and Song, 2020). Retinal ganglion cells can be extremely sensitive to energy variations (Ito and Di Polo, 2017, Liu and Prokosch, 2021) and that can have repercussions on the dendritic architecture, thence on the neural circuitry.

NAD^+ precursors have been used to improve several aspects of retinal metabolism (Hui et al., 2020, Williams et al., 2017b), but we do not know the effects of long term administration of NAM on dendritic architecture in healthy RGCs. To address this issue, normotensive naïve rats have been provided with a NAM enriched diet for four weeks. The intraocular pressure was checked to determine whether NAM affected the normal IOP profile, and immediately post-mortem, dissected retinas were labelled by gene gun delivery of lipophilic dyes (DiOlistic labelling). The RGCs dendritic morphology of randomly labelled RGCs was analysed to determine if NAD adversely affected normal RGC parameters.

4.1.1 Experimental setup

In order to identify the safety and tolerance of long-term NAM administration, two groups of naïve Brown Norway rats (six rats per groups) were exposed for four weeks to NAM enriched diet at two different concentrations (low dose – LNAM – 200 mg/day/kg; high dose – HNAM – 600 mg/day/kg; refer to chapter 2 for a detailed description). Rats IOPs were monitored every other day to exclude any potential secondary effect on IOP profile and therefore classify all rats as normotensive. At the end of the four weeks, the rats were culled by increasing CO_2 concentrations, eyes were promptly enucleated post mortem, and retinas immediately dissected. Flat mounted retinas, with the RGCL oriented upward, were labelled using DiOlistics and nuclei stained post fixation. Treatment efficacy and sustainability was evaluated as a function of dendritic complexity compared to age-matched controls.

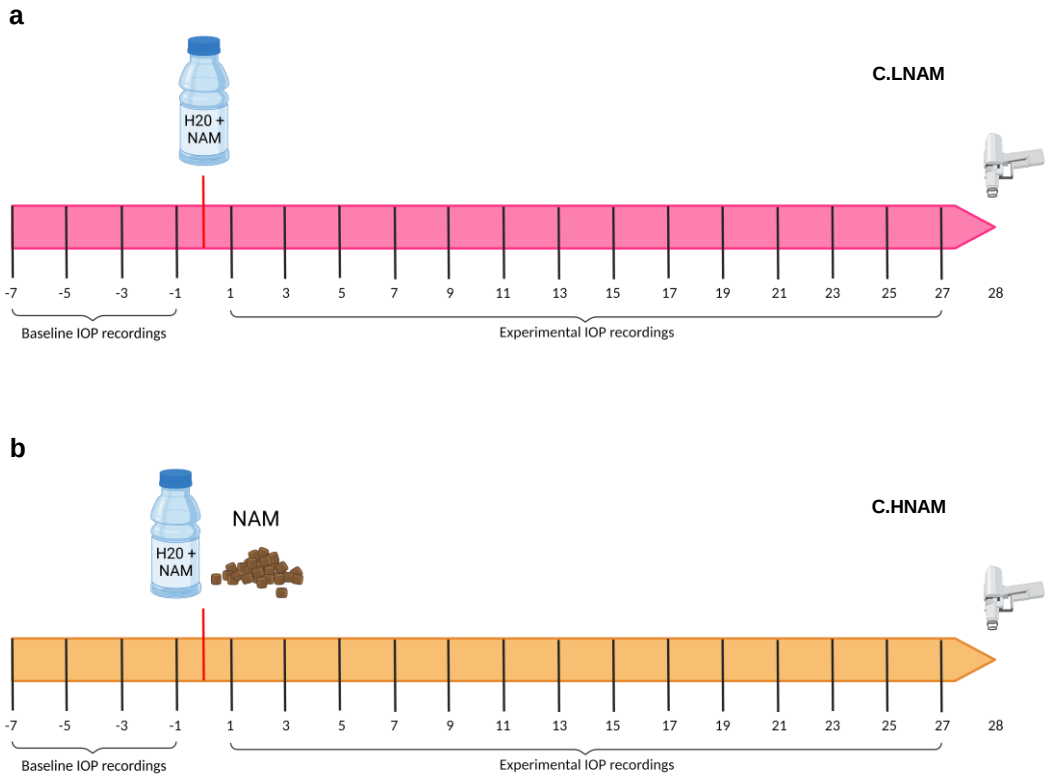

Figure 4. 1. Experimental workflow NAM-treated normotensive Brown Norway rats. a) Low dose NAM treatment (LNAM, 200 mg/day/kg). b) High dose NAM treatment (HNAM, 600 mg/day/kg). Rats were continuously exposed to NAM enriched diet for four weeks. Colour coded according to the experimental groups presented in the results section.

4.2 Results

4.2.1 Nicotinamide adenine mononucleotide does not affect intraocular pressure

Intraocular pressure measurement is the first approach to identify any potential detrimental change that might affect RGC viability. IOPs were monitored for all the experimental period and no changes were detected from the baseline recording, as shown by the single rat and group IOP profiles, but just some insignificant variation due to the rat behaviour during the recordings (Appendix fig. 2; Fig. 4.2).

Both groups maintained their normotensive state indicating that NAM was not interfering with the mechanism that regulate intraocular pressure. Thus, it was hypothesised that if any change would have been detected in the dendritic structure that would not have been related to any pressure change.

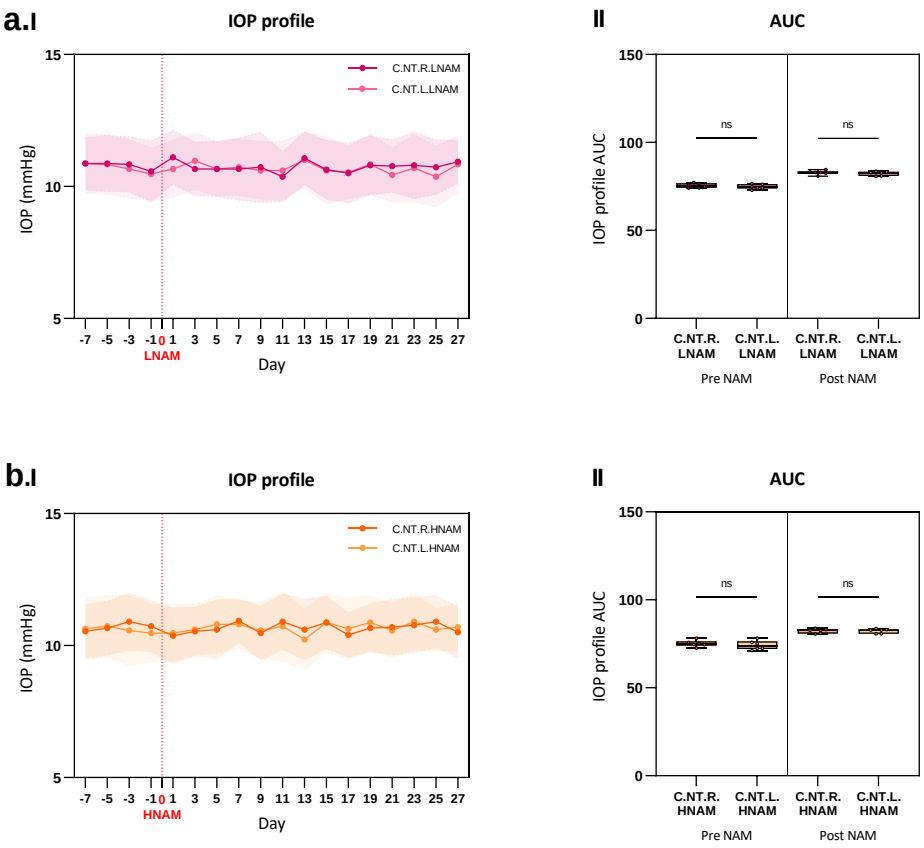

Figure 4. 2. IOP pressure profile of normotensive NAM-treated Brown Norway rats. a) I, C.NT.LNAM group IOP profile. II, area under the IOP profile curve. b) I, C.NT.HNAM group IOP profile. II, area under the IOP profile curve. For the IOP profiles, line represents mean value of complete set of recordings, shaded area ± SD. For the AUC, box and whisker plot represents minimum value, 1st quartile, median, 3rd quartile and maximum value. Each dot represents the values included in the statistical analysis. Ordinary one-way ANOVA followed by Tukey's *post hoc* test; ns = non significant. Post-NAM AUC IOP has been normalised to pre-NAM AUC IOP following: $x(norm.factor) = \frac{\Sigma\ post\ NAM\ recordings}{\Sigma\ pre\ NAM\ recordings}$.

4.2.2 Nicotinamide adenine mononucleotide promotes dendritic plasticity in adult normotensive rats

To evaluate any change in RGC dendritic morphology with NAM treatment, DiOlistically labelled RGCs were individually reconstructed and dendritic structural parameters analysed. RGCs from the NAM normotensive groups were morphologically more complex than their age-matched control (Fig. 4.3 a,b I-III). Scholl analysis revealed a dose-dependent higher level of complexity in the NAM groups mainly gathered between 50 – 150 µm from the soma centre (Fig 4.3 c). The area under the sholl curve (AUC), which is a simplified measure of average dendritic complexity,

did not show any overall significant change between the C.LNAM and C.sham ($p = 0.0915$), while in the C.HNAM there was a significant overall increase in complexity compared to the low dose ($p = 0.0417$) and the sham ($p = <0.0001$. Mean AUC ± SD; C.sham, 4151.87 ± 2120.55; C.LNAM, 4607.61 ± 2182.84; C.HNAM, 5579.29 ± 3138.43; Fig. 4.3 d). However, when the parameters that contributed to the dendritic complexity were analysed individually, the peak in the C.LNAM sholl curve was significant in terms of maximum number of intersections compared to C.sham ($p = 0.0021$; Fig. 4.3 e). In spite of these changes in dendritic complexity, dendritic field area was unaffected (Fig. 4.3 h), even though variations in the total dendritic length were observed among the groups (Fig. 4.3 f). The changes in the shape of the Sholl plot indicated that the change in complexity occurred closers to the cell soma and was not affecting the complexity of the peripheral dendrites. In the C.HNAM, the gain in complexity was greatest in the primary branches, whereas the number of primary branches of the C.LNAM dendritic trees were similar to the C.sham, suggesting a dose-dependent effect for all the dendritic structural parameters (Fig. 4.3 g).

In both the LNAM and HNAM group the RGC counts were similar, with no evidence of clustered cell loss – which is a sign of cell distress and low cell viability – suggesting that NAM treatment did not have an adverse effect on RGC structure (Fig 4.3 i, j). In a further sub analysis of RGCs according to the depth of stratification in the IPL, both ON and OFF centre RGCs demonstrated a similar increase in dendritic complexity in proximal dendrites (Fig. 4.3 k-m). These observation confirmed the safety of high doses of NAM for RGC protection and the lack of any interaction with IOP.

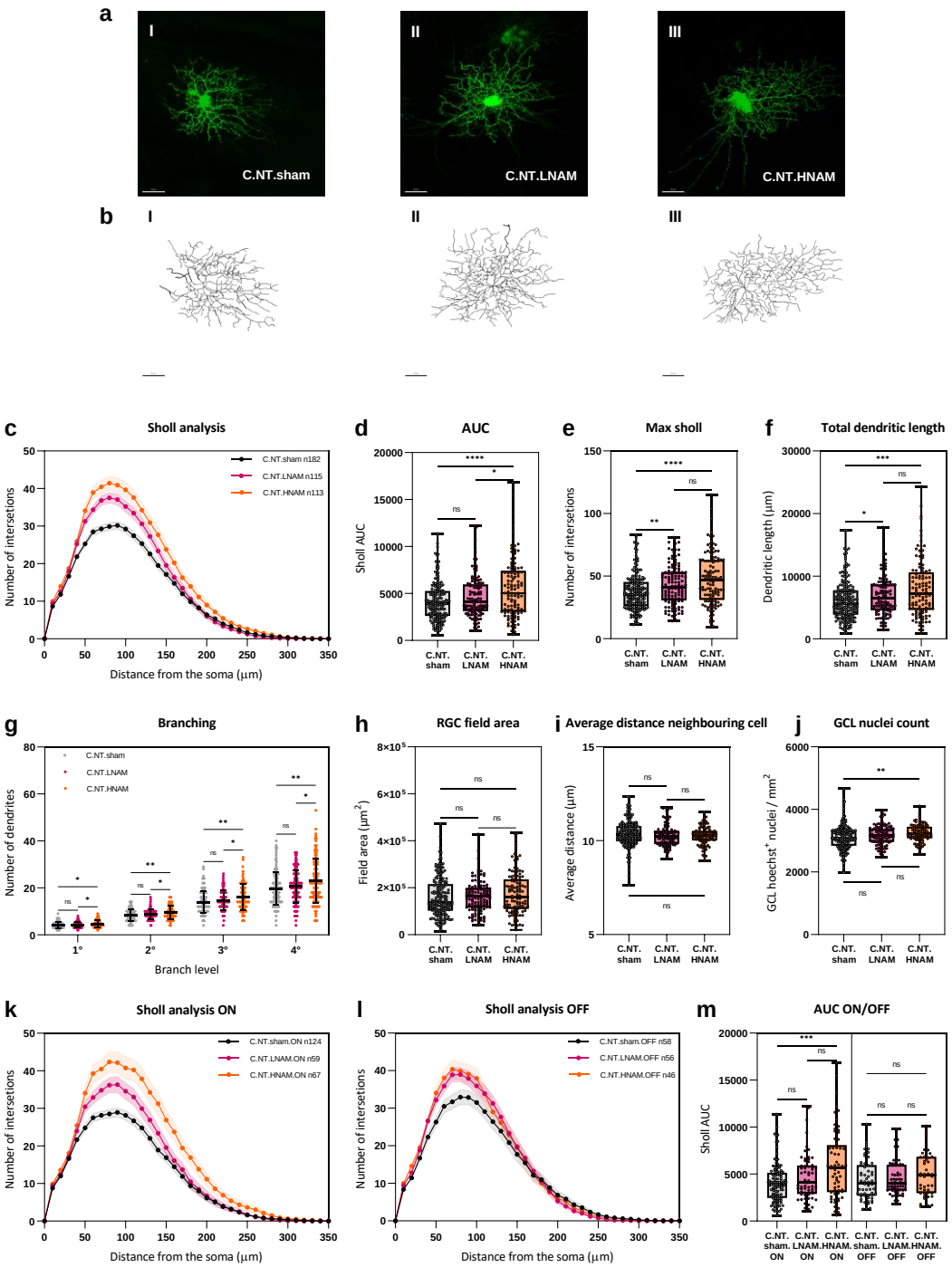

Figure 4. 3. Retinal ganglion cells morphological profile of NAM-treated Brown Norway normotensive rats. a, b) DiOlistically labelled RGCs with corresponding Imaris reconstruction. Scale bar 70 µm, image pixel size 2048 x 2048. c) Sholl analysis of all reconstructed RGCs. Line mean value at each interval; shaded area ± SEM. d) area under the Sholl curve (AUC). e) Maximum number of total dendritic intersetions at the Sholl peak. f) Total dendrites length. g) Number of the dendrites at proximal soma branches. Individual values ± SD. h) Dentritic field area. i) Average distance between neighbouting cells at the GCL. j) Nuclei count at the GCL. k, l) Sholl Analysis of reconstructed RGCs according to their receptive field. m) Area

under the Sholl curve of RGCs divided according to their receptive field. Box and whiskers plot with individual values. Whiskers, minimum and maximum value; box plot, 1st quartile, median and 3rd quartile; dots, individual values. Kruskal-Wallis test followed by uncorred Dunn's test. Ns = non significant, $p > 0.05$; * = $p < 0.05$; ** = $p < 0.01$; *** = $p < 0.001$; **** = $p < 0.0001$.

4.3 Discussion

Retinal ganglion cells have been extensively studied and classified for many years (Sun et al., 2002a, Sun et al., 2002b, Sanes and Masland, 2015), and their changes during development and disease meticulously described (Sernagor et al., 2001, Kim et al., 2021, Tribble et al., 2014). In the absence of an external insult, such as the loss of adjacent cells, studies have not demonstrated any innate plasticity in the adult RGCs. The increase in dendritic complexity in proximal dendrites is an unexpected finding. It is important to note that the receptive field area did not increase in size consistent with the tendency for RGCs to tile and limit receptive field area depending on interactions with adjacent cells.

While the role of NAD^+ precursors in the treatment of metabolic impairments in the pathophysiology of glaucoma has generated considerable interest (Williams et al., 2017c, Cimaglia et al., 2020), the doses used in preliminary clinical evaluation[2] are below those used in experimental models (Hui et al., 2020, De Moraes et al., 2022). NAM is a direct inhibitor of Rho-associated protein kinases (ROCKs; ROCK1 and ROCK2) (Meng et al., 2018). Inhibition of these kinases have been found to promote dendritic and synaptic plasticity (Swanger et al., 2015, Koch et al., 2018) which might explain the increase in dendritic complexity in the NAM groups. ROCKs inhibitors have also been developed to reduce intraocular pressure in glaucoma (Goldhagen et al., 2012), so these collective effects would be beneficial for RGCs.

In summary, the increase in proximal dendritic complexity found in the NAM groups demonstrated that prolonged administration of high doses of NAM does not compromise RGCs viability, that would have otherwise shown sign of dendritic retraction (Tao and Rolls, 2011). The preservation of dendritic tiling ensures that NAM does not interact with predetermined pathway that regulates the retinal mosaic (Reese and Keeley, 2015).

[2] Clinical trial NAM dose in use 1.5g and 3g a day. Human equivalent dose (HED) for Low NAM 2.3g/day; HED High NAM 6.8g/day.

5 Nicotinamide adenine mononucleotide retinal ganglion cells neuroprotection in mouse retinal explant model

5.1 Overview

Accurate assessment of retinal ganglion cells neuroprotection can only be achieved in experimental conditions that mimic disease features. Mouse retinal explants offer this advantage with a well defined injury (*i.e.* axotomy), which allows the precise timing of the insult without being costly and time consuming as an *in vivo* model (Gancharova et al., 2013).

Retinal explants are commonly used to evaluate retinal ganglion cells viability under the effect of different neuroprotective agents or stressors (Pattamatta et al., 2016, Binley et al., 2016), and has helped to gain new insights into retinal degenerative mechanisms (Schnichels et al., 2021, Schnichels et al., 2019, Murali et al., 2019).

Although NAM safety and tolerance was validated *in* vivo, prior to test whether or not NAM could provide sufficient neurotrophic support in *in vivo* ocular hypertension, retinal explants offered the perfect middle ground to test NAM efficacy to protect RGCs in degenerative-trigger conditions.

5.1.1 Experimental setup

To explore whether NAM could have been a suitable neuroprotective agent, this hypothesis was tested using mouse retinal explants (Fig. 5.1).

Three experimental groups were established:

1. Control (labelled as E.0DEV.sham; 0 days ex vivo), where the dissected retinas were immediately processed without culturing time (DiOlistic labelling within 5 minutes of enucleation).
2. Disease (labelled as E.3DEV.sham; 3 days ex vivo), where the dissected retinas were cultured for 72 hr with normal culturing media
3. Disease + NAM (labelled as E.3DEV.NAM; 3 days ex vivo), where the dissected retinas were cultured for 72 hr with culturing media supplemented with nicotinamide at two different concentrations, calculated based on NAM neuroprotective effect achieved in the DBA/2J (2D) nicotinamide trial (Williams et al., 2017b)
    a. 100mM NAM (LNAM)

b. 500mM NAM (HNAM)

Retinal labelling and RGCs morphological analysis were performed as described in chapter 2.

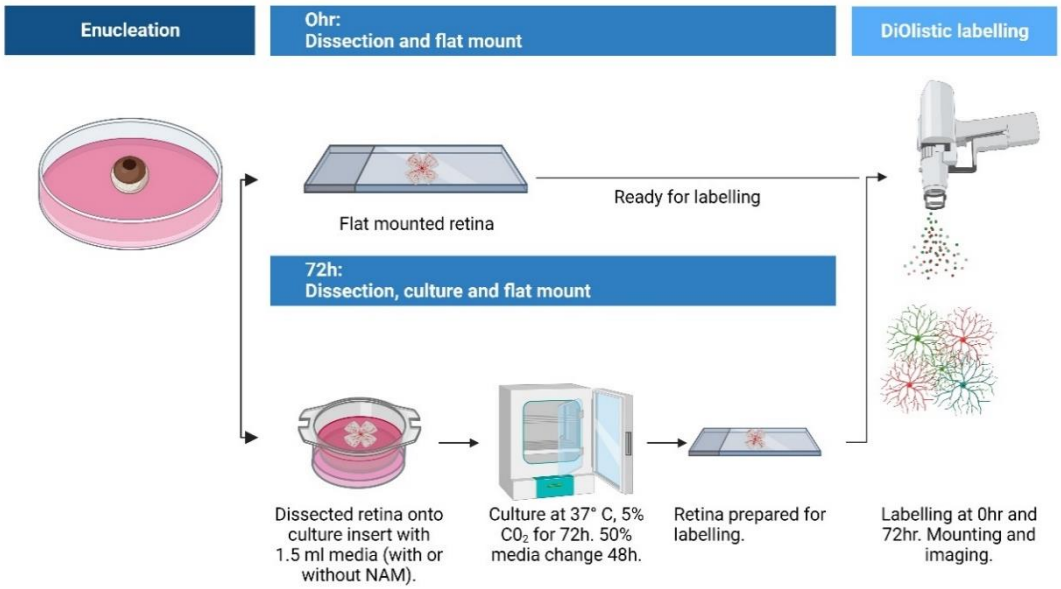

Figure 5. 1. Retinal explant experimental workflow.

5.2 Results

5.2.1 NAM supplemented culturing media mitigates *ex vivo* RGCs degeneration

Sholl analysis of Diolistically labelled RGCs revealed a severe dendritic atrophy within the untreated cultured retinas (E.3DEV.sham) compared to the control group (E.0DEV.sham; Fig. 5.2 c). In contrast, NAM supplemented media mitigated RGCs atrophy to the point that no differences could be observed between NAM groups (E.3DEV.LNAM and E.3DEV.HNAM) and E.0DEV.sham Sholl profiles (Fig. 5.2 c). The Sholl AUC, which represents a measure of overall dendritic complexity, highlighted the marked reduced complexity of E.3DEV.sham RGCs (mean ± SD; E.0DEV.sham 2133.87 ± 897.68; E.3DEV.sham 1121.70 ± 653.61, p = <0.0001; Fig. 5.2 d), while no significant differences could be found in the NAM groups (E.3DEV.LNAM 1983.39 ± 869.19, p = 0.3739; E.3DEV.HNAM 1958.71 ± 882.37, p = 0.2268; Fig. 5.2 d). The number of dendritic intersections in the E.3DEV.sham was reduced compared to E.0DEV.sham (p = <0.0001), identified as max Sholl (Fig. 5.2 e), which was expected considering the profound left shift in the Sholl curve. By contrast, the treated groups did not show any reduction at the Sholl

peak (E.3DEV.LNAM, p = 0.5663; E.3DEV.HNAM, p = 0.5920; Fig. 5.2 e) nor in overall dendritic length (E.3DEV.LNAM, p = 0.3958; E.3DEV.HNAM, p = 0.2712; Fig. 5.2 f). This level of dendritic preservation in both high and low NAM treated retinas was evident from the preservation of primary dendritic branches, confirming that RGCs from treated cultures did not show any sign of degeneration, while the level of complexity of the untreated groups was steadily decreasing at each branch level (Fig. 5.2 g). Although NAM treatment was effective in preserving dendritic complexity in a stressful environment, it did not always preserve the dendritic field area. Some reduction in the dendritic field area was observed within the HNAM group, with almost 18% loss compared to E.0DEV.sham (E.0DEV.sham 87601.18 ± 38233.58; E.3DEV.HNAM 72412.45 ± 38361.56, p = 0.0076; Fig. 5.2 h), while no significant difference was address between E.0DEV.sham and E.3DEV.LNAM (80528.25 ± 42311.47, p = 0.1619). Even though E.3DEV.HNAM showed a reduced field area compared to the control, this reduction was not severe as the 44% field area loss observed in the untreated group E.3DEV.sham (49534.8 ± 29812.48; Fig 5.2 h).

Although RGCs morphology was preserved with NAM enriched media, nuclear counts were reduced in all the cultured groups (mean ± SD; E.0DEV.sham 3606.08 ± 766.84; E.3DEV.sham 2233.66 ± 991.33, p = <0.0001; E.3DEV.LNAM 2997.92 ± 943.70, p = 0.0002; E.3DEV.HNAM 2098 ± 476.47, p = <0.0001; Fig. 5.2 j). As expected, the average distance between neighbouring cells was increased (Fig. 5.2 i). To note, the tissue structure of the cultured retinas was less compact than the E.0DEV.sham non-cultured retina.

A sub analysis of RGCs determined if ON and OFF centred retinal ganglion cells were selectively affected based on the analysis of changes in the inner (ON) and outer (OFF) sublamina distribution of dendrites. Overall, all groups OFF-centre RGCs were less complex. However, only E.3DEV.sham displayed a left shift in the Sholl curve in both sub-classes (Fig. 5.2 k-l), with a significant loss of dendritic complexity (Fig. 5.2 m), while no significant differences were observed between E.0DEV.sham and the treated groups E.3DEV.LNAM and E.3DEV.HNAM (Fig. 5.2.k-m).

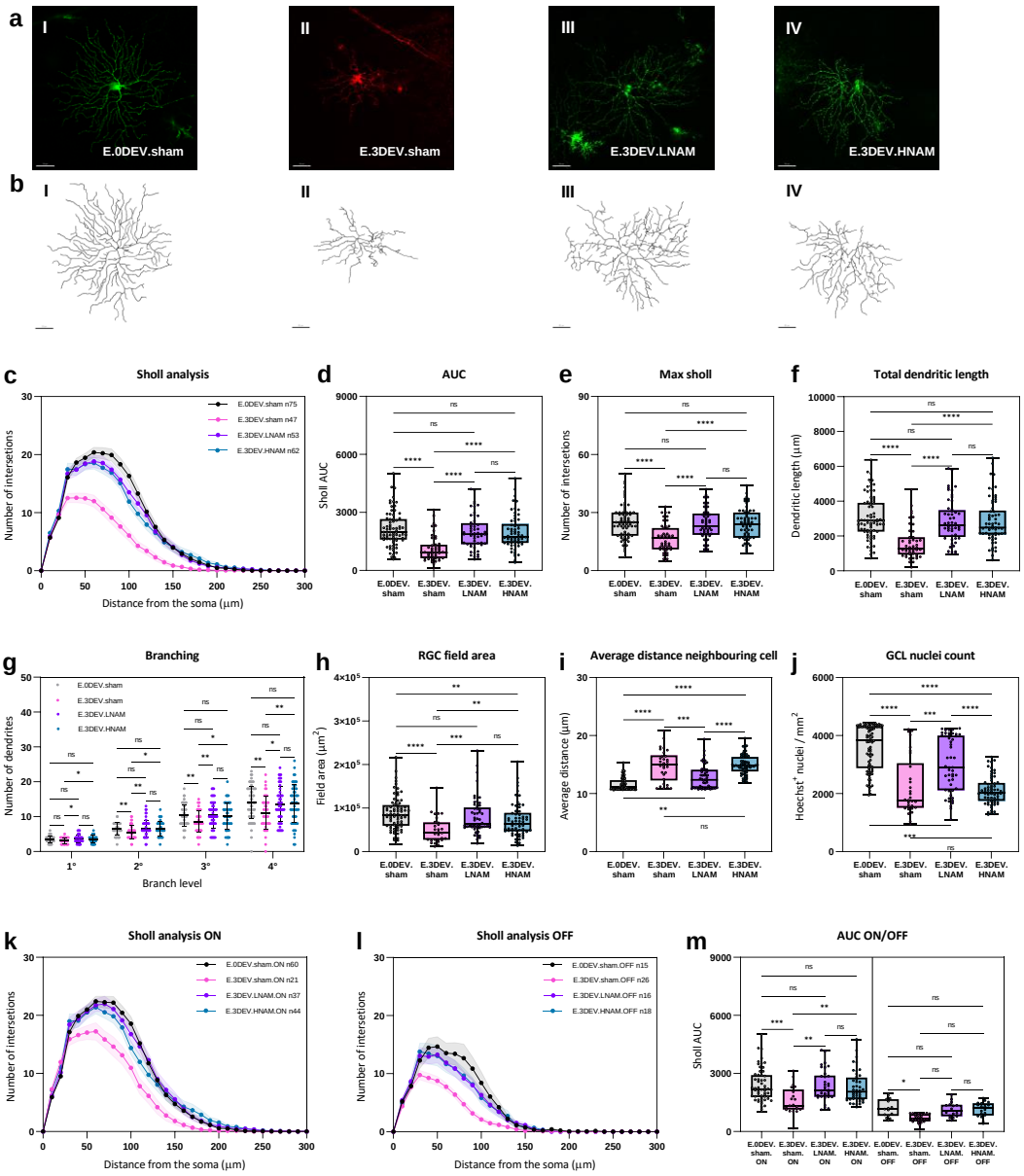

Figure 5. 2. Axotomised retinal ganglion cells morphological profile following 72h culture with NAM supplemented media. a, b) DiOlistically labelled RGCs with corresponding Imaris reconstruction. Scale bar 50 µm, image pixel size 1024 x 1024. c) Sholl analysis of all reconstructed RGCs. Line mean value at each interval; shaded area ± SEM. d) Area under the Sholl curve (AUC). e) Maximum number of total dendritic intersections at the Sholl peak. f) Total dendrites length. g) Number of the dendrites at proximal soma branches. Individual values ± SD. h) Dendritic field area. i) Average distance between neighbouring cells at the GCL. j) Nuclei count at the GCL. k, l) Sholl Analysis of reconstructed RGCs according to their receptive field. m) Area under the Sholl curve of RGCs divided according to their receptive field. Box and whiskers plot with individual values. Whiskers, minimum and maximum value; box plot, 1st quartile, median and 3rd quartile; dots, individual value. Kruskal-Wallis test followed by uncorrected Dunn's test. Ns = non significant, $p > 0.05$; * = $p < 0.05$; ** = $p < 0.01$; *** = $p < 0.001$; **** = $p < 0.0001$. DEV = days *ex vivo*.

5.3 Discussion

Retinal organotypic cultures are a valuable intermediate model to study progressive degeneration and neuroprotection in a controlled environment prior to proceed to *in vivo* studies (Muller et al., 2017). The degeneration of RGCs starts within a few hours after axotomy, with sign of apoptosis already 1 day *ex vivo* (Johnson et al., 2016, Manabe et al., 2002). In light of this, 3 days *ex vivo* endpoint were a good timeframe to measure any potential NAM neuroprotective effect (Binley et al., 2016). Indeed, E.3DEV.sham RGCs lost 48% of dendritic complexity in 72h, while E.3DEV.LNAM less than 7% and E.3DEV.HNAM around 8%, demonstrating that NAM could protect RGCs from dendritic atrophy.

Although RGC dendritic morphology was maintained following NAM treatment, cell loss proceeded in all cultured retinas, surprisingly with a greater degree of cell loss in retinas treated with high dose NAM (E.3DEV.sham 39%; E.3DEV.LNAM 17%; E.3DEV.HNAM 42%). According to Beckers *et. al.* 2019 report (Beckers et al., 2019), dendritic shrinkage (in zebrafish) may be an adaptive response to promote axon regrowth, with dendritic regeneration occurring only after axonal reinnervation. Whether this counteractive interplay takes place in the mammalians CNS is still unknown (Beckers and Moons, 2019), but if that would be possible, in axotomised retinal ganglion cells that mechanism would be brought to the extreme. Hence preventing RGCs dendritic atrophy might potentially promote RGCs death.

A second hypothesis could be that even though NAM supported RGCs structural preservation at the applied concentrations, those doses might have been sufficient only for a fraction of the entire RGC population, and thus the ones lacking this support progressively dying (Alarautalahti et al., 2019).

Considering these results, and the hypothetical potential trade-off between dendritic degeneration and cell survival in RGC degenerative-prone contexts, NAM effect on RGCs connectome was considered worth to be investigated in the BN OHT microbead model of glaucoma.

6 *In vivo* prophylactic and intervention nicotinamide adenine mononucleotide treatment rescues retinal ganglion cells from hypertensive-induced dendritic atrophy

6.1 Overview

Data on the potential effects of nicotinamide treatment on normotensive rats (chapter 4) and retinal explant model (chapter 5), were informative for the design of a study to determine the effect of NAM treatment for RGC protection in glaucoma.

Although some neuroprotective effects have already been addressed using the retinal explants, an *in vivo* model reproduces the more complex physiology seen with clinical glaucoma.

The use of NAM dietary enrichment in models of glaucoma is not new. It has been tested on DBA/2J (D2) mice, and as neuroprotective agent for early neurodegenerative changes in BN model of OHT (Williams et al., 2017c, Williams et al., 2018, Williams et al., 2017b, Tribble et al., 2021c). Although, NAM-derived RGCs neuroprotection was explored in these models, either by the selective RGC marker RNA-binding protein with multiple splicing (RBPMS) or by RNA sequencing, the absence of cell loss does not confirm the absence of RGC degeneration. There is a pressing need to determine whether RGC structure and function can be restored in glaucoma.

RGCs undergo a prolonged phase off shrinkage and remodelling prior to cell death (Morgan, 2012), suggesting that they provide a candidate population that can be treated to restore vision in glaucoma.

Conscious of the effect that NAM supplementation had on retinal explants, there was the need to explore *in vivo* whether RGCs atrophy could be prevented in our standardised model of unilateral glaucoma. The experiments were designed with a translational approach, adapting the treatments to the most frequent clinical scenarios. The standard paradigm for the evaluation of neuroprotective treatment was adopted, with the administration of NAM prior to the onset of glaucoma, but the protective effects of NAM given after the induction of ocular hypertension were also evaluated.

In this chapter the effect of NAM treatment will be described in both scenarios and the experimental groups will be referred as G.NAMproph for NAM prophylactic (Low, LNAMproph

and High, HNAMproph according to the dose), and G.NAMint for NAM intervention (Low, LNAMint and High, HNAMint as above).

6.1.1 Experimental setup

To evaluate whether NAM treatment was preserving RGCs integrity through increasing NAD^+ reservoir (Fig. 6.1), this hypothesis was tested in unilateral hypertensive model of glaucoma.

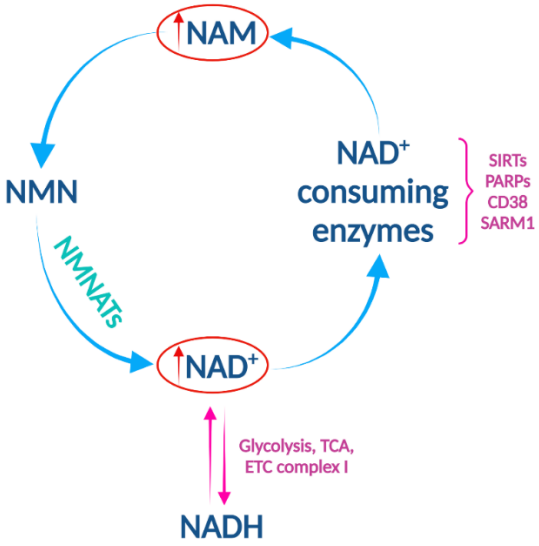

Figure 6. 1. NAD salvage pathway. Increase in NAM, a precursor of NAD, would automatically increase NAD biosynthesis. In a disease context, altering the production of NAD through the salvage pathway may compensate for the increase in NAD consumption or NAD decrease due to age.

The model was induced as explained in chapter 3 and the induction of ocular hypertension assessed with the same technique applied throughout all the project.

The rats were divided in two main experimental groups (Fig. 6.2 a-d):

1) NAM prophylactic treatment (Table 6.1), where the animals were exposed to NAM enriched diet 2 weeks before the induction of ocular hypertension until the end of the experiment, at the following doses:
    a. Low NAM, 200 mg/day/kg (G.LNAMproph), with NAM dissolved in drinking water
    b. High NAM, 600 mg/day/kg (G.HNAMproph), with NAM dissolved in drinking water and irradiated by the manufacturer in custom-made rat food.

Group	NAM dose	Contralateral (NT)	Ipsilateral (HT)
G.LNAMproph	200 mg/day/kg	G.NT.LNAMproph	G.HT.LNAMproph
G.HNAMproph	600 mg/day/kg	G.NT.HNAMproph	G.HT.HNAMproph

Table 6. 1. NAM prophylactic group nomenclature.

2) NAM intervention treatment (Table 6.2), where the animals were exposed to NAM enriched diet 3 days after the induction of ocular hypertension (timed to match IOP peak) until the end of the experiments, at the following doses:
    c. Low NAM, 200 mg/day/kg (G.LNAMint), with NAM dissolved in drinking water
    d. High NAM, 600 mg/day/kg (G.HNAMint), with NAM dissolved in drinking water and irradiated in customised rat food

Group	NAM dose	Contralateral (NT)	Ipsilateral (HT)
G.LNAMint	200 mg/day/kg	G.NT.LNAMint	G.HT.LNAMint
G.HNAMint	600 mg/day/kg	G.NT.HNAMint	G.HT.HNAMint

Table 6. 2. NAM intervention group nomenclature.

Retinal labelling and morphological analysis of RGCs were performed as previously described. In order to estimate NAM neurotrophic support, all the data collected were compared with the positive control C.sham (normotensive untreated group) and the negative control G.sham (unilateral ocular hypertension with no treatment) .

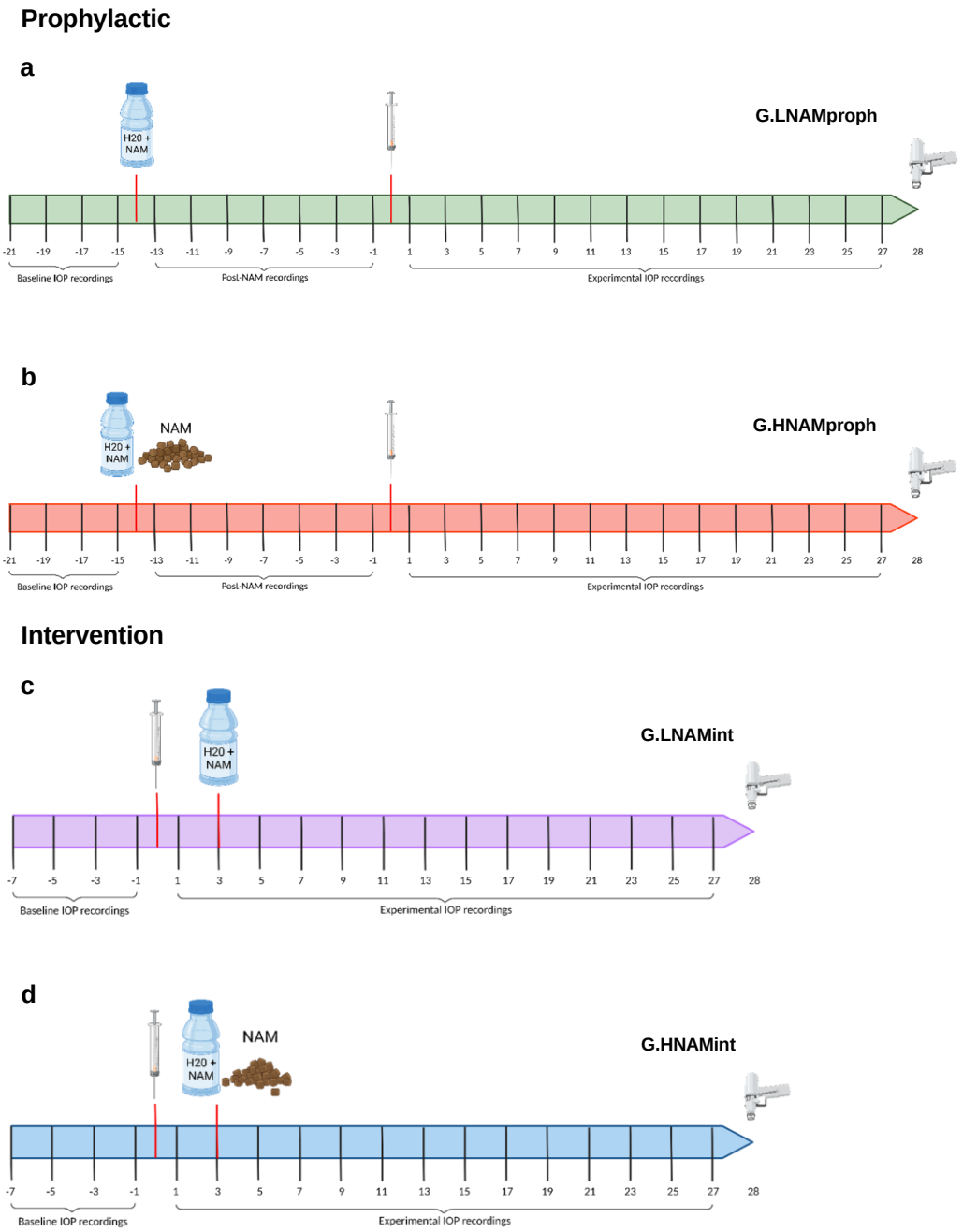

Figure 6. 2. Prophylactic and interventional NAM treatment experimental workflow. Prophylactic treatment, prophylactic treatment was started 2 weeks prior the induction of unilateral ocular hypertension; a) Prophylactic low NAM dose (G.LNAMproph, 200 mg/day/kg), b) Prophylactic high NAM dose (G.HNAMproph, 600 mg/day/kg). Intervention treatment, intervention treatment was started 3 days post induction of unilateral hypertension; c) Intervention low NAM dose (G.LNAMint, 200 mg/day/kg), d) Intervention high NAM dose (G.HNAMint, 600 mg/day/kg).

6.2 Results

6.2.1 NAM prophylactic treatment

6.2.1.1 IOP profile of NAM prophylactic experimental groups

Ocular hypertension was induced on 18 Brown Norway rats treated with NAM at low or high dose two weeks prior to the injection of microbeads. Although NAM has not been shown to affect IOP, BN baseline measurements were recorded a week before NAM treatment and during the experimental period. Six rat were treated with 200 mg/day/kg NAM (LNAMint) and the other twelve with 600 mg/day/kg (HNAMint)[3]. As shown from their IOP profile (Fig 6.3), NAM did not affect intraocular pressure. A chronic and stable increase IOP elevation was maintained in all rats for four weeks (Appendix A.4.1, A.4.2).

The refinement described in chapter 3 allowed the reliable induction of sustained increase in IOP in 100% of BNs, with a significant post MBI difference between the contralateral and the ipsilateral eye (Fig. 6.3 a, b II).

[3] The group size was based on preliminary experiments (data not shown in the thesis) performed to identify the best dose response.

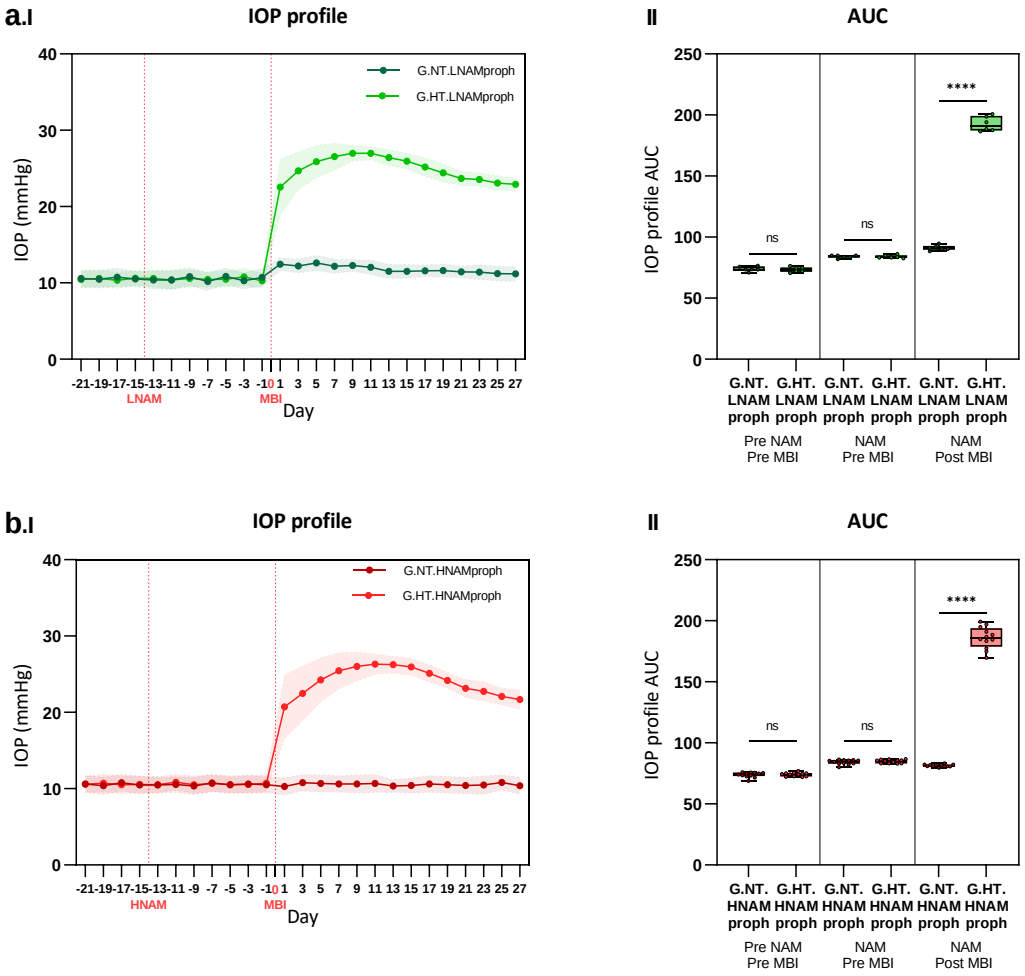

Figure 6. 3. Intraocular pressure profile of prophylactic NAM treated rats with unilateral model of OHT glaucoma. a, I) G.LNAMproph group IOP profile; II) Area under the IOP curve. b, I) G.HNAMproph group IOP profile; II) Area under the IOP curve. Line mean value of complete IOP recordings ; shaded area ± SD. Box and whisker plot. Whiskers, minimum and maximum value; plot, 1st quartile, median and 3rd quartile. Dots, single rat value. Ordinary one-way ANOVA followed by Tukey's *post hoc* test; **** = $p < 0.0001$, ns = non significant, p = > 0.05. NAM pre-MBI AUC IOP has been normalised to pre-NAM pre-MBI AUC IOP following: $x(norm.factor) = \frac{\Sigma\ NAM\ pre\ MBI\ recordings}{\Sigma\ pre\ NAM\ pre\ MBI\ recordings}$. NAM post-MBI IOP AUC has been normalised to pre-NAM pre-MBI AUC IOP following: $x(norm.factor) = \frac{\Sigma\ NAM\ post\ MBI\ recordings}{\Sigma\ pre\ NAM\ pre\ MBI\ recordings}$.

6.2.1.2 Analysis of retinal ganglion cells morphology

The NAM enriched diet was provided for six weeks for the prophylactic group. RGC G.NAMproph parameters were compared with the positive control C.sham (control normotensive) and with the negative control G.sham (untreated unilateral ocular hypertension).

6.2.1.2.1 Low NAM promotes variable degrees of RGCs plasticity following ocular hypertension

It was first determined whether a prophylactic treatment with low dose of NAM would have energetically prepared and supported RGCs capability to react to OHT insult. Sholl analysis of DiOlistically labelled RGCs showed significant preservation of RGCs dendritic morphology (Fig. 6.4 a-b), highlighted by the Sholl curve (Fig. 6.4 c). The Sholl curve showed a greater dendritic density in ipsilateral RGCs (G.HT.LNAMproph) compared to the contralateral RGCs. These changes are summarised with a simplified mathematical representation through the analysis of the AUC, which represents the architectural complexity with a defined number for each RGC analysed. The AUC showed a considerable increase in the G.HT.LNAMproph group, in contrast, no differences were observed between G.NT.LNAMproph and C.sham (G.NT.LNAM proph 4679.00 ± 2766.46 SD, p = 0.3504; G.HT.LNAMproph 5476.30 ± 3300.76, p = 0.0068; Fig. 6.4 d). The number of dendritic intersections at the Sholl peak increased from ≈ 37 in C.sham to ≈ 44 in G.NT.LNAMproph and ≈ 50 in G.HT.HNAMproph (C.sham 37 ± 15 SD ; G.NT.LNAMproph 44 ± 21 SD, p = 0.1186; G.HT.LNAMproph 50 ± 23 SD, p = 0.0005; Fig. 6.4 e), as well as the total length of dendrites (C.sham 6121.01 ± 3123.40 SD; G.NT.LNAMproph 6843.51 ± 3901.76 SD, p = 0.3583; G.HT.LNAMproph 8055.35 ± 4733.64 SD, p = 0.0062; Fig. 6.4 f). Although the increase in neuritic complexity was concentrated between 70 µm and 120µm from the soma, this change did not have any statistical effect on primary branches compared to C.sham (1° G.NT.LNAMproph p = 0.5628, G.HT.LNAMproph p = 0.1630; 2° G.NT.LNAMproph p = 0.9384, G.HT.LNAMproph p = 0.0689; 3° G.NT.LNAMproph p = 0.9877, G.HT.LNAMproph p = 0.1058; 4° G.NT.LNAMproph p = 0.5660, G.HT.LNAMproph p = 0.0558; Fig. 6.4 g), nor influenced the dendritic tiling increasing the dendritic field area (Fig. 6.4 h).

At the GCL, a reduced distance was observed between neighbouring cells and increased cellular density in the treated G.LNAM.proph group (fig. 6.4 i, j). To note, cell count at the GCL was performed counting Hoechst^{+} nuclei. RPBMS staining cannot be performed together with DiOlistics, thus another group of rats would have been required to address RGC specific cell count, and this would have been beyond the budget allocated for the project.

An analysis of the dendritic arborisation according to depth within the IPL did not demonstrate any selective effects of OHT induced damage on ON or OFF RGCs (Fig. 6.4 k-m). However, G.NT.LNAMproph.OFF sample size was very low (n = 6) and it cannot ensure a fair representation of the treatment effect observed in this class.

When compared with the control group C.sham, the low NAM prophylactic treatment offered a discrete neuroprotection from the detrimental effects of OHT. However, to comprehend the magnitude of neuroprotection offered by LNAMproph, the results obtained in G.LNAMproph were compared with the untreated ocular hypertensive model G.sham.

Comparison of ocular hypertensive models, with and without treatment, demonstrated a big difference in the Sholl curves (Fig. 6.5 c), which was reflected in the significant difference between the AUCs, with 49% increase in G.NT.LNAMproph and 114% increase in G.HT.LNAMproph compared to the corresponding untreated condition (G.NT.LNAMproph, $p = 0.0272$; G.HT.LNAMproph, $p = <0.0001$; Fig. 6.5 d). A statistically significant increase was observed in the treated group in the max Sholl and in the total length of dendrites (max sholl, G.NT.LNAMproph, $p = 0.0023$; G.HT.LNAMproph, $p = <0.0001$; Fig. 6.5 e. Total dendritic length, G.NT.LNAMproph, $p = 0.0215$; G.HT.LNAMproph, $p = <0.0001$; Fig. 6.5 f). Similarly, the primary branches did not show atrophic changes, with a consistent increase in complexity at all eccentricities (Fig. 6.5 g). However, no change was observed in the G.NT.LNAMproph RGC area compared to the G.sham matching condition, suggesting some predetermined boundaries between RGCs dendritic extensions (tiling). In contrast, the field area of G.HT.LNAMproph increased compared to G.HT.sham (Fig. 6.5. h).

At the GCL a reduced distance within neighbouring cells was still observed in the G.NT.LNAMproph compared to the untreated counterpart, while any significant difference was addressed within the HT groups (Fig. 6.5 i). Still at the GCL, it was reported an increased cellular density confirming the absence of cell loss (Fig. 6.5 j).

Furthermore, sub-analysis of RGCs classification confirmed that both ON and OFF were equally protected, showing a higher level of complexity compared to the untreated sub-category (Fig. 6.5 k-m).

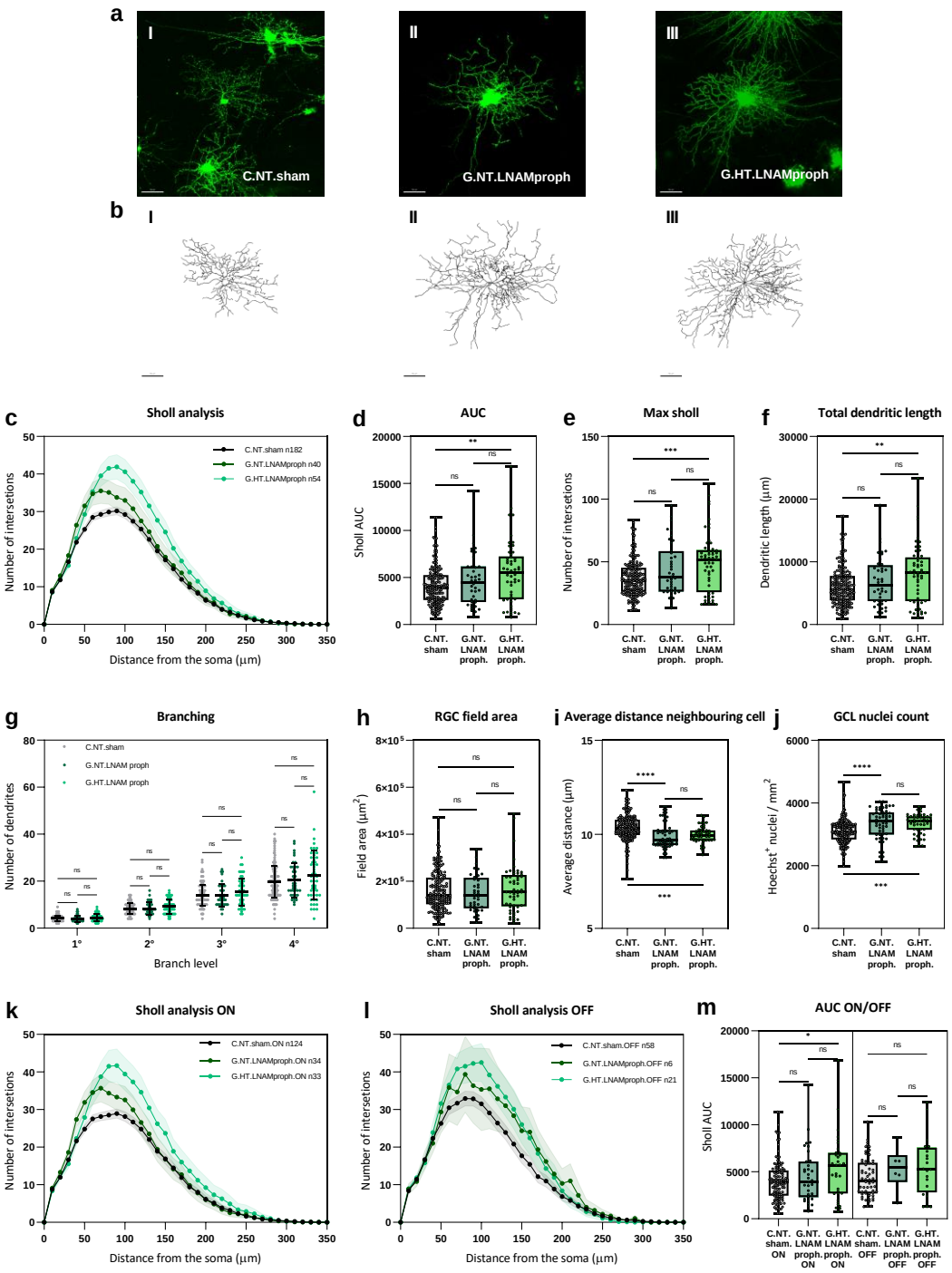

Figure 6. 4. Retinal ganglion cells morphological profile following low dose NAM prophylactic treatment compared to untreated normotensive rats. a, b) DiOlistically labelled RGCs with corresponding Imaris reconstruction. Scale bar 70 µm, image pixel size 2048 x 2048. c) Sholl analysis of all reconstructed RGCs. Line mean value at each interval; shaded area ± SEM. d) Area under the Sholl curve (AUC). e) Maximum number of total dendritic intersections at the Sholl peak. f) Total dendrites length. g) Number of the dendrites at proximal soma branches; individual values ± SD. h) Dendritic field area. i) Average distance between neighbouring cells at the GCL. j) Nuclei count at the GCL. k, l) Sholl Analysis of reconstructed

RGCs according to their receptive field. m) Area under the Sholl curve of RGCs divided according to their receptive field. Box and whiskers plot with individual values. Whiskers, minimum and maximum value; box plot, 1st quartile, median and 3rd quartile; dots, individual values. Kruskal-Wallis test followed by uncorrected Dunn's test. Ns = non significant, p > 0.05; * = p < 0.05; ** = p < 0.01; *** = p < 0.001; **** = p < 0.0001.

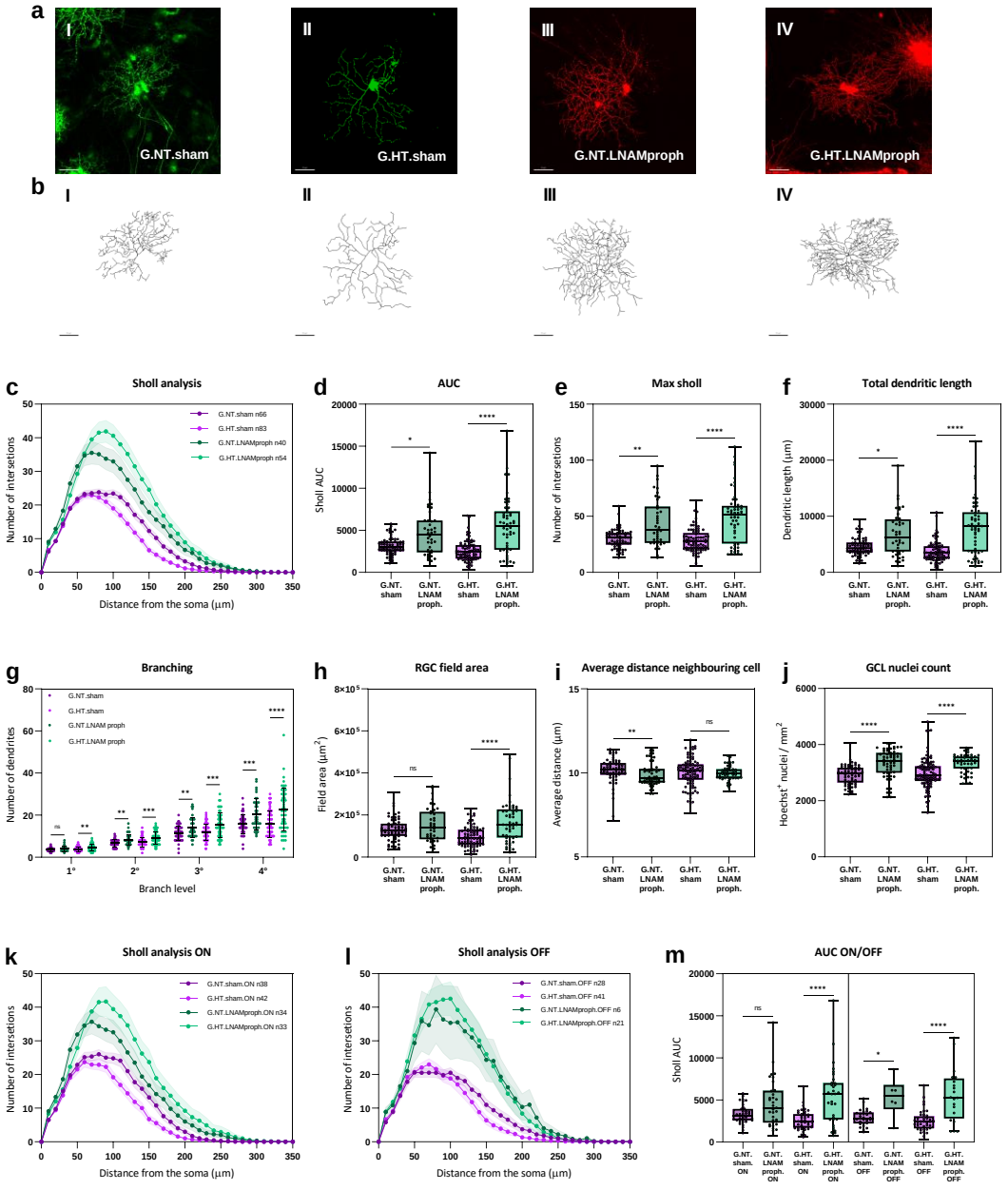

Figure 6. 5. Retinal ganglion cells morphological profile following low NAM prophylactic treatment compared to untreated unilateral OHT glaucoma. a, b) DiOlistically labelled RGCs with corresponding Imaris reconstruction. Scale bar 70 µm, image pixel size 2048 x 2048. c) Sholl analysis of all reconstructed RGCs. Line mean value at each interval; shaded area ± SEM. d) Area under the Sholl curve (AUC). e) Maximum number of total dendritic intersections at the Sholl peak. f) Total dendrites length. g) Number

of the dendrites at proximal soma branches. Individual values ± SD. h) Dendritic field area. i) Average distance between neighbouring cells at the GCL. j) Nuclei count at the GCL. k, l) Sholl Analysis of reconstructed RGCs according to their receptive field. m) Area under the Sholl curve of RGCs divided according to their receptive field. Box and whiskers plot with individual values. Whiskers, minimum and maximum value; box plot, 1st quartile, median and 3rd quartile; dots, individual value. Kruskal-Wallis test followed by uncorrected Dunn's test. Ns = non significant, $p > 0.05$; * = $p < 0.05$; ** = $p < 0.01$; *** = $p < 0.001$; **** = $p < 0.0001$.

6.2.1.2.2 High NAM dose induces the same level of RGCs plasticity in both eyes

To determine if the effects of NAM were dose dependent, a higher NAM dose was tested following the same prophylactic therapeutic regime. Comparison between C.sham and G.HNAMproph revealed a consistent response to the treatment in both contralateral and ipsilateral eyes, with the same Sholl profile and equal increased complexity in G.NT.HNAMproph and G.HT.HNAMproph (Fig. 6.6 c). A peak of 25% AUC increase was measured compared to the untreated normotensive control C.sham (G.NT.HNAMproph 25%, G.HT.HNAMproph 22%), suggesting that NAM was triggering RGCs plasticity (AUCs; G.NT.HNAMproph 5211.65 ± 2909.40 SD, $p = 0.0067$; G.HT.HNAMproph 5093.01 ± 2580.34 SD, $p = 0.0010$; Fig 6.6 d). As consequence of this greater neuritic complexity, an increase in the number of dendritic intersections at the Sholl peak and in the total dendritic length were observed (G.NT.HNAMproph, $p = 0.0006$; G.HT.HNAMproph, $p = 0.0001$; Fig. 6.6 e. G.NT.HNAMproph, $p = 0.0199$; G.HT.HNAMproph, $p = 0.0046$; Fig. 6.6 f). The increase in dendritic complexity was confined between 40 µm and 170 µm from the soma indicating a higher number of primary dendrites (Fig. 6.6 g). In spite of the increase in the complexity of the dendritic trees, the total dendritic field area did not change (Fig. 6.6 h).

High dose NAM preserved a normal cellular disposition at the GCL (C.sham 10.35 ± 0.70 SD; G.NT.HNAMproph 10.16 ± 0.59 SD, $p = 0.0317$; G.HT.HNAMproph, 10.22 ± 0.48 SD, $p = 0.0405$; Fig. 6.6 i), which in the absence of cell loss (Fig. 6.6 j) might indicate that this dose can effectively counteract the pathological cascade triggered by OHT.

Even though RGCs sub-analysis addressed a different response to the treatment depending on the dendritic sub-lamina disposition (ON and OFF RGCs; Fig. 6.6 k-m), overall, high NAM prophylactic produced a more homogeneous response in both ipsilateral and contralateral RGCs. Indeed, when the readouts were compared with G.sham there was a statistically highly significant difference between the two groups.

Improvements in the Sholl profile were observed from the beginning of the Sholl curve (Fig. 6.7 c), with a consequent positive effect on the overall complexity (G.NT.HNAMproph, p = <0.0001; G.HT.HNAMproph, p = <0.0001; Fig. 6.7 d). As it could be expected looking at the Sholl curve, which shows the number of neurites intersection as a function of the distance from the soma, the number of dendritic intersection at the Sholl peak increased as well (G.NT.sham 30.06 ± 8.24 SD, G.NT.HNAMproph 46.77 ± 22.23 SD, p = <0.0001; G.HT.sham 28.55 ± 10.22 SD, G.HT.HNAMproph 45.31 ± 20.06, p = <0.000; Fig. 6.7 e). In view of the marked dendritic atrophy in the G.sham eyes, which drastically affected RGCs architecture, it was no surprise that G.HNAMproph RGCs showed a progressive gain in complexity from the primary branches (Fig. 6.7 g). G.HNAMproph RGCs did not display signs of atrophy nor shrinkage, which was manifested by the significant increase of RGCs dendritic field area compared to G.sham (G.NT.HNAMproph, 169003.68 ± 84702.82, p = 0.0094; G.HT.HNAMproph, 176159.02 ± 80784.70, p = <0.0001; Fig. 6.7 h).

Although the overall distance between neighbouring cells was found to not be statistically significant (G.NT.sham, 10.14 ± 0.78, G.NT.HNAMproph, 10.16 ± 0.59, p = 0.8545; G.HT.sham, 10.03 ± 0.83, G.HT.HNAMproph, 10.22 ± 0.48, p = 0.1037), the individual values from G.HNAMproph group were closer to the values included within the 3rd quartile of the G.sham group (Fig. 6.7 i). In contrast, the cell density at the GCL was significantly higher in the treated group (based on group mean value, G.NT.HNAMproph 14% increase compared to G.NT.sham, G.HT.HNAMproph 13% increase compared to G.HT.sham; Fig.6.7 j).

Analysis of RGCs dendritic architecture according to their IPL lamination detected a greater complexity among OFF-centre RGCs from both ipsilateral and contralateral eyes compared to the untreated counterpart (Fig. 6.7 k-m).

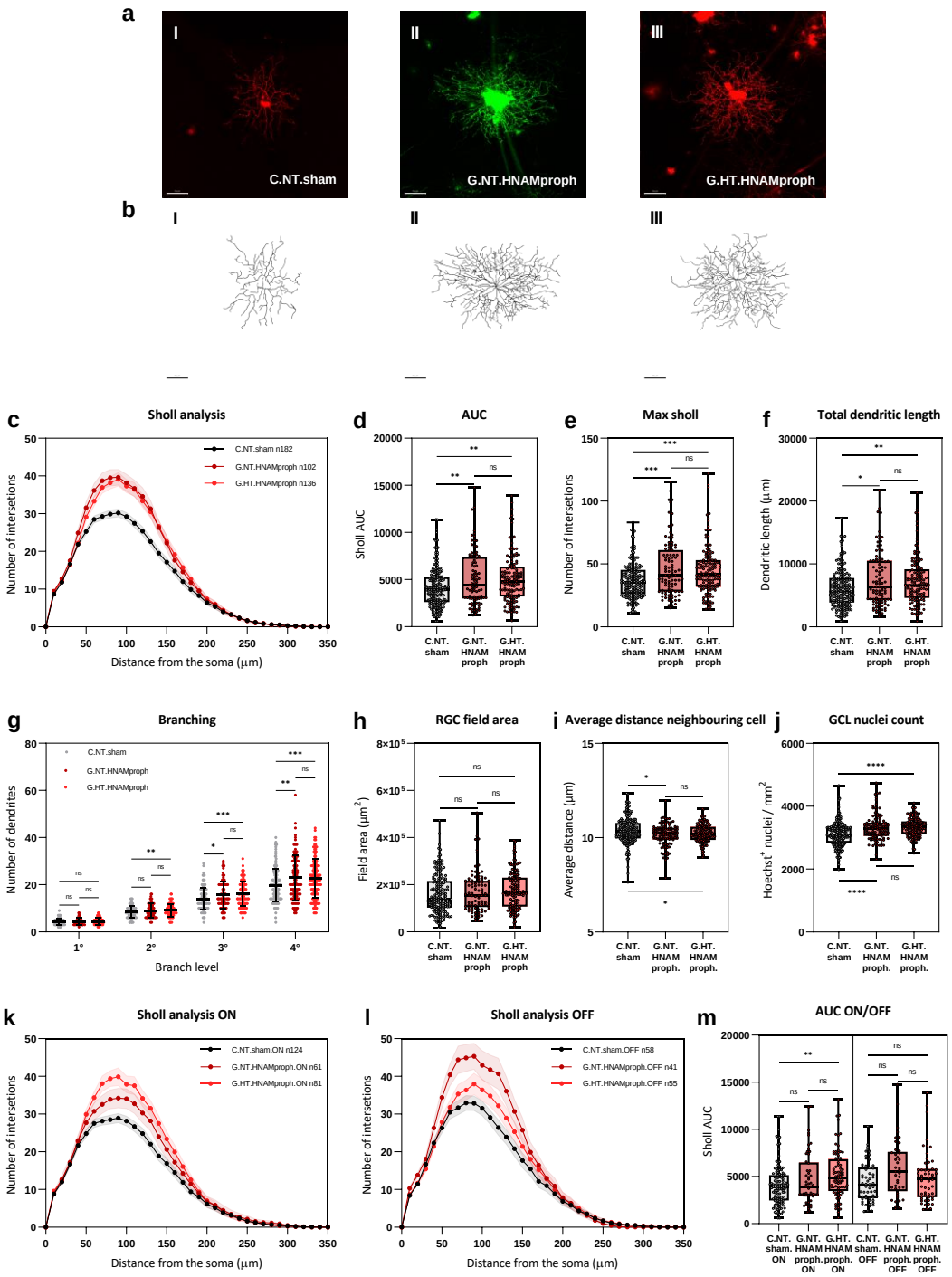

Figure 6. 6. Retinal ganglion cells morphological profile following high dose NAM prophylactic treatment compared to untreated normotensive rats. a, b) DiOlistically labelled RGCs with corresponding Imaris reconstruction. Scale bar 70 µm, image pixel size 2048 x 2048. c) Sholl analysis of all reconstructed RGCs. Line mean value at each interval; shaded area ± SEM. d) Area under the Sholl curve (AUC). e) Maximum number of total dendritic intersections at the Sholl peak. f) Total dendrites length. g) Number of the dendrites at proximal soma branches; individual values ± SD. h) Dendritic field area. i) Average distance between neighbouring cells at the GCL. j) Nuclei count at the GCL. k, l) Sholl Analysis of

reconstructed RGCs according to their receptive field. m) Area under the Sholl curve of RGCs divided according to their receptive field. Box and whiskers plot with individual values. Whiskers, minimum and maximum value; box plot, 1st quartile, median and 3rd quartile; dots, individual value. Kruskal-Wallis test followed by uncorrected Dunn's test. Ns = non significant, p > 0.05; * = p < 0.05; ** = p < 0.01; *** = p < 0.001; **** = p < 0.0001.

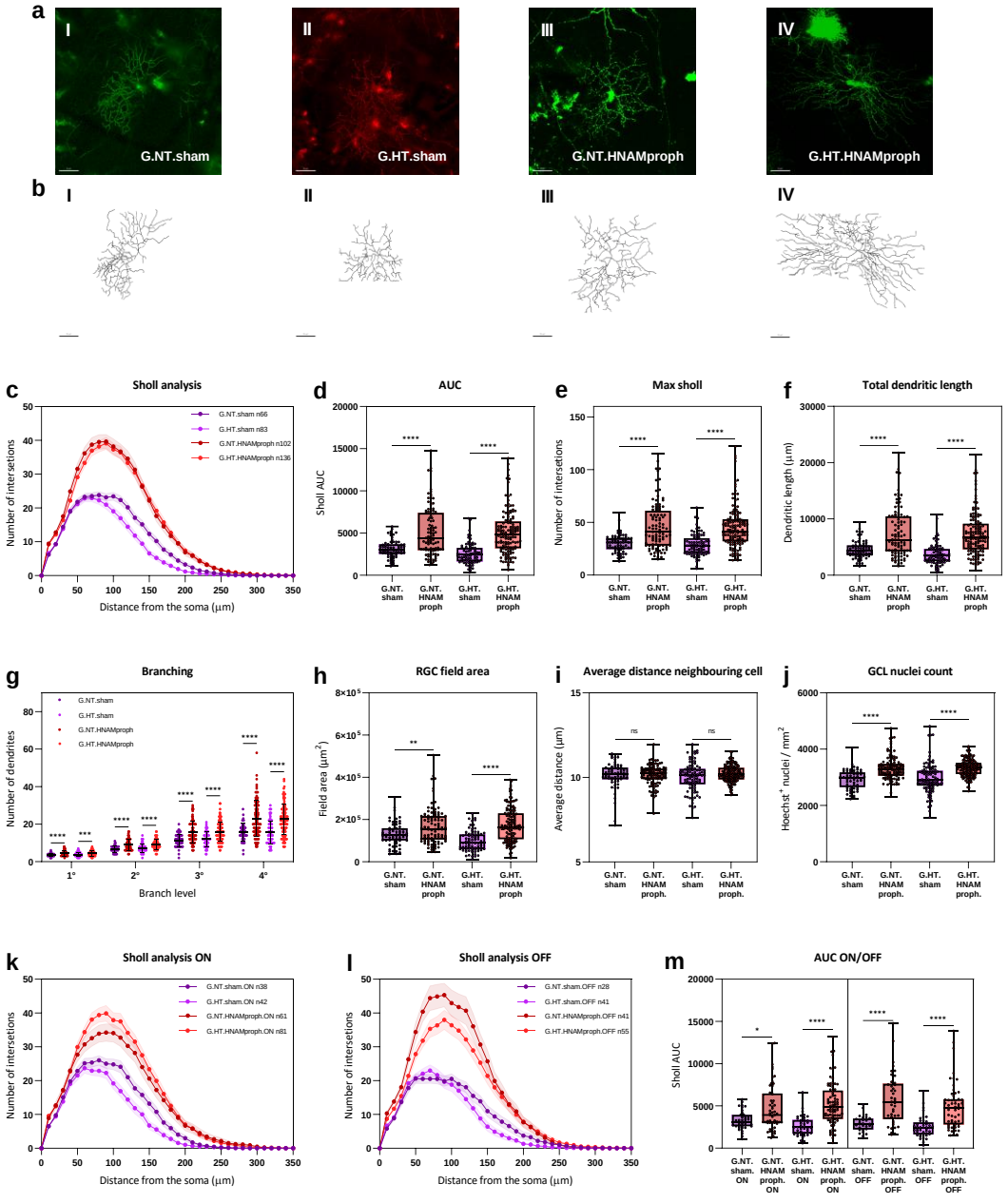

Figure 6. 7. Retinal ganglion cells morphological profile following high NAM prophylactic treatment compared to untreated unilateral OHT glaucoma. a, b) DiOlistically labelled RGCs with corresponding Imaris reconstruction. Scale bar 70 µm, image pixel size 2048 x 2048. c) Sholl analysis of all reconstructed RGCs. Line mean value at each interval; shaded area ± SEM. d) area under the Sholl curve (AUC). e)

Maximum number of total dendritic intersections at the Sholl peak. f) Total dendrites length. g) Number of the dendrites at proximal soma branches. Individual values ± SD. h) Dendritic field area. i) Average distance between neighbouring cells at the GCL. j) Nuclei count at the GCL. k, l) Sholl Analysis of reconstructed RGCs according to their receptive field. m) Area under the Sholl curve of RGCs divided according their receptive field. Box and whiskers plot with individual values. Whiskers, minimum and maximum value; box plot, 1st quartile, median and 3rd quartile; dots, individual value. Kruskal-Wallis test followed by uncorrected Dunn's test. Ns = non significant, $p > 0.05$; * = $p < 0.05$; ** = $p < 0.01$; *** = $p < 0.001$; **** = $p < 0.0001$.

6.2.2 NAM intervention treatment

6.2.2.1 IOP profiles of NAM intervention experimental groups

To assess whether or not NAM treatment was protecting RGCs from glaucomatous damage even following the induction of OHT, OHT was induced in 18 Brown Norway rats[4] and the animals exposed to the NAM intervention treatment 3 days post OHT induction. Even in that case, NAM did not interfere with IOP (Fig. 6.8 a, b), and all the rats with one single microbead injection had a sustained IOP increase for all the experimental period (Appendix A.4.1, 4.2). After the injections, six rat were fed with 200 mg/day/kg NAM (LNAMint) and the other twelve with 600 mg/day/kg (HNAMint).

[4] The group size was based on preliminary experiments (data not shown in the thesis) performed to identify the best dose response.

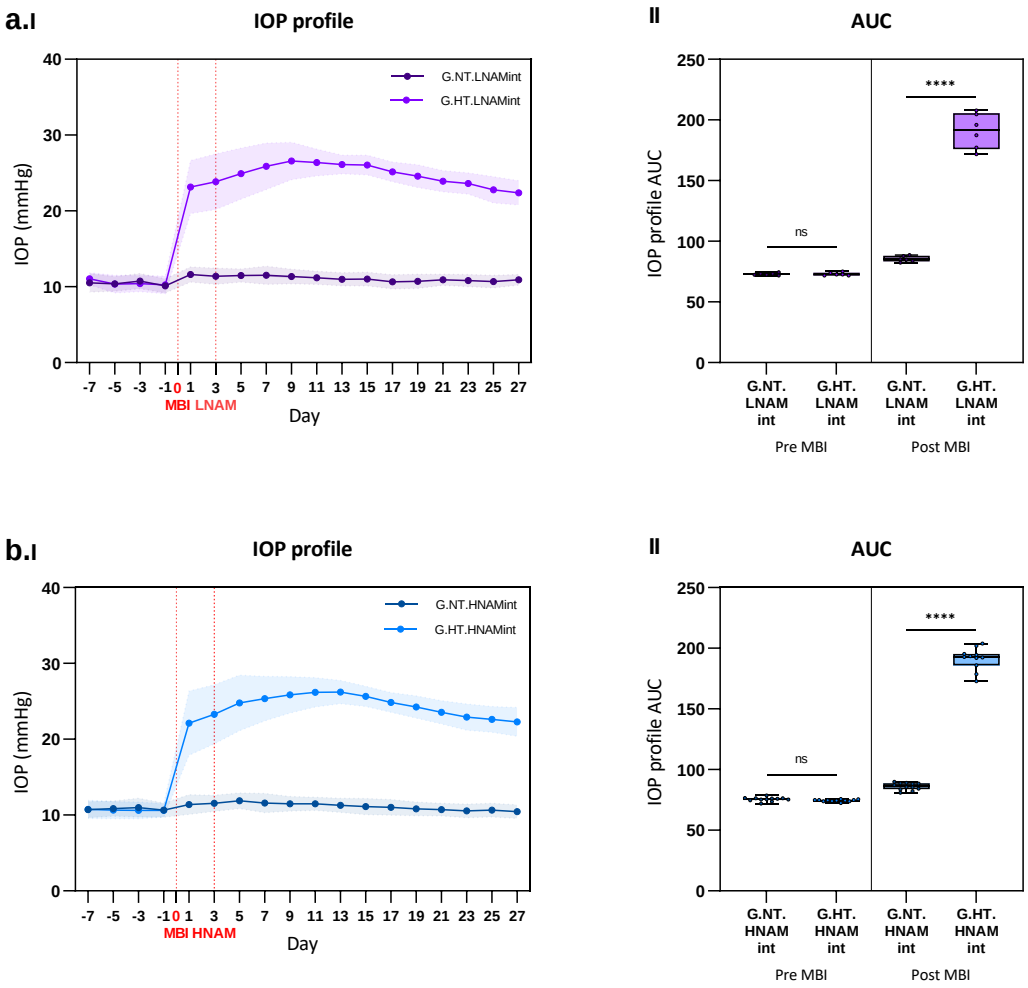

Figure 6. 8. Intraocular pressure profile of NAM intervention treated rats with unilateral model of OHT glaucoma. a, I) G.LNAMint group IOP profile; II) Area under the IOP curve. b, I) G.HNAMint group IOP profile; II) Area under the IOP curve. Line mean value of complete IOP recordings ; shaded area ± SD. Box and whisker plot. Whiskers, minimum and maximum value; plot, 1st quartile, median and 3rd quartile. Dots, single rat value. Ordinary one-way ANOVA followed by Tukey's *post hoc* test; **** = $p < 0.0001$, ns = non significant, p = > 0.05. Post-MBI AUC IOP has been normalised to pre-MBI AUC IOP following: $x(norm.factor) = \frac{\Sigma\ post\ MBI\ recordings}{\Sigma\ pre\ MBI\ recordings}$.

6.2.2.2 Analysis of retinal ganglion cells morphology

The classification of C.sham and G.sham RGCs allowed an accurate comparison with a robust positive and negative control. NAM intervention treatment was tested on models with existing ocular hypertension, thus when RGC G.NAMint parameters will be compared with the positive control C.sham, any non significant difference between the groups has to be read as a positive result (Fig. 6.9 G.LNAMint; Fig. 6.11 G.HNAMint). In contrast, when G.NAMint RGCs parameters

will be compared with the negative control G.sham, statistically significant results represent a positive change (Fig. 6.10 G.LNAMint; Fig.6.12 G.HNAMint).

6.2.2.2.1 Low NAM dose reduces RGCs atrophy following ocular hypertension

Sholl analysis of RGCs from contralateral (NT) and ipsilateral (HT) eyes demonstrated that the neurotrophic support given by LNAMint restored normal dendritic parameters. The benefit was greatest in the contralateral normotensive eye (G.NT.LNAMint), while minimised the atrophy of ipisilateral RGCs (G.HT.LNAMint), when compared to the positive control C.sham (Fig. 6.9 c). The area under Sholl curve (AUC) did not show any significant difference between C.sham (AUC 4151.87 ± 2120.55 SD) and G.NT.LNAMint (AUC 4172.42 ± 2124.87 SD; $p = 0.9815$), while dendritic atrophy in the G.HT.LNAMint could not be completely prevented (AUC 3408.21 ± 2145.56 SD; $p = 0.0016$; Fig. 6.9 d). However, this dendritic retraction was more severe at the periphery, considering that the primary branches were minimally affected (Fig. 6.9 g) and the total number of dendritic intersections at the Sholl peak did not change significantly as well (Fig. 6.9 e). Indeed, that was confirmed by the analysis of the total dendritic length and the dendritic field area, where it was observed a reduction in the G.HT.LNAMint (Fig. 6.9 f, $p = 0.0033$; Fig. 6.9 h, $p = 0.0015$), but no significant changes in the contralateral G.NT.LNAMint.

Analysis at the GCL did not reveal any sign of cell clustering, as a prelude of poor cell viability, nor cell loss (Fig. 6.9 i, j).

Similarly, when RGCs structural responses were analysed according to their receptive field, it could not be noticed any significant difference with the untreated RGC group. G.HT.LNAMint was still the only group showing a left shift in the Sholl curve, in both ON and OFF RGCs. Sub-classes Sholl analysis showed that the dendritic remodelling was more extensive in the ON-centre RGCs (Fig. 6.9 k-m).

Overall, considering that the comparison was between two different physiological conditions, and the fact that all G.LNAMint parameters were similar to C.sham suggests that even at a low dose nicotinamide might partially protect RGCs from glaucomatous damage.

Indeed, when G.LNAMint was compared with G.sham a general positive change was observed. The left shift in the Sholl curve of G.LNAMint was less pronounced than in G.sham (Fig. 6.10 c), and it was observed an overall increased complexity in both contralateral and ipsilateral (AUC G.NT.LNAMint 4172.42 ± 2124.87 SD, G.NT.sham 3140.00 ± 1048.18 SD, $p = 0.0139$; AUC

G.HT.LNAMint 3408.21 ± 2145.56 SD, G.HT.sham 2552.53 ± 1201.66, p = 0.0032; Fig. 6.10 d). Although, Sholl related sub-analysis revealed a slight improvement in several dendritic structural categories (max Sholl, total dendritic length and dendritic field area; Fig. 6.10 e, f and g), analysis of the proximal branches revealed that G.HT.LNAMint was still showing sign of dendritic atrophy with no significant changes compared to G.HT.sham (1° p = 0.7198, 2° p = 0.6179, 3° p = 0.5841, 4° p = 0.1216; Fig. 6.10 g). Despite these atrophic signs, the nuclear count at the GCL highlighted a higher density of Hoechst positive cells (Fig. 6.10 j).

To further extend the observation to ON and OFF centre RGCs, analysis of these RGC classes were performed as well. No significant differences were observed between treated and untreated ON-RGCs, while G.HT.LNAMint.OFF showed an increased complexity compared the OHT untreated RGC group (Fig. 6.10 k-m).

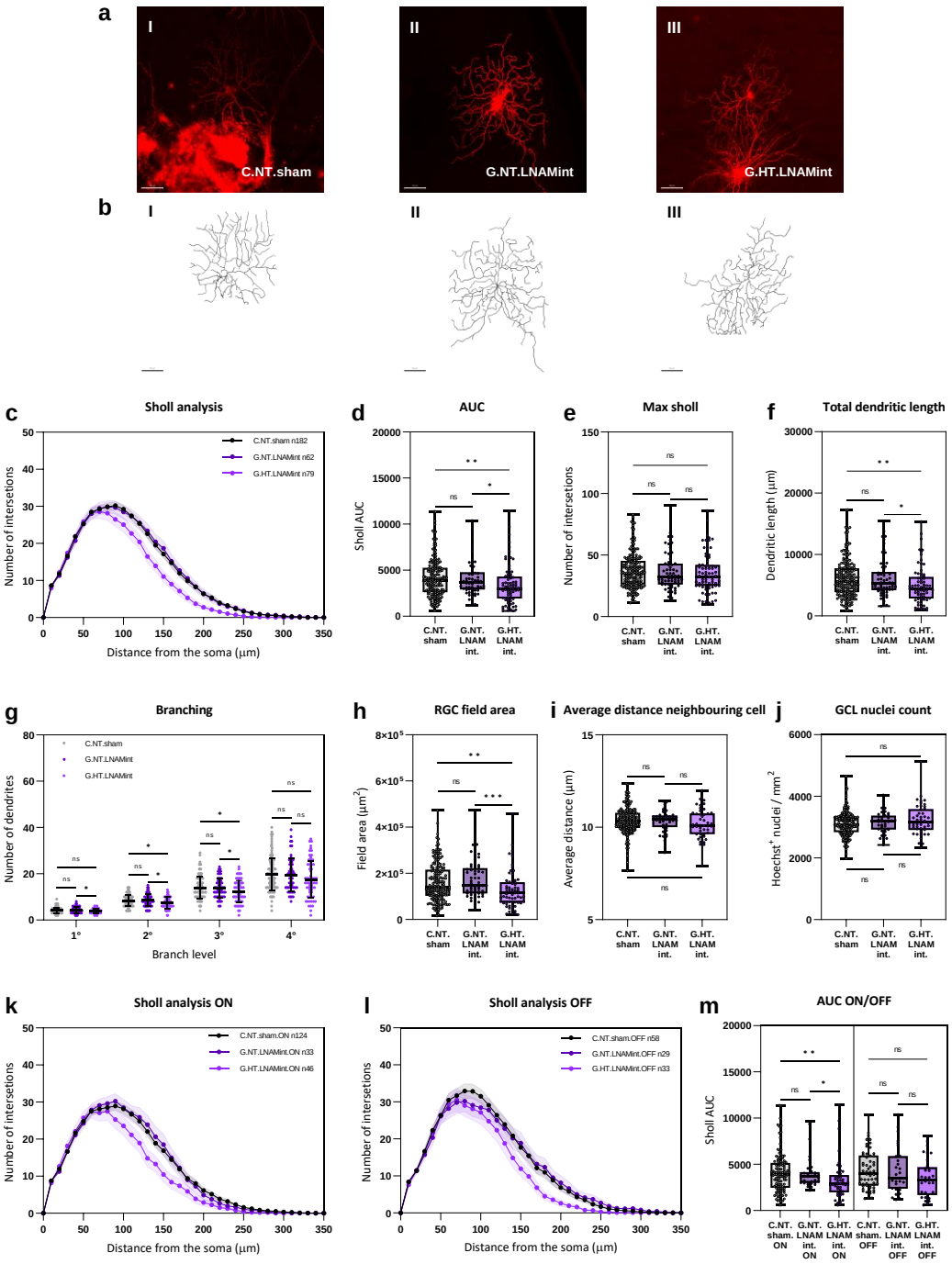

Figure 6. 9. Retinal ganglion cells morphological profile following induction of unilateral ocular hypertension and low NAM intervention treatment compared to untreated normotensive retinal ganglion cells. a, b) DiOlistically labelled RGCs with corresponding Imaris reconstruction. Scale bar 70 µm, image pixel size 2048 x 2048. c) Sholl analysis of all reconstructed RGCs. Line mean value at each interval; shaded area ± SEM. d) Area under the Sholl curve (AUC). e) Maximum number of total dendritic intersections at the Sholl peak. f) Total dendrites length. g) Number of the dendrites at proximal soma branches. Individual values ± SD. h) Dendritic field area. i) Average distance between neighbouring cells at the GCL. j) Nuclei count at the GCL. k, l) Sholl Analysis of reconstructed RGCs according to their receptive

field. m) Area under the Sholl curve of RGCs divided according to their receptive field. Box and whiskers plot with individual values. Whiskers, minimum and maximum value; box plot, 1st quartile, median and 3rd quartile; dots, individual value. Kruskal-Wallis test followed by uncorrected Dunn's test. Ns = non significant, p > 0.05; * = p < 0.05; ** = p < 0.01; *** = p < 0.001.

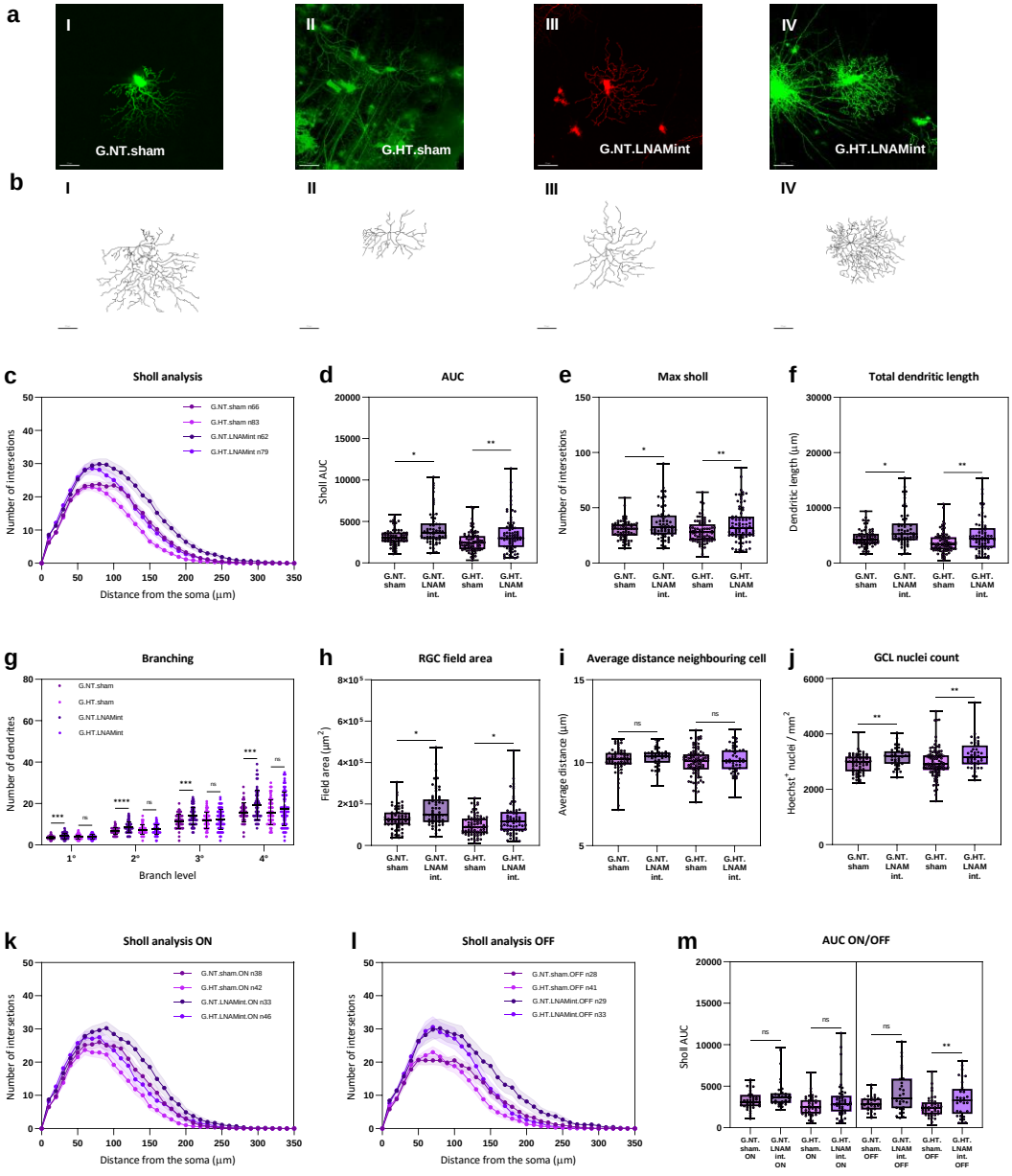

Figure 6. 10. Retinal ganglion cells morphological profile following induction of unilateral ocular hypertension and low dose NAM intervention compared to untreated unilateral OHT retinal ganglion cells profile. a, b) DiOlistically labelled RGCs with corresponding Imaris reconstruction. Scale bar 70 µm, image pixel size 2048 x 2048. c) Sholl analysis of all reconstructed RGCs. Line mean value at each interval; shaded area ± SEM. d) Area under the Sholl curve (AUC). e) Maximum number of total dendritic intersections at the Sholl peak. f) Total dendrites length. g) Number of the dendrites at proximal soma

branches. Individual values ± SD. h) Dendritic field area. i) Average distance between neighbouring cells at the GCL. j) Nuclei count at the GCL. k, l) Sholl Analysis of reconstructed RGCs according to their receptive field. m) Area under the Sholl curve of RGCs divided according to their receptive field. Box and whiskers plot with individual values. Whiskers, minimum and maximum value; box plot, 1st quartile, median and 3rd quartile; dots, individual value. Kruskal-Wallis test followed by uncorrected Dunn's test. Ns = non significant, p > 0.05; * = p < 0.05; ** = p < 0.01; *** = p < 0.001; **** = p < 0.0001.

6.2.2.2.2 High dose of NAM prevents RGCs atrophy following induced ocular hypertension

Sholl analysis revealed a strong RGC preservation following ocular hypertension, without any sign of left shift in the Sholl curve (Fig. 6.11 c). Statistically, no significant difference was detected between C.sham and both NT and HT G.HNAMint groups. G.NT.HNAMint and G.HT.HNAMint showed the same overall dendritic complexity (AUC; G.NT.HNAMint 4480.19 ± 2335.14 SD, p = 0.3103; G.HT.HNAMint 4519.04 ± 2335.14 SD, p = 0.2855; Fig. 6.11 d), characterised by an increased number of dendritic intersection between 50 µm and 100 µm from the soma (G.NT.HNAMint, p = 0.0012; G.HT.HNAMint, p = 0.0158; Fig. 6.11 e). Consistently with the AUC and max Sholl, the effect of HNAMint re-established normal readouts in the total dendritic length and primary branches (Fig. 6.11 f, g). The mean values for the total dendrites length were comparable between the groups, with no significant differences among them (C.sham 6121.012; G.NT.HNAMint 6491.50, p = 0.4206; G.HT.HNAMint 6615.721, p = 0.3576). The same tendency was observed within the proximal branches, with a mean of ≈ 4 in the 1° branches of each group, ≈ 8 in the 2°, ≈ 14 in the 3°, and ≈ 20 in the 4°. Considering that all the other parameters were unchanged in respect to C.sham, a reduction in G.NT.HNAMint dendritic field area was an unexpected observation. No changes were found between C.sham (160982.05 ± 83949.21 SD) and G.HT.HNAMint (148044.12 ± 71140.21 SD; p = 0.2909) and between G.HT.HNAMint and G.NT.HNAMint (134161.33 ± 71623.96 SD; p = 0.1658; Fig. 6.11 h). Although, no significant difference was addressed between the ipsilateral and contralateral RGCs field area, the individual RGCs value of G.HT.HNAMint were close to the values included between the median and the 3rd quartile of the C.sham, while the RGCs individual values of G.NT.HNAMint were similar to the min and the 1st quartile values of C.sham, which may explain the statistical difference (C.sham vs G.NT.HNAMint p = 0.0085).

High NAM intervention was found to be effective not only in regard to the dendritic arbour preservation but also at the GCL. No reduced distance between neighbouring cells (Fig 6.11 i) nor cell loss were observed in the treated groups (C.sham 3112.31 ± 392.82 SD; G.NT.HNAMint 3162.82 ± 362.13 SD, p = 0.3700; G.HT.HNAMint 3090.05 ± 359.32, p = 0.6267; Fig. 6.11 j).

Finally, it was investigated whether or not high dose NAM was exerting the same neuroprotective effect independently of RGCs dendrites laminar depth. Based on ON- and OFF-centre sub-categorisation no significant differences were observed between contralateral and ipsilateral ON and OFF RGCs. In either case their Sholl had the same distribution and no overall difference in their dendritic complexity (Fig. 6.11 k-m).

These results indicate a profound dose dependent neurotrophic support of nicotinamide, which could mitigate OHT-derived dendritic atrophy. Indeed when G.HNAMint readouts were compared with G.sham NAM neuroprotective effect was striking.

An increased neuritic complexity was observed at each Sholl interval (Fig. 6.12 c), which was further confirmed by the AUC, which addressed a significant change in the dendritic tree overall complexity (G.NT.HNAM int, 42% increase, p = 0.0009; G.HT.HNAMint, 77% increase, p = <0.0001; Fig. 6.12 d). As a consequence of this big change, all the parameters showed a switch towards a non-atrophic state, which was well represented by the branching analysis. According to this classification, the two groups G.sham and G.HNAMint were clearly drifting apart, with signs of RGCs atrophy in G.sham and recovery in G.HNAMint. The only exception was the comparison between G.HT.sham and G.HT.HNAMint at the 1° branches that did not reach a threshold of statistical significance (p = 0.0685, with a difference between means of 0.3). All the other comparisons were statistically relevant, with a significant difference between the groups (1° G.NT.HNAMint, p = <0.0001; 2° G.NT.HNAMint p = <0.0001, G.HT.HNAMint p = 0.0088; 3° G.NT.HNAMint, p = <0.0001, G.HT.HNAMint p = 0.0008; 4° G.NT.HNAMint p = <0.0001, G.HT.HNAMint p = <0.0001; Fig. 6.12 h). Similarly, the dendritic field area of the ipsilateral G.HT.HNAMint showed sign of dendritic preservation with intact dendritic tree coverage (p = <0.0001). In contrast, the RGCs field area from the contralateral retina did not reach a statistical significant threshold (p = 0.8565), with very similar mean values (G.NT.sham 130311.10 ± 54383.97; G.NT.HNAMint 134161.33 ± 71623.96; Fig. 6.12 h).

As evidence of this effective neuroprotective environment promoted by NAM high dose, improvements in both cell distribution and density at the GCL were detected as well. A more defined cell distribution was observed, with cells located on average within 10.31 to 10.42 µm from their neighbouring cell (G.NT.HNAMint, p = 0.0304; G.HT.HNAMint, p = 0.0130; Fig. 6.12 i), and normal cell density per mm^2 (G.NT.sham 2926.46 ± 342.48 SD, G.NT.HNAMint 3162.82 ± 362.13 SD, p = 0.0004; G.HT.sham 2967.84 ± 537.96 SD, G.HT.HNAMint 3090.05 ± 359.32 SD, p = 0.0202; Fig. 6.12 j).

As it was expected from the previous comparison with C.sham, even when the labelled RGCs were divided in two main groups according to their IPL depth, both groups of either ipsilateral or contralateral resulted protected from OHT (Fig. 6.12 k-m).

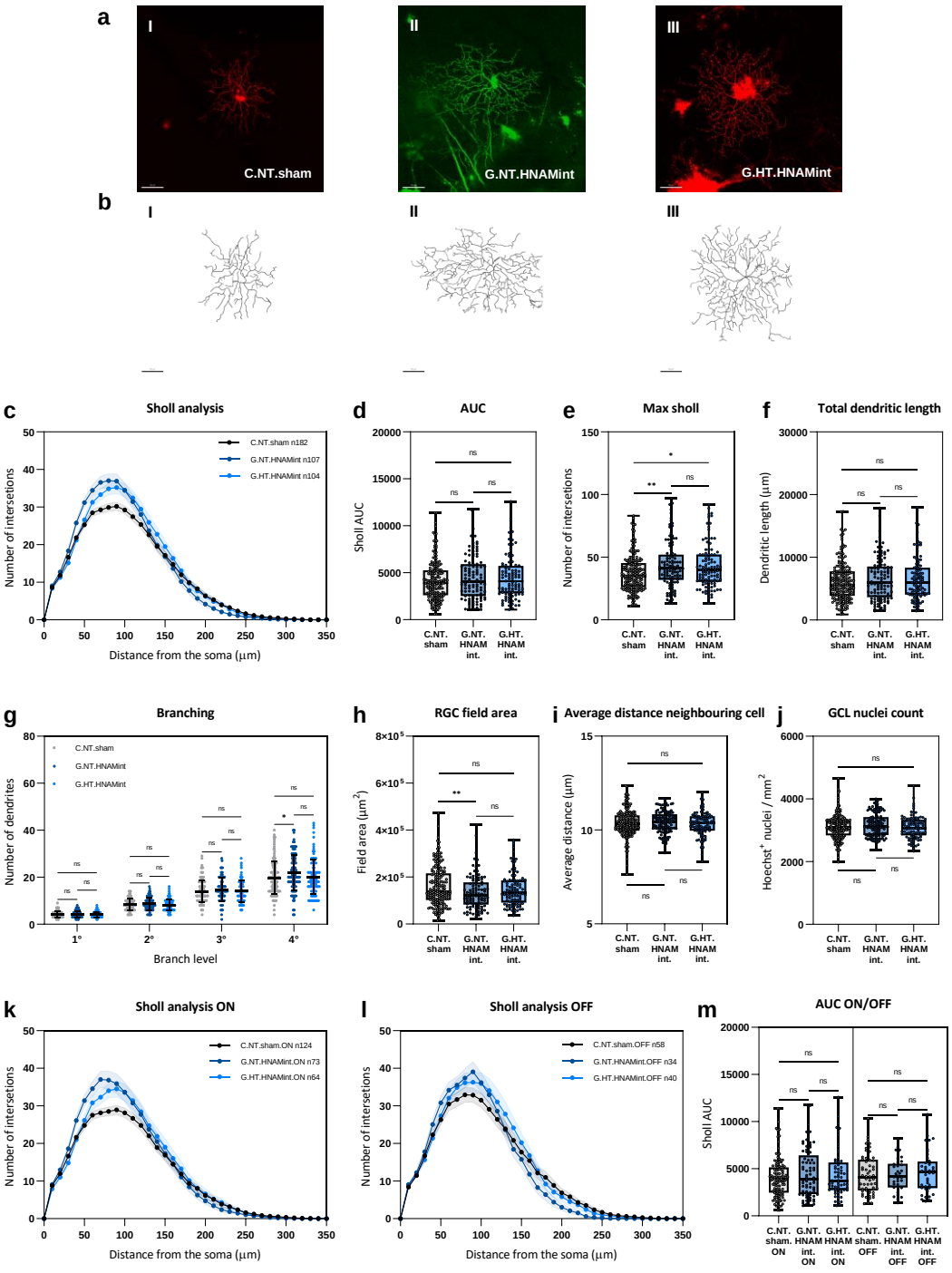

Figure 6. 11. Retinal ganglion cells morphological profile following induction of unilateral ocular hypertension with complementary high dose NAM intervention treatment compared to untreated normotensive retinal ganglion cells. a, b) DiOlistically labelled RGCs with corresponding Imaris reconstruction. Scale bar 70 µm, image pixel size 2048 x 2048. c) Sholl analysis of all reconstructed RGCs.

Line mean value at each interval; shaded area ± SEM. d) Area under the Sholl curve (AUC). e) Maximum number of total dendritic intersections at the Sholl peak. f) Total dendrites length. g) Number of the dendrites at proximal soma branches. Individual values ± SD. h) Dendritic field area. i) Average distance between neighbouring cells at the GCL. j) Nuclei count at the GCL. k, l) Sholl Analysis of reconstructed RGCs according to their receptive field. m) Area under the Sholl curve of RGCs divided according their receptive field. Box and whiskers plot with individual values. Whiskers, minimum and maximum value; box plot, 1st quartile, median and 3rd quartile; dots, individual value. Kruskal-Wallis test followed by uncorrected Dunn's test. Ns = non significant, $p > 0.05$; * = $p < 0.05$; ** = $p < 0.01$.

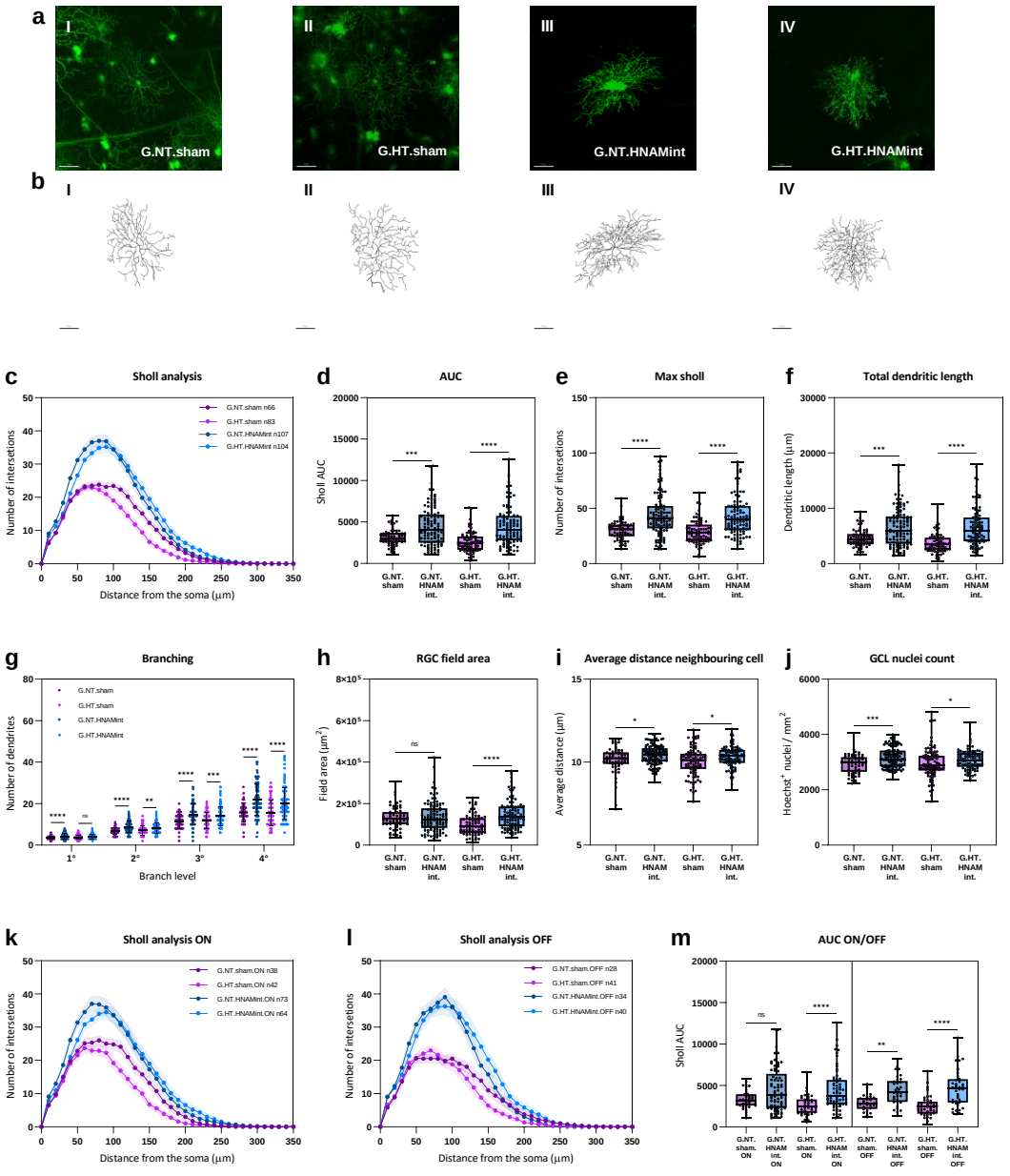

Figure 6. 12. Retinal ganglion cells morphological profile following induction of unilateral ocular hypertension with complementary high dose NAM intervention treatment compared to untreated

unilateral OHT retinal ganglion cells profile. a, b) DiOlistically labelled RGCs with corresponding Imaris reconstruction. Scale bar 70 µm, image pixel size 2048 x 2048. c) Sholl analysis of all reconstructed RGCs. Line mean value at each interval; shaded area ± SEM. d) Area under the Sholl curve (AUC). e) Maximum number of total dendritic intersections at the Sholl peak. f) Total dendrites length. g) Number of the dendrites at proximal soma branches. Individual values ± SD. h) Dendritic field area. i) Average distance between neighbouring cells at the GCL. j) Nuclei count at the GCL. k, l) Sholl Analysis of reconstructed RGCs according to their receptive field. m) Area under the Sholl curve of RGCs divided according to their receptive field. Box and whiskers plot with individual values. Whiskers, minimum and maximum value; box plot, 1st quartile, median and 3rd quartile; dots, individual value. Kruskal-Wallis test followed by uncorrected Dunn's test. Ns = non significant, $p > 0.05$; * = $p < 0.05$; ** = $p < 0.01$; *** = $p < 0.001$; **** = $p < 0.0001$.

6.3 Discussion

The results obtained from both NAM prophylactic and intervention, suggest that nicotinamide can mitigate the insults caused by OHT in a dose-dependent fashion. Structural RGC preservation might suggest that they were functionally preserved as well (Koleske, 2013, Cuntz et al., 2013). However, functional RGC preservation without ERG data can only be supposed and indicates a limitation of the study. A complete investigation would have ideally required a parallel project with functional analysis (ERG) to match the morphological assessment and likely RBPMS cell count to confirm targeted RGCs neuroprotection. Even though treated RGCs displayed morphological preservation with a tendency towards a more complex architecture, which may suggest a plastic predisposition of the RGCs exposed to the treatment, this hypothesis can only be confirmed following changes over time of the same dendritic structure (*e.g.* two photon microscopy (Benninger and Piston, 2013)). Even if that readout would have been very informative, it would have required the establishment of a genetically modified rat with fluorescent tagged RGCs and the optimisation of a diagnostic protocol for RGCs detection, which *per se* is another project.

Although it is difficult to divide the concept of glaucoma degeneration from OHT, especially in experimental models, NAM recovery strategy was designed without a IOP management component (*i.e.* IOP drops), treating the pathology as a neurodegenerative disease with an energy deficit component. The prophylactic and intervention NAM treatments reinforce the evidence that RGCs have the capacity to recover if metabolically supported throughout a period of stress (Crowston et al., 2017, De Moraes et al., 2022, Caprioli, 2013). However, RGCs as all neurons can exist only in three states: "healthy, damaged or dead". Once the ultimate endpoint is reached (i.e. extended dendritic atrophy up to the primary branches, over 50% cell loss) there

is little that can be done. Therefore, the only effective options are given by either prolonging the healthy status or mitigate the damage. In these trials, prophylactic and intervention targeted those two scenarios.

The prophylactic treatment prevented the morphological disease outbreak, providing to the system enough NAD^+ reservoir to tackle OHT related damage (Ventura and Porciatti, 2005, Porciatti and Ventura, 2012). With the intervention it was provided the energy to fight (Petriti et al., 2021). However, in such complex disease as glaucoma, NAD^+ consumption is increased also by other factors that can contribute to worsen RGC damage (*e.g.* SARM1) (Figley et al., 2021, Essuman et al., 2017, Bratkowski et al., 2020) and that may explain why the low NAM was not effective to same extent of high NAM. One of the common feature between the treated groups was the increased complexity of the analysed RGCs. Some studies suggest that IOP damage may promote plasticity in the surviving RGCs with concurrent increase of the dendritic field in order to compensate for the OHT induced dendritic retraction (Ahmed et al., 2001, Kalesnykas et al., 2012). Although no dendritic outgrow was detected over the normal and predetermined dendritic area (Reese and Keeley, 2015), that may explain the more complex architecture of the OFF-centre RGCs. If OFF RGCs are more prone to damage (Della Santina et al., 2013, Della Santina and Ou, 2017, Ou et al., 2016, El-Danaf and Huberman, 2015), it can be assumed that what was observed might have been their response to recovery.

With these premisses, the line between NAM promoted neuroprotection or neurorescue is quite uncertain and a conclusive statement would require a further understanding of NAM triggered mechanism underlying this RGC relief.

7 Nicotinamide adenine mononucleotide-related metabolic changes

7.1 Overview

In the previous chapter it was shown that NAM offers a robust neurotrophic support to RGCs, especially at the highest dose tested. Considering that no IOP management was used together with NAM treatment, this neuroprotection might have been achieved through changes in NAM metabolism.

Tribble *et al.* demonstrated that OHT, even at the earliest stages (3 days after induction), disrupts the main energy-providing pathways (*i. e.* glycolysis, TCA, OXPHOS) in tissue enriched for RGCs, which was prevented with NAM supplementation (Tribble et al., 2021c).

To verify that hypothesis in the BN rat model of chronic ocular hypertension, optic nerves from G.sham, G.HNAMint and G.HNAMproph were analysed at the endpoint of the experimental OHT (4 weeks). The optic nerve is a bundle of RGC's axons, therefore each metabolic change related to the optic nerves directly influences RGCs metabolism.

7.1.1 Experimental setup

To evaluate whether any metabolic shift could be detected after NAM treatment, low molecular weight metabolic analysis[5] were performed on optic nerves from three different experimental groups: G.sham (untreated unilateral glaucoma), G.HNAMproph and G.HNAMint (unilateral glaucoma treated with high dose NAM prior OHT induction, prophylactic, and post OHT induction, intervention). Optic nerves were collected immediately after culling and snap frozen in order to avoid any metabolite deterioration.

The collected optic nerves were shipped to the Metabolomic Swedish Centre for sample processing. Afterwards, all the raw data were normalised to the sample weight and centred with pareto scaling (scales data by dividing each variable by the square root of standard deviation so that each variable has variance equal to 1), and finally analysed with MetaboAnalyst (Chong et al., 2018, Pang et al., 2021) for a detailed understanding on the samples metabolic profiles and pathway analysis (*Rattus norvegicus* KEGG library).

[5] Low molecular weight metabolomics analyse changes in small organic molecules (50-1500 Da) which are involved in biological processes as a substrate or product.

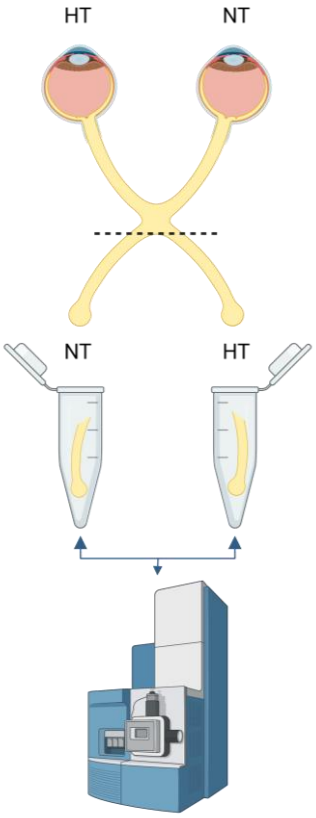

Figure 7. 1. Optic nerves experimental processing. Immediately after culling optic nerves were separated at the optic chiasm in NT (from the contralateral eye) and HT (from the ipsilateral eye). Samples were weighted and immediately frozen with liquid nitrogen. All the samples were stored at –80° C until processed for metabolomic analysis.

7.2 Results

7.2.1 How does nicotinamide treatment influence optic nerves metabolic profile?

It was first investigated whether there were any metabolic differences among the OHT and NT samples within the three groups. Principal component analysis (PCA) separated G.sham in two discrete groups, with no overlap between NT and HT with PC1 describing the biggest part of the variation (83.7 %) and PC2 contributing only for a minimal part (12.4 %). Glycerophosphocholine, arginine and leucine were the main components (loading factors) to determine PC1 (Fig. 7.2 a). In contrast, no separation could be found in any of the two treated groups. In both NAM treated groups PC1 was determining the group characterisation, with NAM in both cases as the highest

loading factor (81.6 %, G.HNAMproph; 90.4 %, G.HNAMint; Fig. 7.2 b, c). The volcano plots[6] showed that NT and HT samples from the NAM treated groups were metabolically similar and no statistical relevant changes were found in the metabolites abundance within the same group (Fig. 7.2 e, f), whereas G.HT.sham had a different metabolic finger print compared to G.NT.sham, with eight upregulated metabolites (*e.g.* glucose-6-phosphate (G6P), glyceraldehyde-3-phosphate (G3P), arachidonic acid (AA), glicerophosphocholine (GPC), methionine (Met)) and two significantly downregulated (*i.e.* phosphoenolpyruvate (PEP), 5-aminolevulinic acid (5-ALA); Fig. 7.2 d).

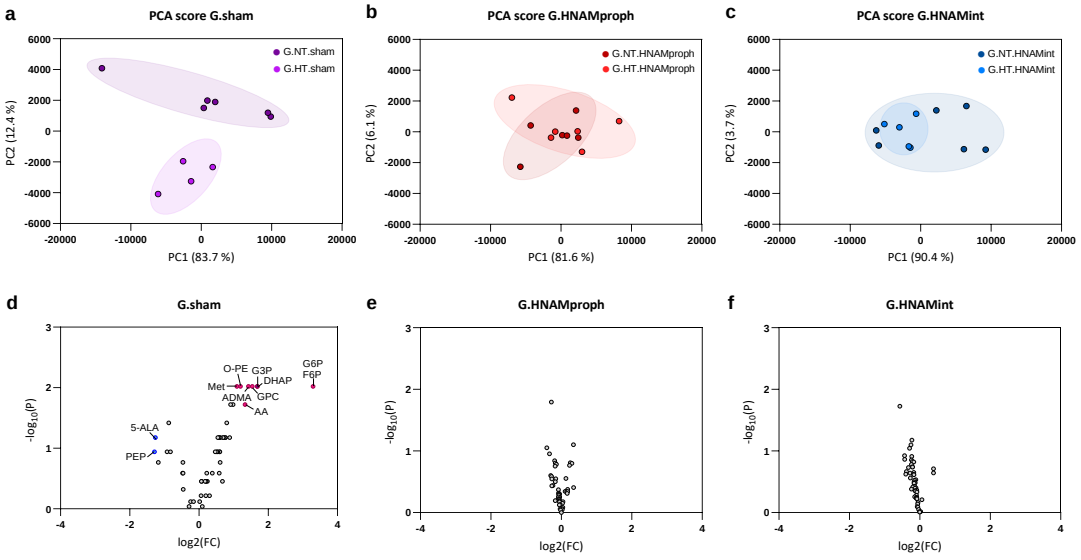

Figure 7. 2. Optic nerves metabolic profile. Principal component analysis describing a) G.sham group, b) G.HNAMproph group and c) G.HNAMint group. Volcano plot for HT vs NT revealed for d) G.sham a significant upregulation of eight metabolites (red dots), and a significant downregulation (blue dots) of two metabolites, while for e) G.HNAMproph and f) G.HNAMint no significant metabolites changes were observed between HT and NT. Significant fold change > ± 2. 5-ALA: 5-aminolevulinic acid; AA: arachidonic acid; ADMA: asymmetric dimethylarginine; DHAP: dihydroxyacetone phosphate; F6P: Fructose-6-phosphate; G3P: glyceraldehyde-3-phosphate; GPC: glycerophosphocholine; G6P: glucose-6-phosphate; Met: methionine; O-PE: O- phosphoethanolamine; PEP: phosphoenolpyruvate.

Pathway analysis revealed that OHT in the untreated animals significantly increased the biochemical activity of the pathways related to arachidonic acid and phenylalanine metabolism,

[6] Volcano plots display the statistical significant difference relative to the magnitude of change for every single metabolite in the comparison. The y axis represents base -2 log fold-change, while the significance shown through the negative base -10 log. All the data points above 1 on the x axis are considered significant. The data point below 0 on the y axis represent down regulated metabolites, while the ones above 0 the upregulated metabolites.

as well as amino acids biosynthesis. The impact of nicotinate and nicotinamide metabolism was lower compared to the other pathways. Pathway disruptions reflected the changes observed in G.sham volcano plot. Prediction of the disrupted metabolites in the pathways evidenced severe decrease of NAD^+, nicotinamide-D-ribonucleotide and L-aspartate especially in the G.HT.sham optic nerves. In addition to that, chronic OHT influenced other pathway which included downstream molecules involved in ATP biosynthesis and oxidative stress (Fig. 7.3 a). In contrast, when NAM treatment was involved the metabolic scenario was completely reversed. Pathway analysis from G.HNAMproph detected an upregulation of the nicotinate and nicotinamide pathway with higher NAD^+ biosynthesis, higher levels of 2-oxoglutarate, L-glutamate and L-aspartate, which are all part of the arginine biosynthesis pathway and connected with the other upregulated pathways (Fig. 7.3 b). In G.HNAMint, pathway analysis revealed an upregulation of the alanine, aspartate and glutamate metabolism together with D-glutamine and D-glutamate metabolism and arginine biosynthesises, which indeed share some of the same downstream molecules that were predicted to have the highest metabolic change (L-aspartate, L-glutamate). In regard to the nicotinamide pathway, even if the treatment duration was shorter compared to the prophylactic, the projected metabolic response was more prominent in the intervention compared to the prophylactic, with changes in both NAM and NAD^+, suggesting a very efficient NAM metabolism (Fig 7.3 c).

These results pointed out that the treated samples were energetically more efficient. In fact, pathway analysis reported improvements in both glycolysis and TCA cycle along with the pentose phosphate pathway, which were disrupted in the G.sham (Appendix A.8 for a complete pathway list, from the most to the least affected).

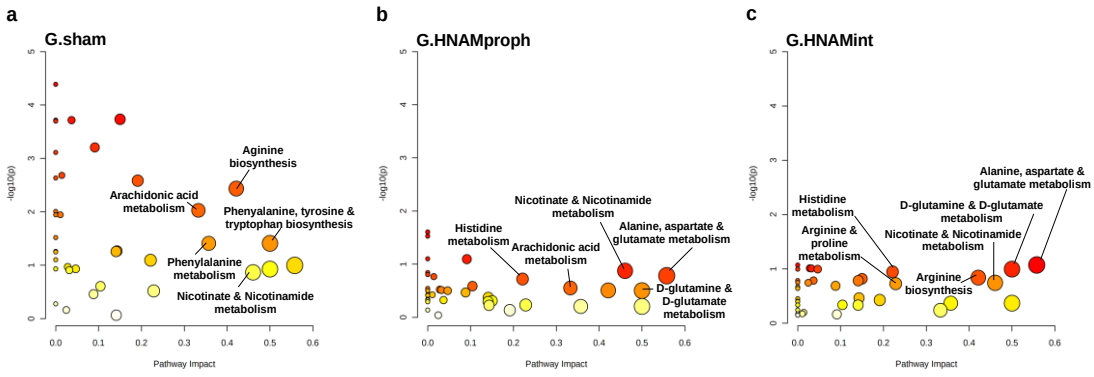

Figure 7. 3. Pathway analysis (KEGG). Metabolites change due to OHT resulted in greater pathway changes in a) G.sham and improvements in the same pathways after NAM treatment in both b) G.HNAMproph and c) G.HNAMint. Red, orange and yellow dots: from high to low impact.

Overall, each treated group was metabolically homogeneous (Fig. 7.2 b, c and e, f) and energetically competent, but the most interesting findings came when NT and HT untreated samples were compared with the corresponding treated conditions (Fig. 7.4).

PCA separated almost completely G.NT.sham/G.NT.HNAMproph and G.NT.sham/G.NT.HNAMint in two discrete groups, with just a minimal overlap. In both cases was PC1 to determine the division, which was arginine for G.NT.sham/G.NT.HNAMproph (Fig. 7.4 a) and nicotinamide for G.NT.sham/G.NT.HNAMint (Fig.7.4 b). Although G.NT.sham and G.NT.HNAMproph had no overlap in the PCA, only one metabolite was found statistically relevant. It was obsereved that glutathione disulfide (GSSG), the oxidised form of glutathione (GSH), was downregulated in the G.NT.HNAMproph while salvage pathway metabolites were slightly upregulated but not enough to be statistically significant (Fig. 7.4 c). In contrast, in G.NT.HNAMint a significant upregulation of NAM and GSH was observed compared to G.NT.sham. At the same time, glutathione disulfide, glyceraldeyde-3-phosphate and dihydroxyacetone phosphate were downregulated (Fig. 7.4 d). A downregulation of two intermediates in the glycolytic pathways may be justified by an adequate amount of ATP in cell. Considering that glucose-6-phosphate and fructose-6-phosphate were significantly upregulated in G.HT.sham (Fig. 7.2 d), that could have been a coping mechanism to the keep up with the energetic demand in the absence of an efficient oxidative phosphorylation in the mitochondria.

Principal component analysis of G.HT.sham/G.HT.HNAMproph (Fig. 7.4 e) and G.HT.sham/G.HT.HNAMint (Fig. 7.4 f) highlighted the metabolic separation between the OHT treated and untreated samples. PCA for G.HT.sham/G.HT.HNAMproph evidenced the metabolic diversity of the two groups with PC1 influencing the metabolic division by 64.8 % (nicotinamide) and PC2 by 25.5 % (glycerophosphocholine, Fig. 7.4 e). In this case the metabolic separation was greater than in the NT counterpart. Eight metabolites were significantly downregulated in G.HT.HNAMproph and among those the greatest difference was found in NMN. In contrast, NAM and NAD^+ were significantly upregulated along with other metabolites (Fig. 7.4 g). Similarly, PCA for G.HT.sham/G.HT.HNAMint revealed even a stronger dichotomy of the groups, still with nicotinamide and glycerophosphocholine determining the division as PC1 and PC2 respectively (Fig. 7.4 f). At a single metabolite level (Fig. 7.4 h), nine molecules were downregulated with NMN among them, but more importantly two fundamental molecules of the salvage pathway were upregulated (NAM and NAD^+), suggesting that the pathway was efficient and there was enough free NAD^+ to allosterically inhibit SARM1.

At the same time, in both G.HT.HNAMproph and G.HT.HNAMint, a further downregulation of the downstream molecules of the glycolytic pathway and GSSG reduction was observed, which may indicate a good ATP reservoir and reduced oxidative stress.

These results not only confirmed that nicotinamide can cross the blood brain barrier and be effective in CNS, but also that the samples were metabolically different, which was the determinant of NAM-derived neuroprotection.

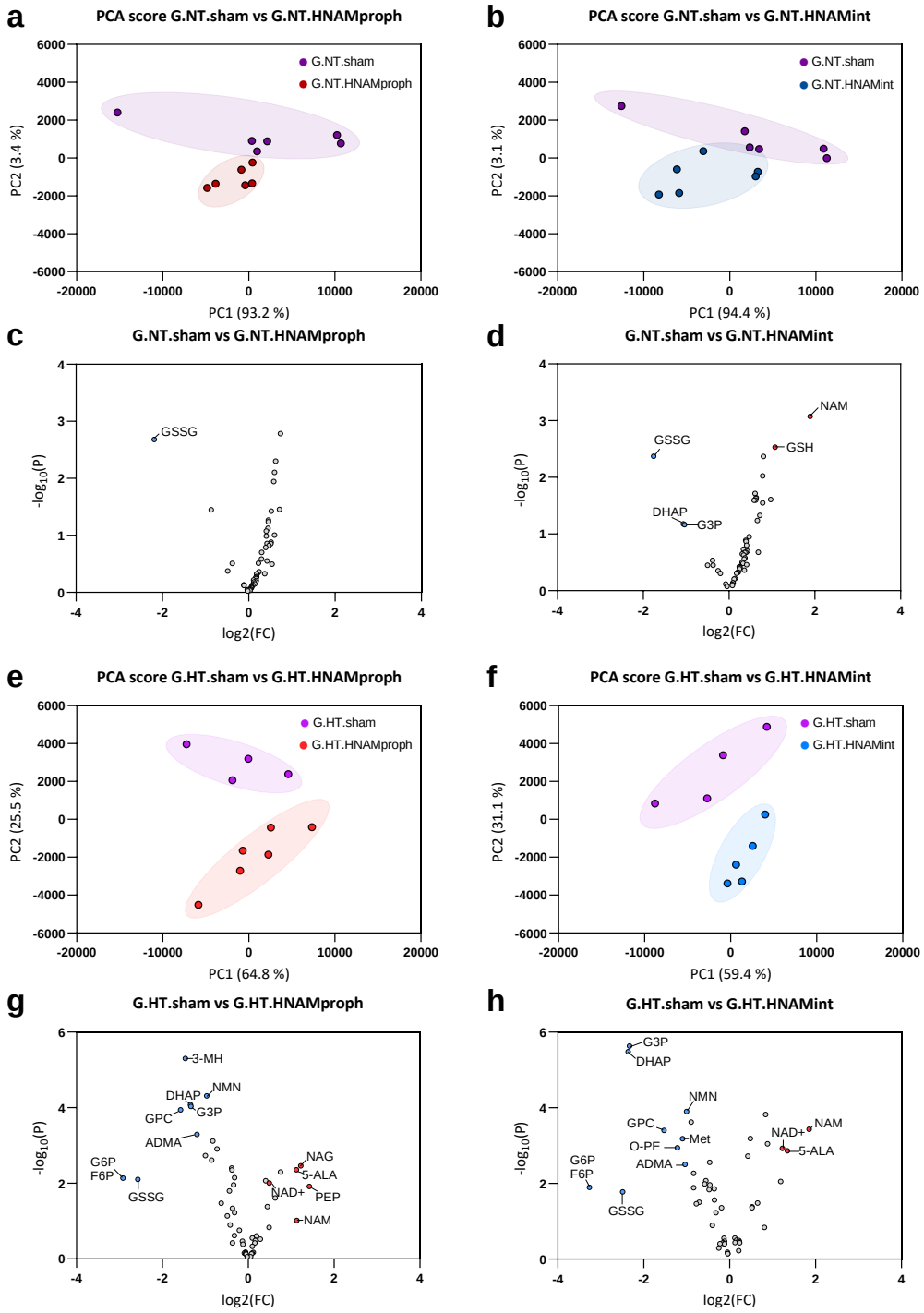

Figure 7. 4. Effect of NAM treatment of optic nerves metabolome. Principal component analysis defined a complete metabolic separation for both contralateral a) G.NT.HNAMproph and b) G.NT.HNAMint compared to G.NTsham. At a single metabolite level c) G.NT.HNAMproph had just one downregulated metabolite compared to the untreated counterpart, while d) G.NT.HNAMint had three downregulated and two upregulated metabolites. Similarly, the ipsilateral groups showed a well defined metabolic separation with both e) G.HT.HNAMproph and f) G.HT.HNAMint forming two discrete groups with no

overlap with the untreated counterpart. In this case we found that in g) G.HT.HNAMproph there were four upregulated metabolites and seven downregulated metabolites. Likewise, h) G.HT.HNAMint had three upregulated metabolites and eight downregulated metabolites. Significant fold change > ± 2. 3-MH: 3-methylhistidine; 5-ALA: 5-ALA: 5-aminolevulinic acid; ADMA: asymmetric dimethylarginine; DHAP: dihydroxyacetone phosphate; F6P: Fructose-6-phosphate; G3P: glyceraldehyde-3-phosphate; GPC: glycerophosphocholine; G6P: glucose-6-phosphate; GSH: glutathione; GSSG: glutathione disulfide; Met: methionine; NAM: nicotinamide adenine mononucleotide; NAD: nicotinamide adenine dinucleotide; NAG: N-acetylglutamate; NMN: nicotinamide mononucleotide; O-PE: O- phosphoethanolamine; PEP: phosphoenolpyruvate.

7.2.2 Changes in NAM salvage pathway

Analysing the metabolites relative abundance normalised to sample weight (m/z = intensity of mass spectrum), in the G.sham an overall disruption of the salvage pathway was observed (Fig 7.5 a-d I). It was found that NMN was significantly upregulated only in G.HT.sham and that its conversion to NAD^+ by NMNAT1/2 was downregulated. A rise in NMN is a clear sign of degeneration and that may explain the profound atrophy found in the untreated RGCs (chapter 3). In contrast, in both G.HNAMproph and G.HNAMint each step of the pathway was quite homogeneous (Fig. 7.5 a-d II-III). Despite a balanced NAM metabolism, it was surprising to find that NAM relative content was higher in G.HNAMint (Fig. 7.5 a III) even though the treatment duration was shorter than in G.HNAMproph.

Although the resources were not enough to analyse optic nerves from all experimental animals, these results suggest with a good level of confidence that the underlying RGCs neuroprotective mechanisms were connected to NAM metabolic support, and likely to SARM1 inhibition, which is highly influenced by NMN:NAD ratio (Fig. 7.6).

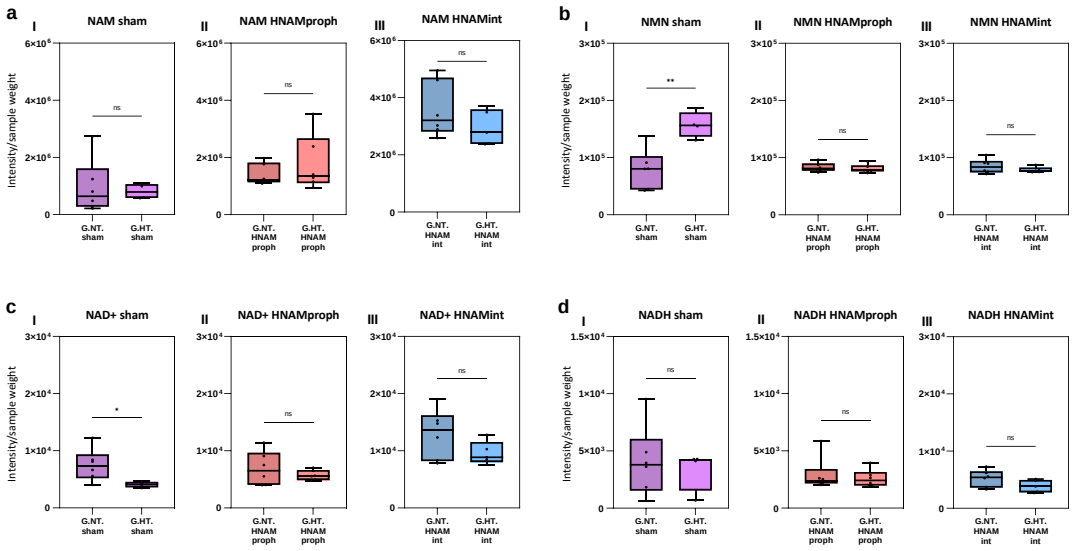

Figure 7. 5. Nicotinamide salvage pathway. Salvage pathway metabolites intensity normalised to the sample weight for the different experimental groups. a) NAM; b) NMN; c) NAD^+; d) NADH. Box and whisker plot with indiidual values. Whiskers, min and max values. Box plot; 1st quartile, median and 3rd quartile. ns = non significant, p > 0.05; * = p < 0.05; ** = p < 0.01.

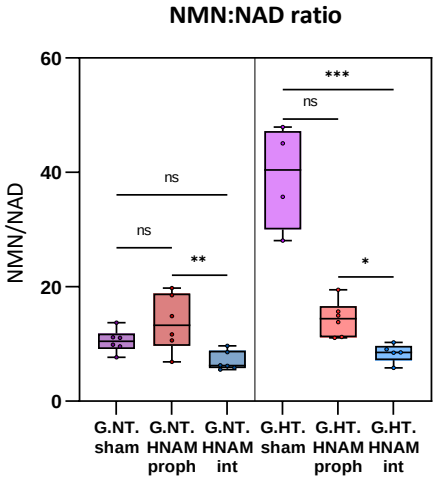

Figure 7. 6. NNM:NAD ratio. Compared to the treated samples, G.HT.sham was the only group showing a molecular shift that could promote SARM1 activation. This mechanism was rescued with NAM supplementation.

7.2.3 Optic nerves oxidative stress and inflammation related metabolites

Besides NAD^+ impaired metabolism, oxidative stress and inflammation influence the outcome of OHT related damage. With metabolic analysis, it could be possible to measure the relative abundance of reduced and oxidised form of glutathione, as well as arachidonic acid (Fig. 7.7 a,

b), which are known as ROS scavenging and inflammatory molecules respectively. GSH to GSSG ratio was significantly higher in the treated groups (Fig. 7.7 a), suggesting a better antioxidant capacity and less oxidative stress. In contrast, arachidonic acid abundance was significantly higher in G.HT.sham group, while no changes could be detected in G.HNAMproph and G.HNAMint, where the metabolite load was almost constant in both NT and HT samples (Fig. 7.7 b).

These data indicate a specific group metabolic finger print, with G.sham characterised by a reduced antioxidant capacity and inflammation in the ipsilateral optic nerves, while the opposite observation can be made for the treated groups.

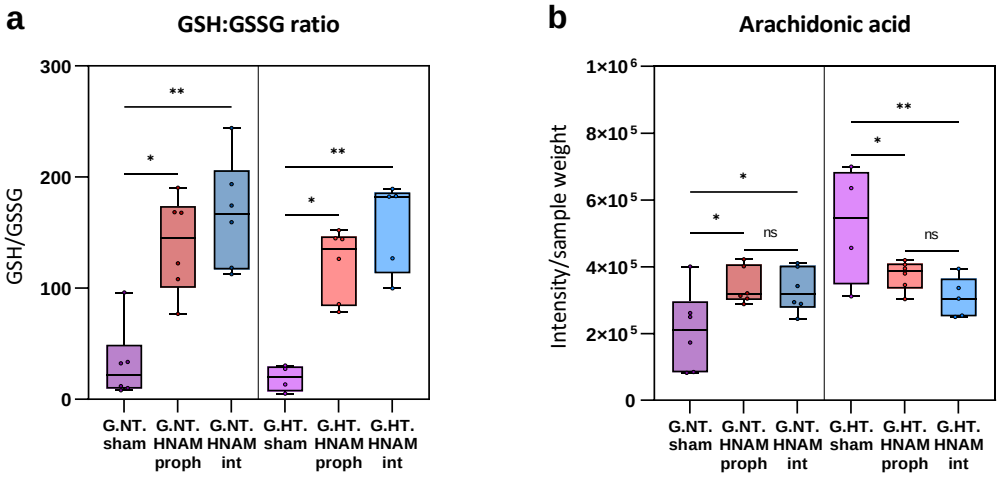

Figure 7. 7. Optic nerve oxidative and inflammatory state. a) GSH:GSSG ratio measures the cellular antioxidant capacity, while the inflammatory state is suggested by b) arachidonic acid sample abundance. Box and whisker plot with indiidual values. Whiskers, min and max values. Box plot; 1st quartile, median and 3rd quartile. Ns = non significant, $p > 0.05$; * = $p < 0.05$; ** = $p < 0.01$.

7.3 Discussion

Brain energy rescue is emerging as one of the most efficient therapeutic concept for age-related neurodegenerative diseases (ANDs) (Mattson and Arumugam, 2018), and glaucoma is among them. Considering that NAD^+ decreases with age and is furtherly reduced in pathological contexts (McReynolds et al., 2020, Blaszczyk, 2020, McReynolds et al., 2021), this reduction may render neurons vulnerable to damage. This assumption appears to be realistic in glaucoma. Williams and Tribble have shown that NAD^+ was depleted in murine models of glaucoma and

that OHT was exacerbating mitochondrial and metabolic disfunctions in their cohorts (Williams et al., 2017c, Tribble et al., 2021c).

In this model it was not assessed whether NAM treatment was directly preventing mitochondrial dysfunction, but it was possible to identify metabolic changes which would have affected mitochondria either directly or indirectly. CNS metabolism is extremely complex and in our treated samples it was possible to identify changes that were beyond the salvage pathway.

At first glance, G.sham group metabolic changes were not related to any NAD^+ precursors but mainly to G6P, 5-ALA and GPC (Fig. 7.2 a, d). These three molecules, which *per se* do not seem to have any connection, may, on the contrary, identify a particular metabolic state in which the neurons sit at. ATP is the biological energy currency and can be produced by a number of distinct cellular processes via four main pathways: glycolysis, TCA cycle, OXPHOS and beta-oxidation (Bonora et al., 2012). The primary energy source is glucose which is catabolised to produce ATP by glycolysis, TCA cycle and OXPHOS, three connected pathway collectively identified as cellular respiration. Cellular respiration gives a net of 38 molecules of ATP per molecule of glucose, with just 2 of them produced outside the mitochondria during glycolysis (cytoplasm). Some of the catabolic steps in the glycolytic pathway requires ATP, while others NAD^+. The reduction of glucose into glucose-6-phosphate (G6P) and fructose-6-phosphate (F6P) requires ATP and the conversion of glycerldeide3-phosphate (G3P) into 1,3biphosphoglycerate requires NAD^+ (Nelson et al., 2008). However, if all the ATP and NAD^+ molecules available are consumed during the first steps of the pathway or to execute other functions, the molecule of glucose that entered in the loop cannot be further catabolised into pyruvate. This picture describes the condition that was observed in G.HT.sham, with a significant increase in G6P, F6P and G3P and a reduction in phosphoenolpyruvate (PEP). Thus, overall this might indicate an ongoing energetic imbalance and likely a desperate attempt to produce at least few molecules of ATP, which failed because the pathway never progressed to the "yielding-energy" phase. In addition to that, 5-aminolevulinic acid (5-ALA; heme amino acid precursor synthesised from glycine and succinyl-CoA in mitochondria), which was found reduced in G.HT.sham and increased in the treated samples, plays an important part in aerobic metabolism and ROS inhibition (Matsuo et al., 2020). Therefore this decrease may confirm energetic deficits and mitochondria related oxidative stress in our model of glaucoma.

However, that picture only described what could have happened in the untreated sample, and thus gave an incomplete overview of all the changes. A detailed characterisation came only

when the untreated samples were compared with their treated counterpart. Starting from the contralateral samples, a significant decrease was observed in GSSG in both G.NT.HNAMproph and G.NT.HNAMint. Glutathione (GSH) is one of the most important scavenger molecules for ROS in the brain. When GSH reacts with radicals it is oxidised into glutathione disulfide (GSSG) by glutathione peroxidase (GPx) and recycled back by glutathione reductase (GR) (Dringen et al., 2000). Therefore, a downregulation of GSSG or upregulation of GSH – with a balanced GSH:GSSG ratio (1.5:1) – indicates a good clearance of ROS (Owen and Butterfield, 2010), suggesting that the untreated contralateral samples might have altered free radicals clearance pathway and thus are exposed to oxidative stress. Then, when the ipsilateral treated samples were compared with the untreated G.HT.sham, it was immediately observed a downregulation of the molecules that were previously found upregulated (*i.e.* G6P, F6P and G3P) and an upregulation of the respective G.sham downregulated molecules (*i.e.* PEP and 5-ALA), suggesting the restoration of a normal cellular homeostasis. In addition, in both G.HT.HNAMproph and G.HT.HNAMint it was detected NMN downregulation and NAM upregulation, and significant NAD^+ upregulation, which was greater in G.HT.HNAMint.

NAM, NMN and NAD^+ in the context of glaucoma are three very important molecules in regard of Wallerian degeneration. Wallerian degeneration refers to the axonal degenerative pathological process led by SARM1 (Sterile alpha and Toll/interleukin-1 receptor [TIR] motif-containing 1), NMN, NAD^+ and NMNAT2 (Hopkins et al., 2021). SARM1 besides being one of the main NAD^+-cleaving enzymes, according to the metabolic environment can switch between two states, an autoinhibitory state driven by Armadillo/HEAT motif (ARM) domain and an active state triggered by the TIR domain (Bratkowski et al., 2020). When an axon is injured (in this context due to OHT) the axonal transport is compromised as well, and since most of the molecules required for axon maintenance are synthesized in the cell body, as for NMNAT2, that alters the balance between NMN and NAD^+ that keeps SARM1 pro-degenerative function silent (Figley and DiAntonio, 2020, Funakoshi and Araki, 2021). In the absence of NMNAT2, NMN cannot be converted into NAD^+, therefore the balance shifts in favour of NMN which binds to the TIR domain and promotes the active state of SARM1 ($SARM1^{TIR}$) (Figley et al., 2021, Essuman et al., 2017). In contrast, when enough NAD^+ is present the ARM domain is not truncated and SARM1 is kept in its inactive state ($SARM1^{ARM}$) (Bratkowski et al., 2020, Jiang et al., 2020, Gerdts et al., 2016, Angeletti et al., 2022).

Looking back at the profound RGCs atrophy and cell loss found in G.sham, if those observations are combined with the metabolic change in G.sham salvage pathway (Fig. 8.5 b and c I), it can

be supposed that OHT triggered RGCs degeneration in all RGC compartments (dendrites, axon, soma) and that NAM treatment was protecting RGCs *in toto*. Also, G.HT.sham samples were the only one expressing glycerophosphocholine upregulation, which has been identified as a sign of neuronal membrane breakdown as a consequence of the neurodegenerative process (Klein, 2000), hence the ultimate proof of cell death (Fricker et al., 2018, Pemberton et al., 2021, Gorman, 2008). In addition to that, a significant reduction of arachidonic acid (AA) was also observed in the treated sample. This polyunsaturated fatty acid can both trigger inflammatory or non-inflammatory reaction depending on its by-products (Das, 2018). If AA metabolites are prostaglandins, thromboxanes or leukotrienes, those will lead to an inflammatory reaction. In contrast, if AA metabolites are resolvins, protectins or maresins the outcome would be anti-inflammatory. Generally is the balance between these metabolites which determines the inflammatory reaction, but it is also true that ROS have modulatory influence on the catabolising enzymes of AA metabolism and may influence the direction of the pathway (Das, 2021, Wang et al., 2021). Thus, it can be supposed that in this case AA might have enabled inflammatory pathways, taking into account all the differences seen by far, as well as the GSH:GSSG ratio coupled with AA increase in G.HT.sham (Fig. 7.7 a and b).

These results suggest that NAM treatment can promote either directly or indirectly a pro-survival state *via* different mechanisms, each of which might be repaired/enhanced/suppressed by modulating NAD^+ and its precursors. NAM-derived neuro-energetic boost provides the resources to keep intact mitochondrial functions, ATP production and ROS defence, which will be beneficial for both axon and dendritic protection (Tribble et al., 2019, Williams et al., 2017b, Baltan et al., 2010, Chrysostomou et al., 2013, Tribble et al., 2021c). For the axonal compartment NAD^+ increase mitigates SARM1 activation and therefore preserves the axons, and likely the connections to dorsal lateral geniculate nucleus and superior colliculus (Sasaki and Milbrandt, 2010, Wang and He, 2009, Risner et al., 2021, Williams et al., 2017a). In addition to that, it was also identified that NAM-metabolic boost restored arginine metabolism that was depleted in G.sham (Fig. 7.2 d; Fig. 7.3 a). Recent findings suggest that arginine methylation, which results in the formation of asymmetric dimethylarginine (ADMA), symmetric dimethylarginine (SDMA) and monomethylated arginine (MMA), represent an important regulatory mechanism in regards of dendritic plasticity and actin cytoskeletal components (Qualmann and Kessels, 2021). Axonal transport relies on actin filaments (Morgan, 2004) and when is interrupted the transfer of information and metabolic material from the retina to the brain (and *vice versa*) cannot be fulfilled (Nuschke et al., 2015, Kevenaar and Hoogenraad, 2015). Therefore, it can be supposed that restoring arginine metabolism might have contributed to maintain axon integrity in the

treated groups and might have been one of the underlying mechanism responsible of RGCs dendritic plasticity.

Overall, it can be said that metabolic changes might be the pivot around which RGC survival revolved. This analysis gives a preliminary understanding on the underling pathological changes that can be encountered in the context of experimental glaucoma. However, due to the disease complexity and the metabolic entanglement, further research will be required to elucidate each mechanism involved.

8 Effect of nicotinamide mononucleotide adenine transferase 2 gene therapy on retinal ganglion cell neuroprotection in an *in vivo* inducible model of glaucoma

8.1 Overview

So far all the possible options to achieve neuroprotection through NAM dietary enrichment have been tested. All these aimed to increase NAD^+ bioavailability. However, another way to ideally achieve the same outcome would be to overexpress NMNAT2, one of the rate limiting enzyme in the salvage pathway, that catalyses the conversion of NMN into NAD^+.

Humans have three paralogues of NMNAT; NMNAT1 mainly expressed in the nucleus, NMNAT3 predominantly expressed in the mitochondria and NMNAT2 cytoplasmic and exclusively expressed in neurons (Brazill et al., 2017). According to different studies, NMNATs, specifically NMNAT1 and NMNAT2, appear to be master regulators of neuronal survival (Tang, 2019).

In the context of glaucoma, mice overexpressing NMNAT1 were found to be protected from glaucomatous induced RGC and axon damage (Zhu et al., 2013), while mice genetically depleted of NMNAT2 were more prone to develop glaucomatous related injury (Williams et al., 2022).

Confident of the neuroprotective effect achieved boosting nicotinamide metabolism through NAM administration, the same paradigm was tested through genetic viral overexpression of *hNMNAT2,* which is highly expressed in RGCs. The experiments were designed to explore if the overexpression of the rate limiting enzyme in the salvage pathway could have provided a protective effect in our model of glaucoma.

In this chapter it will be described the effect of unilateral AVV-hNMNAT2 intravitreal injections in two context. The first, in normotensive animals (T.NT.AAVNMNAT2) in order to evaluate whether or not the intravitreal injection alone would have produced any unexpected change in RGC morphology. The second, in unilateral hypertensive animals (T.G.AAVNMNAT2) in order to examine any effect on RGCs integrity.

8.1.1 Experimental setup

To evaluate whether *hNMNAT2* was preserving RGCs integrity, ideally increasing NAD^+ reservoir (Fig. 8.1), intravitreal injections of AAV-NMNAT2 were performed on normotensive and unilateral hypertensive rats.

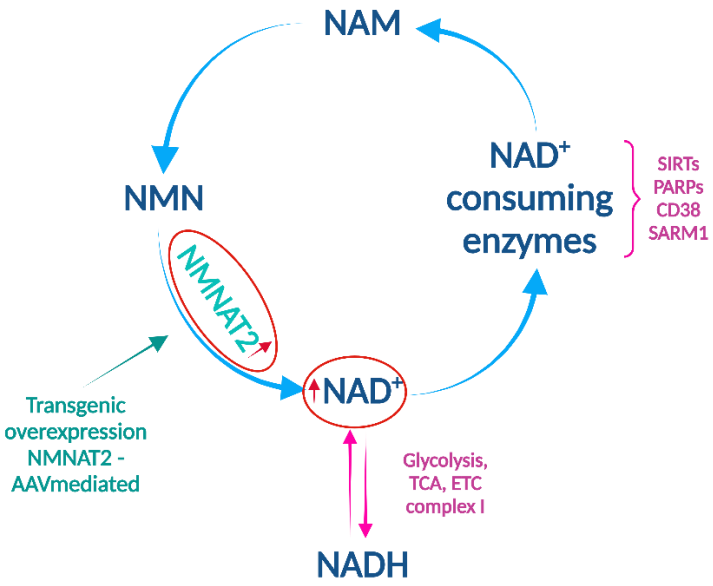

Figure 8. 1. NAD salvage pathway. Increase the expression of NMNAT2, one of the rate limiting enzymes in the salvage pathway, should automatically increase NAD biosynthesis. In a disease context, altering the production of NAD through the salvage pathway may compensate for the increase in NAD consumption or NAD decrease due to age.

Overexpression of *hNMNAT2* was induced through intravitreal injection of an AVV carrier (AAV2 CMV-eGFP-T2A-CMV-NMNAT2, Vector Biolab; 3 µl of $2.2x10^{11}$ gc/ml unilaterally, left eye). A minimum of three weeks were kept between any further procedure to allow the complete expression of the gene and monitor any inflammatory reaction that could have risen from the viral injections. For the hypertensive group, glaucoma was induced as described in chapter 3.

IOP of both groups were monitored constantly throughout the experimental period, and only the rats showing appropriate IOP profiles were included in the analysis.

The rats were divided in two main experimental groups (Fig. 8.2):

1. NMNAT2 unilateral gene therapy on normotensive rats, where the animals were exposed to unilateral NMNAT2 overexpression for a period of 3 weeks. This group will

be referred as T.NT.NMNAT2 (contralateral, T.NT.AAVnull; ipsilateral T.NT.AAVNMNAT2).

2. NMNAT2 unilateral gene therapy on hypertensive rats, where the animals were exposed to unilateral NMNAT2 overexpression for a period of 3 weeks, followed by induction of OHT in the same intravitreally injected eye. As for all the others HT groups OHT was maintained over a period of 4 weeks. This group will be referred as T.G.AAVNMNAT2 (contralateral, T.G.NT.AAVnull; ipsilateral, (T.G.HT.AAVNMNAT2).

Retinal labelling and morphological analysis of RGCs were performed as previously described, with DiOlistics bullets containing a mixture of DiI and DiD to avoid any wavelength overlap with the viral GFP tag.

To estimate NMNAT2-derived neuroprotective effect, all the data collected were compared with the positive control C.sham and the negative control G.sham (only for T.G.AVVNMNAT2).

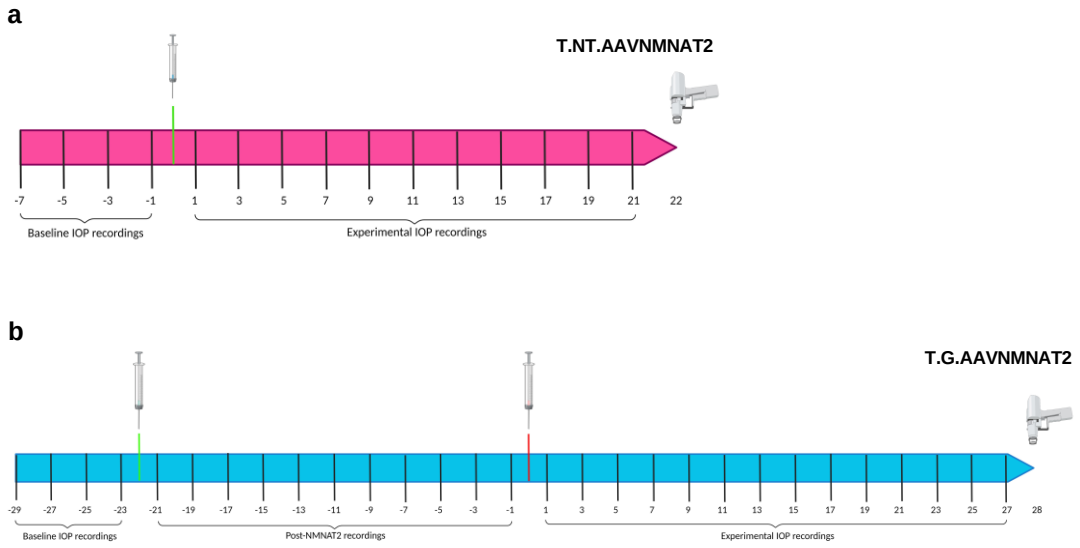

Figure 8. 2. Viral-mediated overexpression of hNMNAT2 experimental workflow. a) Viral-mediated overexpression of *hNMNAT2* in normotensive rats. b) Viral-mediated overexpression of *hNMNAT2* followed by induction of unilateral OHT.

8.2 Results

8.2.1 AVV-mediated hNMNAT2 overexpression in normotensive rats

8.2.1.1 IOP profiles following intravitreal injection with AAV-hNMNAT2

Intravitreal injections in few cases can increase IOP and potentially cause RGCs damage (de Vries et al., 2020). To understand whether or not AAV-NMNAT2 intravitreal injections were causing any change in the animals IOP profiles, all the animals were monitored pre and post injections and their IOP checked every other day.

IOP readouts showed normal IOP profiles after intravitreal injections (IVI; Fig. 8.3 I, II; single animal IOP recording Appendix A.6). This result confirmed that IVIs were not introducing a confounder in the analysis, as dendritic atrophy due to IOP increase, hence it was possible to proceed with RGCs morphological analysis.

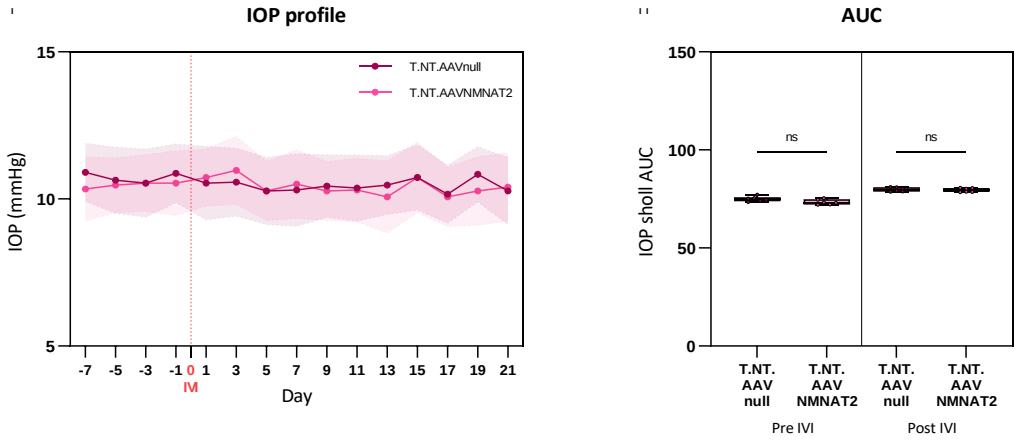

Figure 8. 3. Intraocular pressure profile of normotensive rats unilaterally injected with AAV-NMNAT2. I) T.NT.AAVNMNAT2 group IOP profile; II) Area under the IOP curve. Line mean value of complete IOP recordings ; shaded area ± SD. Box and whisker plot. Whiskers, minimum and maximum value; plot, 1st quartile, median and 3rd quartile. Dots, single rat value. Ordinary one-way ANOVA followed by Tukey's post hoc test; ns = non significant, p = > 0.05. Post-IVI AUC IOP has been normalised to pre-IVI AUC IOP following: $x(norm.\,factor) = \frac{\Sigma\ post\ IVI\ recordings}{\Sigma\ pre\ IVI\ recordings}$.

8.2.1.2 Effect of hNMNAT2 gene therapy on normotensive RGCs morphology

Sholl analysis of DiOlistically labelled RGCs showed that AAV-NMNAT2 injections did not alter Sholl profiles of RGCs of both contralateral and ipsilateral injected eyes compared to C.sham

(Fig. 8.4 c). Although no significant differences were observed within the three Sholl curves, in T.NT.AAVnull the initial Sholl intervals displayed a slightly increased complexity compared to the injected eye and C.sham. However, no difference could be observed in the Sholl AUC (mean ± SD; T.NT.AAVnull 4122.94 ± 2399.13, p = 0.5334; T.NT.AAVNMNAT2 3896.43 ± 1707.83, p = 0.6576; Fig. 8.4 d) neither within the max number of dendritic intersections between the groups (C.sham ≈ 37 ± 15; T.NT.AAVnull ≈ 41 ± 15, p = 0.1876; T.NT.AAVNMNAT2 ≈ 36 ± 13, p = 0.8007; Fig. 8.4 e). Similarly, no significant differences were addressed in the total neurites length (Fig. 8.4 f). At a single branch level, no significant differences were observed between the groups, except for a slight statistically significant decrease within the tertiary branches of T.NT.AAVnull compared to the normotensive untreated control (p = 0.0374; Fig. 8.4 g). Although no relevant changes were addressed as overall dendritic complexity among the groups, analysis of the dendritic field area revealed a reduction of the dendritic spatial coverage of T.NT.AAVnull, while no differences were observed between T.NT.AAVNMNAT2 and C.sham (mean ± SD; C.sham 160982.05 ± 83949.21; T.NT.AAVnull 132035.17 ± 88068.23, p = 0.0194; T.NT.AAVNMNAT2 162841.21 ± 72956.61, p = 0.5866; Fig. 8.4 h).

At the GCL, a 11% decrease was observed in the distance between neighbouring cells of the injected retinas (p = <0.0001), but no differences could be observed with the non injected eyes (p = 0.6450; Fig.8.4 i). Considering that data, it was surprising to observe a 13% increase in the nuclei count of T.NT.AAVNMNAT2 (p = <0.0001; Fig. 8.4 j). However, it has to be taken into account that the confocal laser used to detect Hoechst 33442 might have detected at the GCL some of viral GFP tag. Albeit that should be extremely unlikely considering that Hoechst excitation and emission wavelengths have very little overlap with eGFP (Hoechst 33442, ex. 351nm / em. 454 nm; eGFP, ex. 489 nm / em. 511 nm), it would be better to repeat the experiment to confirm these observations.

To complete the observations of RGC morphological analysis, RGCs were classified according to their dendrites depth in the IPL. According to this classification, no statistical differences were found among the groups, with the ON and OFF of contralateral a bit more complex in the initial part of the Sholl curve and a minimal shift after the peak. Those minimal differences did not affect the overall complexity as measured by the AUC (Fig. 8.4 k-m).

Overall NMNAT2 was well tolerated by RGCs, showing no difference with the normotensive control in regard to dendritic morphology confirming that this experimental approach could be performed on hypertensive rats (next section).

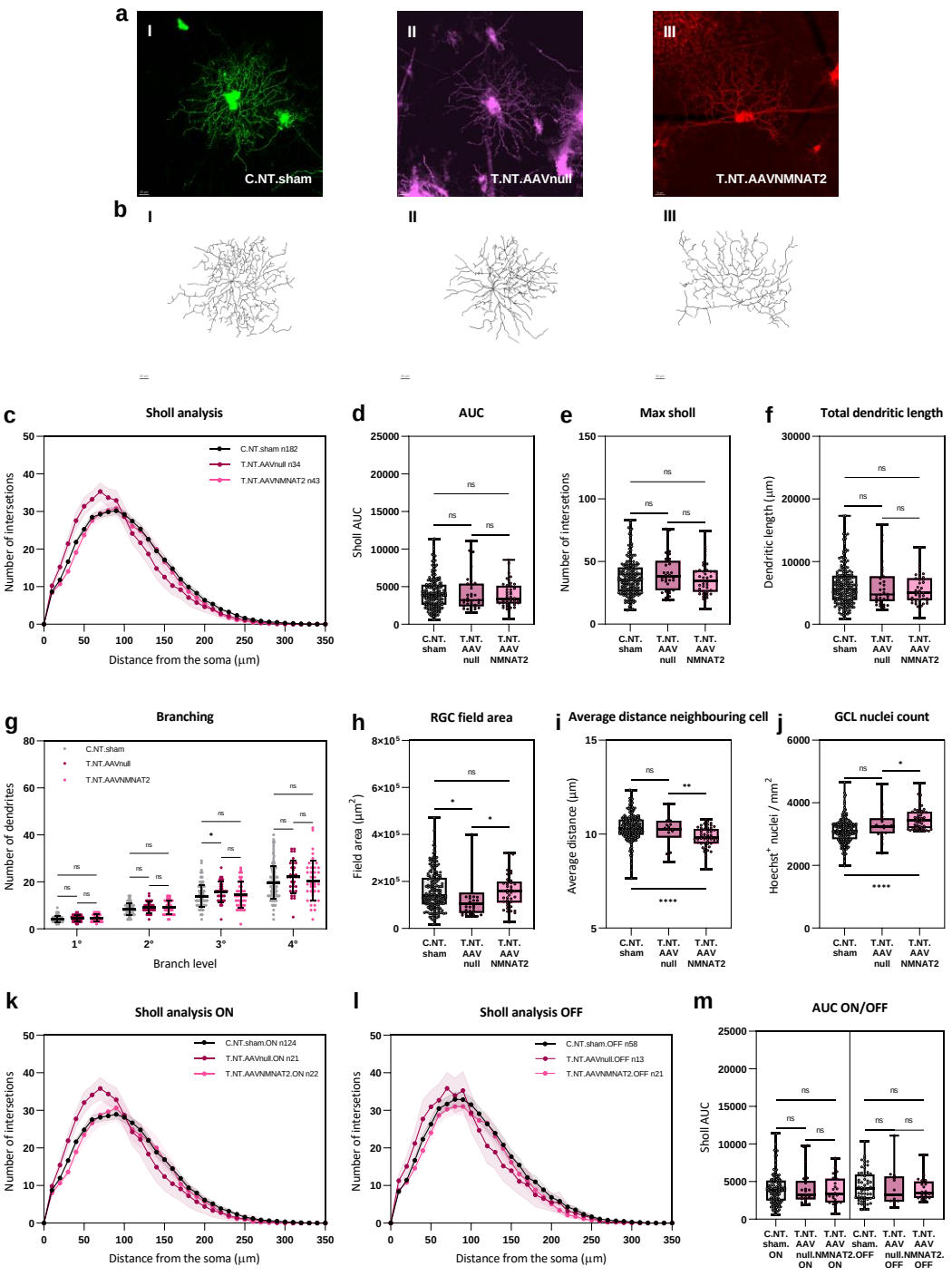

Figure 8. 4. Retinal ganglion cells morphological profile following unilateral intravitreal injection of AAV-NMNAT2 compared to untreated normotensive retinal ganglion cells. a, b) DiOlistically labelled RGCs with corresponding Imaris reconstruction. Scale bar 30 µm, image pixel size 2048 x 2048. c) Sholl analysis of all reconstructed RGCs. Line mean value at each interval; shaded area ± SEM. d) Area under the Sholl curve (AUC). e) Maximum number of total dendritic intersections at the Sholl peak. f) Total dendrites length. g) Number of the dendrites at proximal soma branches. Individual values ± SD. h)

Dendritic field area. i) Average distance between neighbouring cells at the GCL. j) Nuclei count at the GCL. k, l) Sholl Analysis of reconstructed RGCs according to their receptive field. m) Area under the Sholl curve of RGCs divided according their receptive field. Box and whiskers plot with individual values. Whiskers, minimum and maximum value; box plot, 1st quartile, median and 3rd quartile; dots, individual value. Kruskal-Wallis test followed by uncorrected Dunn's test. Ns = non significant, $p > 0.05$; * = $p < 0.05$; ** = $p < 0.01$; **** = $p < 0.0001$.

8.2.2 Can AVV-mediated hNMNAT2 overexpression prevent glaucomatous damage?

8.2.2.1 Do AAV-NMNAT2 intravitreal injections affect the induction of unilateral ocular hypertension?

Unilateral viral mediated overexpression of NMNAT2 was performed on the same eye where intracameral injections of microbeads were going to be performed. Although no changes in normal IOP parameters could be detected in normotensive rats following IVI, it was pivotal to determine whether it was still possible to induce a chronic and moderate IOP increase in intravitreally injected eyes whit just one intracameral microbead injection.

Statistical analysis of IOP profiles revealed no interference of IVIs with the induction of glaucoma (Fig. 8.5; single animal IOP profiles Appendix A.6). All ipsilateral eyes reached a moderate and chronic OHT profile which was maintained for 4 weeks without the need of a second injection.

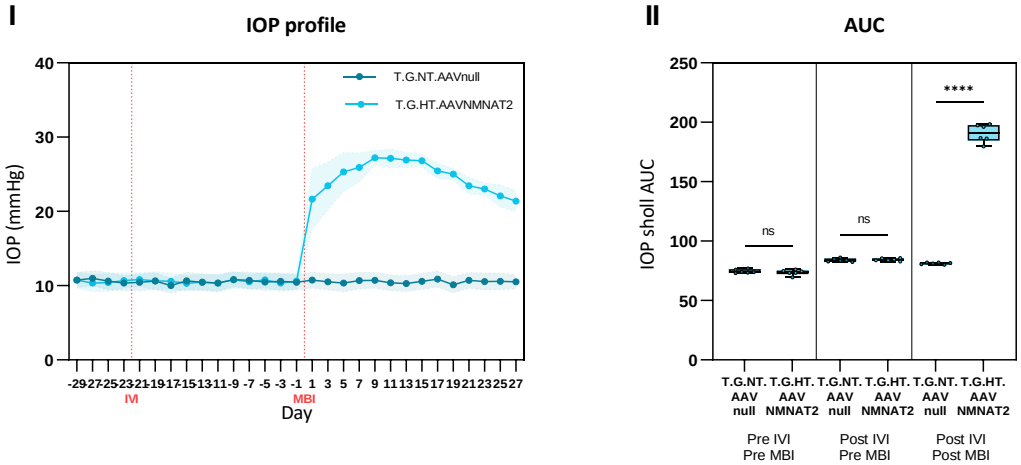

Figure 8. 5. Intraocular pressure profile of AAV-NMNAT2 injected rats followed by the induction unilateral model of OHT glaucoma. I) T.G.AAVNMNAT2 group IOP profile; II) Area under the IOP curve. Line mean value of complete IOP recordings ; shaded area ± SD. Box and whisker plot. Whiskers, minimum and maximum value; plot, 1st quartile, median and 3rd quartile. Dots, single rat value. Ordinary one-way ANOVA followed by Tukey's *post hoc* test; **** = $p < 0.0001$, ns = non significant, $p = > 0.05$. Post-IVI pre-

MBI AUC IOP has been normalised to pre-IVI pre-MBI AUC IOP following: $x(norm.factor) = \frac{\Sigma\ post\ IVI\ pre\ MBI\ recordings}{\Sigma\ pre\ IVI\ pre\ MBI\ recordings}$. Post-IVI post-MBI IOP AUC has been normalised to pre-IVI pre-MBI AUC IOP following: $x(norm.factor) = \frac{\Sigma\ post\ IVI\ post\ MBI\ recordings}{\Sigma\ pre\ IVI\ pre\ MBI\ recordings}$.

8.2.2.2 Can hNMNAT2 gene therapy protect RGC dendrites integrity from OHT damage?

Sholl analysis of Diolistically labelled RGCs showed that RGCs from ipsilateral double injected eyes (IVI and MBI) displayed a greater dendritic complexity within a 50 to 150 µm range from the soma, while the contralateral eye displayed a severe left shift compared to C.sham (Fig 8.6 c). Indeed, the AUC, which is an index of overall complexity, revealed a 30% reduction in the contralateral eye (mean ± SD; C.sham 4151.86 ± 2120.55; T.G.NT.AAVnull 2948.46 ± 1452.34, p = 0.0007), while no statistical differences were found between the ipsilateral and C.sham (T.G.HT.AAVNMNAT2 4699.25 ± 2250.26, p = 0.1402; Fig. 8.6 d). Although a profound left shift was observed in T.G.NT.AAVnull, this change did not affect the number of dendritic intersections at the Sholl peak. Statistical analysis did not reveal any significant change between T.G.NT.AAVnull and C.sham in the max Sholl (p = 0.3040; Fig. 8.6 e), in contrast the overall dendritic reduction deeply affected the total dendrites length, which was 29% less compared to C.sham (p = 0.0009; Fig. 8.6 f). For T.G.HT.AAVNMNAT2, the greater complexity observed in the Sholl profile significantly influenced the number of dendritic intersections at the Sholl peak (20% increase compared to C.sham; p = 0.0102; Fig. 8.6 e), without affecting the total dendritic length (Fig. 8.6 f).

At a branching level, the differences between contralateral and ipsilateral eye with the untreated control were observed since the primary branches, with the number of dendrites progressively deceasing in the contralateral at each branch level and in the ipsilateral progressively increasing (Fig. 8.6 g). All these structural rearrangements had repercussions on the RGCs dendritic area; T.G.NT.AAVnull RGC field areas dramatically decreased compared to both C.sham and T.G.HT.AAVNMNAT2 (mean ± SD; C.sham 160982.05 ± 83949.21; T.G.NT.AAVnull 95440.92 ± 49076.67, p = <0.0001; T.G.HT.AAVNMNAT2 149256.95 ± 68304.75; p vs C.sham = 0.7150, p vs T.G.NT.AAVnull = 0.0003; Fig. 8.6 h).

At the GCL, the distance between neighbouring cells in the contralateral T.G.NT.AAVnull retinas was reduced compared to C.sham, while no significant changes were observed between the ipsilateral T.G.HT.AAVNMNAT2 and C.sham (Fig. 8.6 i). In contrast, the nuclei count of T.G.NT.AAVnull was divided between two extremes (Fig 8.6 j), while the cell density of

T.G.HT.AVVNMNAT2 even if statistically different from C.sham was similar between the analysed sample images (Fig. 8.6 j). Although the data at the GCL had some statistical relevance, it would be preferable to repeat the counting with a specific RGC staining (*i.e.* RBPMS) in order to avoid any misleading speculation.

To confirm that the trend observed in the group Sholl analysis was not related to the different RGCs sub-class response to IVIs, OHT and contralateral effect, ON- and OFF-centre RGCs Sholl analysis were performed as well. The data confirmed the same trend observed in the general Sholl, with the contralateral still showing RGCs dendritic atrophy in both ON- and OFF-centre RGCs while the ipsilateral RGCs ON and OFF profiles were similar to C.sham (Fig. 8.6 k-m).

However, this pilot experiment intended to explore whether gene therapy with NMNAT2 could be an alternative therapeutic approach to protect RGCs from ocular hypertensive damage. Thus, to determine whether AAV-NMNAT2 IVIs protecting RGCs from OHT-related dendritic atrophy, the data were compared with the untreated unilateral hypertensive group G.sham.

From the Sholl profiles it was observed that T.G.HT.AAVNMNAT2 was the only sub-group to not show dendritic atrophy. The contralateral T.G.NT.AAVnull curve had the same profile as both G.sham Sholl curves, indeed they were almost overlapping (Fig. 8.7 c). The same trend was observed for all Sholl-related analysis. The AUC emphasised T.G.HT.AAVNMNAT2 as the only sub-group with a statistically relevant increase of overall complexity (mean ± SD and p values vs T.G.HT.AAVNMNAT2 (149256.95 ± 68304.75); G.NT.sham, 130311.10 ± 54383.97, $p = 0.0006$; G.HT.sham, 97434.28 ± 47712.88, $p = <0.0001$; T.G.NT.AAVnull, 95440.92 ± 49076.67, $p = <0.0001$; Fig. 8.7 d). Similarly, both maximum number of dendritic intersections and total length of dendrites showed that T.G.HT.AAVNMNAT2 was the only sub-group where dendritic preservation could be observed (Fig. 8.7 e, f). Considering the similar Sholl parameters between G.sham and the contralateral T.G.NT.AAVnull, no significant differences were found among the primary branches of those groups. In contrast, genetic overexpression of NMNAT2 in the ipsilateral hypertensive eye contributed to progressive gain of complexity in T.G.HT.AAVNMNAT2 since the primary branches (Fig. 8.7 g).

All these data showed that RGCs from the contralateral eye T.G.NT.AAVnull suffered a severe dendritic atrophy, as confirmed by the analysis of the dendritic field area, where T.G.NT.AAVnull dendritic area readouts were even worse than G.HT.sham ($p = 0.0025$; Fig. 8.7 h).

From the previous experiments it was known that G.sham displayed a severe cell loss. Therefore when the data collected at the GCL were compared with the untreated hypertensive group (Fig. 8.7 i, j), it was confirmed that those specific data could not be trusted due to the inconsistency of the nuclei data from T.G.AAVNMNAT2, in particular for T.G.NT.AAVnull. Therefore, the analysis should be repeated in the future to confirm any observation.

Analysis of ON and OFF RGCs did not add any new unexpected observations, with the contralateral RGCs displaying the same dendritic complexity as the untreated counterparts, and T.G.HT.AAVNMNAT2 as the only group showing preserved dendritic complexity in both sub-categories (Fig. 8.7 k-m).

For a thorough overview of this preliminary gene therapy trial, the two groups exposed to AAV-NMNAT2 were compared as well.

As it can be observed from the Sholl analysis and related parameters, T.NT.AAVnull/NT.AAVNMNAT2 displayed a more homogeneous profile compared to the glaucoma AAVNMNAT2 injected counterpart (Fig. 8.8 c-m). The contralateral effect in the non injected eye (T.G.NT.AAVnull), even within this comparison, was still very severe, which suggests that further experiments should be carried before this can be considered a new therapeutic approach.

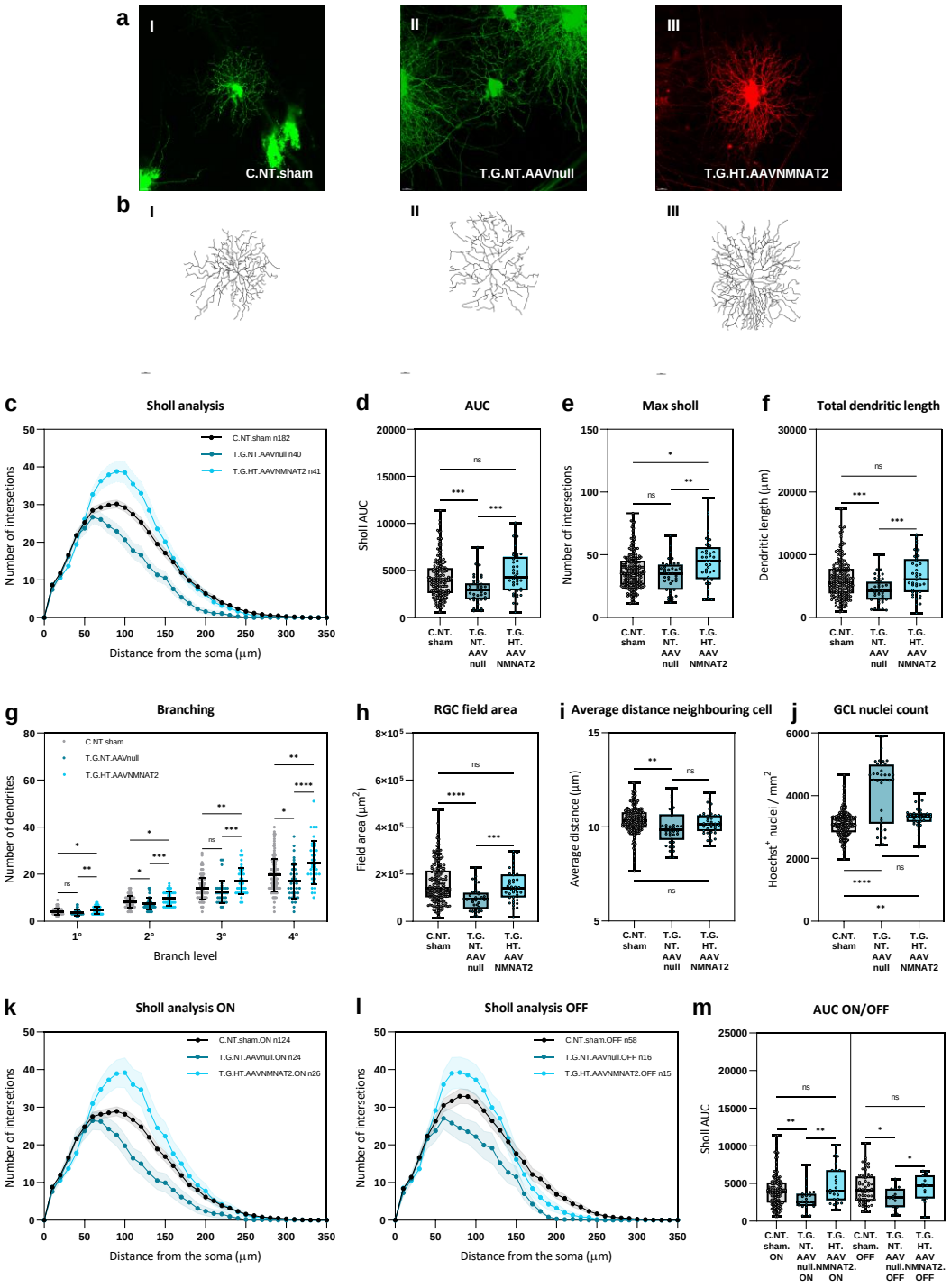

Figure 8. 6. Retinal ganglion cells morphological profile following unilateral intravitreal injection of AAV-NMNAT2 and unilateral induction of ocular hypertension compared to untreated normotensive retinal ganglion cells. a, b) DiOlistically labelled RGCs with corresponding Imaris reconstruction. Scale bar 30 µm, image pixel size 2048 x 2048. c) Sholl analysis of all reconstructed RGCs. Line mean value at each interval; shaded area ± SEM. d) Area under the Sholl curve (AUC). e) Maximum number of total dendritic intersections at the Sholl peak. f) Total dendrites length. g) Number of the dendrites at proximal soma branches. Individual values ± SD. h) Dendritic field area. i) Average distance between neighbouring cells

at the GCL. j) Nuclei count at the GCL. k, l) Sholl Analysis of reconstructed RGCs according to their receptive field. m) Area under the Sholl curve of RGCs divided according their receptive field. Box and whiskers plot with individual values. Whiskers, minimum and maximum value; box plot, 1st quartile, median and 3rd quartile; dots, individual value. Kruskal-Wallis test followed by uncorrected Dunn's test. Ns = non significant, p > 0.05; * = p < 0.05; ** = p < 0.01; *** = p < 0.001; **** = p < 0.0001.

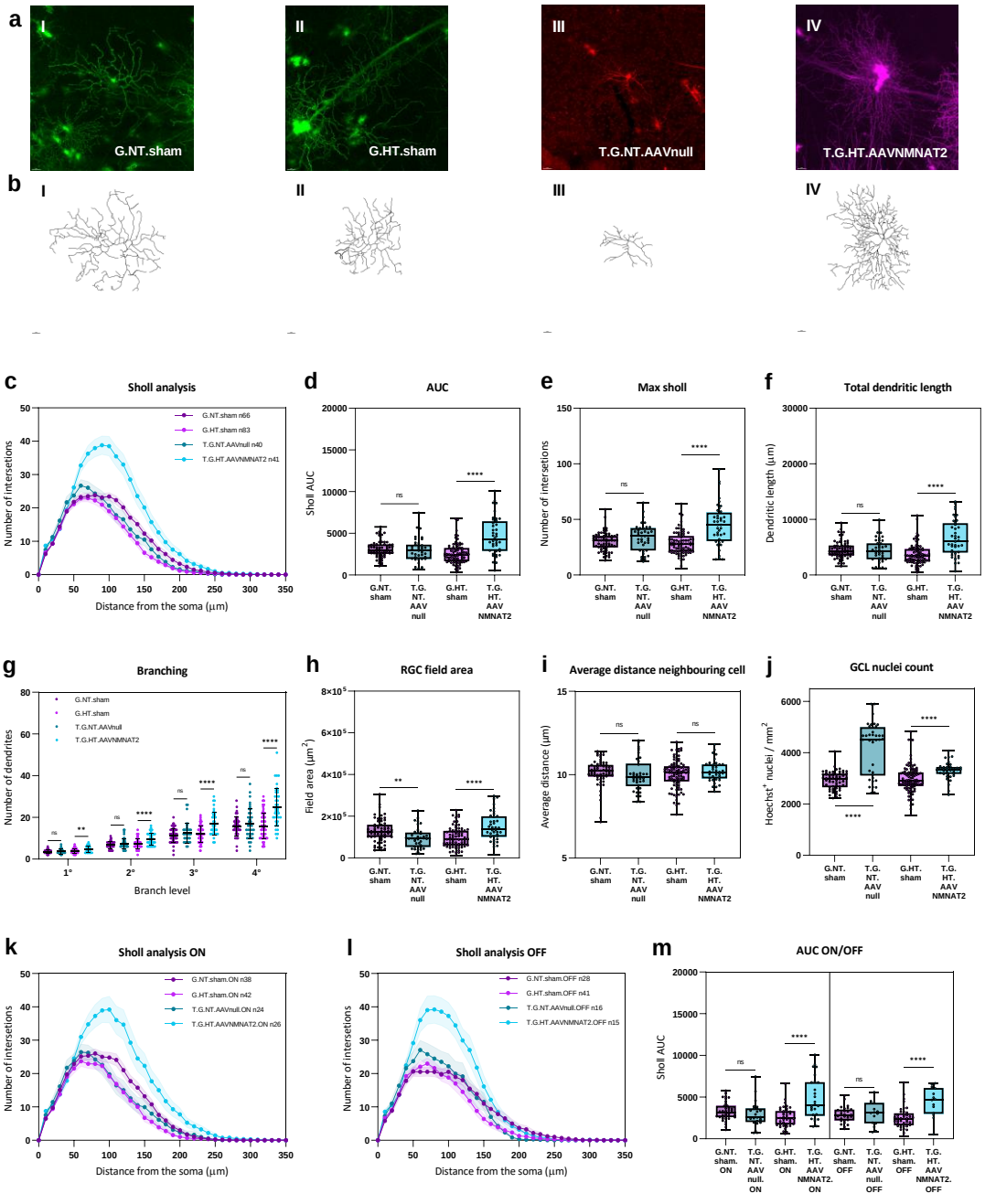

Figure 8. 7. Retinal ganglion cells morphological profile following unilateral AAV-NMNAT2 injection and induction of unilateral ocular hypertension ocular compared to untreated unilateral OHT retinal ganglion cells profile. a, b) DiOlistically labelled RGCs with corresponding Imaris reconstruction. Scale bar 30 µm, image pixel size 2048 x 2048. c) Sholl analysis of all reconstructed RGCs. Line mean value at each

interval; shaded area ± SEM. d) Area under the Sholl curve (AUC). e) Maximum number of total dendritic intersections at the Sholl peak. f) Total dendrites length. g) Number of the dendrites at proximal soma branches. Individual values ± SD. h) Dendritic field area. i) Average distance between neighbouring cells at the GCL. j) Nuclei count at the GCL. k, l) Sholl Analysis of reconstructed RGCs according to their receptive field. m) Area under the Sholl curve of RGCs divided according their receptive field. Box and whiskers plot with individual values. Whiskers, minimum and maximum value; box plot, 1st quartile, median and 3rd quartile; dots, individual value. Kruskal-Wallis test followed by uncorrected Dunn's test. Ns = non significant, p > 0.05; * = p < 0.05; ** = p < 0.01; **** = p < 0.0001.

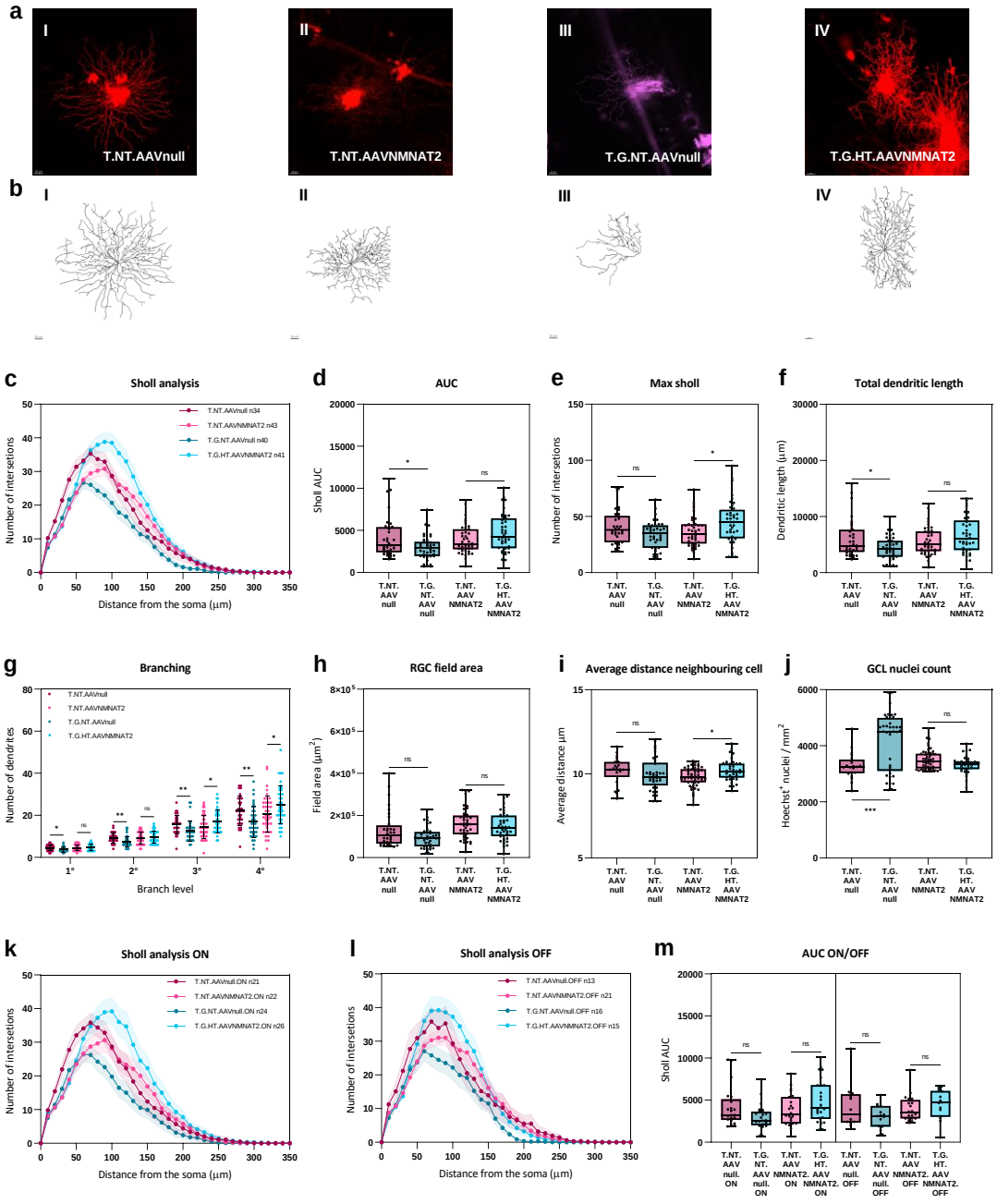

Figure 8. 8. Retinal ganglion cells morphological profile following unilateral AAV-NMNAT2 injection and induction of unilateral ocular hypertension ocular compared to normotensive unilaterally intravitreally injected AAV-NMNAT2 retinal ganglion cells profile. a, b) DiOlistically labelled RGCs with corresponding Imaris reconstruction. Scale bar 30 µm, image pixel size 2048 x 2048. c) Sholl analysis of all reconstructed RGCs. Line mean value at each interval; shaded area ± SEM. d) Area under the Sholl curve (AUC). e) Maximum number of total dendritic intersections at the Sholl peak. f) Total dendrites length. g) Number of the dendrites at proximal soma branches. Individual values ± SD. h) Dendritic field area. i) Average distance between neighbouring cells at the GCL. j) Nuclei count at the GCL. k, l) Sholl Analysis of reconstructed RGCs according to their receptive field. m) Area under the Sholl curve of RGCs divided according their receptive field. Box and whiskers plot with individual values. Whiskers, minimum and maximum value; box plot, 1st quartile, median and 3rd quartile; dots, individual value. Kruskal-Wallis test followed by uncorrected Dunn's test. Ns = non significant, $p > 0.05$; * = $p < 0.05$; ** = $p < 0.01$.

8.3 Discussion

Before the outcome of the experiments will be discussed, there are few technical issues that arose during DiOlistics labelling which are worth mentioning.

As we explained in chapter 2, Diolistic labelling relies on ballistic delivery of fluorescent particles which diffuse in the cells. To perform these experiments the dyes combination has been adjusted in order to avoid any overlap between the fluorescent spectra. Although it seems trivial, that small adjustment slightly compromised the labelling outcome.

DiD spectrum does not fall within the human visible wavelengths (Rodriguez-Carmona and Barbur, 2017), therefore when retinas labelling was checked only DiI labelled RGCs were seen. When the DiI was randomly dispersed on at least 30% of the retina surface the tissue was not re-shot, but this did not happen for all the samples. In some cases the re-shooting has produced an unintentional over labelling which affected the ability to completely separate some RGCs. Due to that some cells were excluded from the analysis, which drastically reduced the sample size.

With that been said, both NMNAT2 experiments have been useful to understand several aspects of NAD^+ neurotrophic support that could not have been noticed with a systemic delivery route.

First of all, NMNAT2 overexpression was not harmful to RGCs in neither condition. Focusing the attention on the injected eyes, in the normotensive animals nothing changed compared to a naïve Sholl profile, while in the glaucoma some improvements could even be observed. Both observations, at a minor degree, were consistent with the results obtained with a NAM enriched

diet. However, in the NAM experiments both eyes were protected, the concentration the animals were exposed to was known, and the impact this had on their metabolism. In these experiments, two main things could not be controlled. The contralateral effect and the extent in which *NMNAT2* overexpression was influencing NAD^+ metabolism.

RGCs from T.G.NT.AAVnull, the contralateral non injected eye, displayed a severe dendritic atrophy which might have been caused by the lack neurotrophic support given by NAD^+ metabolism, and thus might have been exposed to the contralateral OHT effect. This scenario could not be observed in the NAM experiments due to the systemic delivery route. Although severe, this effect emphasised that the pathophysiology of glaucoma should be regarded as a complex neurodegenerative disease where OHT is just one of the symptoms. Contralateral degeneration has been observed in different models of retina diseases (Lucas-Ruiz et al., 2021). This degeneration appears to be caused by uncontrolled glia activation and retrograde degenerative inputs from the affected brain areas (Sapienza et al., 2016). Glia activation triggers an extended neuroinflammatory reaction that jeopardises neuronal viability, and improving NAD^+ metabolism, among its multiple therapeutic potentials, seems to have also anti-inflammatory properties (Rajman et al., 2018). That might explain why this effect was not noticed before, with the exception of G.sham. In light of this result, if NMNAT2 intravitreal gene therapy were to be pursued as treatment strategy, it should be considered to overexpress NMNAT2 in the contralateral eye as well, possibly considering NAM supplementation to support NMNAT2 activity.

The other factor that might have influenced the experimental outcome could have been the overexpression efficiency. Given the increased complexity in T.G.HT.AAVNMNAT2, it can be assumed that NMNAT2 overexpression was successful. However, it has to be considered NMNAT2 does not operate only in the salvage pathway (Brazill et al., 2017), but serves as substrate for multiple signalling pathways as well (Verdin, 2015, Lavado-Roldan and Fernandez-Chacon, 2016, Zhai et al., 2008). Due to this “multitasking” role, cellular level of NMNAT2 may vary depending on the context and physiological state (Moriya, 2015, Munkacsy et al., 2019). Therefore, for a future experimental outlook, it should be considered to perform NMNAT2 quantitative studies in order to inject the proper amount of gene copies to fulfil the cellular requirement in a degenerative state.

Beside the unexpected outcome of this trial, it is well established that NMNAT2 exerts neuroprotective functions against various insults (Pottorf et al., 2018), and that its

overexpression has been found to rescue RGCs from glaucomatous damage (Fang et al., 2022). Interestingly, when Liu *et al.* (Liu et al., 2021) employed the same viral construct as Fang et al. (Fang et al., 2022) (AAV-mSncg-NMNAT2Δex6 (Wang et al., 2020, Yang et al., 2016, Miao et al., 2016)) they did not observe any neuroprotective effect nor improved visual functions in their experimental groups.

Although there are some controversies, there is enough evidence which emphasises NMNAT2 role as key molecule in axon maintenance (Waller and Collins, 2021, Icso and Thompson, 2022, Gilley and Coleman, 2010, Gilley et al., 2018) and RGCs homeostasis (Fang et al., 2022, Williams et al., 2022) but, in order to be translated into an effective treatment, further studies are needed to clarify NMNAT2 neuroprotective mechanisms in a disease context.

9 General discussion and conclusions

One of the most characteristic features of glaucoma is the degeneration and loss of retinal ganglion cells (Morgan et al., 2006). However, while RGC cell death contributes to visual loss, dendritic atrophy, which influences the ability to process visual information (Agostinone and Di Polo, 2015) is a significant contributing factor.

The one and only unmodifiable risk factor for glaucoma is age. Age alters the metabolic state of the cells (Blaszczyk, 2020), and for cells as RGCs which live on a metabolic knife edge, that renders the latter vulnerable to IOP related stress (Harder et al., 2020, Morgan, 2012). Although OHT is one of the modifiable factors, RGCs continue to degenerate even when IOP decreases or is normal (*e.g.* normotensive glaucoma) (Boland and Quigley, 2007). This lack of RGC resilience even when the stressors are eradicated might be due to a complex bioenergetic failure (Casson et al., 2021).

The work in this project has focussed on the disruption of NAD^+ metabolism as an additional factor to be considered in driving retinal ganglion cell damage in glaucoma. Neuronal survival relies on NAD^+ as the main redox cofactor for energy production, and RGCs as the most energy demanding neurons rely on NAD^+ for their energetic support (Cimaglia et al., 2020). Williams *et al.* have reported multiple evidence of NAD^+ imbalance in several murine models of glaucoma (Tribble et al., 2021c, Williams et al., 2018, Williams et al., 2017b) and there is evidence that suggests that prior to cell death RGCs enter into a "comatose" state due to lack of energetic support (Fry et al., 2018). Relief of RGC stress does not mean only IOP reduction, but indicates improvement of mitochondrial function, decrease of oxidative stress and inflammation (Calkins, 2021, Calkins, 2012, Qu et al., 2010).

To date, little is known about NAD^+ long-term exposure effect on RGCs connectome, except for the dendritic preservation shown in retinal explants (Tribble et al., 2021c).

Considering the ongoing clinical trials for NAD^+-glaucoma based therapy and the compelling need to understand more about the effect of this molecule, this project intended to explore NAD^+ metabolism efficacy for RGCs neuroprotection in a rat *in vivo* model of induced chronic ocular hypertension. In the next sections the principal findings of this thesis will be summarised, and future direction for research in this area will be proposed.

9.1 Main findings

9.1.1 NAD^+ precursor nicotinamide adenine mononucleotide long term administration is well tolerated and does not influence intraocular pressure

NAM is the best tolerated NAD^+ precursor and the one with least side effects. However, the need to use upper physiological levels of nicotinamide to increase NAD^+ metabolism and to contain NAD^+ age decline, has raised some concern about the safety and tolerance of long-term administration of that molecule (Hwang and Song, 2020, Conze et al., 2019).

In light of the differences between clinical trial doses and *in vivo* research (human dose in trial 200 mg/kg; animal dose from 200 to 900 mg/kg), it was important to determine whether experimental doses of NAM were well tolerated and whether they had any adverse effect on IOP and RGCs normal parameters.

Monitoring NT BN IOPs for six weeks, four of which with NAM enriched diet (200 mg/kg/day and 600 mg/kg/day), established that NAM had no interaction with IOP and did not compromise RGCs viability. All RGCs showed a notable increase in dendritic complexity when exposed to the molecule. Neuroplasticity in fully differentiated adult RGCs has not been previously documented, but among NAM multiple function there is the direct inhibition of ROCKs (Meng et al., 2018). ROCKs inhibition has been shown to promote dendritic and synaptic plasticity (Swanger et al., 2015, Koch et al., 2018). Considering that all the rats were exposed to the same light cycle from birth (12h light/12h dark), with no differences observed between ON and OFF centre RGCs dendritic density (Tian and Copenhagen, 2001, Tian and Copenhagen, 2003, Bodnarenko and Chalupa, 1993), NAM was the only new factor that could have promoted this change. Whether or not this has improved BN visual acuity is not known, but this confirms that NAM can positively influence RGCs connectome.

9.1.2 Retinal ganglion cell dendritic neuroprotection with dietary NAM is substantial and dose-dependent

NAM retinal ganglion cell neuroprotection has been tested throughout all this project in two well-established models of acute (retinal explants) and chronic (*in vivo* OHT) retinal injury. In both models NAM supplementation showed a substantial neuroprotective effect toward RGCs dendrites.

RGCs from axotomised NAM supplemented retinal explants (both low NAM and high NAM) displayed the same level of complexity as non cultured RGCs, but between 20% to 40% cell loss. These observations suggest that dendritic preservation may not necessarily improve cell survival. Indeed the Moons group has made the argument that dendritic preservation after axonal injury might interfere with RGCs regenerative capacity and therefore promote cell death (Beckers and Moons, 2019). In this case, dendritic atrophy is regarded as an adaptive response to ensure cell survival and the preservation of afferent connections. The implication is that treatments to enhance dendritic preservation / regeneration may increase the risk of afferent loss and cell death. An important qualifier is that retinal ganglion cell axotomy is an acute injury, whose effects are visible within hours of optic nerve resection and manifest with cell loss (Manabe et al., 2002). It might be possible that NAD^+ synthesis, from its precursor NAM, was not rapid enough and thus could not fulfil RGCs neuroprotective requirements at the same pace of the concurrent cell loss. Even though it would be nice to explore NAD biosynthesis dynamics, that would not be enough to explain the greater cell loss in E.3DEV.HNAM compared to the untreated retinal explants.

In vivo, NAM treatment afforded a high level of RGC preservation. With NAM prophylactic and intervention treatment only high NAM provided the same level of protection in the ipsilateral (OHT) and contralateral (NT) eyes, while with low NAM the effect was partial. These results are highly relevant for clinical use of nicotinamide precursors and highlight a dose-dependent effect of nicotinamide. Low NAM AED of 200 mg/kg/day corresponds to HED 2.27 g/day (based on an average weight of 70 kg) (Nair and Jacob, 2016), which exceeds the current dose reported in clinical trials (NCT05275738, 2022, NCT05405868, 2022). By contrast, high NAM (AED 600 mg/kg/day; HED 6.80 g/day) provided the same level of protection in both eyes, preserving normal RGCs dendritic structure even when administered after the induction of ocular hypertension. However, the highest dose of NAM in the available pharmaceutical formulations is 500 mg per tablet, which suggests that high dose NAM may raise adherence issues. The dose effect suggests that new formulation of high dose NAM and alternative routes (e.g. local ocular delivery) should be considered.

9.1.3 NAM neuroprotective effects are achieved through a pro-survival metabolic switch

RGCs have a high bioenergetic demand which renders them vulnerable to mitochondrial dysfunction and metabolic failure. Physiological aging is characterised by decreased metabolic

activity and increase in mitochondrial stress, which may promote neurodegenerative disease outbreak when combined with other cofactors (Jadeja et al., 2020, Fang et al., 2017, Lautrup et al., 2019, Casson et al., 2021). OHT is the characterising cofactor of glaucoma, that, even at its earliest stages, produces major metabolic disruption which escape the neuronal compensatory mechanisms and influence RGCs viability (Tribble et al., 2021c, Tribble et al., 2019, Williams et al., 2017b, Kouassi Nzoughet et al., 2019). NAD^+ decrease has been found to be the main driver of this neuroenergetic failure, and considering that 80% of NAD^+ biosynthesis comes from the salvage pathway, whose synthesising enzymes are highly expressed in the inner retina and optic nerve/optic nerve head (Tribble et al., 2023), it is not surprising that glaucomatous injury in those areas influences RGCs fate.

The project was based on the assumption that OHT disrupts NAD^+ metabolism and as a consequence influence RGCs resistance and/or resilience to damage. Although *ex vivo* and *in vivo* RGCs morphologic readouts demonstrated NAD^+-related dendritic neuroprotection, there was the need to understand how this protection was achieved. Optic nerves metabolic analysis identified distinct metabolic profiles between G.sham, prophylactic and intervention HNAM treated groups. Whilst the defining factor for this distinction was driven by NAD^+ related metabolites, detrimental changes within the G.sham group were also associated with the three main cellular respiration pathways, confirming the expected OHT-related energy deficits in the untreated group. In addition to that, GSH:GSSG ratio was found significantly decreased within G.sham, highlighting the inefficient antioxidant capacity caused by the lack of NAM supplementation. Free ROS promote mitochondrial damage and inflammatory reaction (Mittal et al., 2013, Guo et al., 2013), which have been documented as pathological finger print in glaucoma. Furthermore, this may also explain the severe atrophy in G.sham as well as the contralateral effect that may have been promoted by arachidonic acid related inflammatory reactions.

However, within the picture of RGCs degeneration/survival, salvage pathway analysis identified a pro-Wallerian degeneration shift only in the untreated samples. Wallerian degeneration is the well known mechanisms of axonal degeneration triggered by SARM1 activation influenced by NAD^+ depletion (Gilley et al., 2018, Di Stefano et al., 2015, Angeletti et al., 2022, Waller and Collins, 2021, Figley and DiAntonio, 2020, Figley et al., 2021, Essuman et al., 2017). OHT compromises NMNAT2 transport from the soma to the axons, and NAM in the absence of NMNAT2 cannot complete its conversion to NAD^+. Increasing levels of NMN, the intermediate NAM by-product in the salvage pathway, allosterically activate SARM1 ($SARM1^{TIR}$), hence just

minor alterations in the NNM:NAD ratio might be sufficient to trigger SARM1, which in contrast is allosterically inhibited by NAD^+.

These results suggest that NAM treatment is an effective neuroprotective agent for all RGCs compartments. Its effects do not only provide a neuroenergetic boost, which for itself might be sufficient to fulfil RGCs energy requirements, but negatively interfere with pro-degenerative mechanism enhancing cellular survival capability.

9.1.4 NMNAT2 overexpression in the OHT eye protects ipsilateral RGCs from dendritic atrophy but does not prevent contralateral degeneration

Systemic NAD^+ precursors delivery have the advantage that they increase nicotinamide metabolism in the whole system, whereas local overexpression of NMNAT2 acts only in the target area. In the absence of OHT damage or degenerative injuries the lack of systemic NAD^+ increase should not be an issue, as observed in the normotensive model with intravitreal delivery of AVV-NMNAT2. In contrast, when the same level of NMNAT2 overexpression was applied to a model of ocular hypertension only the ipsilateral eye was protected from glaucomatous induced dendritic pruning.

OHT is not a focal injury, but has repercussions in multiple areas. Therefore, if NAD^+ metabolism is increased only where the physical damage appears, there might be the risk that local overactivity of NMNAT2, in order to fulfil is enzymatic role, might withdraw NAM from other cellular compartments where it might be needed. To confirm this hypothesis, the ideal experiment (outside the scope of the current work) would have been to combine NMNAT2 overexpression with NAM dietary enrichment. Without this data is only possible to confirm that NMNAT2 overexpression did not harm RGCs but was not enough to counteract the contralateral OHT effect.

9.2 Conclusions and future work

The findings of this project suggest that the restoration of NAD^+ biosynthesis/metabolism can protect from OHT induced damage. However, NAM intervention data, which are the most relevant for a translation approach, highlighted issues with regard to the appropriate NAM dose for RGC protection.. Dendritic atrophy, even if minor, may compromise cell viability and affect the transfer of visual information from the eye to the brain (Bargmann and Marder, 2013, Agostinone and Di Polo, 2015). A detailed investigation of RGCs functional changes and

preservation of central afferent connection were outside the scope of this project, but it would be interesting to explore whether or not NAM treatment may influence RGCs function and central connection in a dose-dependent fashion, and whether the increased plastic competence plays a part in that as well. In addition to that, metabolic analysis revealed that glaucoma is much more than a simple optic neuropathy, which supports the continuous research effort in finding the underlying disease mechanisms instead of focusing only on OHT damage. Further more, it would be interesting to understander whether NAM can be used to reverse RGC degeneration and whether it can be used to prepare neurons for regenerative treatment (following the Moons argument, Beckers and Moons, 2019, Beckers *et al*., 2019).

References

AGOSTINONE, J. & DI POLO, A. 2015. Retinal ganglion cell dendrite pathology and synapse loss: Implications for glaucoma. *Progress in Brain Research,* 220**,** 199-216.

AHMED, F. A. K. M., CHAUDHARY, P. & SHARMA, S. C. 2001. Effects of increased intraocular pressure on rat retinal ganglion cells. *International Journal of Developmental Neuroscience,* 19**,** 209-218.

ALARAUTALAHTI, V., RAGAUSKAS, S., HAKKARAINEN, J. J., UUSITALO-JARVINEN, H., UUSITALO, H., HYTTINEN, J., KALESNYKAS, G. & NYMARK, S. 2019. Viability of Mouse Retinal Explant Cultures Assessed by Preservation of Functionality and Morphology. *Investigative Ophthalmology & Visual Science,* 60**,** 1914-1927.

ALMASIEH, M., WILSON, A. M., MORQUETTE, B., CUEVA VARGAS, J. L. & DI POLO, A. 2012. The molecular basis of retinal ganglion cell death in glaucoma. *Progress in Retinal and Eye Research,* 31**,** 152-81.

ANDERSON, M. G., SMITH, R. S., HAWES, N. L., ZABALETA, A., CHANG, B., WIGGS, J. L. & JOHN, S. W. M. 2002. Mutations in genes encoding melanosomal proteins cause pigmentary glaucoma in DBA/2J mice. *Nature Genetics,* 30**,** 81-85.

ANDERSON, S., BANKIER, A. T., BARRELL, B. G., DE BRUIJN, M. H. L., COULSON, A. R., DROUIN, J., EPERON, I. C., NIERLICH, D. P., ROE, B. A., SANGER, F., SCHREIER, P. H., SMITH, A. J. H., STADEN, R. & YOUNG, I. G. 1981. Sequence and organization of the human mitochondrial genome. *Nature,* 290**,** 457-465.

ANGELETTI, C., AMICI, A., GILLEY, J., LORETO, A., TRAPANOTTO, A. G., ANTONIOU, C., MERLINI, E., COLEMAN, M. P. & ORSOMANDO, G. 2022. SARM1 is a multi-functional NAD(P)ase with prominent base exchange activity, all regulated bymultiple physiologically relevant NAD metabolites. *iScience,* 25**,** 103812.

ARMSTRONG, R. A. & CUBBIDGE, R. C. 2019. The Eye and Vision: An Overview. *Handbook of Nutrition, Diet, and the Eye.*

BAI, S. & SHELINE, C. T. 2013. NAD(+) maintenance attenuates light induced photoreceptor degeneration. *Experimental eye research,* 108**,** 76-83.

BALTAN, S., INMAN, D. M., DANILOV, C. A., MORRISON, R. S., CALKINS, D. J. & HORNER, P. J. 2010. Metabolic vulnerability disposes retinal ganglion cell axons to dysfunction in a model of glaucomatous degeneration. *Journal of Neuroscience,* 30**,** 5644-52.

BANEKE, A. J., LIM, K. S. & STANFORD, M. 2016. The Pathogenesis of Raised Intraocular Pressure in Uveitis. *Current Eye Research,* 41**,** 137-49.

BARGMANN, C. I. & MARDER, E. 2013. From the connectome to brain function. *Nature Methods,* 10**,** 483-90.

BECKERS, A. & MOONS, L. 2019. Dendritic shrinkage after injury: a cellular killer or a necessity for axonal regeneration? *Neural Regeneration Research,* 14**,** 1313-1316.

BECKERS, A., VAN DYCK, A., BOLLAERTS, I., VAN HOUCKE, J., LEFEVERE, E., ANDRIES, L., AGOSTINONE, J., VAN HOVE, I., DI POLO, A., LEMMENS, K. & MOONS, L. 2019. An Antagonistic Axon-Dendrite Interplay Enables Efficient Neuronal Repair in the Adult Zebrafish Central Nervous System. *Molecular Neurobiology,* 56**,** 3175-3192.

BENNINGER, R. K. P. & PISTON, D. W. 2013. Two-Photon Excitation Microscopy for the Study of Living Cells and Tissues. *Current Protocols in Cell Biology,* 59**,** 4.11.1-4.11.24.

BERGEN, A. A. 2017. Nicotinamide, iRPE-in-a dish, and age-related macular degeneration therapy development. *Stem cell investigation,* 4**,** 81-81.

BINLEY, K. E., NG, W. S., BARDE, Y.-A., SONG, B., MORGAN, J. E. & KIRIK, D. 2016. Brain-derived neurotrophic factor prevents dendritic retraction of adult mouse retinal ganglion cells. *European Journal of Neuroscience*.

BINLEY, K. E., NG, W. S., TRIBBLE, J. R., SONG, B. & MORGAN, J. E. 2014. Sholl analysis: a quantitative comparison of semi-automated methods. *Journal of Neuroscience Methods,* 225**,** 65-70.

BISWAS, S. & WAN, K. H. 2019. Review of rodent hypertensive glaucoma models. *Acta Ophthalmologica,* 97**,** e331-e340.

BLASZCZYK, J. W. 2020. Energy Metabolism Decline in the Aging Brain-Pathogenesis of Neurodegenerative Disorders. *Metabolites,* 10.

BODEUTSCH, N. & THANOS, S. 2000. Migration of phagocytotic cells and development of the murine intraretinal microglial network: An in vivo study using fluorescent dyes. *Glia,* 32**,** 91-101.

BODNARENKO, S. R. & CHALUPA, L. M. 1993. Stratification of ON and OFF ganglion cell dendrites depends on glutamate-mediated afferent activity in the developing retina. *Nature,* 364**,** 144-146.

BOGAN, K. L. & BRENNER, C. 2008. Nicotinic acid, nicotinamide, and nicotinamide riboside: a molecular evaluation of NAD+ precursor vitamins in human nutrition. *Annual Review of Nutrition,* 28**,** 115-30.

BOIKO, T., VAN WART, A., CALDWELL, J. H., LEVINSON, S. R., TRIMMER, J. S. & MATTHEWS, G. 2003. Functional Specialization of the Axon Initial Segment by Isoform-Specific Sodium Channel Targeting. *The Journal of Neuroscience,* 23**,** 2306.

BOLAND, M. V. & QUIGLEY, H. A. 2007. Risk Factors and Open-angle Glaucoma: Classification and Application. *Journal of Glaucoma,* 16.

BONORA, M., PATERGNANI, S., RIMESSI, A., DE MARCHI, E., SUSKI, J. M., BONONI, A., GIORGI, C., MARCHI, S., MISSIROLI, S., POLETTI, F., WIECKOWSKI, M. R. & PINTON, P. 2012. ATP synthesis and storage. *Purinergic Signal,* 8**,** 343-57.

BOULTON, M. & DAYHAW-BARKER, P. 2001. The role of the retinal pigment epithelium: Topographical variation and ageing changes. *Eye,* 15**,** 384-389.

BRAIDY, N., BERG, J., CLEMENT, J., KHORSHIDI, F., POLJAK, A., JAYASENA, T., GRANT, R. & SACHDEV, P. 2019. Role of Nicotinamide Adenine Dinucleotide and Related Precursors as Therapeutic Targets for Age-Related Degenerative Diseases: Rationale, Biochemistry, Pharmacokinetics, and Outcomes. *Antioxidants & Redox Signaling,* 30**,** 251-294.

BRAKEDAL, B., DÖLLE, C., RIEMER, F., MA, Y., NIDO, G. S., SKEIE, G. O., CRAVEN, A. R., SCHWARZLMÜLLER, T., BREKKE, N., DIAB, J., SVERKELI, L., SKJEIE, V., VARHAUG, K., TYSNES, O.-B., PENG, S., HAUGARVOLL, K., ZIEGLER, M., GRÜNER, R., EIDELBERG, D. & TZOULIS, C. 2022. The NADPARK study: A randomized phase I trial of nicotinamide riboside supplementation in Parkinson's disease. *Cell Metabolism,* 34**,** 396-407.e6.

BRATKOWSKI, M., XIE, T., THAYER, D. A., LAD, S., MATHUR, P., YANG, Y. S., DANKO, G., BURDETT, T. C., DANAO, J., CANTOR, A., KOZAK, J. A., BROWN, S. P., BAI, X. & SAMBASHIVAN, S. 2020. Structural and Mechanistic Regulation of the Pro-degenerative NAD Hydrolase SARM1. *Cell Reports,* 32**,** 107999.

BRAZILL, J. M., LI, C., ZHU, Y. & ZHAI, R. G. 2017. NMNAT: It's an NAD(+) synthase... It's a chaperone... It's a neuroprotector. *Current Opinion in Genetics and Development,* 44**,** 156-162.

BRILL, M., WAXMAN, S., MOORE, J. & JOYNER, R. 1977. Conduction velocity and spike configuration in myelinated fibres: computed dependence on internode distance. *Journal of Neurology, Neurosurgery & Psychiatry,* 40**,** 769-774.

BRINGMANN, A., IANDIEV, I., PANNICKE, T., WURM, A., HOLLBORN, M., WIEDEMANN, P., OSBORNE, N. N. & REICHENBACH, A. 2009. Cellular signaling and factors involved in Müller cell gliosis: Neuroprotective and detrimental effects. *Progress in Retinal and Eye Research,* 28**,** 423-451.

BROWN, T. M. 2010. Pellagra: An Old Enemy of Timeless Importance. *Psychosomatics,* 51**,** 93-97.

BULL, N. D., JOHNSON, T. V., WELSAPAR, G., DEKORVER, N. W., TOMAREV, S. I. & MARTIN, K. R. 2011. Use of an adult rat retinal explant model for screening of potential retinal ganglion cell neuroprotective therapies. *Investigative Ophthalmology & Visual Science,* 52**,** 3309-20.

CALKINS, D. J. 2012. Critical pathogenic events underlying progression of neurodegeneration in glaucoma. *Progress in Retinal and Eye Research,* 31**,** 702-19.

CALKINS, D. J. 2021. Adaptive responses to neurodegenerative stress in glaucoma. *Progress in Retinal and Eye Research,* 84**,** 100953.

CAMACHO-PEREIRA, J., TARRAGO, M. G., CHINI, C. C. S., NIN, V., ESCANDE, C., WARNER, G. M., PURANIK, A. S., SCHOON, R. A., REID, J. M., GALINA, A. & CHINI, E. N. 2016. CD38 Dictates Age-Related NAD Decline and Mitochondrial Dysfunction through an SIRT3-Dependent Mechanism. *Cell Metabolism,* 23**,** 1127-1139.

CAMPBELL, J. M. 2022. Supplementation with NAD(+) and Its Precursors to Prevent Cognitive Decline across Disease Contexts. *Nutrients,* 14.

CANTO, C., MENZIES, K. J. & AUWERX, J. 2015. NAD(+) Metabolism and the Control of Energy Homeostasis: A Balancing Act between Mitochondria and the Nucleus. *Cell Metabolism,* 22**,** 31-53.

CAPRIOLI, J. 2013. Glaucoma: A Disease of Early Cellular Senescence. *Investigative Ophthalmology & Visual Science,* 54**,** ORSF60-ORSF67.

CASSON, R. J., CHIDLOW, G., CROWSTON, J. G., WILLIAMS, P. A. & WOOD, J. P. M. 2021. Retinal energy metabolism in health and glaucoma. *Progress in Retinal and Eye Research,* 81**,** 100881.

CASTRO-PORTUGUEZ, R. & SUTPHIN, G. L. 2020. Kynurenine pathway, NAD+ synthesis, and mitochondrial function: Targeting tryptophan metabolism to promote longevity and healthspan. *Experimental Gerontology,* 132**,** 110841.

CHAN, J. W., CHAN, N. C. Y. & SADUN, A. A. 2021. Glaucoma as Neurodegeneration in the Brain. *Eye Brain,* 13**,** 21-28.

CHIDLOW, G., WOOD, J. P. M., SIA, P. I. & CASSON, R. J. 2019. Distribution and Activity of Mitochondrial Proteins in Vascular and Avascular Retinas: Implications for Retinal Metabolism. *Investigative Ophthalmology & Visual Science,* 60**,** 331-344.

CHONG, J., SOUFAN, O., LI, C., CARAUS, I., LI, S., BOURQUE, G., WISHART, D. S. & XIA, J. 2018. MetaboAnalyst 4.0: towards more transparent and integrative metabolomics analysis. *Nucleic Acids Research,* 46**,** W486-W494.

CHONG, J., WISHART, D. S. & XIA, J. 2019. Using MetaboAnalyst 4.0 for Comprehensive and Integrative Metabolomics Data Analysis. *Current Protocols in Bioinformatics,* 68**,** e86.

CHOW, S.-C., WANG, H., & SHAO, J. 2007. Sample Size Calculations in Clinical Research. *Chapman and Hall/CRC.* .

CHRYSOSTOMOU, V., REZANIA, F., TROUNCE, I. A. & CROWSTON, J. G. 2013. Oxidative stress and mitochondrial dysfunction in glaucoma. *Current Opinion in Pharmacology,* 13**,** 12-5.

CHUANG, C. F. & BARGMANN, C. I. 2005. A Toll-interleukin 1 repeat protein at the synapse specifies asymmetric odorant receptor expression via ASK1 MAPKKK signaling. *Genes & Development,* 19**,** 270-81.

CHUNG, H. T. & JOE, Y. 2014. Antagonistic crosstalk between SIRT1, PARP-1, and -2 in the regulation of chronic inflammation associated with aging and metabolic diseases. *Integrative Medicine Research,* 3**,** 198-203.

CIMAGLIA, G., VOTRUBA, M., MORGAN, J. E., ANDRÉ, H. & WILLIAMS, P. A. 2020. Potential Therapeutic Benefit of NAD+ Supplementation for Glaucoma and Age-Related Macular Degeneration. *Nutrients,* 12.

CLAES, M., DE GROEF, L. & MOONS, L. 2019. Target-Derived Neurotrophic Factor Deprivation Puts Retinal Ganglion Cells on Death Row: Cold Hard Evidence and Caveats. *International Journal of Molecular Sciences,* 20.

CLAES, M. & MOONS, L. 2022. Retinal Ganglion Cells: Global Number, Density and Vulnerability to Glaucomatous Injury in Common Laboratory Mice. *Cells,* 11.

CLAES, M., SANTOS, J. R. F., MASIN, L., COOLS, L., DAVIS, B. M., ARCKENS, L., FARROW, K., DE GROEF, L. & MOONS, L. 2021. A Fair Assessment of Evaluation Tools for the Murine Microbead Occlusion Model of Glaucoma. *International Journal of Molecular Sciences,* 22.

COLEMAN, A. L. & MIGLIOR, S. 2008. Risk Factors for Glaucoma Onset and Progression. *Survey of Ophthalmology,* 53**,** S3-S10.

CONE, F. E., STEINHART, M. R., OGLESBY, E. N., KALESNYKAS, G., PEASE, M. E. & QUIGLEY, H. A. 2012. The effects of anesthesia, mouse strain and age on intraocular pressure and an improved murine model of experimental glaucoma. *Experimental Eye Research,* 99**,** 27-35.

CONFORTI, L., FANG, G., BEIROWSKI, B., WANG, M. S., SORCI, L., ASRESS, S., ADALBERT, R., SILVA, A., BRIDGE, K., HUANG, X. P., MAGNI, G., GLASS, J. D. & COLEMAN, M. P. 2007. NAD+ and axon degeneration revisited: Nmnat1 cannot substitute for WldS to delay Wallerian degeneration. *Cell Death & Differentiation,* 14**,** 116-127.

CONLON, R., SAHEB, H. & AHMED, II 2017. Glaucoma treatment trends: a review. *Canadian Journal of Ophthalmology,* 52**,** 114-124.

CONZE, D., BRENNER, C. & KRUGER, C. L. 2019. Safety and Metabolism of Long-term Administration of NIAGEN (Nicotinamide Riboside Chloride) in a Randomized, Double-Blind, Placebo-controlled Clinical Trial of Healthy Overweight Adults. *Scientific Reports,* 9**,** 9772.

COUNTRY, M. W. 2017. Retinal metabolism: A comparative look at energetics in the retina. *Brain Research,* 1672**,** 50-57.

COVARRUBIAS, A. J., PERRONE, R., GROZIO, A. & VERDIN, E. 2020. NAD(+) metabolism and its roles in cellular processes during ageing. *Nature Review Molecular Cell Biology*.

CRAGG, B. & THOMAS, P. 1957. The relationships between conduction velocity and the diameter and internodal length of peripheral nerve fibres. *The Journal of physiology,* 136**,** 606.

CRAWLEY, L., ZAMIR, S. M., CORDEIRO, M. F. & GUO, L. 2012. Clinical Options for the Reduction of Elevated Intraocular Pressure. *Ophthalmology and Eye Diseases,* 4**,** OED.S4909.

CROWSTON, J. G., FAHY, E. T., FRY, L., TROUNCE, I. A., VAN WIJNGAARDEN, P., PETROU, S. & CHRYSOSTOMOU, V. 2017. Targeting retinal ganglion cell recovery. *Eye (Lond),* 31**,** 196-198.

CUNNANE, S. C., TRUSHINA, E., MORLAND, C., PRIGIONE, A., CASADESUS, G., ANDREWS, Z. B., BEAL, M. F., BERGERSEN, L. H., BRINTON, R. D., DE LA MONTE, S., ECKERT, A., HARVEY, J., JEGGO, R., JHAMANDAS, J. H., KANN, O., LA COUR, C. M., MARTIN, W. F., MITHIEUX, G., MOREIRA, P. I., MURPHY, M. P., NAVE, K. A., NURIEL, T., OLIET, S. H. R., SAUDOU, F., MATTSON, M. P., SWERDLOW, R. H. & MILLAN, M. J. 2020. Brain energy rescue: an

emerging therapeutic concept for neurodegenerative disorders of ageing. *Nature Review Drug Discovery*.

CUNNINGHAM, E. T. & ZIERHUT M, 2017. Uveitic ocular hypertension and glaucoma. *Ocular Immunology and Inflammation,* 25(6), 737-739.

CUNTZ, H., FORSTNER, F., SCHNELL, B., AMMER, G., RAGHU, S. V. & BORST, A. 2013. Preserving Neural Function under Extreme Scaling. *PLOS ONE,* 8**,** e71540.

CURCIO, C. A. & ALLEN, K. A. 1990. Topography of ganglion cells in human retina. *Journal of Comparative Neurology,* 300**,** 5-25.

CVENKEL, B. & KOLKO, M. 2020. Current Medical Therapy and Future Trends in the Management of Glaucoma Treatment. *Journal of Ophthalmology,* 2020**,** 6138132.

DAS, U. N. 2018. Ageing: Is there a role for arachidonic acid and other bioactive lipids? A review. *Journal of Advanced Research,* 11**,** 67-79.

DAS, U. N. 2021. Essential Fatty Acids and Their Metabolites in the Pathobiology of Inflammation and Its Resolution. *Biomolecules,* 11.

DE MORAES, C. G., JOHN, S. W. M., WILLIAMS, P. A., BLUMBERG, D. M., CIOFFI, G. A. & LIEBMANN, J. M. 2022. Nicotinamide and Pyruvate for Neuroenhancement in Open-Angle Glaucoma: A Phase 2 Randomized Clinical Trial. *JAMA Ophthalmology,* 140**,** 11-18.

DE VRIES, V. A., BASSIL, F. L. & RAMDAS, W. D. 2020. The effects of intravitreal injections on intraocular pressure and retinal nerve fiber layer: a systematic review and meta-analysis. *Scientific Reports,* 10**,** 13248.

DELLA SANTINA, L., INMAN, D. M., LUPIEN, C. B., HORNER, P. J. & WONG, R. O. L. 2013. Differential Progression of Structural and Functional Alterations in Distinct Retinal Ganglion Cell Types in a Mouse Model of Glaucoma. *The Journal of Neuroscience,* 33**,** 17444.

DELLA SANTINA, L. & OU, Y. 2017. Who's lost first? Susceptibility of retinal ganglion cell types in experimental glaucoma. *Experimental Eye Resesearch,* 158**,** 43-50.

DI STEFANO, M., NASCIMENTO-FERREIRA, I., ORSOMANDO, G., MORI, V., GILLEY, J., BROWN, R., JANECKOVA, L., VARGAS, M. E., WORRELL, L. A., LORETO, A., TICKLE, J., PATRICK, J., WEBSTER, J. R., MARANGONI, M., CARPI, F. M., PUCCIARELLI, S., ROSSI, F., MENG, W., SAGASTI, A., RIBCHESTER, R. R., MAGNI, G., COLEMAN, M. P. & CONFORTI, L. 2015. A rise in NAD precursor nicotinamide mononucleotide (NMN) after injury promotes axon degeneration. *Cell Death & Differentiation,* 22**,** 731-42.

DIN, N. M., ISA, H., TAYLOR, S. R. J., BARTON, K. & LIGHTMAN, S. L. 2014. Intraocular pressure elevation in uveitis. *Expert Review of Ophthalmology,* 7**,** 45-59.

DOWLING, J. E. 1987. *The retina: an approachable part of the brain*, Harvard University Press.

DOWLING, J. E. 2015. Retina: An Overview. *Reference Module in Biomedical Sciences.* Elsevier.

DRINGEN, R., GUTTERER, J. M. & HIRRLINGER, J. 2000. Glutathione metabolism in brain. *European Journal of Biochemistry,* 267**,** 4912-4916.

EASTLAKE, K., JAYARAM, H., LUIS, J., HAYES, M., KHAW, P. T. & LIMB, G. A. 2021. Strain Specific Responses in a Microbead Rat Model of Experimental Glaucoma. *Current Eye Research,* 46**,** 387-397.

EL-DANAF, R. N. & HUBERMAN, A. D. 2015. Characteristic Patterns of Dendritic Remodeling in Early-Stage Glaucoma: Evidence from Genetically Identified Retinal Ganglion Cell Types. *The Journal of Neuroscience,* 35**,** 2329.

ELMORE, S. 2007. Apoptosis: a review of programmed cell death. *Toxicologic Pathology,* 35**,** 495-516.

ESSUMAN, K., SUMMERS, D. W., SASAKI, Y., MAO, X., DIANTONIO, A. & MILBRANDT, J. 2017. The SARM1 Toll/Interleukin-1 Receptor Domain Possesses Intrinsic NAD(+) Cleavage Activity that Promotes Pathological Axonal Degeneration. *Neuron,* 93**,** 1334-1343 e5.

FALK, M. J., ZHANG, Q., NAKAMARU-OGISO, E., KANNABIRAN, C., FONSECA-KELLY, Z., CHAKAROVA, C., AUDO, I., MACKAY, D. S., ZEITZ, C., BORMAN, A. D., STANISZEWSKA, M., SHUKLA, R., PALAVALLI, L., MOHAND-SAID, S., WASEEM, N. H., JALALI, S., PERIN, J. C., PLACE, E., OSTROVSKY, J., XIAO, R., BHATTACHARYA, S. S., CONSUGAR, M., WEBSTER, A. R., SAHEL, J.-A., MOORE, A. T., BERSON, E. L., LIU, Q., GAI, X. & PIERCE, E. A. 2012. NMNAT1 mutations cause Leber congenital amaurosis. *Nature genetics,* 44**,** 1040-1045.

FANG, E. F., LAUTRUP, S., HOU, Y., DEMAREST, T. G., CROTEAU, D. L., MATTSON, M. P. & BOHR, V. A. 2017. NAD(+) in Aging: Molecular Mechanisms and Translational Implications. *Trends in Molecular Medicine,* 23**,** 899-916.

FANG, E. F., SCHEIBYE-KNUDSEN, M., BRACE, L. E., KASSAHUN, H., SENGUPTA, T., NILSEN, H., MITCHELL, J. R., CROTEAU, D. L. & BOHR, V. A. 2014. Defective mitophagy in XPA via PARP-1 hyperactivation and NAD(+)/SIRT1 reduction. *Cell,* 157**,** 882-896.

FANG, E. F., SCHEIBYE-KNUDSEN, M., CHUA, K. F., MATTSON, M. P., CROTEAU, D. L. & BOHR, V. A. 2016. Nuclear DNA damage signalling to mitochondria in ageing. *Nature Review Molecular Cell Biology,* 17**,** 308-21.

FANG, F., ZHUANG, P., FENG, X., LIU, P., LIU, D., HUANG, H., LI, L., CHEN, W., LIU, L., SUN, Y., JIANG, H., YE, J. & HU, Y. 2022. NMNAT2 is downregulated in glaucomatous RGCs, and RGC-specific gene therapy rescues neurodegeneration and visual function. *Molecular Therapy*.

FAUL, F., ERDFELDER, E., LANG, A.-G. & BUCHNER, A. 2007. G*Power 3: A flexible statistical power analysis program for the social, behavioral, and biomedical sciences. *Behavior Research Methods,* 39**,** 175-191.

FELICITAS BERGER, C. L., MATHIAS DAHLMANN AND MATHIAS ZIEGLER 2005. Subcellular Compartmentation and Differential Catalytic Properties of the Three Human Nicotinamide Mononucleotide Adenylyltransferase Isoforms. *Journal of Biological Chemistry*.

FERNANDES, K. A., HARDER, J. M., WILLIAMS, P. A., RAUSCH, R. L., KIERNAN, A. E., NAIR, K. S., ANDERSON, M. G., JOHN, S. W., HOWELL, G. R. & LIBBY, R. T. 2015. Using genetic mouse models to gain insight into glaucoma: Past results and future possibilities. *Experimental Eye Research,* 141**,** 42-56.

FICARROTTA, K. R., BELLO, S. A., MOHAMED, Y. H. & PASSAGLIA, C. L. 2018. Aqueous Humor Dynamics of the Brown-Norway Rat. *Investigative Ophthalmology & Visual Science,* 59**,** 2529-2537.

FIGLEY, M. D. & DIANTONIO, A. 2020. The SARM1 axon degeneration pathway: control of the NAD(+) metabolome regulates axon survival in health and disease. *Current Opinion in Neurobiology,* 63**,** 59-66.

FIGLEY, M. D., GU, W., NANSON, J. D., SHI, Y., SASAKI, Y., CUNNEA, K., MALDE, A. K., JIA, X., LUO, Z., SAIKOT, F. K., MOSAIAB, T., MASIC, V., HOLT, S., HARTLEY-TASSELL, L., MCGUINNESS, H. Y., MANIK, M. K., BOSANAC, T., LANDSBERG, M. J., KERRY, P. S., MOBLI, M., HUGHES, R. O., MILBRANDT, J., KOBE, B., DIANTONIO, A. & VE, T. 2021. SARM1 is a metabolic sensor activated by an increased NMN/NAD(+) ratio to trigger axon degeneration. *Neuron,* 109**,** 1118-1136 e11.

FINKEL, T., DENG, C.-X. & MOSTOSLAVSKY, R. 2009. Recent progress in the biology and physiology of sirtuins. *Nature,* 460**,** 587-591.

FISHER, C. R. & FERRINGTON, D. A. 2018. Perspective on AMD Pathobiology: A Bioenergetic Crisis in the RPE. *Investigative Ophthalmology & Visual Science,* 59**,** AMD41-AMD47.

FLETCHER, R. S., RATAJCZAK, J., DOIG, C. L., OAKEY, L. A., CALLINGHAM, R., DA SILVA XAVIER, G., GARTEN, A., ELHASSAN, Y. S., REDPATH, P., MIGAUD, M. E., PHILP, A., BRENNER, C., CANTO, C. & LAVERY, G. G. 2017. Nicotinamide riboside kinases display redundancy in mediating nicotinamide mononucleotide and nicotinamide riboside metabolism in skeletal muscle cells. *Molecular Metabolism,* 6**,** 819-832.

FRANCESCHI, C., GARAGNANI, P., PARINI, P., GIULIANI, C. & SANTORO, A. 2018. Inflammaging: a new immune-metabolic viewpoint for age-related diseases. *Nature Review Endocrinology,* 14**,** 576-590.

FRICKER, M., TOLKOVSKY, A. M., BORUTAITE, V., COLEMAN, M. & BROWN, G. C. 2018. Neuronal Cell Death. *Physiological Reviews,* 98**,** 813-880.

FRY, L. E., FAHY, E., CHRYSOSTOMOU, V., HUI, F., TANG, J., VAN WIJNGAARDEN, P., PETROU, S. & CROWSTON, J. G. 2018. The coma in glaucoma: Retinal ganglion cell dysfunction and recovery. *Progress in Retinal and Eye Research,* 65**,** 77-92.

FULOP, T., LARBI, A., DUPUIS, G., LE PAGE, A., FROST, E. H., COHEN, A. A., WITKOWSKI, J. M. & FRANCESCHI, C. 2017. Immunosenescence and Inflamm-Aging As Two Sides of the Same Coin: Friends or Foes? *Frontiers in Immunology,* 8**,** 1960.

FULOP, T., LARBI, A., PAWELEC, G., KHALIL, A., COHEN, A. A., HIROKAWA, K., WITKOWSKI, J. M. & FRANCESCHI, C. 2021. Immunology of Aging: the Birth of Inflammaging. *Clin Rev Allergy Immunol***,** 1-14.

FUNAKOSHI, M. & ARAKI, T. 2021. Mechanism of initiation and regulation of axonal degeneration with special reference to NMNATs and Sarm1. *Neuroscience Research*.

GAN, W.-B., GRUTZENDLER, J., WONG, W. T., WONG, R. O. L. & LICHTMAN, J. W. 2000. Multicolor "DiOlistic" Labeling of the Nervous System Using Lipophilic Dye Combinations. *Neuron,* 27**,** 219-225.

GANCHAROVA, O. S., MANSKIKH, V. N., ZAMYATNIN, A. A., JR. & PHILIPPOV, P. P. 2013. Organotypic culture of neural retina as a research model of neurodegeneration of ganglion cells. *Biochemistry (Mosc),* 78**,** 1280-6.

GAO, J., WANG, W. Y., MAO, Y. W., GRAFF, J., GUAN, J. S., PAN, L., MAK, G., KIM, D., SU, S. C. & TSAI, L. H. 2010. A novel pathway regulates memory and plasticity via SIRT1 and miR-134. *Nature,* 466**,** 1105-9.

GERDTS, J., SUMMERS, D. W., MILBRANDT, J. & DIANTONIO, A. 2016. Axon Self-Destruction: New Links among SARM1, MAPKs, and NAD+ Metabolism. *Neuron,* 89**,** 449-60.

GIBBS, R. A., WEINSTOCK, G. M., METZKER, M. L., MUZNY, D. M., SODERGREN, E. J., SCHERER, S., SCOTT, G., STEFFEN, D., WORLEY, K. C., BURCH, P. E., OKWUONU, G., HINES, S., LEWIS, L., DERAMO, C., DELGADO, O., DUGAN-ROCHA, S., MINER, G., MORGAN, M., HAWES, A., GILL, R., HOLT, C. R. A., ADAMS, M. D., AMANATIDES, P. G., BADEN-TILLSON, H., BARNSTEAD, M., CHIN, S., EVANS, C. A., FERRIERA, S., FOSLER, C., GLODEK, A., GU, Z., JENNINGS, D., KRAFT, C. L., NGUYEN, T., PFANNKOCH, C. M., SITTER, C., SUTTON, G. G., VENTER, J. C., WOODAGE, T., SMITH, D., LEE, H.-M., GUSTAFSON, E., CAHILL, P., KANA, A., DOUCETTE-STAMM, L., WEINSTOCK, K., FECHTEL, K., WEISS, R. B., DUNN, D. M., GREEN, E. D., BLAKESLEY, R. W., BOUFFARD, G. G., DE JONG, P. J., OSOEGAWA, K., ZHU, B., MARRA, M., SCHEIN, J., BOSDET, I., FJELL, C., JONES, S., KRZYWINSKI, M., MATHEWSON, C., SIDDIQUI, A., WYE, N., MCPHERSON, J., ZHAO, S., FRASER, C. M., SHETTY, J., SHATSMAN, S., GEER, K., CHEN, Y., ABRAMZON, S., NIERMAN, W. C., GIBBS, R. A., WEINSTOCK, G. M., HAVLAK, P. H., CHEN, R., JAMES DURBIN, K., EGAN, A., REN, Y., SONG, X.-Z., LI, B., LIU, Y., QIN, X., CAWLEY, S., WEINSTOCK, G. M., WORLEY, K. C., COONEY, A. J., GIBBS, R. A., D'SOUZA, L. M., MARTIN, K., QIAN WU, J., GONZALEZ-GARAY, M. L., JACKSON, A. R., KALAFUS, K. J., MCLEOD, M. P., MILOSAVLJEVIC, A., VIRK, D., VOLKOV, A., WHEELER, D. A., et al. 2004. Genome sequence of the Brown Norway rat yields insights into mammalian evolution. *Nature,* 428**,** 493-521.

GILLEY, J. & COLEMAN, M. P. 2010. Endogenous Nmnat2 is an essential survival factor for maintenance of healthy axons. *PLoS biology,* 8**,** e1000300-e1000300.

GILLEY, J., MAYER, P. R., YU, G. & COLEMAN, M. P. 2018. Low levels of NMNAT2 compromise axon development and survival. *Human Molecular Genetics,* 28**,** 448-458.

GILMOUR, B. C., GUDMUNDSRUD, R., FRANK, J., HOV, A., LAUTRUP, S., AMAN, Y., ROSJO, H., BRENNER, C., ZIEGLER, M., TYSNES, O. B., TZOULIS, C., OMLAND, T., SORAAS, A., HOLMOY, T., BERGERSEN, L. H., STORM-MATHISEN, J., NILSEN, H. & FANG, E. F. 2020. Targeting NAD(+) in translational research to relieve diseases and conditions of metabolic stress and ageing. *Mechanism of Ageing and Development,* 186**,** 111208.

GOLDHAGEN, B., PROIA, A. D., EPSTEIN, D. L. & RAO, P. V. 2012. Elevated Levels of RhoA in the Optic Nerve Head of Human Eyes With Glaucoma. *Journal of Glaucoma,* 21.

GORMAN, A. M. 2008. Neuronal cell death in neurodegenerative diseases: recurring themes around protein handling. *Journal of Cell and Molecular Medicine,* 12**,** 2263-80.

GREEN, D. R. & REED, J. C. 1998. Mitochondria and apoptosis. *Science*, 281, 1309-1312.

GREGG, R. G., MCCALL, M. A. & MASSEY, S. C. 2013. Function and Anatomy of the Mammalian Retina. *Retina.*

GRÜNERT, U. 2009. Retinal Bipolar Cells. *In:* BINDER, M. D., HIROKAWA, N. & WINDHORST, U. (eds.) *Encyclopedia of Neuroscience.* Berlin, Heidelberg: Springer Berlin Heidelberg.

GUERREIRO, S., PRIVAT, A. L., BRESSAC, L. & TOULORGE, D. 2020. CD38 in Neurodegeneration and Neuroinflammation. *Cells,* 9.

GUO, C., SUN, L., CHEN, X. & ZHANG, D. 2013. Oxidative stress, mitochondrial damage and neurodegenerative diseases. *Neural Regeneration Research,* 8**,** 2003-14.

HARADA, T., HARADA, C., NAKAMURA, K., QUAH, H.-M. A., OKUMURA, A., NAMEKATA, K., SAEKI, T., AIHARA, M., YOSHIDA, H., MITANI, A. & TANAKA, K. 2007. The potential role of glutamate transporters in the pathogenesis of normal tension glaucoma. *The Journal of Clinical Investigation,* 117**,** 1763-1770.

HARDEN, A., YOUNG, W. J. & MARTIN, C. J. 1906a. The alcoholic ferment of yeast-juice. *Proceedings of the Royal Society of London. Series B, Containing Papers of a Biological Character,* 77**,** 405-420.

HARDEN, A., YOUNG, W. J. & MARTIN, C. J. 1906b. The alcoholic ferment of yeast-juice. Part II.—The coferment of yeast-juice. *Proceedings of the Royal Society of London. Series B, Containing Papers of a Biological Character,* 78**,** 369-375.

HARDER, J. M., GUYMER, C., WOOD, J. P. M., DASKALAKI, E., CHIDLOW, G., ZHANG, C., BALASUBRAMANIAN, R., CARDOZO, B. H., FOXWORTH, N. E., DEERING, K. E., OUELLETTE, T. B., MONTGOMERY, C., WHEELOCK, C. E., CASSON, R. J., WILLIAMS, P. A. & JOHN, S. W. M. 2020. Disturbed glucose and pyruvate metabolism in glaucoma with neuroprotection by pyruvate or rapamycin. *Proceedings of the National Academy of Sciences,* 117**,** 33619.

HARVEY, A. R. & ROBERTSON, D. 1992. Time-course and extent of retinal ganglion cell death following ablation of the superior colliculus in neonatal rats. *Journal of Comparative Neurology,* 325**,** 83-94.

HEGYI, J., SCHWARTZ, R. A. & HEGYI, V. 2004. Pellagra: Dermatitis, dementia, and diarrhea. *International Journal of Dermatology,* 43**,** 1-5.

HIKOSAKA, K., YAKU, K., OKABE, K. & NAKAGAWA, T. 2021. Implications of NAD metabolism in pathophysiology and therapeutics for neurodegenerative diseases. *Nutritional Neuroscience,* 24**,** 371-383.

HOLLOWS, F. C. & GRAHAM, P. A. 1966. Intra-ocular pressure, glaucoma, and glaucoma suspects in a defined population. *British Journal of Ophthalmology,* 50**,** 570.

HONIG, M. G. & HUME, R. I. 1986. Fluorescent carbocyanine dyes allow living neurons of identified origin to be studied in long-term cultures. *Journal of Cell Biology,* 103**,** 171-187.

HOPKINS, E. L., GU, W., KOBE, B. & COLEMAN, M. P. 2021. A Novel NAD Signaling Mechanism in Axon Degeneration and its Relationship to Innate Immunity. *Frontiers in Molecular Biosciences,* 8**,** 703532.

HOYNG, P. F. J. & KITAZAWA, Y. 2002. Medical Treatment of Normal Tension Glaucoma. *Survey of Ophthalmology,* 47**,** S116-S124.

HUANG, W., XU, Q., SU, J., TANG, L., HAO, Z. Z., XU, C., LIU, R., SHEN, Y., SANG, X., XU, N., TIE, X., MIAO, Z., LIU, X., XU, Y., LIU, F., LIU, Y. & LIU, S. 2022. Linking transcriptomes with morphological and functional phenotypes in mammalian retinal ganglion cells. *Cell Reports,* 40**,** 111322.

HUI, F., TANG, J., WILLIAMS, P. A., MCGUINNESS, M. B., HADOUX, X., CASSON, R. J., COOTE, M., TROUNCE, I. A., MARTIN, K. R., VAN WIJNGAARDEN, P. & CROWSTON, J. G. 2020. Improvement in inner retinal function in glaucoma with nicotinamide (vitamin B3) supplementation: A crossover randomized clinical trial. *Clinical & Experimental Ophthalmology,* n/a.

HWANG, E. S. & SONG, S. B. 2020. Possible Adverse Effects of High-Dose Nicotinamide: Mechanisms and Safety Assessment. *Biomolecules,* 10.

ICSO, J. D. & THOMPSON, P. R. 2022. The chemical biology of NAD(+) regulation in axon degeneration. *Current Opinion in Chemical Biology,* 69**,** 102176.

INMAN, D. M. & HORNER, P. J. 2007. Reactive nonproliferative gliosis predominates in a chronic mouse model of glaucoma. *Glia,* 55**,** 942-953.

ISHIKAWA, M., YOSHITOMI, T., ZORUMSKI, C. F. & IZUMI, Y. 2015. Experimentally Induced Mammalian Models of Glaucoma. *Biomed Research International,* 2015**,** 281214.

ITO, Y. A., BELFORTE, N., CUEVA VARGAS, J. L. & DI POLO, A. 2016. A Magnetic Microbead Occlusion Model to Induce Ocular Hypertension-Dependent Glaucoma in Mice. *Journal of Visualized Experiments***,** e53731.

ITO, Y. A. & DI POLO, A. 2017. Mitochondrial dynamics, transport, and quality control: A bottleneck for retinal ganglion cell viability in optic neuropathies. *Mitochondrion,* 36**,** 186-192.

JADEJA, R. N., THOUNAOJAM, M. C., BARTOLI, M. & MARTIN, P. M. 2020. Implications of NAD(+) Metabolism in the Aging Retina and Retinal Degeneration. *Oxidative Medicine and Cellular Longevity,* 2020**,** 2692794.

JAN, Y.-N. & JAN, L. Y. 2010. Branching out: mechanisms of dendritic arborization. *Nature Reviews Neuroscience,* 11**,** 316-328.

JAVLE, M. & CURTIN, N. J. 2011. The role of PARP in DNA repair and its therapeutic exploitation. *British Journal of Cancer,* 105**,** 1114-1122.

JIA, L., CEPURNA, W. O., JOHNSON, E. C. & MORRISON, J. C. 2000. Effect of General Anesthetics on IOP in Rats with Experimental Aqueous Outflow Obstruction. *Investigative Ophthalmology & Visual Science,* 41**,** 3415-3419.

JIANG, C., MOORE, M. J., ZHANG, X., KLASSEN, H., LANGER, R. & YOUNG, M. 2007. Intravitreal injections of GDNF-loaded biodegradable microspheres are neuroprotective in a rat model of glaucoma. *Molecular Vision,* 13**,** 1783-92.

JIANG, Y., LIU, T., LEE, C. H., CHANG, Q., YANG, J. & ZHANG, Z. 2020. The NAD(+)-mediated self-inhibition mechanism of pro-neurodegenerative SARM1. *Nature,* 588**,** 658-663.

JOHNSON, T. V., OGLESBY, E. N., STEINHART, M. R., CONE-KIMBALL, E., JEFFERYS, J. & QUIGLEY, H. A. 2016. Time-Lapse Retinal Ganglion Cell Dendritic Field Degeneration Imaged in Organotypic Retinal Explant Culture. *Investigative Ophthalmology & Visual Science,* 57**,** 253-64.

JOHNSON, T. V. & TOMAREV, S. I. 2010. Rodent models of glaucoma. *Brain Research Bulletin,* 81**,** 349-58.

JONAS, J. B., AUNG, T., BOURNE, R. R., BRON, A. M., RITCH, R. & PANDA-JONAS, S. 2017. Glaucoma. *The Lancet,* 390**,** 2183-2193.

JORNAYVAZ, F. R. & SHULMAN, G. I. 2010. Regulation of mitochondrial biogenesis. *Essays in Biochemistry,* 47**,** 69-84.

JU, W. K., PERKINS, G. A., KIM, K. Y., BASTOLA, T., CHOI, W. Y. & CHOI, S. H. 2022. Glaucomatous optic neuropathy: Mitochondrial dynamics, dysfunction and protection in retinal ganglion cells. *Progress in Retinal and Eye Research***,** 101136.

KAGEYAMA, G. H. & WONG-RILEY, M. T. 1984. The histochemical localization of cytochrome oxidase in the retina and lateral geniculate nucleus of the ferret, cat, and monkey, with particular reference to retinal mosaics and ON/OFF-center visual channels. *The Journal of Neuroscience,* 4**,** 2445.

KALESNYKAS, G., OGLESBY, E. N., ZACK, D. J., CONE, F. E., STEINHART, M. R., TIAN, J., PEASE, M. E. & QUIGLEY, H. A. 2012. Retinal Ganglion Cell Morphology after Optic Nerve Crush and Experimental Glaucoma. *Investigative Ophthalmology & Visual Science,* 53**,** 3847-3857.

KANAMORI, A., NAKAMURA, M., NAKANISHI, Y., YAMADA, Y. & NEGI, A. 2005. Long-term glial reactivity in rat retinas ipsilateral and contralateral to experimental glaucoma. *Experimental Eye Research,* 81**,** 48-56.

KARLSTETTER, M., SCHOLZ, R., RUTAR, M., WONG, W. T., PROVIS, J. M. & LANGMANN, T. 2015. Retinal microglia: just bystander or target for therapy? *Progress in Retinal and Eye Research,* 45**,** 30-57.

KATSYUBA, E. & AUWERX, J. 2018. Chapter 3 - NAD+ Modulation: Biology and Therapy. *In:* GUARENTE, L., MOSTOSLAVSKY, R. & KAZANTSEV, A. (eds.) *Introductory Review on Sirtuins in Biology, Aging, and Disease.* Academic Press.

KATSYUBA, E., ROMANI, M., HOFER, D. & AUWERX, J. 2020. NAD+ homeostasis in health and disease. *Nature Metabolism,* 2**,** 9-31.

KAUPPINEN, A., SUURONEN, T., OJALA, J., KAARNIRANTA, K. & SALMINEN, A. 2013. Antagonistic crosstalk between NF-kappaB and SIRT1 in the regulation of inflammation and metabolic disorders. *Cellular Signaling,* 25**,** 1939-48.

KEVENAAR, J. T. & HOOGENRAAD, C. C. 2015. The axonal cytoskeleton: from organization to function. *Frontiers in Molecular Neuroscience,* 8.

KHAN, N. A., AURANEN, M., PAETAU, I., PIRINEN, E., EURO, L., FORSSTRÖM, S., PASILA, L., VELAGAPUDI, V., CARROLL, C. J., AUWERX, J. & SUOMALAINEN, A. 2014. Effective treatment of mitochondrial myopathy by nicotinamide riboside, a vitamin B3. *EMBO Molecular Medicine,* 6**,** 721-731.

KIM, K. Y., PERKINS, G. A., SHIM, M. S., BUSHONG, E., ALCASID, N., JU, S., ELLISMAN, M. H., WEINREB, R. N. & JU, W. K. 2015. DRP1 inhibition rescues retinal ganglion cells and their axons by preserving mitochondrial integrity in a mouse model of glaucoma. *Cell Death & Disease,* 6**,** e1839-e1839.

KIM, U. S., MAHROO, O. A., MOLLON, J. D. & YU-WAI-MAN, P. 2021. Retinal Ganglion Cells-Diversity of Cell Types and Clinical Relevance. *Frontiers in Neurology,* 12**,** 661938.

KLEIN, J. 2000. Membrane breakdown in acute and chronic neurodegeneration: focus on choline-containing phospholipids. *Journal of Neural Transmission,* 107**,** 1027-1063.

KNIP, M., DOUEK, I. F., MOORE, W. P. T., GILLMOR, H. A., MCLEAN, A. E. M., BINGLEY, P. J., GALE, E. A. M. & FOR THE, E. G. 2000. Safety of high-dose nicotinamide: a review. *Diabetologia,* 43**,** 1337-1345.

KOCH, J. C., TATENHORST, L., ROSER, A.-E., SAAL, K.-A., TÖNGES, L. & LINGOR, P. 2018. ROCK inhibition in models of neurodegeneration and its potential for clinical translation. *Pharmacology & Therapeutics,* 189**,** 1-21.

KOLB H., F. E., NELSON R. 1995. The Organization of the Retina and Visual System. Salt Lake City UT: Webvision .

KOLESKE, A. J. 2013. Molecular mechanisms of dendrite stability. *Nature Review Neuroscience,* 14**,** 536-50.

KONG, G. Y. X., VAN BERGEN, N. J., TROUNCE, I. A. & CROWSTON, J. G. 2009. Mitochondrial Dysfunction and Glaucoma. *Journal of Glaucoma,* 18**,** 93-100.

KOUASSI NZOUGHET, J., CHAO DE LA BARCA, J. M., GUEHLOUZ, K., LERUEZ, S., COULBAULT, L., ALLOUCHE, S., BOCCA, C., MULLER, J., AMATI-BONNEAU, P., GOHIER, P., BONNEAU, D., SIMARD, G., MILEA, D., LENAERS, G., PROCACCIO, V. & REYNIER, P. 2019. Nicotinamide Deficiency in Primary Open-Angle Glaucoma. *Investigative Ophthalmology & Visual Science,* 60**,** 2509-2514.

KROEMER, G., DALLAPORTA, B. & RESCHE-RIGON, M. 1998. The mitochondrial death/lfe regulator in apoptosis and necrosis. *Annual Review of Physiology,* 60, 619-642.

LAMBIASE, A., ALOE, L., CENTOFANTI, M., PARISI, V., MANTELLI, F., COLAFRANCESCO, V., MANNI, G. L., BUCCI, M. G., BONINI, S. & LEVI-MONTALCINI, R. 2009. Experimental and clinical evidence of neuroprotection by nerve growth factor eye drops: Implications for glaucoma. *Proceedings of the National Academy of Sciences,* 106**,** 13469.

LANGMANN, T. 2007. Microglia activation in retinal degeneration. *Journal of Leukocyte Biology,* 81**,** 1345-51.

LAUTRUP, S., SINCLAIR, D. A., MATTSON, M. P. & FANG, E. F. 2019. NAD(+) in Brain Aging and Neurodegenerative Disorders. *Cell Metabolism,* 30**,** 630-655.

LAVADO-ROLDAN, A. & FERNANDEZ-CHACON, R. 2016. Two for the Price of One: A Neuroprotective Chaperone Kit within NAD Synthase Protein NMNAT2. *PLoS Biology,* 14**,** e1002522.

LEAVER, S. G., CUI, Q., PLANT, G. W., ARULPRAGASAM, A., HISHEH, S., VERHAAGEN, J. & HARVEY, A. R. 2006. AAV-mediated expression of CNTF promotes long-term survival and regeneration of adult rat retinal ganglion cells. *Gene Therapy,* 13**,** 1328-1341.

LEE, S., VAN BERGEN, N. J., KONG, G. Y., CHRYSOSTOMOU, V., WAUGH, H. S., O'NEILL, E. C., CROWSTON, J. G. & TROUNCE, I. A. 2011. Mitochondrial dysfunction in glaucoma and emerging bioenergetic therapies. *Experimental Eye Research,* 93**,** 204-12.

LEWKOWICZ, D., WILLERMAIN, F., RELVAS, L. J., MAKHOUL, D., JANSSENS, S., JANSSENS, X. & CASPERS, L. 2015. Clinical Outcome of Hypertensive Uveitis. *Journal of Ophthalmology,* 2015**,** 974870.

LI, C. & WU, L. E. 2021. Risks and rewards of targeting NAD(+) homeostasis in the brain. *Mechanism of Ageing and Development,* 198**,** 111545.

LIAO, C., ASHLEY, N., DIOT, A., MORTEN, K., PHADWAL, K., WILLIAMS, A., FEARNLEY, I., ROSSER, L., LOWNDES, J., FRATTER, C., FERGUSON, D. J. P., VAY, L., QUAGHEBEUR, G., MORONI, I., BIANCHI, S., LAMPERTI, C., DOWNES, S. M., SITARZ, K. S., FLANNERY, P. J., CARVER, J., DOMBI, E., EAST, D., LAURA, M., REILLY, M. M., MORTIBOYS, H., PREVO, R., CAMPANELLA, M., DANIELS, M. J., ZEVIANI, M., YU-WAI-MAN, P., SIMON, A. K., VOTRUBA, M. & POULTON, J. 2017. Dysregulated mitophagy and mitochondrial organization in optic atrophy due to OPA1 mutations. *Neurology,* 88**,** 131-142.

LIBBY, R. T., ANDERSON, M. G., PANG, I.-H., ROBINSON, Z. H., SAVINOVA, O. V., COSMA, I. M., SNOW, A. M. Y., WILSON, L. A., SMITH, R. S., CLARK, A. F. & JOHN, S. W. M. 2005. Inherited glaucoma in DBA/2J mice: Pertinent disease features for studying the neurodegeneration. *Visual Neuroscience,* 22**,** 637-648.

LIN, JONATHAN B., KUBOTA, S., BAN, N., YOSHIDA, M., SANTEFORD, A., SENE, A., NAKAMURA, R., ZAPATA, N., KUBOTA, M., TSUBOTA, K., YOSHINO, J., IMAI, S.-I. & APTE, RAJENDRA S. 2016. NAMPT-Mediated NAD+ Biosynthesis Is Essential for Vision In Mice. *Cell Reports,* 17**,** 69-85.

LIN, T. Y., CHEN, P. J., YU, H. H., HSU, C. P. & LEE, C. H. 2020. Extrinsic Factors Regulating Dendritic Patterning. *Frontiers in Cellular Neuroscience,* 14**,** 622808.

LIU, H. & PROKOSCH, V. 2021. Energy Metabolism in the Inner Retina in Health and Glaucoma. *International Journal of Molecular Sciences,* 22.

LIU, P., HUANG, H., FANG, F., LIU, L., LI, L., FENG, X., CHEN, W., DALAL, R., SUN, Y. & HU, Y. 2021. Neuronal NMNAT2 Overexpression Does Not Achieve Significant Neuroprotection in Experimental Autoimmune Encephalomyelitis/Optic Neuritis. *Frontiers in Cellular Neuroscience,* 15.

LOMBARD, D. B., TISHKOFF, D. X. & BAO, J. 2011. Mitochondrial sirtuins in the regulation of mitochondrial activity and metabolic adaptation. *Handbook of Experimental Pharmacology,* 206**,** 163-88.

LORETO, A., HILL, C. S., HEWITT, V. L., ORSOMANDO, G., ANGELETTI, C., GILLEY, J., LUCCI, C., SANCHEZ-MARTINEZ, A., WHITWORTH, A. J., CONFORTI, L., DAJAS-BAILADOR, F. & COLEMAN, M. P. 2019. Mitochondrial impairment activates the Wallerian pathway through depletion of NMNAT2 leading to SARM1-dependent axon degeneration. *Neurobiology of Disease,* 134**,** 104678.

LUCAS-RUIZ, F., GALINDO-ROMERO, C., ALBALADEJO-GARCIA, V., VIDAL-SANZ, M. & AGUDO-BARRIUSO, M. 2021. Mechanisms implicated in the contralateral effect in the central nervous system after unilateral injury: focus on the visual system. *Neural Regeneration Research,* 16**,** 2125-2131.

LUNDT, S. & DING, S. 2021. NAD(+) Metabolism and Diseases with Motor Dysfunction. *Genes (Basel),* 12.

MA, K., CHEN, G., LI, W., KEPP, O., ZHU, Y. & CHEN, Q. 2020. Mitophagy, Mitochondrial Homeostasis, and Cell Fate. *Frontiers in Cell and Developmental Biology,* 8**,** 467.

MAC NAIR, C. E. & NICKELLS, R. W. 2015. Neuroinflammation in Glaucoma and Optic Nerve Damage. *Progress in Molecular Biology and Translational Science,* 134**,** 343-63.

MAGNI, G., AMICI, A., EMANUELLI, M., RAFFAELLI, N. & RUGGIERI, S. 2009. Enzymology of NAD+ synthesis. *Advances in Enzymology and Relatated Areas of Molecular Biology,* 73**,** 135-82.

MAGNI, G., ORSOMANDO, G., RAFFELLI, N. & RUGGIERI, S. 2008. Enzymology of mammalian NAD metabolism in health and disease. *Frontiers in Bioscience-Landmark,* 13**,** 6135-6154.

MALAVASI, F., DEAGLIO, S., FUNARO, A., FERRERO, E., HORENSTEIN, A. L., ORTOLAN, E., VAISITTI, T. & AYDIN, S. 2008. Evolution and Function of the ADP Ribosyl Cyclase/CD38 Gene Family in Physiology and Pathology. *Physiological Reviews,* 88**,** 841-886.

MANABE, S.-I., KASHII, S., HONDA, Y., YAMAMOTO, R., KATSUKI, H. & AKAIKE, A. 2002. Quantification of axotomized ganglion cell death by explant culture of the rat retina. *Neuroscience Letters,* 334**,** 33-36.

MARQUIS, R. E. & WHITSON, J. T. 2005. Management of Glaucoma: Focus on Pharmacological Therapy. *Drugs & Aging,* 22**,** 1-21.

MARSHAK, D. W. 2009. Retinal Ganglion Cells: Anatomy. *In:* SQUIRE, L. R. (ed.) *Encyclopedia of Neuroscience.* Oxford: Academic Press.

MARTENS, C. R., DENMAN, B. A., MAZZO, M. R., ARMSTRONG, M. L., REISDORPH, N., MCQUEEN, M. B., CHONCHOL, M. & SEALS, D. R. 2018. Chronic nicotinamide riboside supplementation is well-tolerated and elevates NAD(+) in healthy middle-aged and older adults. *Nature Communication,* 9**,** 1286.

MATSUO, K., YABUKI, Y. & FUKUNAGA, K. 2020. 5-aminolevulinic acid inhibits oxidative stress and ameliorates autistic-like behaviors in prenatal valproic acid-exposed rats. *Neuropharmacology,* 168**,** 107975.

MATTSON, M. P. & ARUMUGAM, T. V. 2018. Hallmarks of Brain Aging: Adaptive and Pathological Modification by Metabolic States. *Cell metabolism,* 27**,** 1176-1199.

MCKINNON, S. J., SCHLAMP, C. L. & NICKELLS, R. W. 2009. Mouse models of retinal ganglion cell death and glaucoma. *Experimental Eye Research,* 88(4), 816-824.

MCREYNOLDS, M. R., CHELLAPPA, K. & BAUR, J. A. 2020. Age-related NAD(+) decline. *Experimental Gerontology,* 134**,** 110888.

MCREYNOLDS, M. R., CHELLAPPA, K., CHILES, E., JANKOWSKI, C., SHEN, Y., CHEN, L., DESCAMPS, H. C., MUKHERJEE, S., BHAT, Y. R., LINGALA, S. R., CHU, Q., BOTOLIN, P., HAYAT, F., DOKE, T., SUSZTAK, K., THAISS, C. A., LU, W., MIGAUD, M. E., SU, X., RABINOWITZ, J. D. & BAUR, J. A. 2021. NAD+ flux is maintained in aged mice despite lower tissue concentrations. *Cell Systems,* 12**,** 1160-1172.e4.

MEHMEL, M., JOVANOVIC, N. & SPITZ, U. 2020. Nicotinamide Riboside-The Current State of Research and Therapeutic Uses. *Nutrients,* 12.

MELIK PARSADANIANTZ, S., REAUX-LE GOAZIGO, A., SAPIENZA, A., HABAS, C. & BAUDOUIN, C. 2020. Glaucoma: A Degenerative Optic Neuropathy Related to Neuroinflammation? *Cells,* 9.

MENG, Y., REN, Z., XU, F., ZHOU, X., SONG, C., WANG, V. Y.-F., LIU, W., LU, L., THOMSON, J. A. & CHEN, G. 2018. Nicotinamide Promotes Cell Survival and Differentiation as Kinase Inhibitor in Human Pluripotent Stem Cells. *Stem Cell Reports,* 11**,** 1347-1356.

MIAO, L., YANG, L., HUANG, H., LIANG, F., LING, C. & HU, Y. 2016. mTORC1 is necessary but mTORC2 and GSK3β are inhibitory for AKT3-induced axon regeneration in the central nervous system. *eLife,* 5**,** e14908.

MILLS, K. F., YOSHIDA, S., STEIN, L. R., GROZIO, A., KUBOTA, S., SASAKI, Y., REDPATH, P., MIGAUD, M. E., APTE, R. S., UCHIDA, K., YOSHINO, J. & IMAI, S. I. 2016. Long-Term Administration of Nicotinamide Mononucleotide Mitigates Age-Associated Physiological Decline in Mice. *Cell Metabolism,* 24**,** 795-806.

MITTAL, M., SIDDIQUI, M. R., TRAN, K., REDDY, S. P. & MALIK, A. B. 2013. Reactive Oxygen Species in Inflammation and Tissue Injury. *Antioxidants & Redox Signaling,* 20**,** 1126-1167.

MORABIA, A. 2008. Joseph Goldberger's research on the prevention of pellagra. *Journal of the Royal Society of Medicine,* 101**,** 566-568.

MORGAN, J. E. 2002. Retinal ganglion cell shrinkage in glaucoma. *Journal of glaucoma,* 11**,** 365-370.

MORGAN, J. E. 2004. Circulation and axonal transport in the optic nerve. *Eye (Lond),* 18**,** 1089-95.

MORGAN, J. E. 2012. Retina ganglion cell degeneration in glaucoma: an opportunity missed? A review. *Clinical & Experimental Ophthalmology,* 40**,** 364-8.

MORGAN, J. E., DATTA, A. V., ERICHSEN, J. T., ALBON, J. & BOULTON, M. E. Retinal Ganglion Cell Remodelling in Experimental Glaucoma. *In:* HOLLYFIELD, J. G., ANDERSON, R. E. & LAVAIL, M. M., eds. Retinal Degenerative Diseases, 2006// 2006 Boston, MA. Springer US, 397-402.

MORGAN, J. E. & TRIBBLE, J. R. 2015. Microbead models in glaucoma. *Experimental Eye Research,* 141**,** 9-14.

MORI, V., AMICI, A., MAZZOLA, F., DI STEFANO, M., CONFORTI, L., MAGNI, G., RUGGIERI, S., RAFFAELLI, N. & ORSOMANDO, G. 2014. Metabolic profiling of alternative NAD biosynthetic routes in mouse tissues. *PloS one,* 9**,** e113939.

MORIYA, H. 2015. Quantitative nature of overexpression experiments. *Molecular Biology of the Cell,* 26**,** 3932-9.

MORRISON, J. C., JIA, L., CEPURNA, W., GUO, Y. & JOHNSON, E. 2009. Reliability and sensitivity of the TonoLab rebound tonometer in awake Brown Norway rats. *Investigative Ophthalmology & Visual Science,* 50**,** 2802-8.

MORRISON, J. C., JOHNSON, E. & CEPURNA, W. O. 2008. Rat models for glaucoma research. *Glaucoma: An Open Window to Neurodegeneration and Neuroprotection.*

MUENCH, N. A., PATEL, S., MAES, M. E., DONAHUE, R. J., IKEDA, A. & NICKELLS, R. W. 2021. The Influence of Mitochondrial Dynamics and Function on Retinal Ganglion Cell Susceptibility in Optic Nerve Disease. *Cells,* 10.

MULLER, B., WAGNER, F., LORENZ, B. & STIEGER, K. 2017. Organotypic Cultures of Adult Mouse Retina: Morphologic Changes and Gene Expression. *Investigative Ophthalmology & Visual Science,* 58**,** 1930-1940.

MUNEMASA, Y. & KITAOKA, Y. 2012. Molecular mechanisms of retinal ganglion cell degeneration in glaucoma and future prospects for cell body and axonal protection. *Frontiers in Cellular Neuroscience,* 6**,** 60.

MUNKACSY, G., HERMAN, P. & GYORFFY, B. 2019. Independent validation of induced overexpression efficiency across 242 experiments shows a success rate of 39. *Scientific Reports,* 9**,** 343.

MURALI, A., RAMLOGAN-STEEL, C. A., ANDRZEJEWSKI, S., STEEL, J. C. & LAYTON, C. J. 2019. Retinal explant culture: A platform to investigate human neuro-retina. *Clinical & Experimental Ophthalmology,* 47**,** 274-285.

NAIK, S., PANDEY, A., LEWIS, S. A., SADASHIVA, S. R. B. & MUTALIK, S. 2020. Neuroprotection: A versatile approach to combat glaucoma. *European Journal of Pharmacology***,** 173208.

NAIR, A. B. & JACOB, S. 2016. A simple practice guide for dose conversion between animals and human. *Journal of Basic and Clinical Pharmacy,* 7**,** 27-31.

NASS, S. & NASS, M. M. 1963. INTRAMITOCHONDRIAL FIBERS WITH DNA CHARACTERISTICS. II. ENZYMATIC AND OTHER HYDROLYTIC TREATMENTS. *Journal of Cell Biology,* 19**,** 613-29.

NCT05275738, T. 2022. The Glaucoma Nicotinamide Trial. https://ClinicalTrials.gov/show/NCT05275738.

NCT05405868, N. 2022. Nicotinamide in Glaucoma. https://ClinicalTrials.gov/show/NCT05405868.

NEISHABOURI, A. M. & FAISAL, A. A. 2011. The metabolic efficiency of myelinated vs unmyelinated axons. *BMC Neuroscience,* 12**,** P100.

NELSON, D. L., LEHNINGER, A. L. & COX, M. M. 2008. *Lehninger principles of biochemistry*, Macmillan.

NI, H.-M., WILLIAMS, J. A. & DING, W.-X. 2015. Mitochondrial dynamics and mitochondrial quality control. *Redox Biology,* 4**,** 6-13.

NISSANKA, N. & MORAES, C. T. 2018. Mitochondrial DNA damage and reactive oxygen species in neurodegenerative disease. *FEBS Letters,* 592**,** 728-742.

NUSCHKE, A. C., FARRELL, S. R., LEVESQUE, J. M. & CHAUHAN, B. C. 2015. Assessment of retinal ganglion cell damage in glaucomatous optic neuropathy: Axon transport, injury and soma loss. *Experimental Eye Research,* 141**,** 111-24.

OSTERLOH, J. M., YANG, J., ROONEY, T. M., FOX, A. N., ADALBERT, R., POWELL, E. H., SHEEHAN, A. E., AVERY, M. A., HACKETT, R., LOGAN, M. A., MACDONALD, J. M., ZIEGENFUSS, J. S., MILDE, S., HOU, Y.-J., NATHAN, C., DING, A., BROWN, R. H., CONFORTI, L., COLEMAN, M., TESSIER-LAVIGNE, M., ZÜCHNER, S. & FREEMAN, M. R. 2012. dSarm/Sarm1 Is Required for Activation of an Injury-Induced Axon Death Pathway. *Science,* 337**,** 481-484.

OU, Y., JO, R. E., ULLIAN, E. M., WONG, R. O. L. & DELLA SANTINA, L. 2016. Selective Vulnerability of Specific Retinal Ganglion Cell Types and Synapses after Transient Ocular Hypertension. *The Journal of Neuroscience,* 36**,** 9240.

OWEN, J. B. & BUTTERFIELD, D. A. 2010. Measurement of oxidized/reduced glutathione ratio. *Methods in Molecular Biology,* 648**,** 269-77.

PANG, I. H. & CLARK, A. F. 2020. Inducible rodent models of glaucoma. *Progress in Retinal and Eye Research,* 75**,** 100799.

PANG, Z., CHONG, J., ZHOU, G., DE LIMA MORAIS, D. A., CHANG, L., BARRETTE, M., GAUTHIER, C., JACQUES, P. E., LI, S. & XIA, J. 2021. MetaboAnalyst 5.0: narrowing the gap between raw spectra and functional insights. *Nucleic Acids Research,* 49**,** W388-W396.

PANG, Z., ZHOU, G., EWALD, J., CHANG, L., HACARIZ, O., BASU, N. & XIA, J. 2022. Using MetaboAnalyst 5.0 for LC–HRMS spectra processing, multi-omics integration and covariate adjustment of global metabolomics data. *Nature Protocols,* 17**,** 1735-1761.

PARRISH, J. Z., EMOTO, K., KIM, M. D. & JAN, Y. N. 2007. Mechanisms that regulate establishment, maintenance, and remodeling of dendritic fields. *Annual Review of Neuroscience,* 30**,** 399-423.

PATTAMATTA, U., MCPHERSON, Z. & WHITE, A. 2016. A mouse retinal explant model for use in studying neuroprotection in glaucoma. *Experimental Eye Research,* 151**,** 38-44.

PAZZAGLIA, S. & PIOLI, C. 2019. Multifaceted Role of PARP-1 in DNA Repair and Inflammation: Pathological and Therapeutic Implications in Cancer and Non-Cancer Diseases. *Cells,* 9.

PEARSON, H. E. & THOMPSON, T. P. 1993. Atrophy and Degeneration of Ganglion Cells in Central Retina Following Loss of Postsynaptic Target Neurons in the Dorsal Lateral Geniculate Nucleus of the Adult Cat. *Experimental Neurology,* 119**,** 113-119.

PEMBERTON, J. M., POGMORE, J. P. & ANDREWS, D. W. 2021. Neuronal cell life, death, and axonal degeneration as regulated by the BCL-2 family proteins. *Cell Death & Differentiation,* 28**,** 108-122.

PETRITI, B., WILLIAMS, P. A., LASCARATOS, G., CHAU, K. Y. & GARWAY-HEATH, D. F. 2021. Neuroprotection in Glaucoma: NAD(+)/NADH Redox State as a Potential Biomarker and Therapeutic Target. *Cells,* 10.

PFEIFFER, R. L., MARC, R. E., KONDO, M., TERASAKI, H. & JONES, B. W. 2016. Muller cell metabolic chaos during retinal degeneration. *Experimental Eye Research,* 150**,** 62-70.

PICKLES, S., VIGIÉ, P. & YOULE, R. J. 2018. Mitophagy and Quality Control Mechanisms in Mitochondrial Maintenance. *Current Biology,* 28**,** R170-R185.

POLJSAK, B. & MILISAV, I. 2018. Vitamin B3 forms as precursors to NAD+: Are they safe? *Trends in Food Science & Technology,* 79**,** 198-203.

PORCIATTI, V. & VENTURA, L. M. 2012. Retinal ganglion cell functional plasticity and optic neuropathy: a comprehensive model. *Journal of Neuroophthalmology,* 32**,** 354-8.

POTTORF, T., MANN, A., FROSS, S., MANSEL, C. & VOHRA, B. P. S. 2018. Nicotinamide Mononucleotide Adenylyltransferase 2 maintains neuronal structural integrity through the maintenance of golgi structure. *Neurochemistry International,* 121**,** 86-97.

PREISS, J. & HANDLER, P. 1958a. Biosynthesis of diphosphopyridine nucleotide I. Identification of intermediates. *Journal of Biological Chemistry,* 233**,** 488-492.

PREISS, J. & HANDLER, P. 1958b. Biosynthesis of diphosphopyridine nucleotide II. Enzymatic aspects. *Journal of Biological Chemistry,* 233**,** 493-500.

PRUSKY, G. T., HARKER, K. T., DOUGLAS, R. M. & WHISHAW, I. Q. 2002. Variation in visual acuity within pigmented, and between pigmented and albino rat strains. *Behavioural Brain Research,* 136**,** 339-348.

QU, J., WANG, D. & GROSSKREUTZ, C. L. 2010. Mechanisms of retinal ganglion cell injury and defense in glaucoma. *Experimental Eye Research,* 91**,** 48-53.

QUALMANN, B. & KESSELS, M. M. 2021. The Role of Protein Arginine Methylation as Post-Translational Modification on Actin Cytoskeletal Components in Neuronal Structure and Function. *Cells,* 10.

QUIGLEY, H. A. 2011. Glaucoma. *Lancet,* 377**,** 1367-77.

RAJMAN, L., CHWALEK, K. & SINCLAIR, D. A. 2018. Therapeutic Potential of NAD-Boosting Molecules: The In Vivo Evidence. *Cell Metabolism,* 27**,** 529-547.

RAMIREZ, A. I., DE HOZ, R., SALOBRAR-GARCIA, E., SALAZAR, J. J., ROJAS, B., AJOY, D., LOPEZ-CUENCA, I., ROJAS, P., TRIVINO, A. & RAMIREZ, J. M. 2017. The Role of Microglia in Retinal Neurodegeneration: Alzheimer's Disease, Parkinson, and Glaucoma. *Frontiers in Aging Neuroscience,* 9**,** 214.

RAMÍREZ, A. I., SALAZAR, J. J., DE HOZ, R., ROJAS, B., GALLEGO, B. I., SALINAS-NAVARRO, M., ALARCÓN-MARTÍNEZ, L., ORTÍN-MARTÍNEZ, A., AVILÉS-TRIGUEROS, M., VIDAL-SANZ, M., TRIVIÑO, A. & RAMÍREZ, J. M. 2010. Quantification of the Effect of Different Levels of IOP in the Astroglia of the Rat Retina Ipsilateral and Contralateral to Experimental Glaucoma. *Investigative Ophthalmology & Visual Science,* 51**,** 5690-5696.

RAMÍREZ, A. I., SALAZAR, J. J., DE HOZ, R., ROJAS, B., GALLEGO, B. I., SALOBRAR-GARCÍA, E., VALIENTE-SORIANO, F. J., TRIVIÑO, A. & RAMIREZ, J. M. 2015. Chapter 7 - Macro- and microglial responses in the fellow eyes contralateral to glaucomatous eyes. *In:* BAGETTA, G. & NUCCI, C. (eds.) *Progress in Brain Research.* Elsevier.

RASHID, K., AKHTAR-SCHAEFER, I. & LANGMANN, T. 2019. Microglia in Retinal Degeneration. *Frontiers in Immunology,* 10.

RATAJCZAK, J., JOFFRAUD, M., TRAMMELL, S. A. J., RAS, R., CANELA, N., BOUTANT, M., KULKARNI, S. S., RODRIGUES, M., REDPATH, P., MIGAUD, M. E., AUWERX, J., YANES, O., BRENNER, C. & CANTÓ, C. 2016. NRK1 controls nicotinamide mononucleotide and nicotinamide riboside metabolism in mammalian cells. *Nature Communications,* 7**,** 13103.

REDZA-DUTORDOIR, M. & AVERILL-BATES, D. A. 2016. Activation of apoptosis signalling pathways by reactive oxygen species. *Biochimica et Biophysica Acta,* 1863**,** 2977-2992.

REESE, B. E. & KEELEY, P. W. 2015. Design principles and developmental mechanisms underlying retinal mosaics. *Biological Reviews of the Cambridge Philosophical Society,* 90**,** 854-76.

RHO, S., PARK, I., SEONG, G. J., LEE, N., LEE, C. K., HONG, S. & KIM, C. Y. 2014. Chronic ocular hypertensive rat model using microbead injection: comparison of polyurethane, polymethylmethacrylate, silica and polystyene microbeads. *Current Eye Research,* 39**,** 917-27.

RISNER, M. L., PASINI, S., MCGRADY, N. R., D'ALESSANDRO, K. B., YAO, V., COOPER, M. L. & CALKINS, D. J. 2021. Neuroprotection by Wld(S) depends on retinal ganglion cell type and age in glaucoma. *Molecular Neurodegeneration,* 16**,** 36.

RODRIGUEZ-CARMONA, M. & BARBUR, J. L. 2017. 3 - Variability in normal and defective colour vision: Consequences for occupational environments. *In:* BEST, J. (ed.) *Colour Design (Second Edition).* Woodhead Publishing.

RONGVAUX, A., ANDRIS, F., VAN GOOL, F. & LEO, O. 2003. Reconstructing eukaryotic NAD metabolism. *Bioessays,* 25**,** 683-690.

SALINAS-NAVARRO, M., MAYOR-TORROGLOSA, S., JIMÉNEZ-LÓPEZ, M., AVILÉS-TRIGUEROS, M., HOLMES, T. M., LUND, R. D., VILLEGAS-PÉREZ, M. P. & VIDAL-SANZ, M. 2009. A computerized analysis of the entire retinal ganglion cell population and its spatial distribution in adult rats. *Vision Research,* 49**,** 115-126.

SAMSEL, P. A., KISISWA, L., ERICHSEN, J. T., CROSS, S. D. & MORGAN, J. E. 2011. A novel method for the induction of experimental glaucoma using magnetic microspheres. *Investigative Ophthalmology & Visual Science,* 52**,** 1671-5.

SANES, J. R. & MASLAND, R. H. 2015. The Types of Retinal Ganglion Cells: Current Status and Implications for Neuronal Classification. *Annual Review of Neuroscience,* 38**,** 221-246.

SAPIENZA, A., RAVEU, A. L., REBOUSSIN, E., ROUBEIX, C., BOUCHER, C., DEGARDIN, J., GODEFROY, D., ROSTENE, W., REAUX-LE GOAZIGO, A., BAUDOUIN, C. & MELIK PARSADANIANTZ, S. 2016. Bilateral neuroinflammatory processes in visual pathways induced by unilateral ocular hypertension in the rat. *Journal of Neuroinflammation,* 13**,** 44.

SAPPINGTON, R. M., CARLSON, B. J., CRISH, S. D. & CALKINS, D. J. 2010. The microbead occlusion model: a paradigm for induced ocular hypertension in rats and mice. *Investigative Ophthalmology & Visual Science,* 51**,** 207-16.

SASAKI, Y., ENGBER, T. M., HUGHES, R. O., FIGLEY, M. D., WU, T., BOSANAC, T., DEVRAJ, R., MILBRANDT, J., KRAUSS, R. & DIANTONIO, A. 2020. cADPR is a gene dosage-sensitive biomarker of SARM1 activity in healthy, compromised, and degenerating axons. *Experimental Neurology,* 329**,** 113252.

SASAKI, Y., MARGOLIN, Z., BORGO, B., HAVRANEK, J. J. & MILBRANDT, J. 2015. Characterization of Leber Congenital Amaurosis-associated NMNAT1 Mutants. *The Journal of biological chemistry,* 290**,** 17228-17238.

SASAKI, Y. & MILBRANDT, J. 2010. Axonal degeneration is blocked by nicotinamide mononucleotide adenylyltransferase (Nmnat) protein transduction into transected axons. *The Journal of biological chemistry,* 285**,** 41211-41215.

SCHNICHELS, S., KIEBLER, T., HURST, J., MALIHA, A. M., LOSCHER, M., DICK, H. B., BARTZ-SCHMIDT, K. U. & JOACHIM, S. C. 2019. Retinal Organ Cultures as Alternative Research Models. *Alternatives to Laboratory Animals,* 47**,** 19-29.

SCHNICHELS, S., PAQUET-DURAND, F., LOSCHER, M., TSAI, T., HURST, J., JOACHIM, S. C. & KLETTNER, A. 2021. Retina in a dish: Cell cultures, retinal explants and animal models for common diseases of the retina. *Progress in Retinal and Eye Research,* 81**,** 100880.

SCHOBER, M. S., CHIDLOW, G., WOOD, J. P. & CASSON, R. J. 2008. Bioenergetic-based neuroprotection and glaucoma. *Clinical & Experimantal Ophthalmology,* 36**,** 377-85.

SCHONDORF, D. C., IVANYUK, D., BADEN, P., SANCHEZ-MARTINEZ, A., DE CICCO, S., YU, C., GIUNTA, I., SCHWARZ, L. K., DI NAPOLI, G., PANAGIOTAKOPOULOU, V., NESTEL, S., KEATINGE, M., PRUSZAK, J., BANDMANN, O., HEIMRICH, B., GASSER, T., WHITWORTH, A. J. & DELEIDI, M. 2018. The NAD+ Precursor Nicotinamide Riboside Rescues Mitochondrial Defects and Neuronal Loss in iPSC and Fly Models of Parkinson's Disease. *Cell Reports,* 23**,** 2976-2988.

SCHWEINFURTH, M. K. 2020. The social life of Norway rats (Rattus norvegicus). *Elife,* 9.

SERNAGOR, E., EGLEN, S. J. & WONG, R. O. L. 2001. Development of Retinal Ganglion Cell Structure and Function. *Progress in Retinal and Eye Research,* 20**,** 139-174.

SHAREEF, S. R., GARCIA-VALENZUELA, E., SALIERNO, A., WALSH, J. & SHARMA, S. C. 1995. Chronic ocular hypertension following episcleral venous occlusion in rats. *Experimental eye research,* 61**,** 379-82.

SHELINE, C. T., ZHOU, Y. & BAI, S. 2010. Light-induced photoreceptor and RPE degeneration involve zinc toxicity and are attenuated by pyruvate, nicotinamide, or cyclic light. *Molecular vision,* 16**,** 2639-2652.

SHERAZEE, N. & ALVAREZ, V. A. 2013. DiOlistics: delivery of fluorescent dyes into cells. *Methods in Molecular Biology,* 940**,** 391-400.

SHOLL, D. A. 1953. Dendritic organization in the neurons of the visual and motor cortices of the cat. *Journal of anatomy,* 87**,** 387-406.

SHPILKA, T. & HAYNES, C. M. 2018. The mitochondrial UPR: mechanisms, physiological functions and implications in ageing. *Nature Reviews Molecular Cell Biology,* 19**,** 109-120.

SMEDOWSKI, A., PIETRUCHA-DUTCZAK, M., KAARNIRANTA, K. & LEWIN-KOWALIK, J. 2014. A rat experimental model of glaucoma incorporating rapid-onset elevation of intraocular pressure. *Scientific Reports,* 4**,** 5910.

SMITH, A. J. & LILLEY, E. 2019. The Role of the Three Rs in Improving the Planning and Reproducibility of Animal Experiments. *Animals (Basel),* 9.

SMITH, P. 1879. Glaucoma: its causes, symptoms, pathology and treatment. *London: J.A. Churchill*.

SOTO, I. & HOWELL, G. R. 2014. The complex role of neuroinflammation in glaucoma. *Cold Spring Harbor Perspective in Medicine,* 4.

STEIN, L. R. & IMAI, S.-I. 2014. Specific ablation of Nampt in adult neural stem cells recapitulates their functional defects during aging. *The EMBO Journal,* 33**,** 1321-1340.

STRØMLAND, Ø., DIAB, J., FERRARIO, E., SVERKELI, L. J. & ZIEGLER, M. 2021. The balance between NAD+ biosynthesis and consumption in ageing. *Mechanisms of Ageing and Development,* 199**,** 111569.

SUN, W., LI, N. & HE, S. 2002a. Large-scale morophological survey of rat retinal ganglion cells. *Visual Neuroscience,* 19**,** 483-93.

SUN, W., LI, N. & HE, S. 2002b. Large-scale morphological survey of mouse retinal ganglion cells. *Journal of Comparative Neurology,* 451**,** 115-26.

SWANGER, S. A., MATTHEYSES, A. L., GENTRY, E. G. & HERSKOWITZ, J. H. 2015. ROCK1 and ROCK2 inhibition alters dendritic spine morphology in hippocampal neurons. *Cellular Logistics,* 5**,** e1133266.

TANG, B. L. 2019. Why is NMNAT Protective against Neuronal Cell Death and Axon Degeneration, but Inhibitory of Axon Regeneration? *Cells,* 8**,** 267.

TANG, Z., ZHANG, S., LEE, C., KUMAR, A., ARJUNAN, P., LI, Y., ZHANG, F. & LI, X. 2011. An optic nerve crush injury murine model to study retinal ganglion cell survival. *Journal of Visualized Experiments*.

TAO, J. & ROLLS, M. M. 2011. Dendrites Have a Rapid Program of Injury-Induced Degeneration That Is Molecularly Distinct from Developmental Pruning. *Journal of Neuroscience,* 31**,** 5398-5405.

TEZEL, G. 2021. Multifactorial Pathogenic Processes of Retinal Ganglion Cell Degeneration in Glaucoma towards Multi-Target Strategies for Broader Treatment Effects. *Cells,* 10.

THAM, Y.-C., LI, X., WONG, T. Y., QUIGLEY, H. A., AUNG, T. & CHENG, C.-Y. 2014. Global Prevalence of Glaucoma and Projections of Glaucoma Burden through 2040: A Systematic Review and Meta-Analysis. *Ophthalmology,* 121**,** 2081-2090.

TIAN, N. & COPENHAGEN, D. R. 2001. Visual Deprivation Alters Development of Synaptic Function in Inner Retina after Eye Opening. *Neuron,* 32**,** 439-449.

TIAN, N. & COPENHAGEN, D. R. 2003. Visual Stimulation Is Required for Refinement of ON and OFF Pathways in Postnatal Retina. *Neuron,* 39**,** 85-96.

TRIBBLE, J. R., CROSS, S. D., SAMSEL, P. A., SENGPIEL, F. & MORGAN, J. E. 2014. A novel system for the classification of diseased retinal ganglion cells. *Visual Neuroscience,* 31**,** 373-80.

TRIBBLE, J. R., HAGSTROM, A., JUSSEAUME, K., LARDNER, E., WONG, R. C., STALHAMMAR, G. & WILLIAMS, P. A. 2023. NAD salvage pathway machinery expression in normal and glaucomatous retina and optic nerve. *Acta Neuropathologica Communication,* 11**,** 18.

TRIBBLE, J. R., KOKKALI, E., OTMANI, A., PLASTINO, F., LARDNER, E., VOHRA, R., KOLKO, M., ANDRE, H., MORGAN, J. E. & WILLIAMS, P. A. 2021a. When Is a Control Not a Control? Reactive Microglia Occur Throughout the Control Contralateral Pathway of Retinal Ganglion Cell Projections in Experimental Glaucoma. *Translational Vision Science & Technology,* 10**,** 22.

TRIBBLE, J. R., OTMANI, A., KOKKALI, E., LARDNER, E., MORGAN, J. E. & WILLIAMS, P. A. 2021b. Retinal Ganglion Cell Degeneration in a Rat Magnetic Bead Model of Ocular Hypertensive Glaucoma. *Translational Vision Science & Technology,* 10**,** 21.

TRIBBLE, J. R., OTMANI, A., SUN, S., ELLIS, S. A., CIMAGLIA, G., VOHRA, R., JOE, M., LARDNER, E., VENKATARAMAN, A. P., DOMINGUEZ-VICENT, A., KOKKALI, E., RHO, S., JOHANNESSON, G., BURGESS, R. W., FUERST, P. G., BRAUTASET, R., KOLKO, M., MORGAN, J. E., CROWSTON, J. G., VOTRUBA, M. & WILLIAMS, P. A. 2021c. Nicotinamide provides neuroprotection in glaucoma by protecting against mitochondrial and metabolic dysfunction. *Redox Biology,* 43**,** 101988.

TRIBBLE, J. R., VASALAUSKAITE, A., REDMOND, T., YOUNG, R. D., HASSAN, S., FAUTSCH, M. P., SENGPIEL, F., WILLIAMS, P. A. & MORGAN, J. E. 2019. Midget retinal ganglion cell dendritic and mitochondrial degeneration is an early feature of human glaucoma. *Brain Communication,* 1**,** fcz035.

TSAI, J. C., WU, L., WORGUL, B., FORBES, M. & CAO, J. 2005. Intravitreal Administration of Erythropoietin and Preservation of Retinal Ganglion Cells in an Experimental Rat Model of Glaucoma. *Current Eye Research,* 30**,** 1025-1031.

URCOLA, J. H., HERNANDEZ, M. & VECINO, E. 2006. Three experimental glaucoma models in rats: comparison of the effects of intraocular pressure elevation on retinal ganglion cell size and death. *Experimental Eye Research,* 83**,** 429-37.

VAN DE VEN, R. A. H., SANTOS, D. & HAIGIS, M. C. 2017. Mitochondrial Sirtuins and Molecular Mechanisms of Aging. *Trends in Molecular Medicine,* 23**,** 320-331.

VAN DEN BERG, R. A., HOEFSLOOT, H. C., WESTERHUIS, J. A., SMILDE, A. K. & VAN DER WERF, M. J. 2006. Centering, scaling, and transformations: improving the biological information content of metabolomics data. *BMC Genomics,* 7**,** 142.

VANDERWALL, K. B., LU, B., ALFARO, J. S., ALLSOP, A. R., CARR, A. S., WANG, S. & MEYER, J. S. 2020. Differential susceptibility of retinal ganglion cell subtypes in acute and chronic models of injury and disease. *Scientific Reports,* 10**,** 17359.

VECINO, E., RODRIGUEZ, F. D., RUZAFA, N., PEREIRO, X. & SHARMA, S. C. 2016. Glia–neuron interactions in the mammalian retina. *Progress in Retinal and Eye Research,* 51**,** 1-40.

VEENHUIS, S. J. G., VAN OS, N. J. H., JANSSEN, A. J. W. M., VAN GERVEN, M. H. J. C., COENE, K. L. M., ENGELKE, U. F. H., WEVERS, R. A., TINNEVELT, G. H., TER HEINE, R., VAN DE WARRENBURG, B. P. C., WEEMAES, C. M. R., ROELEVELD, N. & WILLEMSEN, M. A. A. P. 2021. Nicotinamide Riboside Improves Ataxia Scores and Immunoglobulin Levels in Ataxia Telangiectasia. *Movement Disorders,* 36**,** 2951-2957.

VENTURA, L. M. & PORCIATTI, V. 2005. Restoration of retinal ganglion cell function in early glaucoma after intraocular pressure reduction: A pilot study. *Ophthalmology,* 112**,** 20-27.

VERDIN, E. 2015. NAD+ in aging, metabolism, and neurodegeneration. *Science,* 350**,** 1208.

VIDAL-SANZ, M., SALINAS-NAVARRO, M., NADAL-NICOLAS, F. M., ALARCON-MARTINEZ, L., VALIENTE-SORIANO, F. J., DE IMPERIAL, J. M., AVILES-TRIGUEROS, M., AGUDO-BARRIUSO, M. & VILLEGAS-PEREZ, M. P. 2012. Understanding glaucomatous damage: anatomical and functional data from ocular hypertensive rodent retinas. *Progress in Retinal and Eye Research,* 31**,** 1-27.

VIEGAS, F. O. & NEUHAUSS, S. C. F. 2021. A Metabolic Landscape for Maintaining Retina Integrity and Function. *Frontiers in Molecular Neuroscience,* 14**,** 656000.

VON KORTZFLEISCH, V. T., KARP, N. A., PALME, R., KAISER, S., SACHSER, N. & RICHTER, S. H. 2020. Improving reproducibility in animal research by splitting the study population into several 'mini-experiments'. *Scientific Reports,* 10**,** 16579.

WALLER, A. V. 1850. XX. Experiments on the section of the glossopharyngeal and hypoglossal nerves of the frog, and observations of the alterations produced thereby in the structure of their primitive fibres. *Philosophical Transactions of the Royal Society of London***,** 423-429.

WALLER, T. J. & COLLINS, C. A. 2021. An NAD+/NMN balancing act by SARM1 and NMNAT2 controls axonal degeneration. *Neuron,* 109**,** 1067-1069.

WANG, B., WU, L., CHEN, J., DONG, L., CHEN, C., WEN, Z., HU, J., FLEMING, I. & WANG, D. W. 2021. Metabolism pathways of arachidonic acids: mechanisms and potential therapeutic targets. *Signal Transduction and Targeted Therapy,* 6**,** 94.

WANG, J. & HE, Z. 2009. NAD and axon degeneration: from the Wlds gene to neurochemistry. *Cell Adhesion & Migration,* 3**,** 77-87.

WANG, Q., ZHUANG, P., HUANG, H., LI, L., LIU, L., WEBBER, H. C., DALAL, R., SIEW, L., FLIGOR, C. M., CHANG, K.-C., NAHMOU, M., KREYMERMAN, A., SUN, Y., MEYER, J. S., GOLDBERG, J. L. & HU, Y. 2020. Mouse γ-Synuclein Promoter-Mediated Gene Expression and Editing in Mammalian Retinal Ganglion Cells. *The Journal of Neuroscience,* 40**,** 3896.

WANG, Y., XU, E., MUSICH, P. R. & LIN, F. 2019. Mitochondrial dysfunction in neurodegenerative diseases and the potential countermeasure. *CNS Neuroscience & Therapeutics,* 25**,** 816-824.

WÄSSLE, H., PEICHL, L. & BOYCOTT, B. B. 1981. Dendritic territories of cat retinal ganglion cells. *Nature,* 292**,** 344-345.

WAXMAN, S. G. 1980. Determinants of conduction velocity in myelinated nerve fibers. *Muscle Nerve,* 3**,** 141-50.

WEBER, A. J. & HARMAN, C. D. 2005. Structure–function relations of parasol cells in the normal and glaucomatous primate retina. *Investigative ophthalmology & visual science,* 46**,** 3197-3207.

WEBER, A. J., KAUFMAN, P. L. & HUBBARD, W. C. 1998. Morphology of single ganglion cells in the glaucomatous primate retina. *Investigative ophthalmology & visual science,* 39**,** 2304-2320.

WEBER, A. J., VISWANÁTHAN, S., RAMANATHAN, C. & HARMAN, C. D. 2010. Combined Application of BDNF to the Eye and Brain Enhances Ganglion Cell Survival and Function in the Cat after Optic Nerve Injury. *Investigative Ophthalmology & Visual Science,* 51**,** 327-334.

WEINREB, R. N., AUNG, T. & MEDEIROS, F. A. 2014. The pathophysiology and treatment of glaucoma: a review. *JAMA,* 311**,** 1901-11.

WILLIAMS, P. A., HARDER, J. M., CARDOZO, B. H., FOXWORTH, N. E. & JOHN, S. W. M. 2018. Nicotinamide treatment robustly protects from inherited mouse glaucoma. *Communicative & Integrative Biology,* 11**,** e1356956.

WILLIAMS, P. A., HARDER, J. M., FOXWORTH, N. E., CARDOZO, B. H., COCHRAN, K. E. & JOHN, S. W. M. 2017a. Nicotinamide and WLD(S) Act Together to Prevent Neurodegeneration in Glaucoma. *Frontiers in Neuroscience,* 11**,** 232.

WILLIAMS, P. A., HARDER, J. M., FOXWORTH, N. E., COCHRAN, K. E., PHILIP, V. M., PORCIATTI, V., SMITHIES, O. & JOHN, S. W. M. 2017b. Vitamin B3 modulates mitochondrial vulnerability and prevents glaucoma in aged mice. *Science,* 355**,** 756.

WILLIAMS, P. A., HARDER, J. M. & JOHN, S. W. M. 2017c. Glaucoma as a Metabolic Optic Neuropathy: Making the Case for Nicotinamide Treatment in Glaucoma. *Journal of Glaucoma,* 26**,** 1161-1168.

WILLIAMS, P. A., MARSH-ARMSTRONG, N., HOWELL, G. R., LASKER, I. I. O. A. & GLAUCOMATOUS NEURODEGENERATION, P. 2017d. Neuroinflammation in glaucoma: A new opportunity. *Experimental eye research,* 157**,** 20-27.

WILLIAMS, P. A., MORGAN, J. E. & VOTRUBA, M. 2010. Opa1 deficiency in a mouse model of dominant optic atrophy leads to retinal ganglion cell dendropathy. *Brain,* 133**,** 2942-51.

WILLIAMS, P. A., TRIBBLE, J. R., JÖE, M., BRANCALE, A., VARRICCHIO, C., COLEMAN, M., GILLEY, J., LORETO, A., WHEELOCK, C. & JOHANNESSON, G. 2022. Targeting NMNAT2 for neuroprotection in glaucoma. *Investigative Ophthalmology & Visual Science,* 63**,** 1134-1134.

WILSEY, L. J. & FORTUNE, B. 2016. Electroretinography in glaucoma diagnosis. *Current Opinion in Ophthalmology,* 27.

XIA, J. & WISHART, D. S. 2011. Web-based inference of biological patterns, functions and pathways from metabolomic data using MetaboAnalyst. *Nature Protocols,* 6**,** 743-760.

XIE, N., ZHANG, L., GAO, W., HUANG, C., HUBER, P. E., ZHOU, X., LI, C., SHEN, G. & ZOU, B. 2020. NAD(+) metabolism: pathophysiologic mechanisms and therapeutic potential. *Signal Transduction and Targeted Therapy,* 5**,** 227.

YAMADA, M., MIZUGUCHI, M., OTSUKA, N., IKEDA, K. & TAKAHASHI, H. 1997. Ultrastructural localization of CD38 immunoreactivity in rat brain. *Brain Research,* 756**,** 52-60.

YANG, L., LI, S., MIAO, L., HUANG, H., LIANG, F., TENG, X., XU, L., WANG, Q., XIAO, W., RIDDER, W. H., FERGUSON, T. A., CHEN, D. F., KAUFMAN, R. J. & HU, Y. 2016. Rescue of

Glaucomatous Neurodegeneration by Differentially Modulating Neuronal Endoplasmic Reticulum Stress Molecules. *The Journal of Neuroscience,* 36**,** 5891.

YANG, Y. & SAUVE, A. A. 2016. NAD(+) metabolism: Bioenergetics, signaling and manipulation for therapy. *Biochimica et biophysica acta,* 1864**,** 1787-1800.

YU, D.-Y. & CRINGLE, S. J. 2001. Oxygen Distribution and Consumption within the Retina in Vascularised and Avascular Retinas and in Animal Models of Retinal Disease. *Progress in Retinal and Eye Research,* 20**,** 175-208.

YU, D.-Y., CRINGLE, S. J., BALARATNASINGAM, C., MORGAN, W. H., YU, P. K. & SU, E.-N. 2013. Retinal ganglion cells: Energetics, compartmentation, axonal transport, cytoskeletons and vulnerability. *Progress in Retinal and Eye Research,* 36**,** 217-246.

ZENG, L., MING, C., LI, Y., SU, L.-Y., SU, Y.-H., OTECKO, N. O., DALECKY, A., DONNELLAN, S., APLIN, K., LIU, X.-H., SONG, Y., ZHANG, Z.-B., ESMAILIZADEH, A., SOHRABI, S. S., NANAEI, H. A., LIU, H.-Q., WANG, M.-S., AG ATTEYNINE, S., ROCAMORA, G., BRESCIA, F., MORAND, S., IRWIN, D. M., PENG, M.-S., YAO, Y.-G., LI, H.-P., WU, D.-D. & ZHANG, Y.-P. 2018. Out of Southern East Asia of the Brown Rat Revealed by Large-Scale Genome Sequencing. *Molecular Biology and Evolution,* 35**,** 149-158.

ZHAI, R. G., ZHANG, F., HIESINGER, P. R., CAO, Y., HAUETER, C. M. & BELLEN, H. J. 2008. NAD synthase NMNAT acts as a chaperone to protect against neurodegeneration. *Nature,* 452**,** 887-91.

ZHANG, W., XIE, Y., WANG, T., BI, J., LI, H., ZHANG, L. Q., YE, S. Q. & DING, S. 2010. Neuronal protective role of PBEF in a mouse model of cerebral ischemia. *Journal of Cerebral Blood Flow & Metabolism,* 30**,** 1962-1971.

ZHU, Y., ZHANG, L., SASAKI, Y., MILBRANDT, J. & GIDDAY, J. M. 2013. Protection of Mouse Retinal Ganglion Cell Axons and Soma from Glaucomatous and Ischemic Injury by Cytoplasmic Overexpression of Nmnat1. *Investigative Ophthalmology & Visual Science,* 54**,** 25-36.

ZHU, Y., ZHAO, K.-K., TONG, Y., ZHOU, Y.-L., WANG, Y.-X., ZHAO, P.-Q. & WANG, Z.-Y. 2016. Exogenous NAD+ decreases oxidative stress and protects H2O2-treated RPE cells against necrotic death through the up-regulation of autophagy. *Scientific Reports,* 6**,** 26322.

Appendix

A.1 C.sham single rat IOP profiles

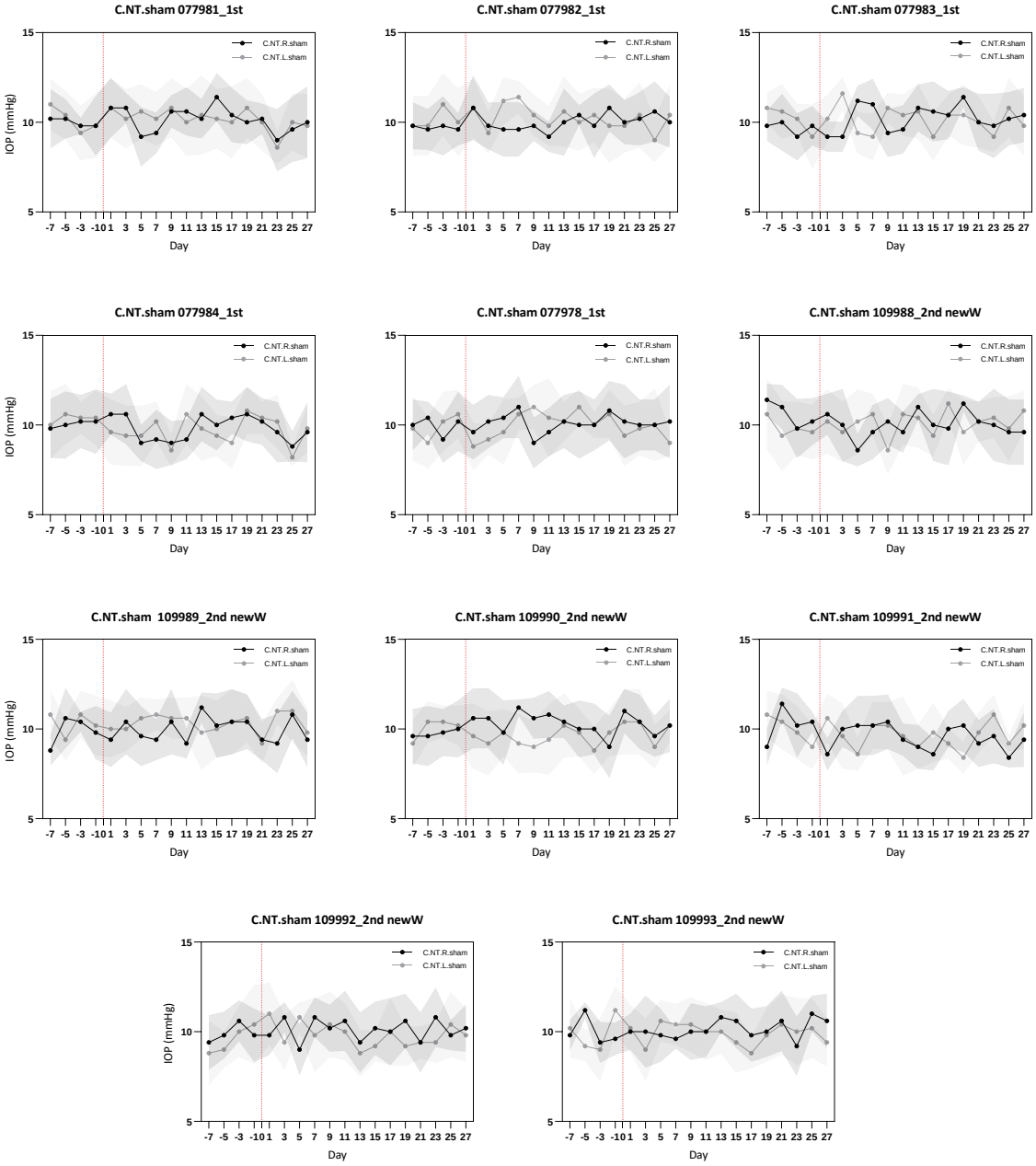

Appendix figure. 1. C.sham, normotensive control single animal IOP profiles. Line represents mean value of complete set of recordings, shaded area ± SD.

A.2 G.sham single rat IOP profiles

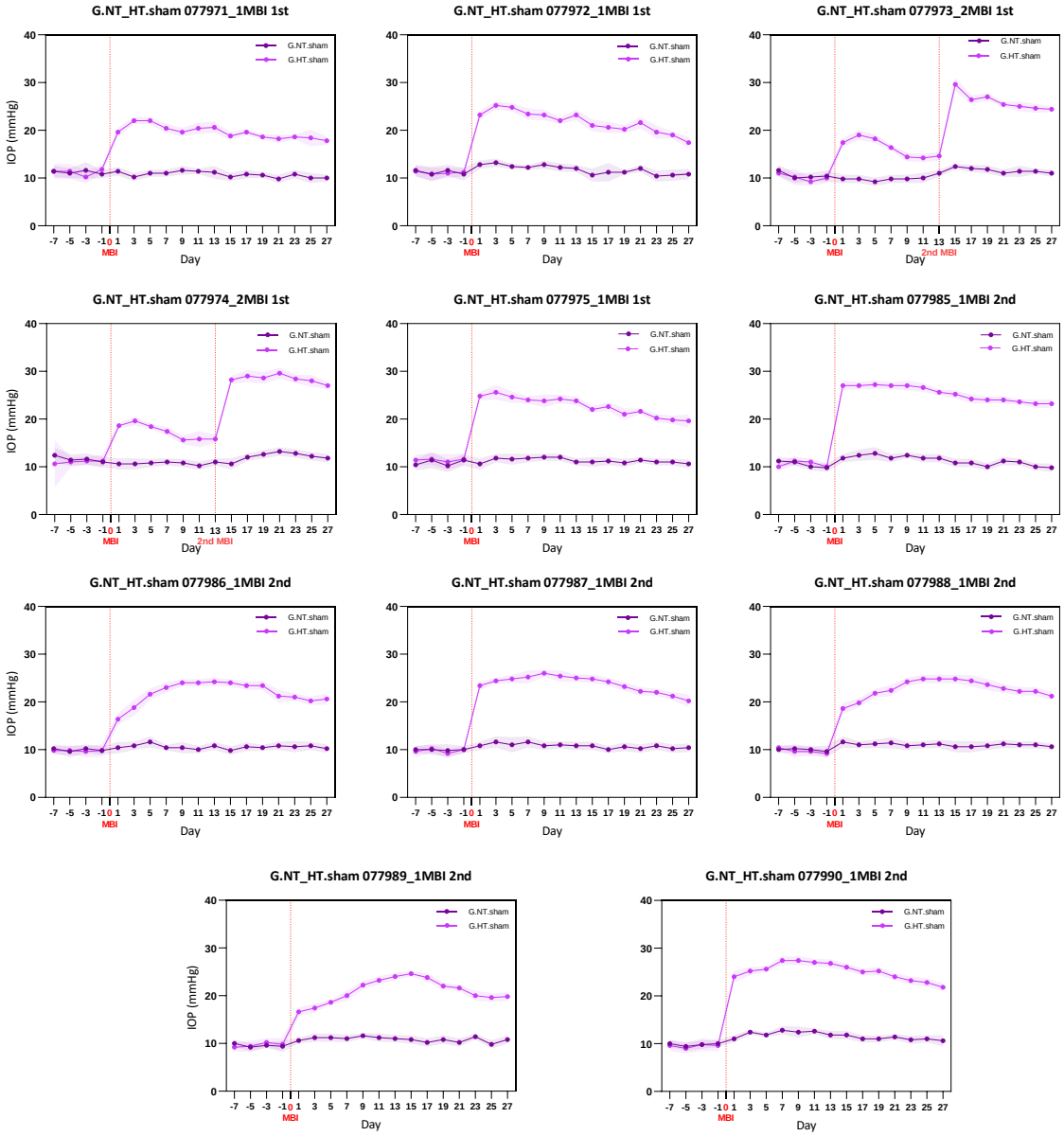

Appendix figure 2. G.sham, hypertensive untreated controls single animal IOP profiles. Line represents mean value of complete set of recordings, shaded area ± SD.

A.3 C.LNAM and C.HNAM single rat IOP profiles

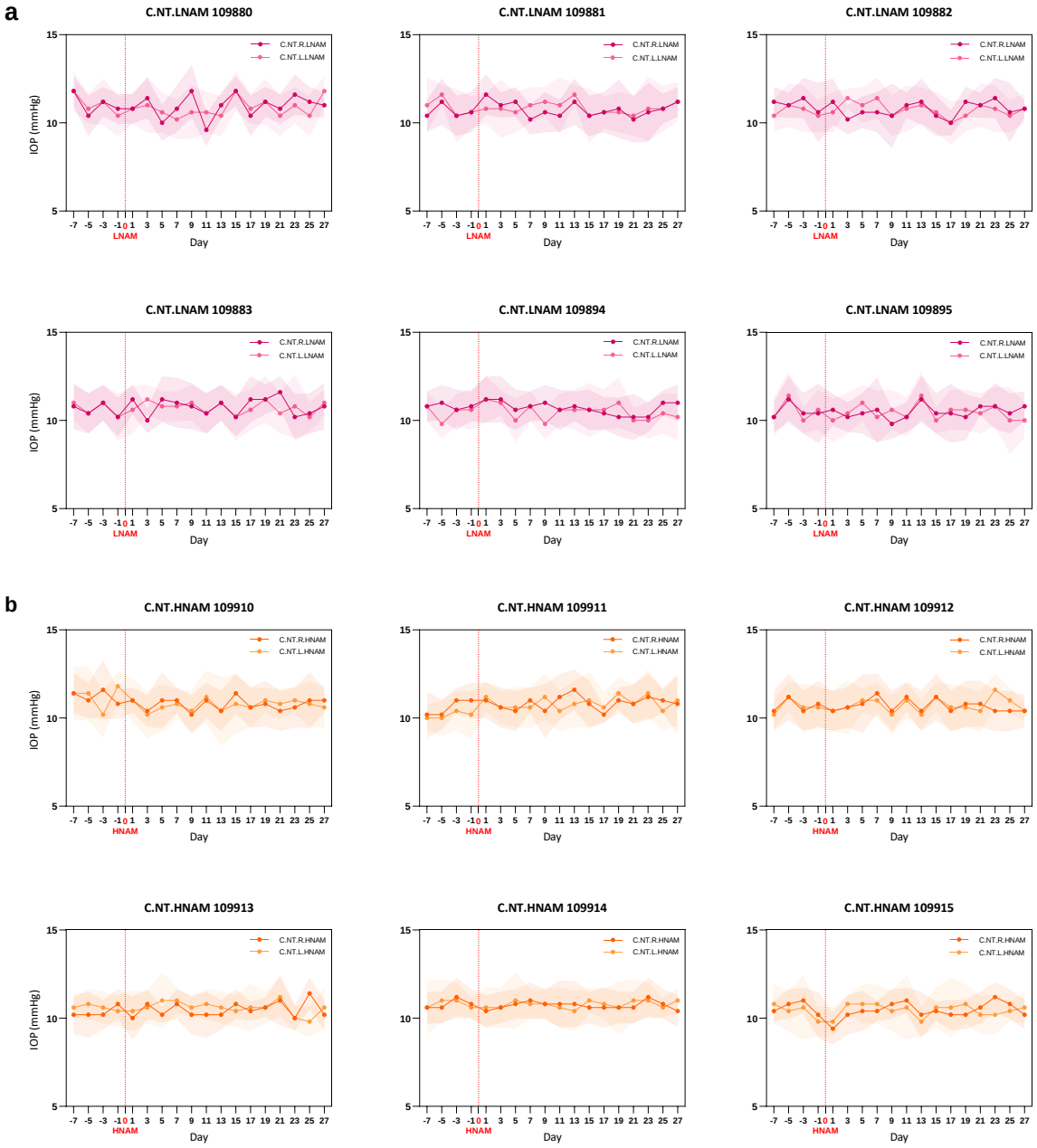

Appendix figure 3. Normotensive NAM treated single animal IOP profiles. a) C.NT.LNAM single rat IOP profiles during the experimental period. b) C.NT.HNAM single rats IOP profiles during the experimental period. group IOP profile. Line represents mean value of complete set of recordings, shaded area ± SD.

A.4 NAM prophylactic treatment single rat IOP profiles

A.4.1 Low NAM prophylactic

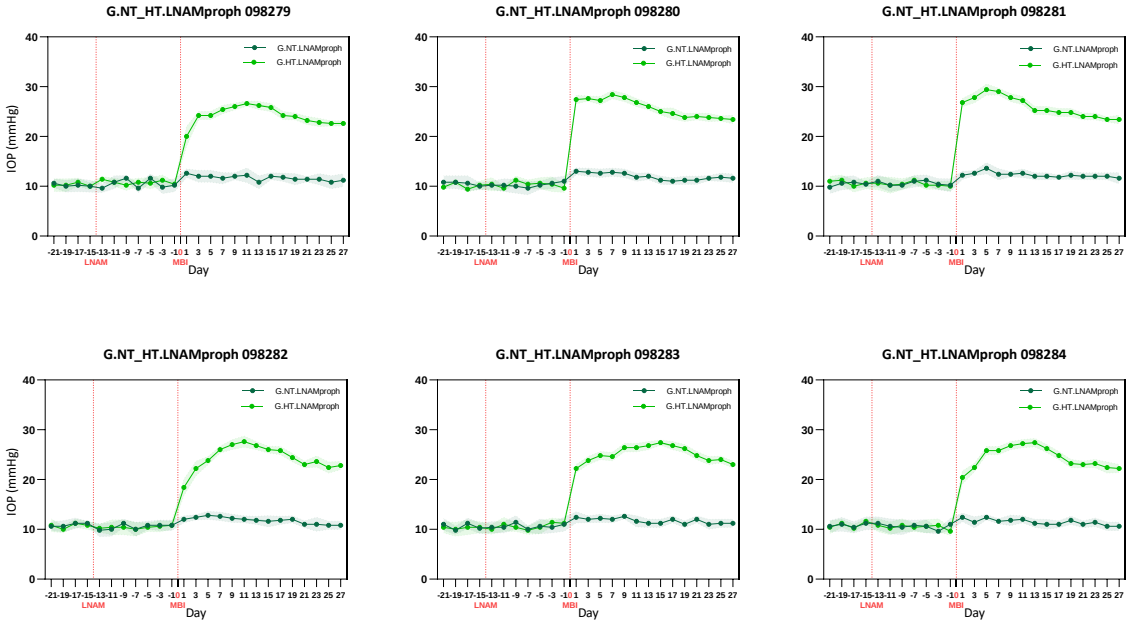

Appendix figure. 4. Low NAM dose prophylactic treatment single animal IOP profiles. Line represents mean value of complete set of recordings, shaded area ± SD.

A.4.2 High NAM prophylactic

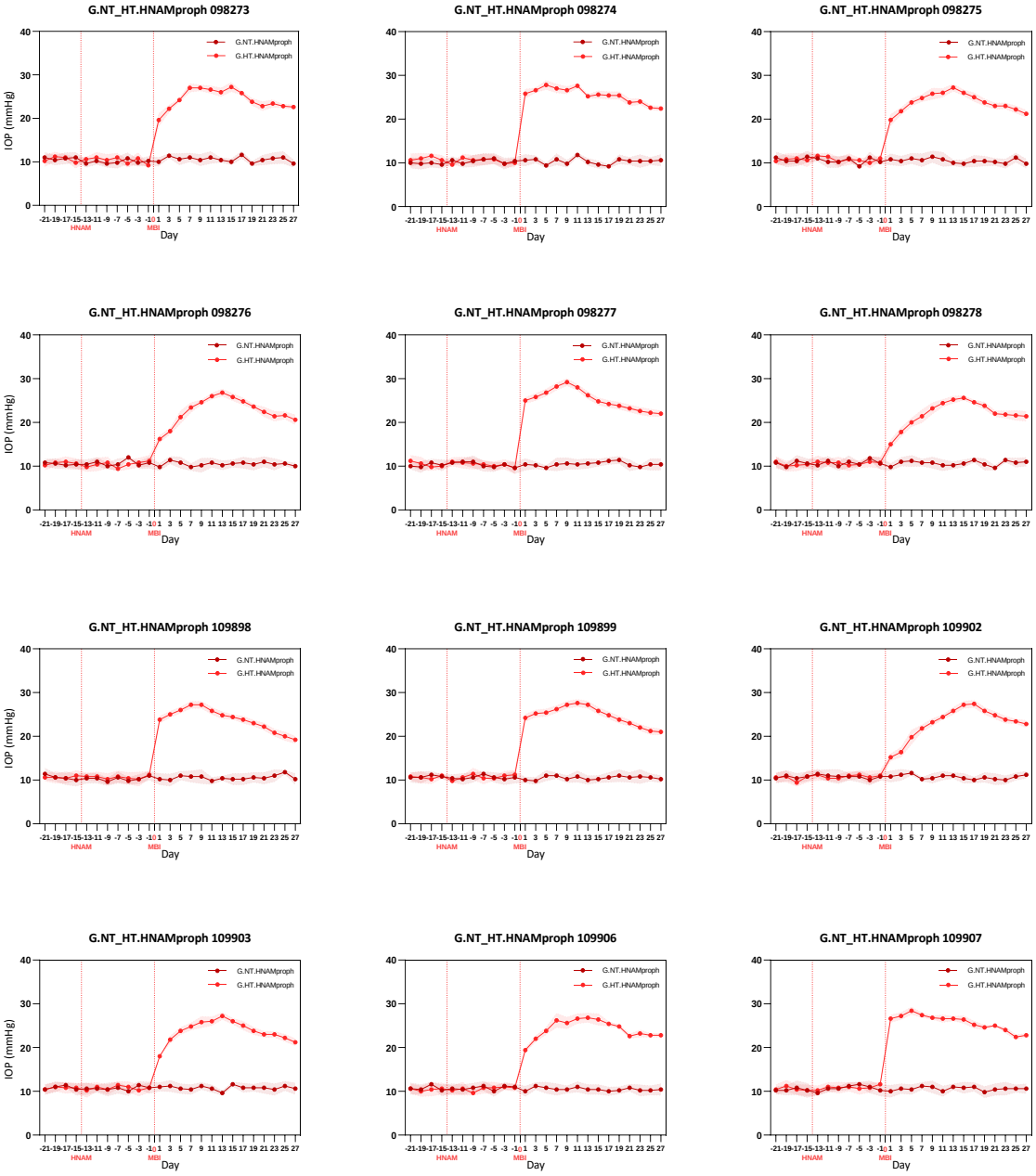

Appendix figure. 5. High NAM dose prophylactic treatment single animal IOP profiles. Line represents mean value of complete set of recordings, shaded area ± SD.

A.5 NAM intervention treatment single rat IOP profiles

A.5.1 Low NAM intervention

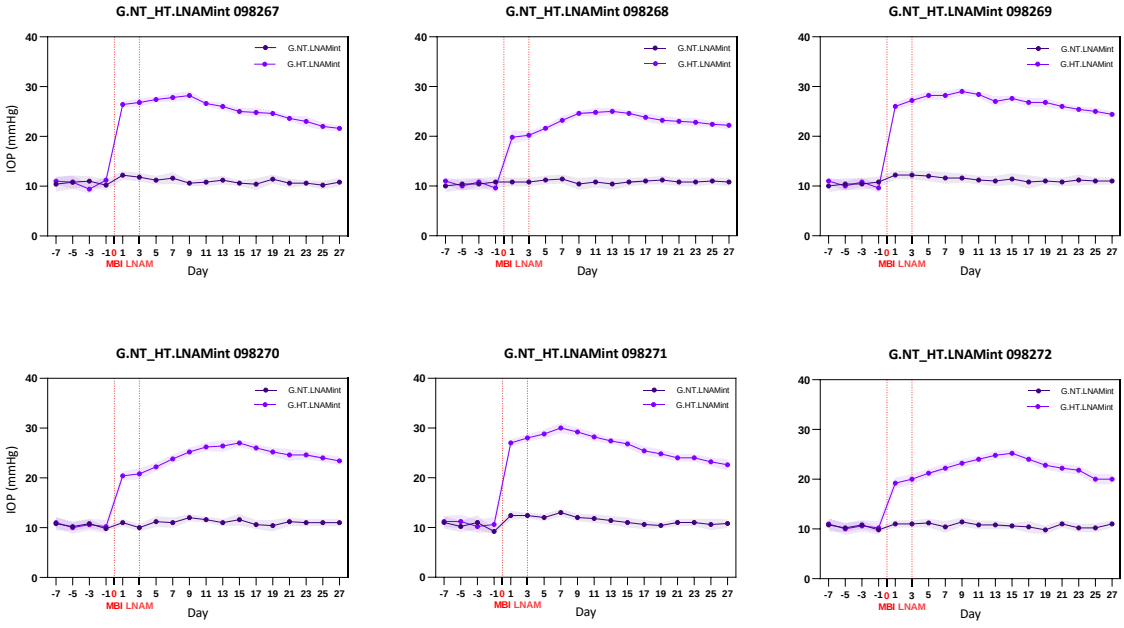

Appendix figure. 6. Low NAM dose intervention treatment single animal IOP profiles. Line represents mean value of complete set of recordings, shaded area ± SD.

A.5.2 High NAM intervention

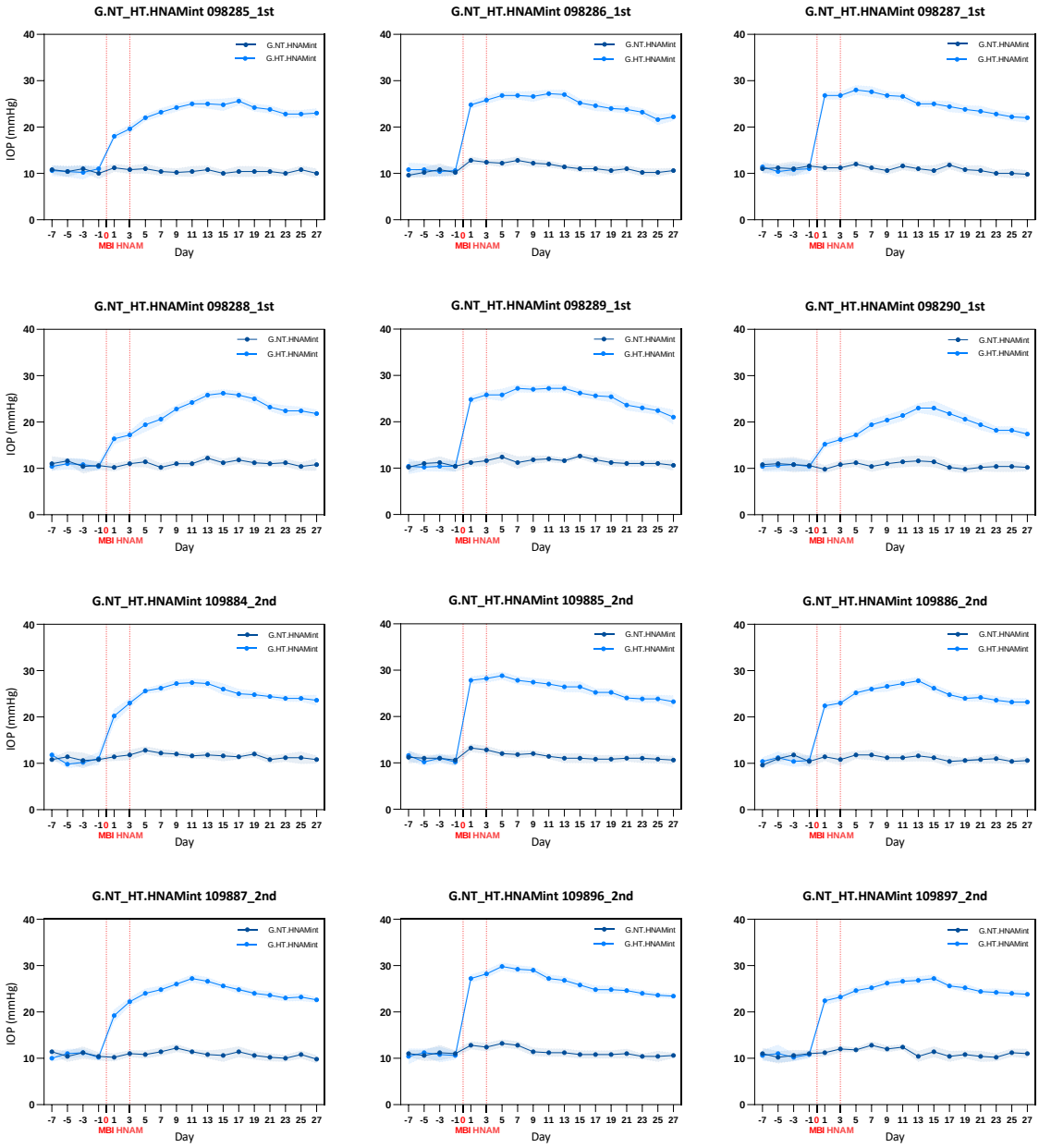

Appendix figure. 7. High NAM dose intervention treatment single animal IOP profiles. Line represents mean value of complete set of recordings, shaded area ± SD.

A.6 NMNAT2 gene therapy single rat IOP profile

A.6.1 T.NT.AAVNMNAT2

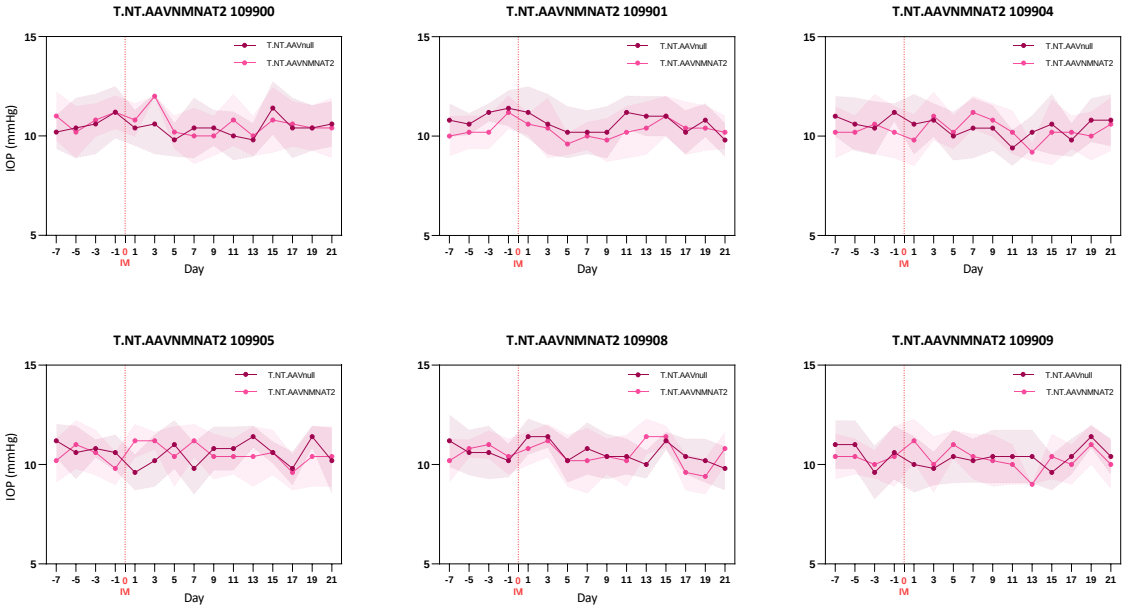

Appendix figure. 8. Normotensive AAV-NMNAT2 injected single animal IOP profiles. Line represents mean value of complete set of recordings, shaded area ± SD.

A.6.2 T.G.AAVNMNAT2

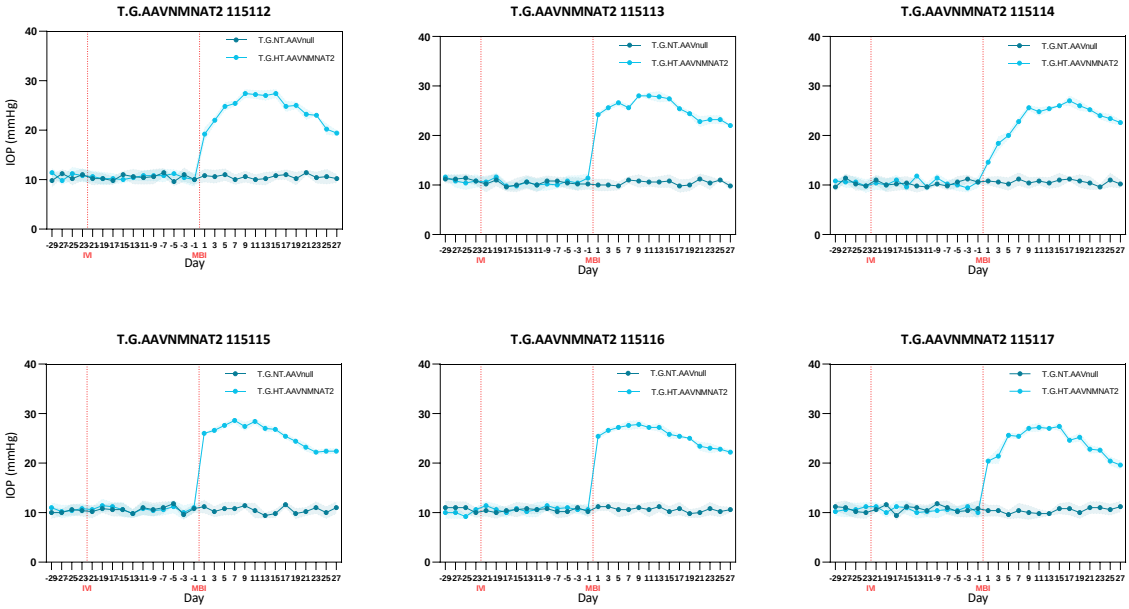

Appendix figure. 9. Normotensive AAV-NMNAT2 injected single animal IOP profiles. Line represents mean value of complete set of recordings, shaded area ± SD.

A.7 Metabolic pathway complete list

A.7.1 G.sham changed metabolic pathways

Pantothenate and CoA biosynthesis

Pentose phosphate pathway

Fructose and mannose metabolism

Inositol phosphate metabolism

Glycerolipid metabolism

Glycerophospholipid metabolism

Ether lipid metabolism

Sphingolipid metabolism

Aminoacyl-tRNA biosynthesis

Glycolysis / Gluconeogenesis

Arginine biosynthesis

Arachidonic acid metabolism

Biosynthesis of unsaturated fatty acids

Valine, leucine and isoleucine degradation

Valine, leucine and isoleucine biosynthesis

β-Alanine metabolism

Phenylalanine, tyrosine and tryptophan biosynthesis

Phenylalanine metabolism

Tryptophan metabolism

Biotin metabolism

Lysine degradation

Glycine, serine and threonine metabolism

Pyruvate metabolism

Histidine metabolism

Alanine, aspartate and glutamate metabolism

Glutathione metabolism

Glyoxylate and dicarboxylate metabolism

Nitrogen metabolism

D-glutamine and D-glutamate metabolism

Nicotinate and nicotinamide metabolism

Cysteine and methionine metabolism

Arginine and proline metabolism

TCA cycle

Riboflavin metabolism

Tyrosine metabolism

Purine metabolism

A.7.2 G.HNAMproph changed metabolic pathways

Pantothenate and CoA biosynthesis

β-Alanine metabolism

Ether lipid metabolism

Glycerophospholipid metabolism

Nicotinate and nicotinamide metabolism

Riboflavin metabolism

Glycine, serine and threonine metabolism

Alanine, aspartate and glutamate metabolism

Sphingolipid metabolism

Histidine metabolism

Cysteine and methionine metabolism

Arachidonic acid metabolism

Biosynthesis of unsaturated fatty acids

Butanoate metabolism

Arginine biosynthesis

D-glutamine and D-glutamate metabolism

Glutathione metabolism

Glyoxylate and dicarboxylate metabolism

Nitrogen metabolism

TCA cycle

Valine, leucine and isoleucine biosynthesis

Aminoacyl-tRNA biosynthesis

Purine metabolism

Glycerolipid metabolism

Fructose and mannose metabolism

Inositol phosphate metabolism

Pentose phosphate pathway

Lysine degradation

Biotin metabolism

Arginine and proline metabolism

Tryptophan metabolism

Phenylalanine, tyrosine and tryptophan biosynthesis

Phenylalanine metabolism

Pyruvate metabolism

Glycolysis / Gluconeogenesis

Tyrosine metabolism

A.7.3 G.HNAMint changed metabolic pathways

Alanine, aspartate and glutamate metabolism

Glycine, serine and threonine metabolism

Butanoate metabolism

D-glutamine and D-glutamate metabolism

Glyoxylate and dicarboxylate metabolism

Nitrogen metabolism

Glutathione metabolism

Histidine metabolism

Arginine biosynthesis

Pentose phosphate pathway

Fructose and mannose metabolism

Inositol phosphate metabolism

Purine metabolism

Glycerolipid metabolism

Tyrosine metabolism

Nicotinate and nicotinamide metabolism

Arginine and proline metabolism

TCA cycle

Aminoacyl-tRNA biosynthesis

β-Alanine metabolism

Tryptophan metabolism

Riboflavin metabolism

Glycolysis / Gluconeogenesis

Pantothenate and CoA biosynthesis

Pyruvate metabolism

Phenylalanine, tyrosine and tryptophan biosynthesis

Phenylalanine metabolism

Cysteine and methionine metabolism

Biotin metabolism

Lysine degradation

Biosynthesis of unsaturated fatty acids

Arachidonic acid metabolism

Sphingolipid metabolism

Valine, leucine and isoleucine degradation

Valine, leucine and isoleucine biosynthesis

Glycerophospholipid metabolism

Ether lipid metabolism

A.8 List of materials

A.8.1 Reagents

B27	10889-038, Gibco™; Thermo Fisher Scientific
Dichloromethane	D7566-500ML, Sigma
DiD' solid; DiIC$_{18}$(5) solid (1,1'-Dioctadecyl-3,3,3',3'-Tetramethylindodicarbocyanine, 4-Chlorobenzenesulfonate Salt)	D7757, Invitrogen™; Thermo Fisher Scientific
DiI Stain (1,1'-Dioctadecyl-3,3,3',3'-Tetramethylindocarbocyanine Perchlorate ('DiI'; DiIC$_{18}$(3)))	D282, Invitrogen™; Thermo Fisher Scientific
DiO'; DiOC$_{18}$(3) (3,3'-Dioctadecyloxacarbocyanine Perchlorate)	D275, Invitrogen™; Thermo Fisher Scientific
Dynabeads™ M-450 Epoxy	14011, Invitrogen™; Thermo Fisher Scientific
FluorSave Reagent	345789, Millipore®; Sigma-Aldrich
Glass beads, acid-washed (425-600 µm)	G8772, Sigma-Aldrich
GlutaMAX	35050-61, Gibco™; Thermo Fisher Scientific
Hank's Balanced Salt Solution (HBSS)	24020-091, Gibco™; Thermo Fisher Scientific
Hoescht 33342	62249, Thermo Scientific; Thermo Fisher Scientific
Methylene chloride	M1550000, European Pharmacopoeia (EP); Sigma-Aldrich
N2	17502-048, Gibco™; Thermo Fisher Scientific
Neurobasal-A Medium	10888-022, Gibco™; Thermo Fisher Scientific
Nicotinamide (NAM)	BIN0610, Apollo Scientific Ltd
Paraformaldehyde 4%, pH 6.9	100496500, Sigma-Aldrich
PBS (10X), pH 7.4	70011-044, Gibco™; Thermo Fisher Scientific

Penicillin Streptomycin	15140-122, Gibco™; Thermo Fisher Scientific
Tungsten M-25 Microcarrier, 1.7 µm	1652269, Bio-Rad
Tungsten powder, APS < 1µm, 99.95% (metal basis)	44210, Alfa Aesar; Thermo Fisher Scientific

A.8.2 Solutions

Phosphate Buffered Saline (PBS) 10%

80 g Solidum Chloride (NaCl), 2 g Potassium Chloride (KCl), 14.4 g Sodium Phosphate (Na_2HPO_4), 2.4 g Potassium Phosphate (KH_2PO_4) were dissolved in 800 ml of ddH_2O. The pH was adjusted to ph 7.4, and the volume adjusted to 1 l adding ddH_2O.

Retinal explant media

For 10 ml media: 100 µl N-2 supplement (100X), 200 µl B-27 supplement (50X), 100 µl Pen/Strep (10000 U/ml), 25 µl GlutaMAX supplement (200mM), 9.565 ml Neurobasal-A Medium.

A.8.3 Consumables

6 well plate	10578911, Corning™ Costar™; Fischer Scientific
BD Microlance stainless steel needles (Brown 26 G)	10703815, Fisher Scientific
BD Microlance stainless steel needles (Orange 25 G)	12389169, Fisher Scientific
Eppendorf 1.5 ml	0030121023, Eppendorf
Falcon cell culture inserts, 3 µm pore size (use with 6 well plate)	353092, Falcon; Fisher Scientific
Falcon tube 15 ml	339650, Nunc™; Thermo Fisher Scientific
Falcon tube 50 ml	339652, Nunc™; Thermo Fisher Scientific
Millicell, cell culture inserts 0.4 µm pore size, 30mm diameter	PICMORG50, Merck Millipore; Fischer Scientific
Tefzel Tubing	1652441, Bio-Rad

Thermo Scientific Superfrost Plus Adhesion slides J1800AMNZ pack of 72	10149870, Fisher Scientific

A.8.4 Equipment

Disposable transducer for Icare TonoLab tonometer	1736010, Icare; Eickemeyer
Helios® Gene gun	1652432, Bio-Rad
Leica SP8 lightning confocal microscope	Leica
LSM 780 Carl Zeiss confocal microscope	Zeiss
NanoFil needle, 33 G bevelled	NF33BV-2, World Precision Instruments
NanoFil needle, 35 G bevelled	NF35BV-2, World Precision Instruments
NanoFil syringe, 10 µl	NANOFIL-10, World Precision Instruments
NanoFil syringe, 100 µl	NANOFIL-100, World Precision Instruments
Pierse notched forceps	2-100E, Duckworth & Kent
TonoLab rebound tonometer	Icare
Vannas scissors (straight)	1-110, Duckworth & Kent

A.8.5 Medications

Chloramphenicol 0.5 % Minims	PL03468/0069, Bausch & Lomb
Isoflurane 200 % inhalation vapour, liquid	Piramal Healthcare UK Ltd
Oxybuprocaine hydrochloride 0.4 % Minims	PL03468/0053, Bausch & Lomb
Viscotears liquid gel	PL13757/0020, Bausch & Lomb